# University of Sussex

**A University of Sussex DPhil thesis**

Available online via Sussex Research Online:

http://sro.sussex.ac.uk/

This thesis is protected by copyright which belongs to the author.

This thesis cannot be reproduced or quoted extensively from without first obtaining permission in writing from the Author

The content must not be changed in any way or sold commercially in any format or medium without the formal permission of the Author

When referring to this work, full bibliographic details including the author, title, awarding institution and date of the thesis must be given

Please visit Sussex Research Online for more information and further details

Novel insights into the DNA interstrand cross-link repair in

*Schizosaccharomyces pombe*:

characterisation of Fan1 through standard and high-throughput

genetic analysis

Yari Fontebasso

A thesis submitted for the degree of Doctor of Philosophy at the University of Sussex

April 2011

I hereby declare that this thesis has not been and will not be, submitted in whole or in part to another University for the award of any other degree.


Signature…………………………………………………………………………………………………………………………

# Acknowledgements

*My most heartfelt thanks go to Professor Tony Carr and Dr Jo Murray, who in a moment of distraction allowed me to sneak in their laboratories and work for them. Their constant, unobtrusive help provided me with the best balance between need for support and independence of thought.*

*Thanks to Dr Matt Neale for seizing me by the scruff of my neck and keeping me on the right track of my PhD during our meetings.*

*Thanks to Dr Tim Humphrey for being such a kind host during the work done in his lab. I regard the time spent in Oxford as some of the most intense and fulfilling experiences in my studies. Unfortunately I managed to reciprocate only by giving him a bunch of advice on how to maintain a correct posture while running. I'm particularly grateful to Anoushka for her help and for stopping me from scrapping some data that in fact were not too bad, after all.*

*Thanks to Dr Sean Collins for keeping replying to all my silly questions. He somehow managed to make sense of some really obscure high-throughput computational analyses.*

*Thanks to Izumi Miyabe for not getting upset when I asked him to share a piece of his unpublished data (note for the examiners: this data has been properly referenced in the thesis).*

*Thanks to Amon Tobin for providing me with a proper inspirational electro-beat during the writing-up.*

*Genuine thanks to Marvin for being such a reliable, high-throughput companion of late nights in the lab.*

*Thanks to my lab colleagues and to the people around the Genome Centre. They made me realise how important is to have valuable and supportive people around me. I made them realise what it means having to do with a scientist with a temperamental Mediterranean heart. In particular, personal thanks go to Stephi, Georgina, Bernie, Katie, Mariella and Jean. They managed to keep me afloat in the most troubled moments of my PhD. How on earth they could put up with all my moaning is still a mystery to me.*

*Special thanks go to Michela for the unique mix of personal support and inspirational scientific discussions. She gave me the feeling that I could actually comprehend issues at the interface between philosophy, molecular biology and quantum physics. Mine is just a feeling. I wish she can get some of those answers for real, one day.*

*Un ringraziamento davvero speciale alla mia famiglia. Mamma, papà, Giayes: senza il vostro costante aiuto e supporto non sarei qui, a tentare di realizzare quello che per me è importante nella vita.*

# UNIVERSITY OF SUSSEX

YARI FONTEBASSO

A thesis submitted for the degree of Doctor of Philosophy

*"Novel insights into the DNA interstrand cross-link repair in Schizosaccharomyces pombe: characterisation of Fan1 through standard and high-throughput genetic analysis"*

FAN1/MTMR15 (Fanconi anemia-associated nuclease 1 / Myotubularin-related protein 15) is a protein originally identified from a set of size-fractionated human brain cDNA libraries coding for large proteins *in vitro* (Nagase et al., 1999). FAN1 is widely conserved across eukaryotes, with the notable exception of *S. cerevisiae* (Smogorzewska et al., 2010; MacKay et al., 2010; Kratz et al., 2010; Liu et al., 2010; Shereda et al., 2010). Recent work has shown that FAN1 is a novel component of the Fanconi Anemia repair DNA pathway in higher eukaryotes (Smogorzewska et al., 2010; MacKay et al., 2010; Kratz et al., 2010; Yoshikiyo et al., 2010; Liu et al., 2010; Shereda et al., 2010).

My work presents a biochemical and genetic characterisation of the FAN1 *Schizosaccharomyces pombe* ortholog Fan1. I show that, in contrast with the situation in higher eukaryotes, Fan1 in *S. pombe* does not strongly interact with components of the mismatch repair pathway. The disruption of *fan1* causes a mild sensitivity to interstrand cross-linking agents, dramatically augmented by the concomitant deletion of the nuclease Pso2, suggesting a role for Fan1 in the resolution of DNA interstrand cross-links. Further genetic interactions are explored by use of an automated high-throughput screen, where a non-epistatic relationship is found with Pli1, a component of the SUMOylation pathway. Finally, I show that three conserved residues in the VRR_nuc nuclease domain are required for Fan1 activity in DNA repair. Taken together, the data presented points at a role for *S. pombe* Fan1 in the resolution of adducts created by DNA interstrand cross-linking agents.

# Table of Contents

## Chapter Three
## BIOCHEMICAL CHARACTERISATION OF FAN1 IN SCHIZOSACCHAROMYCES POMBE ................................................................................................... 107

## Chapter Six
## PHENOTYPIC ANALYSIS OF FAN1<sup>SP</sup> POINT MUTANTS........................... 173

## Chapter Seven
## FINAL DISCUSSION AND CONCLUSIONS ............................................. 181

## Appendix 1
## USE OF THE Ch16 DOUBLE-STRAND BREAK REPAIR SYSTEM TO INVESTIGATE THE FUNCTIONAL INTERACTION BETWEEN Rqh1$^{Sp}$ AND Crb2$^{Sp}$ IN RECOMBINATIONAL DNA REPAIR

## Appendix 2
## SUPPLEMENTARY FIGURES

## 10   References

# List of figures

# List of tables

# Abbreviation list

| | |
|---|---|
| 14152 / 14152N (strain) | fan1::kanMX6 / fan1::natMX6 deletion mutant (derived from Bioneer® deletion set) |
| 3909 / 3909N (strain) | fan1::kanMX6 / fan1::natMX6 deletion mutant (derived from Paul Nurse's strain collection) |
| 5-FOA | 5-fluoroorotic acid |
| 9-1-1 clamp complex | complex composed of: Rad9-Hus1-Rad1 (*Homo sapiens*, *Schizosaccharomyces pombe*); Rad17-Mec3-Ddc1 (*Saccharomyces cerevisiae*) |
| A | adenine |
| ade | adenine |
| AP site | apurinic or apyrimidinic site |
| BER | base excision repair |
| BIR | break-induced replication |
| bp | base pair |
| C | cytosine |
| Ch16 | minichromosome derived from chromosome III used in this study |
| ChIP | chromatin Immunoprecipitation |
| cispl | cisplatin |
| co | crossing-over |
| CPT | camptothecin |
| cyh | cycloheximide |
| Δ / -d / D | deletion (gene) |
| DDRs | DNA damage responses |
| DMSO | dimethyl sulfoxide |
| DNA | deoxyribonucleic acid |
| DSB | double strand breaks |
| dsDNA | double strand DNA |
| Ec / *E. coli* | *Escherichia coli* |
| ECL | enhanced chemi-luminescence |
| EDTA | ethylene diaminetetra-acetate |
| EJ | end-joining |
| ELN | extremely low nitrogen |
| EMM | Edinburgh minimal media |
| ER | estrogen receptor |
| FA | Fanconi anemia |
| FAN1, Fan1 | Fanconi anemia-associated nuclease 1, or FANCD2/FANCI-associated nuclease 1 |
| G | guanine |
| G418 | geneticin |
| GC | gene conversion |
| GC (plate) | YEA plate containing geneticin and cycloheximide |

| | |
|---|---|
| GNC (plate) | YEA plate containing geneticin, nurseothricin and cycloheximide |
| HBD | hormone binding domain |
| his | histidine |
| HJ / dHJ | Holliday junction / double Holliday junction |
| HN1 | 2-dimethylaminoethylchloride hydrochloride, monofunctional nitrogen mustard |
| HN2 | mechlorethamine hydrochloride, bifunctional nitrogen mustard |
| HO | HO endonuclease |
| HR | homologous recombination |
| Hs / *H. sapiens* | *Homo sapiens* |
| HU | Hydroxyurea |
| ICL | interstrand cross-link |
| ID complex | Complex composed of FANCD2-FANCI (*Homo sapiens*) |
| IDL | small insertion/deletion (loops) |
| inv | invertase promoter |
| invHO | invertase promoter - HO |
| IP / co-IP | immunoprecipitation / co-immunoprecipitation |
| kan | kanamycin |
| kDA | kiloDalton |
| leu | leucine |
| LOH | loss of heterozygosity |
| LTGC | long-tract gene conversion |
| MGH | minichromosome carrying the MATa, G418 and His markers |
| MMC | mitomycin C |
| MMR | mismatch repair |
| MMS | methyl methanesulfonate |
| MRN/MRX complex | complex composed of: Mre11-Rad50-Nbs1 (*Homo sapiens*, *Schizosaccharomyces pombe*); Mre11-Rad50-Xrs2 (*Saccharomyces cerevisiae*) |
| NAT | nourseothricin |
| NER | nucleotide excision repair |
| NHEJ | nonhomologous end-joining |
| nmt | no-message in thiamine |
| o/n | overnight |
| ORF | open reading frame |
| PAGE | polyacrylamide gel electrophoresis |
| PBS | phosphate buffered saline |
| PCR | polymerase chain reaction |
| PEM-2 | pombe epistatic mapper 2 |
| PFGE | pulse-field gel electrophoresis |
| Q | query mutant |
| r,R *(following a genetic marker)* | resistant |
| ROS | Reactive Oxygen Species |

| | |
|---|---|
| rpm | revolutions per minute |
| rt | room temperature |
| s, S *(following a genetic marker)* | sensitive |
| Sc / *S. cerevisiae* | *Saccharomyces cerevisiae* |
| SCC | sister-chromatid conversion |
| SDS | sodium dodecyl sulphate |
| SDSA | synthesis-dependent strand annealing |
| SGA | synthetic genetic array |
| SL | synthetic lethal |
| Sp / *S. pombe* | *Schizosaccharomyces pombe* |
| SS | synthetic sick |
| SSA | single strand annealing |
| SSB | single strand breaks |
| ssDNA | single strand DNA |
| T | thymine |
| TBE | tris-borate-EDTA |
| TCA | trichloroacetic acid |
| TE | tris-EDTA |
| TLS | Translesion synthesis |
| ura | uracil |
| UV | ultra-violet |
| W-C | Watson-Crick (pairing) |
| WCE | whole cell extract |
| wt | wild type |
| YE /YEA | yeast extract / yeast extract agar |
| YFL | Yari Fontebasso (deletion) Library |
| YFP | Yari Fontebasso Plasmid |
| YFS | Yari Fontebasso Strain |
| YNB | yeast nitrogen base |

Chapter One

INTRODUCTION

## 1.1 DNA damage and response pathways

The maintenance of genomic stability is of paramount importance in living cells. Every day cellular DNA is damaged by exogenous, environmental factors such as background radiation and sunlight. In addition, endogenous harmful by-products of cell metabolism and errors induced by enzymes involved in DNA processing constitute continuous threats which are intrinsic to cellular growth and development (Ciccia and Elledge, 2010). The damage occurring to the DNA double helix can be broadly classified into three categories, according to the nature of the lesion: single-strand breaks (SSBs) occur when a discontinuity is generated on only one of the two complementary DNA strands; double-strand breaks (DSBs) involve both the DNA strands; a third group of lesions comprises local alterations of the standard base pairing or hydrogen-bond configuration such as base chemical modifications, base-base mismatches and DNA covalent intra- and inter-strand cross-links. Cells have developed an intricate network of tightly regulated repair mechanisms which detect and address different forms of DNA damage, in order to minimise any fatal effect which may arise as a consequence of it. SSBs are repaired by the single-strand break repair system, whereas DSBs are tackled by either nonhomologous end-joining (NHEJ) or homologous recombination (HR). The third category of DNA lesion is processed by specific mechanisms such as base excision repair (BER), mismatch repair (MMR), nucleotide excision repair (NER) and interstrand cross-link repair (Ciccia and Elledge, 2010).

## 1.2 Structure of this chapter

### 1.2.1 Aim of this chapter

The aim of this introductory chapter is to provide a background for the work presented in the subsequent sections. First, a general overview will be given of the organisation of the DNA damage responses and of the DNA checkpoints, the mechanisms by which living cells sense and respond to insults at their genetic material (sections 1.3 - 1.4). Then, a brief section will outline the single-strand repair pathway (section 1.5). It should be noted that this section is

intentionally schematic and has been added for completeness, since this topic is not directly relevant to the work presented in the following chapters of results. The DNA double-strand break repair system will be discussed in sections 1.6 – 1.8 primarily from a mechanistic perspective, where the role of the various components will be described with preference towards better understood mechanisms and model organisms. A special emphasis will be given to the repair of double strand breaks by homologous recombination processes (section 1.8), as this aspect is relevant to one of the sections of results (appendix 1). For completeness, basic aspects of DNA double-strand break repair by non-homologous end joining will also be illustrated in section 1.7 The major body of this introduction will focus on specific mechanisms of DNA damage responses aimed at the repair of chemical alterations to the DNA structure (sections 1.9 – 1.12). In particular, the final section 1.12 will present a detailed discussion of the interstrand cross-link repair pathway, the main subject of the work presented in this thesis.

### 1.2.2 Notes on the use of nomenclature used for protein names

While being conserved in most of its fundamental aspects, the detailed mechanisms and the components of the response to DNA damage can differ between organisms. Those differences will be highlighted where necessary. The following superscripts have been used to define protein names: [Hs], *Homo sapiens*; [Sp], *Schizosaccharomyces pombe*; [Sc], *Saccharomyces cerevisiae* [Ec], *Escherichia coli*. However, superscripts have been omitted when the context is specific in respect of the model organism discussed. In addition, superscripts have been occasionally omitted when a molecular mechanism is presented as a general concept, or when a mechanism is conserved across all the organisms discussed. As a guide for the following initial sections, table 1.1 presents a summary of the known homologs of the main players in the DNA damage checkpoint in fission yeast, humans and budding yeast.

## 1.3 DNA damage responses

Cells respond to insults to their genome by coordinating a series of signal transduction pathways whose primary aim is to restore the integrity of the genetic material. The key initial step shared by all the DNA damage responses (DDRs) is sensing the DNA lesions. Downstream components acting as mediators are thought to act as bridges to functionally connect different response factors. Effectors are then identified as the responsible proteins for end-point effects of the damage responses such as the induction of cell-cycle arrest and the promotion of DNA repair. Overall, the signals from early to late steps of the damage response define signal transduction pathways named signal cascades.

## 1.4 DNA checkpoints

One of the most crucial consequences of the activation of DNA damage responses is the induction of cell cycle arrest in order to allow time for DNA repair (Zhou and Elledge, 2000). The orchestration of cell cycle transitions during DNA repair is controlled by DNA checkpoint proteins. It is now clear that, although mainly conserved across eukaryotes (see table 1.1), the mechanisms and the players involved in DNA checkpoints differ between humans, *S. cerevisiae* and *S. pombe*. In this section, an overview is presented of the current model of DNA checkpoint signalling and the details of mechanisms underlying the functioning of DNA checkpoints, focusing on *S. pombe* as a model organism.

The concept of DNA damage checkpoint was initially formulated following studies of the Rad9[Sc] (homolog of *S. pombe* Crb2 and human 53BP1) mutant in *S. cerevisiae*, which failed to delay mitosis after DNA damage (Weinert and Hartwell, 1988). Thus, it was proposed that this DNA damage checkpoint linked DNA repair and progression through the cell cycle. Rad9 was proposed to perform a surveillance function, sensing DNA damage and signalling to the cell cycle machinery to delay progression until repair of damage has been accomplished.

### 1.4.1 DNA checkpoints in S. pombe

Two major DNA checkpoints have been identified in *S. pombe*: the first acts in G2 and is called G2/M DNA damage checkpoint; the second acts in S phase and is called replication (or S phase) checkpoint. The effect of both these checkpoints is to halt the transition from G2 to mitosis (Carr, 2002).

The G2/M checkpoint was shown to be conserved in fission yeast following the observation of a delayed onset of mitosis in cells irradiated with UV (Rowley et al., 1992; al-Khodairy and Carr, 1992). al-Khodairy and Carr (1992) showed four mutants (*rad1*-d, *rad3*-d, *rad9*-d and *rad17*-d) to be unable to arrest in mitosis following exposure to UV, indicating a role for the corresponding proteins in the damage checkpoint. Enoch et al. (1992) showed that these proteins and Hus1 (the third component of the heterotrimeric 9-1-1 clamp complex Rad9-Rad1-Hus1) were also required for the S phase replication checkpoint following HU-induced cell cycle arrest. Subsequent work identified Rad26 as a further DNA checkpoint protein (al-Khodairy et al., 1994), which is now known to interact and be phosphorylated by Rad3 following DNA damage (Edwards et al., 1999). This phosphorylation is the earliest biochemical marker of Rad3 function and occurs independently of all the other checkpoint proteins (Edwards et al., 1999). The effector kinase Chk1 has been shown to be a central regulator of the DNA damage checkpoint, downstream of Rad3, Rad26 and the 9-1-1 complex (Walworth et al., 1993; al-Khodairy et al., 1994). Importantly, Walworth et al. (1993) presented also the first evidence for the connection between the damage checkpoint and the progression through the cell cycle by control of the cell cycle kinase Cdc2. Subsequent work by Saka et al. (1997) identified Crb2 as a checkpoint mediator required for the activation of Chk1 in response to DNA damage.

Additional work identified genes required only for proficient cell cycle arrest following exposure to hydroxyurea (HU), an agent which arrests S phase by depleting the cellular nucleotide pool. In response to S-phase arrest or to DNA damage perturbing the progression of

the replication fork, phosphorylation and activation of the serine/threonine kinase Cds1 is an essential prerequisite (Murakami and Okayama, 1995; Lindsay et al., 1998). The mediator Mrc1 has been shown to be essential for the activation of Cds1 (Alcasabas et al., 2001). In addition to delaying mitosis, this intra-S phase checkpoint stabilises stalled replication forks and prevents late origin firing (Lindsay et al., 1998; Santocanale and Diffley, 1998).

The components discussed above constitute the DNA damage and replication checkpoints in *S. pombe*. However, a high degree of conservation has been found throughout eukaryotes (table 1.1).

### 1.4.2 **Sensing the damage**

As discussed above, the phospho-inositide 3 kinase (PI3K)-like kinase Rad3 has been identified as a key activator of the DNA damage response in *S. pombe*. This is the homolog of Mec1[Sc] and ATR[Hs], originally identified as homologs of Rad3[Sp]. It has been speculated that distinct structure-dependent sensors elicit specific DNA damage responses (Zhou and Elledge, 2000). A

| Description | Fission yeast | Human | Budding yeast |
|---|---|---|---|
| *phospho-inositide 3 kinase (PI3K)-like kinase* | Rad3 | ATR | Mec1 |
| *ATR-interacting protein* | Rad26 | ATRIP | Ddc2 |
| *phospho-inositide 3 kinase (PI3K)-like kinase* | Tel1 | ATM | Tel1 |
| *Rfc1 homolog* | Rad17 | Rad17 | Rad24 |
| *9-1-1 clamp* | Rad9 | Rad9 | Rad17 |
| | Hus1 | Hus1 | Mec3 |
| | Rad1 | Rad1 | Ddc1 |
| *MRX complex* | Rad32 | Mre11 | Mre11 |
| | Rad50 | Rad50 | Rad50 |
| | Nbs1 | Nbs1 | Xrs2 |
| *Mediator/checkpoint protein (BRCT protein)* | Crb2 | 53BP1, MDC1, BRCA1? | Rad9 |
| *Mediator (BRCT protein)* | Mrc1 | Claspin | Mrc1 |
| *Mediator (BRCT protein)* | Rad4/Cut5 | TopBP1 | Dpb11 |
| *Signaling kinase* | Chk1 | Chk1 | Chk1 |
| *Signaling kinase* | Cds1 | Chk2 | Rad53 |

**Table 1.1 | Homologs of DNA checkpoint proteins in fission yeast, human and budding yeast.**

common intermediate able to trigger DNA damage responses is ssDNA coated with the single-strand binding protein RPA (Zou and Elledge, 2003). Another PI3-like kinase, ATM[Hs] (Tel1[Sp,Sc]) plays an important role in DNA damage checkpoint in higher eukaryotes (Zhou and Elledge, 2000), whereas its role in yeast appears to be confined at the control of telomere length (Greenwell et al., 1995). ATR and ATM kinases in mammalian cells have been associated with the role of sensor proteins, although the extent of their involvement in the damage response pathways is clearly much broader (see 1.4.3). A brief overview is given below of proteins that have been associated with the role of sensors of the DNA damage and replication checkpoint.

ATR binds to ssDNA (one of the hallmarks of DNA damage) coated with the single-strand binding protein RPA dependently on the interaction with its partner ATRIP (Zou and Elledge, 2003). However, studies in *Xenopus laevis* have indicated that this localisation is not sufficient for ATR activation. In this system, ATR signalling is dependent on the additional colocalisation of the 9-1-1 complex, involved in checkpoint activation in higher and lower eukaryotes (Parrilla-Castellar et al., 2004; Cimprich and Cortez, 2008). Interestingly, in *S. cerevisiae* the colocalisation of the Ddc2[Sc]-Mec1[Sc] (orthologs of ATRIP[Hs] – ATR[Hs]) and the 9-1-1 (composed of Rad17-Mec3-Ddc1 in *S. cerevisiae*) complexes is sufficient to activate the DDR even in the absence of damage (Bonilla et al., 2008). However, the model for ATR activation appears to be more complicated than previously thought and may require the additional presence of structures that resemble stalled replication forks, as shown in *Xenopus* egg extracts (MacDougall et al., 2007). Indeed, the structural similarity of the 9-1-1 complex with the sliding trimeric clamp PCNA (Proliferating Cell Nuclear Antigen, a processivity factor involved in eukaryotic replication) suggests that the 9-1-1 complex could act as an emergency sliding platform for the recruitment of DNA repair factors to the site of damage following replicational stress (Parrilla-Castellar et al., 2004). In this scenario, ATR-dependent mechanisms may act more specifically in response to DNA damage impeding the progression of the replication fork, rather than to generic DNA damage (Cimprich and Cortez, 2008).

The role of ATM appears to be more limited and directed at the response to DNA DSBs. The heterotrimeric MRN (Mre11[Hs,Sc]/Rad32[Sp] - Rad50[Hs,Sp ,Sc] − Nbs1[Hs,Sp] / Xrs2[Sc]) complex has been implicated as a sensor protein and this complex is required for ATM activation (evidence reviewed in Lamarche et al., 2010). Interestingly, the artificial targeting of DNA repair factors such as NBS1[Hs], MRE11[Hs] and ATM[Hs] elicited a DNA damage response in the absence of any lesion in mammalian cells (Soutoglou and Misteli, 2008). Despite this seductive simplicity, it is increasingly clear that the ATR and ATM pathways are interconnected and further studies are required to unravel the biological significance of this cross-talk (Parrilla-Castellar *et al.*, 2004).

### 1.4.3    The downstream effects of the damage responses

Primary physiological targets of the damage responses are the orchestration of cell-cycle transitions, the regulation of DNA transcription, the coordination of DNA repair and the induction of apoptotic responses (Zhou and Elledge, 2000). However, recent work has shown that the scope of the biochemical consequences following the activation of damage-induced responses is more extensive than previously appreciated. A large-scale proteomic analysis identified more than 700 targets for ATR[Hs] and ATM[Hs], encompassing previously expected proteins involved in processes such as RNA splicing, the spindle checkpoint and chromatin remodelling (Matsuoka et al., 2007). A wider complexity can be envisaged following the potential identification of additional targets for the downstream kinases Chk1 and Chk2.

Beyond these unexpected far-reaching effects, the significant enrichment shown for factors involved in DNA repair mechanisms (Matsuoka *et al.*, 2007) confirms the critical role for the DNA damage responses in directly surveilling and maintaining the integrity of the cellular genome.

### 1.4.4    The mediators of the damage responses

Following the initial activation, the damage response pathways depend on a wide range of posttranslational modifications which act as mediating elements for protein-protein interactions (Ciccia and Elledge, 2010). As seen above, ATR[Hs] (Rad3[Sp], Mec1[Sc]) and ATM[Hs]

(Tel1[Sp,Sc]) play a key role as upstream transducers in the response to DNA damage. ATR and ATM control the downstream stages of the cascade by phosphorylating targets such as the two serine/threonine kinases Chk1[Hs] (Chk1[Sp,Sc]) and Chk2[Hs] (Cds1[Sp], Rad53[Sc]) respectively, which in turn phosphorylate other downstream mediators and effectors (Zhou and Elledge, 2000).

An important mediator identified in mammalian cells and yeast is the checkpoint protein 53BP1[Hs] (Crb2[Sp], Rad9[Sc]), which has been shown to play additional direct roles in recombination. Importantly, a requirement was shown for Crb2 for proficient cell cycle arrest in response to UV (Saka et al., 1997). This activity was suggested to rely on direct interactions of Crb2 with the BRCT protein Rad4/Cut5 and the kinase Chk1 (Saka et al., 1997).

### 1.4.5 A model for the DNA checkpoint in *S. pombe*

Taken together, the above data suggest a model for the DNA damage checkpoint in *S. pombe* where the Rad9-Rad1-Hus1 complex is firstly loaded at damage sites by Rad17 and independently of the phospho-inositide 3 kinase (PI3K)-like kinase Rad3 (in complex with its binding partner Rad26). If the damage occurs during replication, Mrc1 acts as a mediator to activate Cds1, which in turn acts on the Cdc2 kinase to prevent the progression into mitosis. In contrast, if the damage occurs in the G2 phase, Crb2 and Rad4/Cut5 mediate the signal to Chk1, which in turn exerts a similar action to halt the cell cycle.

### 1.4.6 The role of Crb2 in DNA damage checkpoint and repair

Crb2, homolog of human 53BP1 and *S. cerevisiae* Rad9, is a central component of the DNA damage checkpoint and the DNA damage responses in *S. pombe*. Interestingly, while the DNA repair functions appear to be conserved between Crb2[Sp], 53BP1[Hs] and Rad9[Sc], the DNA checkpoint role of 53BP1 seems to play a limited role compared to the yeast homologs (Carr, 2002; Ward et al., 2006). As a background for the work presented in chapter 8, this section provides an overview of the current knowledge on Crb2 as a player in DNA damage checkpoint responses. Further aspects about this protein, in particular the role in the DNA damage checkpoint and its interaction with Rqh1[Sp], are discussed in section 8.1.1.

Crb2[Sp] is directly recruited to Ionizing Radiation (IR)- induced DSBs through interactions between its Tudor and BRCT domains with modified histones (Du et al., 2006; Greeson et al., 2008). The crucial role for Crb2 in the DSB response pathway is confirmed by data showing that, following UV irradiation, Crb2 is phosphorylated and in turn required for phosphorylation and activation of Chk1 (Saka et al., 1997; Mochida et al., 2004). However, Tudor domains are dispensable for Crb2 recruitment to DSBs induced by the HO endonuclease (Du et al., 2006).

A number of studies emphasise the importance of CDK phosphorylation on Crb2-T215 in DSB repair. This aspect was first characterised by Esashi and Yanagida (1999). Importantly, a pathway of recruitment occurring in the absence of histone phosphorylation and methylation seems to be dependent on the phosphorylation of T215 (Du et al., 2006). This residue has been shown to be critical for the association between Crb2 and the BRCT chromatin-bound protein Rad4/Cut5 (Du et al., 2006). Furthermore, T215 phosphorylation by Cdk1 has been suggested to be required for the subsequent Rad3-dependent hyperphosphorylation of Crb2 upon DNA damage (Esashi and Yanagida, 1999). The effect of mutations of the T215 residue on the DNA repair functions of Crb2 has been shown directly by the fact that *crb2*-T215A cells are more sensitive than wt to IR (Caspari et al., 2002). The T215A mutation has been suggested to cause a deficiency in the checkpoint function of Crb2, although this seems to be dependent on the doses of DNA damaging agent used (this aspect is further discussed in section 8.1.1). However, it is interesting to note that *crb2*-T215A cells are as hypersensitive as *crb2*-d cells to the DNA damaging agent camptothecin (CPT), although significantly less hypersensitive to UV and IR (Greeson et al., 2008). This data suggests that the phosphorylation of Crb2-T215 is differentially required in response to distinct subsets of lesions. Interestingly, this CDK phosphorylation regulates Crb2 activity through the cell cycle, as recruitment of Crb2 to DSBs is blocked at early stages of the S-phase, indicating that Crb2 may be involved in DNA repair only at specific stages of the cell cycle (Du et al., 2003; Nakamura et al., 2004; Du et al., 2006).

## 1.5    DNA Single-strand break repair

This section is included to complete the description of the types of DNA damage with a brief overview of the current model for the repair of single strand breaks. As little is known about this repair pathway in *S. pombe* and no yeast homolog has been found for the central component PARP1, the overview illustrated below is based mostly on reviewed data from mammalian systems.

### 1.5.1    Sources of SSBs

Single-strand breaks (SSBs) in living cells can arise as a consequence of a variety of processes. Attacks by reactive oxygen species (ROS) such as hydrogen peroxide are amongst the most common causes of SSBs (reviewed in Caldecott, 2008). SSBs are also produced as molecular intermediates of physiological processes like the relaxation of DNA topological stress by topoisomerases belonging to the subfamilies IA and IB (Wang, 2002) or the removal of damaged bases by the base excision repair (BER) system (Robertson et al., 2009). Unrepaired SSBs can eventually lead to the fatal impairment of fundamental physiological process such as DNA replication and transcription (Caldecott, 2008).

### 1.5.2    Overview of the single-strand repair system in mammalian cells

The current model for the repair of SSBs distinguishes different repair pathways depending on the cause of damage. In the case of breaks that are consequences of damage to the DNA sugar (like those caused by ROS), the primary SSB sensor is poly(ADP-ribose) polymerase 1 (PARP1[Hs]). Upon binding with DNA breaks, PARP1 functions by adding chains of poly(ADP-ribose) onto itself and other target proteins (Caldecott, 2008). PARP1 binding on DNA is rapidly reversed by degradation of poly(ADP-ribose) chains by poly(ADP-ribose) glycohydrolase PARG (Fisher et al., 2007; Caldecott, 2008). Although multiple roles have been attributed to PARP1[Hs] (reviewed in Caldecott, 2008), the main role for this component appears to be the recruitment of XRCC1 (X-ray repair cross-complementing protein 1). It has been proposed that XRCC1 acts as a scaffold for the assembly of components downstream of the SSB repair pathway (Whitehouse et al.,

2001). The second step in the SSB repair is the DNA end processing, which restores the standard 3'-hydroxyl and 5'-phosphate termini. This step is carried out by a diverse range of enzymes: PNKP, APE1, TDP1 and APTX (the functional details related to these enzymes can be found in Caldecott, 2008). Once the conventional ends have been restored, a gap filling step can occur where the damaged DNA strand is resynthesized to its original length. Gaps of a single nucleotide are repaired by Polβ in a pathway termed short-patch repair. Alternatively, when the gap filling step is extended for 2-12 nucleotides, a process called long-patch repair occurs which requires the flap endonuclease 1 FEN1 and is stimulated by PCNA and PARP1.

SSBs induced as a consequence of the abortive activity of TOP1 are repaired by TDP1 (tyrosyl-DNA phosphodiesterase 1) and PNKP (polynucleotide kinase 3'-phosphatase) (Caldecott, 2008).

The final step of SSBR is the ligation of the single-stranded gaps, carried out preferentially by LIG1 in long-patch repair and LIG3α in short-patch repair (Caldecott, 2008).

Indirect SSBs created as intermediates of the base excision repair pathway are discussed in 1.9.

## 1.6    DNA Double-strand breaks

Among the different types of DNA damage, double-strand breaks (DSB) are particularly dangerous in that the complementary strand cannot be used as a template for repair.

DSBs can be caused by exogenous, endogenous or specialized factors. Exogenous agents are represented by ionizing radiation, environmental mutagens or anticancer drugs. In addition, endogenous by-products of cell metabolism (e.g. free radicals), replication single-stranded breaks in DNA, collapsed forks or dysfunctional telomere end processing can all lead to formation of DSBs. However, this type of lesion naturally occurs as intermediates in several specialized cellular processes including meiosis, V(D)J recombination, immunoglobulin class switching and possibly B-cell somatic hypermutation (van Gent et al., 2001).

The importance of accurate DNA DSB repair is confirmed by accumulating indications in higher eukaryotes of direct links between inappropriate DSB repair and tumorigenesis (Pierce et al., 2001).

Cells possess two distinct ways to repair a DSB repair: homologous recombination (HR) and non-homologous end-joining (NHEJ). The first requires extensive sequence homology as a template to repair the break, thus as a consequence homologous recombination is potentially an error-free repair pathway. In contrast, NHEJ is generally error-prone, as the two cut ends are ligated together with little or no requirement for sequence homology (Haber, 2000).

### 1.6.1 HR versus NHEJ: the pathway choice

The preference towards either pathway of DNA double-strand break repair is determined by several factors and only recently studies have begun to shed light on the subject (reviewed in Shrivastav et al., 2008).

Firstly, it is increasingly clear that the choice between homologous recombination and non-homologous end joining is largely dependent on the phase of the cell cycle. Given its requirement for sequence homology, HR is used after DNA replication, when a sister chromatid is present. On the other hand, NHEJ can be used irrespectively of the presence of homologous sequences. Several reports are now beginning to unravel the relationship between the cell cycle and the choice of DSB repair pathway. It appears that cyclin-dependent protein kinases are directly involved in this aspect. In *S. cerevisiae*, DSB repair by homologous recombination in G1 is limited, with recombination being controlled at the level of resection by Clb (S and G2 cyclins)-CDK activity (Aylon et al., 2004). Importantly, CDK1 (Cdc28[Sc]) is required for efficient 5'-3' resection and inhibition of Cdc28[Sc] results in abolished HR and increased NHEJ (Ira et al., 2004). In particular, this control seems to be exerted in the budding yeast by CDK over the endonuclease Sae2[Sc] (Huertas et al., 2008).

Secondly, the nature of the lesion should be taken into consideration. For instance, in the case of DNA DSBs as consequences of chemical damage or discontinuities to only one DNA strand,

NHEJ cannot always be used, as only a single free end may be generated. In contrast, when DNA damage produces two double-stranded ends, both HR and NHEJ can be potentially utilised, opening the possibility of the choice between the two modalities of repair.

Thirdly, competition between HR and NHEJ components appears also to play an important role. In *S. cerevisiae*, Mre11 accumulates at unresected DSB ends and processing near the breaks in G1 is inhibited by competition with NHEJ (Ira et al., 2004; Zierhut and Diffley, 2008). Furthermore, the lack of the NHEJ proteins yKu[Sc], Lif1[Sc] or Dnl4[Sc] increases 5' DSB end degradation in G1 (Clerici et al., 2008).

Finally, differences in the use of HR versus NHEJ have been reported for lower and higher eukaryotes. In yeast, most of double-stranded breaks are repaired by HR. This is preferred to NHEJ, which has been shown to be very limited and inefficient (Prudden et al., 2003; further evidence reviewed in Shrivastav et al., 2008). In contrast, the use of NHEJ in mammalian cells is extensive and accounts for the repair of majority of DSBs (Shrivastav et al., 2008).

Taken together, the data so far indicate that pathway choice in DSB repair is more intricate than previously thought and it is possible that additional novel unknown factors may still add to the complexity of the scenario.

## 1.7    DNA Double-strand break repair: non-homologous end joining

As discussed above, repair by non-homologous end joining is inefficient and utilized very limitedly in yeast DSB repair. However, the key NHEJ components are present and conserved across eukaryotes. The section below presents a brief overview of the components of this repair pathway from data from lower and higher eukaryotes.

### 1.7.1    Non-homologous end joining: key players in higher and lower eukaryotes

The term non-homologous end joining (NHEJ) was proposed following the observation of imprecise repair occurring in *S. cerevisiae* in the absence of a homologous donor (Moore and Haber, 1996). NHEJ is now defined as a process whereby two cut DNA duplexes are rejoined

together with little or no requirement for sequence homology. The two broken ends are firstly protected by high-affinity binding proteins. The further downstream events lead to the re-association of the two broken molecules and the final re-ligation. Although components exquisitely critical for NHEJ have been identified, many proteins acting in this pathway share functions in single-strand break repair. Indeed, the key difference between the two processes is the need for re-associating overhangs when both the DNA strands, rather than only one of them, are cut.

The widely conserved heterodimer Ku70/Ku80 is a central component of NHEJ in higher as well as lower eukaryotes (Daley et al., 2005). Ku binds DNA ends with high affinity and is considered to be a docking platform for enzymes involved in the downstream NHEJ (Lieber, 2010). In vertebrate NHEJ, the kinase DNA-PKcs phosphorylates Artemis, and the endonuclease activity of the DNA-PKcs:Artemis complex is thought to be involved in the step of 5' and 3' overhang processing (Ma et al., 2002). Further downstream, DNA synthesis is performed by family X polymerases such as Polµ and Polλ (Lieber, 2010). The XRCC4:DNA ligase IV is a crucial complex able to ligate ends that share microhomology as well as incompatible ends (Gu et al., 2007). The latter activity is facilitated by Ku and XLF (XRCC4-like factor) (Gu et al., 2007; Tsai et al., 2007). Other accessory components participate in processing 5' and 3' DNA ends in vertebrate NHEJ: polynucleotide kinase (PNK), aprataxin (APTX), and APLF, all interacting with XRCC4 and whose precise role is still a matter of debate (Lieber, 2010).

Despite being less important for DSB repair, all the key NHEJ components are conserved in yeast. In the budding yeast, Ku and DNA ligase IV are present (Yku70$^{Sc}$, Yku80$^{Sc}$, Dnl4$^{Sc}$) (Daley et al., 2005). The fundamental interaction between XRCC4 (Lif1$^{Sc}$) and DNA ligase IV (Dnl4$^{Sc}$) is also maintained (Herrmann et al., 1998). Pol4$^{Sc}$, the only polymerase X in *S. cerevisiae*, has also been associated with NHEJ (Wilson and Lieber, 1999). However, homologs of other components such as DNA-PKcs and Artemis have not been identified (Daley et al., 2005). In the fission yeast *S. pombe*, the key *S. cerevisiae* NHEJ components are present, with the exception

of XRCC4 (Raji and Hartsuiker, 2006). Interestingly, a notable difference between *S. cerevisiae* versus *S. pombe* and *H. sapiens* NHEJ is the involvement of the MRX[Sc] (Mre11[Sc]- Rad50[Sc] - Xrs2[Sc]) complex. Although its exact role is still unknown, it has been proposed that the tethering capabilities of the trimer may facilitate repair by keeping the severed overhangs in proximity. However, a more direct role in assisting Ku and Dnl4[Sc] has also been suggested (Daley et al., 2005).

### 1.7.2   A model for non-homologous end joining

Based on data from *S. cerevisiae*, a model for NHEJ has been proposed by Daley et al. (2005) where the MRX complex promptly binds DSBs internally to Ku. Dnl4[Sc] (DNA ligase IV) is then recruited to the DSB. After the pairing of the overhangs, ligation is attempted. If unsuccessful, a series of rounds of DNA end processing and ligation attempts follow. Thus, this model postulates an iterative process where the choreography of DSB repair by NHEJ is dictated by the relative affinity of NHEJ components for distinct DNA ends.

A similar scenario might occur in vertebrates, with the additional role for DNA-PKcs in recruiting XRCC4:DNA ligase IV, which then ligates the two DNA ends. In this context, Artemis might be involved in the iterative ligation/processing rounds. The physical interaction shown for DNA-PKcs with XRCC4:DNA ligase IV and Artemis (Daley et al., 2010) would lend support to this model.

## 1.8    DNA Double-strand break repair: homologous recombination

### 1.8.1   Overview of homologous recombination processes

Three main mechanisms can be grouped under the definition of homologous recombination processes: single-strand annealing (SSA), break-induced replication (BIR) and gene conversion (GC) (Haber, 2000). The process called single-strand annealing occurs when a DSB is created between two flanking homologous regions. In this scenario, these homologous regions can be used to direct annealing and ligation of the two DNA strands, leading to deletion of the

sequence between the repeats (fig. 1.1a). In cases where single-ended DSBs are generated (e.g. from a collapsed replication fork), a repair mechanism called break-induced replication can occur (fig. 1.1b). By this pathway, DNA replication continues to the end of a chromosome, or until a converging fork is encountered.

However, it is usually common to refer to homologous recombination as a synonym for gene conversion, as it is still unclear whether and to what extent SSA and BIR represent physiological alternatives to GC *in vivo*, or whether they just represent failed GC events (reviewed in Paques and Haber, 1999). For this reason, the overview presented in this section focuses on homologous recombination as intended for gene conversion.

Gene conversion is a uni-directional transfer of genetic information to a broken DNA molecule from a homologous template, usually a sister chromatid or a homologous chromosome. Gene conversion, like all the other proposed homologous recombination mechanisms, begins with a 5'-3' resection at the DSB to expose a long 3'-ended single-stranded DNA filament which invades a homologous region forming a so-called D-loop (displacement loop) (fig. 1.1, top). Gene conversion can lead to crossover events, and two models have been proposed for this mechanism.

According to the model proposed by Szostak and colleagues (Szostak et al., 1983), following the formation of the D loop by strand invasion, the second resected end on the broken duplex (the one not engaged in the D loop formation) is captured to the D-loop. A double Holliday junction is then formed whose resolution leads to either crossing-over or non-crossing-over structures, depending on the direction by which the junctions are resolved (fig. 1.1c). In the second model, called synthesis-dependent strand annealing (SDSA) (fig. 1.1c, bottom), the newly synthesized leading strand is displaced from the donor and re-annealed to its original partner. Consequently, this mechanism leads to non-crossover events only.

Thus, overall the essential steps in homologous recombination can be summarised as follows: first, the double strand break is recognised; second, the duplex is resected from the 5' to the 3'
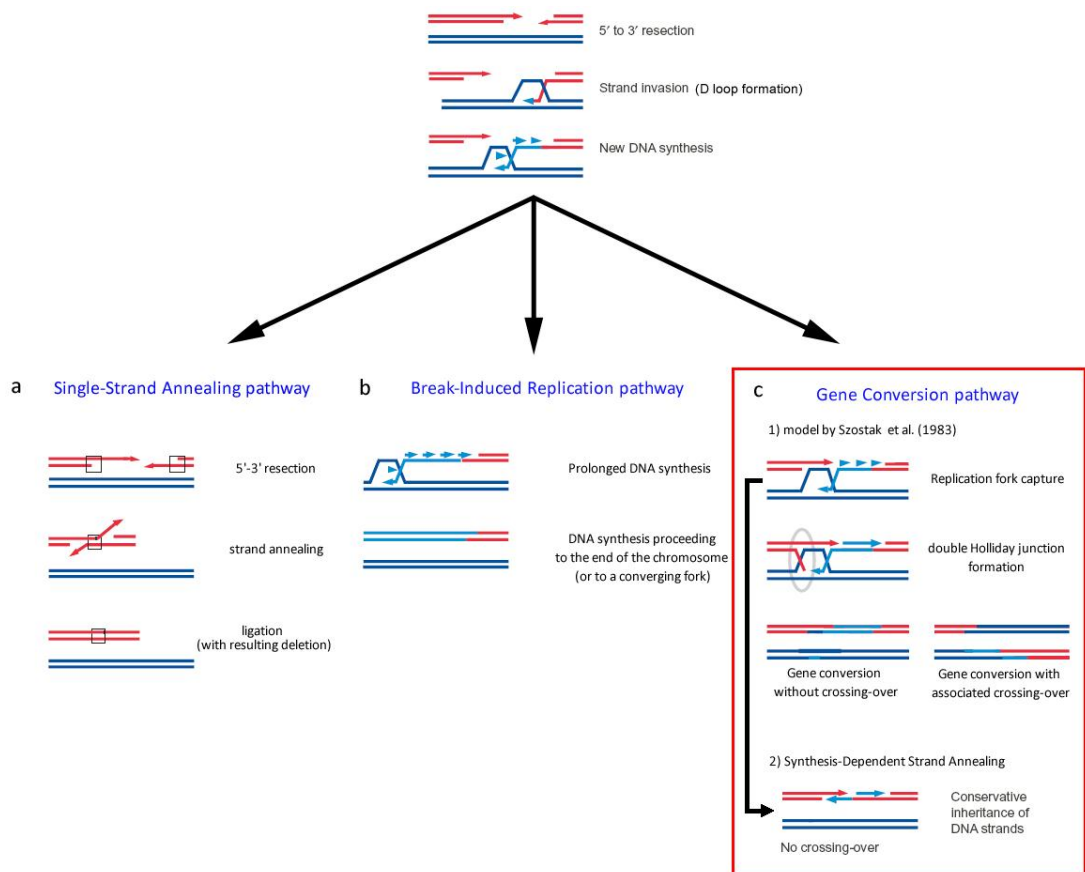
**Figure 1.1 | Pathways of homologous recombination (adapted from Haber, 2000).** a. Single strand annealing, occurring when two homologous regions flanking a DSB are used to direct the annealing step. b. Break-induced replication, occuring when DNA replication proceeds to the end of the chromosome or to a converging fork. c. Gene conversion, as a model proposed by Szostak et al. (1983) (top) or as synthesis-dependent strand annealing (bottom). See text for more details.

end to provide a single-stranded filament for the subsequent strand invasion; a D-loop is formed between the above single DNA strand and a homologous template strand, either from a sister chromatid or a homologous chromosome; finally, the second end is captured and a double Holliday junction is formed which is then resolved, leading to either crossing-over or non crossing-over products.

### 1.8.2 Step 1: DSB recognition

The heterotrimeric MRN (Mre11[Hs,Sc]/Rad32[Sp] - Rad50[Hs,Sp ,Sc] − Nbs1[Hs,Sp] / Xrs2[Sc]) complex is recruited at early stages of DSB repair in *S. cerevisiae* (Lisby et al., 2004). As seen above, this complex has been implicated at the early stages of DSB recognition. In the context of homologous recombination, data indicates that an additional role for this complex would be in tethering broken DNA molecules, keeping the partners close to each other in order to facilitate

the downstream molecular mechanisms. Firstly, it has been shown that clustering of damaged chromosome ends is reduced in MRN-deficient cells (Aten et al., 2004). Secondly, structural work in human cells indicates that the 50-nm long coiled coil of Rad50[Hs] can tether broken DNA ends (de Jager et al., 2001). Interestingly, in yeast it has been reported that the apex interaction that connects two Rad50 coiled coils is essential for wild-type resistance to DNA damaging agents (Wyman and Kanaar, 2006). In this context, a functional role has been has been proposed in *S. pombe* where Rad50 would promote the use of sister chromatids as templates for repair (Hartsuiker et al., 2001).

### 1.8.3    Step 2: DNA end resection

The following steps in homologous recombination require the creation of a single-stranded 3'-hydroxyl overhang in a process named DNA 5'-3' resection. Two types of DNA breaks should be distinguished: 'clean' DSB ends, with standard 5'-P and 3'-OH, like those resulting from the activity of endonucleases; 'dirty' DSB ends, with modified termini or protein-DNA adducts that require further processing in order to restore standard termini.  It appears that the role of the many enzymes associated with DNA resection is not always overlapping, and some specificity for specific structures exists.

In *S. cerevisiae,* the MRX (Mre11[Sc] - Rad50[Sc] – Xrs2[Sc]) complex has been shown to play a crucial role in the resection of 'clean' breaks created by the HO endonuclease, whereas the ability to perform gene conversion *per se* is only marginally affected in *mrx* null mutants (Sugawara and Haber, 1992; Ivanov et al., 1994). Thus, the mechanistic details of this requirement are still not clear. Rather than having a direct role in the processive 5'-3' resection, Mre11[Sc] nuclease activity is required only for the initial clipping of 'dirty' ends (Krogh and Symington, 2004). A similar role has been shown in *S. pombe*, where the Mre11 ortholog Rad32[Sp] is involved in the removal of Top2 and Top1 from the 5' and 3' ends, respectively (Hartsuiker et al., 2009). In the fission yeast and mammals, however, the endonucleolytic activity of the complex (Mre11[Hs],

Rad32[Sp]) seems to be more crucial for DSB repair than in the budding yeast (Williams et al., 2008; Buis et al., 2008).

Work in *S. cerevisiae* has shown that the endonuclease Sae2 plays a role in the transition from the initial resection steps to the following end processing (Lisby *et al.*, 2004). This finding would suggest a role for Sae2 as a regulator of 5'-3' processive resection further to the activity of the MRX complex. Intriguingly, in *S. pombe* the Sae2 homolog Ctp1 participates in DNA end resection in concert with the MRN complex (Limbo et al., 2007). A role for this protein in processing 'dirty' DNA ends has been identified that overlaps with Rad32[Sp] in the removal of 5'-bound Top2 (Hartsuiker *et al.*, 2009). A functional interaction with the MRN complex has been also demonstrated for the human homolog CtIP (Sartori et al., 2007), confirming the crucial conserved involvement of this component in these initial steps of recombination.

The extensive processing required for the generation of a 3'-overhang suggests the requirement for a 5'-3' exonuclease. In the budding and the fission yeast, Exo1 seems to be a good candidate, as deletion of *exo1* impairs resection (Llorente and Symington, 2004; Moreau et al., 2001; Tomita et al., 2003). However, the finding that resection and homologous recombination in Exo1-deficient cells still occur (Tran et al., 2004) indicates that other unknown nucleases or mechanisms are involved in shortening the 5'-3' DNA tracts.

Studies in *S. cerevisiae* and mammalian cells have suggested that a possible parallel mechanism for DNA end resection may involve the combined activity of the helicase Sgs1[Sc]/BLM[Hs] and a single-strand-specific endo- or exonuclease. Deletion of both Sgs1[Sc] and Exo1[Sc] did not abolish gene conversion, suggesting that the combined activity of these two enzymes is not absolutely required for the initial steps of recombination (Mimitou and Symington, 2008). However, a resection defect was shown for *sgs1*[Sc]/*bml*[Hs] deletion mutants, and resection required Sgs1 helicase domain. The Exo1 nuclease activity was also required (Mimitou and Symington, 2008; Zhu et al., 2008; Gravel et al., 2008). It has been proposed that a two-step mechanism of resection occurs, where intermediates created by the initial

trimming (MRN complex and Sae2) are processed via either of two resection pathways: the first led by Exo1; the second involving Sgs1 in association with a nuclease (Mimitou and Symington, 2008). It has been suggested that this enzyme is the endonuclease/helicase Dna2[Sc] (Zhu *et al.*, 2008). However, it should be noted that the assays employed in the two above studies (Mimitou and Symington, 2008; Zhu et al., 2008) are based on a single-strand annealing system in which the cellular background is devoid of the recombination protein Rad51[Sc]. This was done in order to exclude the contribution of Rad51-dependent molecular events such as break-induced replication. However, it cannot be excluded that the resection operated by Sgs1[Sc] in this background can in fact be an artefact of the system used. Thus, further work is needed to establish more precisely the extent and the mechanisms of the involvement of RecQ helicases in the resection step of homologous recombination.

### 1.8.4    **Step 3: strand invasion**

The ssDNA generated following the resection step is thought to be rapidly bound by the abundant single-strand binding protein RPA. The central step in homologous recombination is the assembly of a nucleoprotein filament, composed of DNA and recombination proteins belonging to the Rad52 epistasis group (Krogh and Symington, 2004). Biochemical data from lower and higher eukaryotes indicate that the recombinase Rad51 catalyses an ATP-dependent strand exchange reaction between a single-stranded circular DNA and a homologous linear duplex (Sung, 1994; Namsaraev and Berg, 1997). However, in yeast Rad51 is not always required for all recombination events and is often less important than Rad52 *in vivo* (Paques and Haber, 1999). It has been shown that Rad52 in *S. cerevisiae* acts by forming a complex with RPA bound to ssDNA and by recruiting Rad51, which then displaces RPA (Sugiyama and Kowalczykowski, 2002). Biochemical data indicate that other two proteins, Rad55 and Rad57, form a stable heterodimer which has been implicated in mediating the assembly of the Rad51 nucleoprotein filament (Sung, 1997). Another component that localises to the Rad51 nucleoprotein filament is Rad54. It has been shown that this enzyme, belonging to the

Swi2/Snf2 family of chromatin remodelling proteins, promotes Rad51-dependent pairing of homologous DNA through a change in the topological conformation of the double helix (Petukhova et al., 1999). This process, where the nucleoprotein filament invades a homologous duplex through the formation of a D-loop, is called strand invasion. The topological changes induced by Rad54 appear to be a requirement for strand invasion and DNA pairing (Petukhova et al., 1999; Van Komen et al., 2000).

### 1.8.5 Holliday Junction resolution

The Szostak model of recombination predicts the generation of a recombination intermediate called double Holliday junction (dHJ; fig. 1.1; Szostak et al., 1983). According to this model, the final products of recombination can be crossover or non-crossover type, depending on the directionality by which the double Holliday junction is resolved. Crossover events can occur between sister chromatids (SCE, Sister Chromatid Exchange) or between homologous chromosomes or regions in the genome. SCE are usually not deleterious, as sisters have identical sequences. Thus, the most obvious reason to suppress crossover events is to prevent exchanges between repetitive sequences in the genome, which could lead to harmful chromosomal rearrangements. For this reason, crossovers events are usually suppressed in favour of non-crossover events: by using the synthesis-dependent strand annealing (SDSA) pathway (fig. 1.1c), by biased resolution of Holliday junctions (fig. 1.1c), or by using a Holliday junction dissolution pathway (Wu and Hickson, 2003; Wu and Hickson, 2006).

The mechanism for HJ resolution has been elusive for decades. Although studies in *S. pombe* initially suggested that the complex Mus81$^{Sp}$/Eme1$^{Sp}$ was a promising candidate for in vivo HJ resolution, these proteins lack the biochemical properties of canonical HJ resolvases, such as activity towards static HJs *in vitro* (evidence reviewed in Svendsen and Harper, 2010). A role for Mus81$^{Sp}$/Eme1$^{Sp}$ has been proposed where these enzymes act on intermediates generated during HJ resolution, rather than on fully formed HJs (Osman et al., 2003). In multicellular

eukaryotes, *in vitro* cleavage of HJs has been shown for the SLX1[Hs]/SLX4[Hs] complex, whereas the fungal ortholog appears to lack this activity (Svendsen and Harper, 2010).

The first classical HJ resolvases involved in eukaryotic nuclear metabolism, GEN1[Hs] and Yen1[Sc], have been recently identified in *S. cerevisiae* and mammalian cells, respectively (Ip et al., 2008). *S. pombe* lacks an obvious ortholog of these enzymes. This finding might explain the prominent role for Mus81[Sp]/Eme1[Sp] in this organism (Ip *et al.*, 2008).

However, in the context of double Holliday junctions formed during gene conversion, it is still unclear whether and how these resolvases are controlled *in vivo* to allow a biased resolution towards non-crossover products.

### 1.8.6 RecQ helicases and Holliday junction dissolution

The RecQ family of helicases is a class of enzymes highly conserved across species and required for the maintenance of genome stability. Their importance is substantiated by the fact that three human RecQ homologs are defective in cancer-prone syndromes (Bernstein et al., 2010). Yeasts have only one main RecQ homologue (Sgs1 in *S. cerevisiae*, Rqh1 in *S. pombe*), while five members are present in human (BLM, WRN, RECQ1, RECQ4, RECQ5).

One of the most prominent roles for RecQ helicases is their role in suppressing deleterious consequences arising from homologous recombination processes. As seen above, depending on the particular pathways chosen for HR-mediated repair of DNA damage, the final products can be crossover or non-crossover type (fig. 1.1c). In this context, RecQ helicases appear to be involved in suppressing crossover events, which could be potentially deleterious. Studies involving Rqh1[Sp], Sgs1[Sc] and BLM[Hs] have shown that these helicases are functionally associated with two binding partners, topoisomerase Top3[Sc] (TOPOIII[Hs]) and Rmi[Sc] (Rmi[Sp], RMI1[Hs]/BLAP75) (Laursen et al., 2003; Gangloff et al., 1994; Johnson et al., 2000; Wu et al., 2000; Mullen et al., 2005; Chang et al., 2005). These associations have proved to be important for the activity of these helicases in homologous recombination. In *S. cerevisiae*, Sgs1 is required to suppress crossovers during DSB repair and it has been proposed to process double Holliday junctions

(Ira et al., 2003). Sgs1 is also required for resolution of Rad51-dependent recombination intermediates arising from perturbed replication (Liberi et al., 2005). Likewise, in *S. pombe* early work has shown that *rqh1* null cells have high levels of recombination and fail to properly segregate chromosomes (Stewart et al., 1997). Similarly to the situation in *S. cerevisiae*, fission yeast Rqh1-Top3 are involved with Rhp51 (homolog of Rad51[Sc]) in response to UV- and IR-induced damage in G2 (Murray et al., 1997; Caspari et al., 2002; Laursen et al., 2003). The central role of RecQ helicases in suppressing potentially deleterious homologous recombination processes has been recently highlighted by showing that Sgs1[Sc] is critically required to suppress formation of multichromatid joint molecules during meiosis (Oh et al., 2007). Together with other studies on human BLM[Hs] helicase, these lines of evidence have suggested four roles for RecQ helicases in homologous recombination processes: 1) at the resection stage of homologous recombination, it has been recently demonstrated that Sgs1[Sc], in collaboration with other nucleases such as Sae2, Exo1 and Dna2, is able to resect 5' ends, allowing exposure of 3' tails required for subsequent processing by the HR machinery (Mimitou and Symington, 2008; Zhu et al., 2008; Gravel et al., 2008); 2) at later stages of homologous recombination, RecQ helicases disrupt the formation of D-loops (van Brabant et al., 2000; Bachrati et al., 2006; Wu et al., 2001); 3) as suggested from studies in Drosophila, BLM helicase may assist the SDSA pathway (see fig. 1.1c), by facilitating DNA synthesis after formation of the D-loop and/or by disrupting the D-loop to allow reannealing of the extended strand to the original broken molecule (Adams et al., 2003; McVey et al., 2004); 4) a late role for RecQ helicases at double Holliday junctions has been shown *in vitro* for BLM[Hs] in association with its functional partner TOPOIII[Hs]. In a process called double Holliday junction dissolution, BLM[Hs] would process these structures into a hemicatenane structure by its branch-migrating activity, and TOPOIII[Hs] would decatenate these intermediates into a non-crossover product (Wu and Hickson, 2003). RMI[Hs] has been shown to be a stimulating factor in this process (Wu and Hickson, 2006; Raynard et al., 2006).

## 1.9 Repair of chemically altered DNA bases: Base Excision Repair

### 1.9.1 Mutation avoidance pathways: Base Excision Repair and Mismatch Repair

The most common base-base interaction within the DNA helix is the standard G/C – A/T Watson-Crick (W-C) pairing. Although alternative physiological base pairings exist, generally deviations from the standard W-C hydrogen bond configuration lead to threats to genome stability (Kunz et al., 2009). Another type of DNA mismatch is the misalignment of two complementary strands known as insertion/deletion loops (IDLs) (Jiricny, 2006; Kunz et al., 2009). Two main pathways (reviewed in Kunz et al., 2009) deal with both these types of base mispairings: base excision repair (BER), responding to mispairings arising as a consequence of DNA damage; postreplicative mismatch repair (MMR), specialized in misincorporation errors generated by DNA polymerases.

This section will give only a brief overview of the first repair pathway, whereas the next section will present a more detailed discussion about the mutation avoidance by MMR.

### 1.9.2 Core BER components in eukaryotes

Base Excision Repair is a highly conserved pathway which deals with damage to DNA bases in the form of alkylation, deamination and oxidation. Such chemical alterations can be deleterious for living organisms, as they can lead to deviations from the canonical Watson-Crick base pairing (Robertson et al., 2009).

BER acts by replacing the damaged base with the correct one and restoring the integrity of the affected DNA strand. The BER reaction is initiated by DNA glycosylases, which recognise and remove the damaged base, irrespective of whether this is located on the nascent or the template strand. This cleavage creates either an apurinic or apyrimidinic (AP) site. Thus far, 11 different DNA glycosylases have been identified in mammalian cells (Robertson et al., 2009). A common molecular mechanism appears to be shared by these proteins where the removal of the target base is performed by cleaving the N-glycosydic bond between the affected base and the proximal deoxyribose (Roberston et al., 2009).

The resulting AP site is further processed by either an AP endonuclease or an AP lyase, whose reaction generates a single nucleotide gap in the DNA strand. The difference between the two types of enzymes is in the side where the incision of the DNA is performed: 5' or 3' to the AP site, respectively (Boiteux et al., 1987; O'Connor and Laval, 1989; Robson and Hickson, 1991). Finally, the single-stranded gap is filled by DNA polymerase beta (POLB[Hs]) and the nick ligated by DNA ligase III (LIG3[Hs]) (Sobol et al., 1996; Kubota et al., 1996; Wei et al., 1995).

The importance of BER for genomic stability is confirmed by the high degree of conservation for the key components of the pathway from bacteria to mammals (Robertson et al., 2009).

### 1.9.3    Short-patch and long-patch BER

It has been shown that human BER can be reconstituted *in vitro* with only four enzymes: a uracil-DNA glycosylase (UNG[Hs]), the AP endonuclease APEX1[Hs], the polymerase POLB[Hs], and either the ligase LIG3[Hs] or LIG1[Hs] (Kubota et al., 1996). However, further work by Frosina et al. (1996) proposed the existence of two distinct BER pathways in mammalian cells. The case of a single-nucleotide gap directly processed by POLB[Hs] and LIG3[Hs] was called short-patch BER, whereas the case where a longer gap is created was named long-patch BER (Frosina et al., 1996). In the latter pathway, following the endonucleolytic activity of APEX1[Hs], POLB[Hs] exerts its additional strand-displacement activity which leads to the generation of a flap structure that needs to be processed by the flap endonuclease FEN1[Hs] prior to ligation (Frosina et al., 1996; Robertson et al., 2009).

Interestingly, XRCC1[Hs] has been shown to be recruited to repair sites promptly after the activity of a DNA glycosylase or an AP endonuclease during short-patch BER (Kubota et al., 1996). In this context, it has been suggested that XRCC1[Hs] would function as a scaffold protein, similarly to the situation in the general single-strand DNA repair (see 1.5.2 and Kubota *et al.*, 1996). On the other hand, PCNA[Hs] appears to be required specifically for long-patch BER (Robertson et al., 2009). However, the significance and the mechanism underlying the choice of either repair pathway are still obscure.

## 1.10   Repair of base-base mismatches: Mismatch Repair Pathway

### 1.10.1   Overview of the mismatch repair pathway

The estimated mutation rate during DNA replication in eukaryotic cells is lower than 1 mutation every $10^9$ bases copied. Replicative DNA polymerases are hi-fidelity enzymes, capable of error rates as low as 1 error every $10^7$ insertions as a result of their proofreading activity (McCulloch and Kunkel, 2008). In order to achieve a further 100-fold decrease in mutation events, cells use correction pathways acting downstream of replication, of which postreplicative MMR is the most prominent one (McCulloch and Kunkel, 2008; Kunz et al., 2009). Errors in nucleotide incorporation arise during either semi-conservative replication or synthesis associated with DNA repair, the most common causes being nucleotide pool imbalances (Roberts and Kunkel, 1988; Bebenek et al., 1992) or contaminations with chemically altered nucleotides (reviewed in Kunz et al., 2009). MMR deals with four types of mismatches within the DNA helix: non-Watson/Crick pairings; small insertion/deletion loops (IDLs); DNA bases-uracil mispairings (e.g. GU mispairings); chemical modification of DNA bases (e.g. 8-oxo-7,8-dihydroguanine, or 8-oxo-G) which lead to mismatches due to alterations of the hydrogen-bonding potential (Kunz et al., 2009). MMR in prokaryotes and eukaryotes can be divided into four steps: the first step is the recognition of the DNA lesion; the second step is the assembly of the repair complex; the third step is the identification of the nascent DNA strand; the final fourth step is the excision of the affected base and the resynthesis and ligation of the DNA strand (Jiricny, 2006). Although the general repair mechanisms are conserved, specific molecular differences distinguish prokaryotic, higher and lower eukaryotic systems. A schematic overview of the MMR pathway based on studies of reconstituted human MMR in vitro is shown in fig. 1.2.

### 1.10.2   Mismatch repair pathway in *E. coli*

To date most of the mechanistic insights in the MMR pathway derive from studies of the MutS, MutL and MutH complexes (collectively named MutHLS system) in *E. coli*.  MutS homodimers

recognize IDLs (1-4 nt in length) and a variety of base-base mismatches (Spampinato et al., 2009; Kunz et al., 2009). MutS then recruits a homodimer of MutL; the formation of this ternary complex is dependent on ATP and activates the latent endonuclease MutH (Jiricny, 2006). In prokaryotes, the specificity of the MMR pathway for mispairings occurring on newly synthesized DNA strands following DNA replication is due to MutH preferential binding to Dam methylation on GATC sequences, which are transiently unmethylated shortly after the transit of the DNA polymerase (Welsh et al., 1987; Au et al., 1992). MutH generates a nick which provides an entry point for the single strand binding protein SSB and the DNA helicase II (UvrD). This enzyme unwinds the DNA, facilitating the further exonucleolitic degradation by either 5'-3' (RecJ or ExoVII) or 3'-5' (ExoI or ExoX) nucleases, depending on where the mismatch is located (Burdett et al., 2001; Spampinato et al., 2009). Finally, the affected strand is resynthesized and ligated by DNA polymerase III and DNA ligase (Kunz et al., 2009).

### 1.10.3 **The mammalian mismatch repair system**

The MMR pathway in eukaryotes differs from the MutHLS system in that the proteins involved are heterodimers instead of homodimers (table 1.2). The initial steps of the pathway are similar to the *E. coli* system, whereas the steps downstream appear to differ. The initial recognition step is carried out by two heterodimers: MSH2 and MSH6 form MutSα, dealing with base-base mismatches and 1-2 IDLs; MSH2 and MSH3 constitute MutSβ, which binds larger IDLs (Kunz et al., 2009). The precise role of the MutL heterodimers is still unclear. MLH1[Hs] and PMS2[Hs] form MutLα, the most important MutL complex in human MMR. This dimer is involved in general MMR, including single base-base and short IDL mismatches (Kunkel and Erie, 2005; Kunz et al., 2009). MLH1[Hs] and PMS1[Hs] form MutLβ, which could provide a backup role for MutLα, although its function is still unknown (Räschle et al., 1999). MLH1[Hs] heterodimerizes with MLH3[Hs] to form MutLγ, whose primary role seems to be in meiotic recombination (Lipkin et al., 2002).

Although it has been shown that MutLα and MutLβ interact to form a ternary complex with

| | E.coli | H. sapiens | S. pombe | S. cerevisiae |
|---|---|---|---|---|
| **MutS** | MSH2 | Msh2 | Msh2 |
| | MSH3 | Swi4 | Msh3 |
| | MSH6 | Msh6 | Msh6 |
| **MutL** | MLH1 | Mlh1 | Mlh1 |
| | PMS2 | Pms1 | Pms1 |
| | - | - | Mlh2 |
| | MLH3 | - | Mlh3 |
| | PMS1* | - | - |
| **MutH** | - | - | - |
| - | EXO1 | Exo1 | Exo1 |

**Table 1.2 MMR factors of prokaryotic and eukaryotic model organisms.**
**\*hPMS1 is closely related to Mlh2$^{Sc}$, but it is not considered as ortholog**
**because of significant structural dissimilarities. Adapted from Marti et**
**al., 2002**
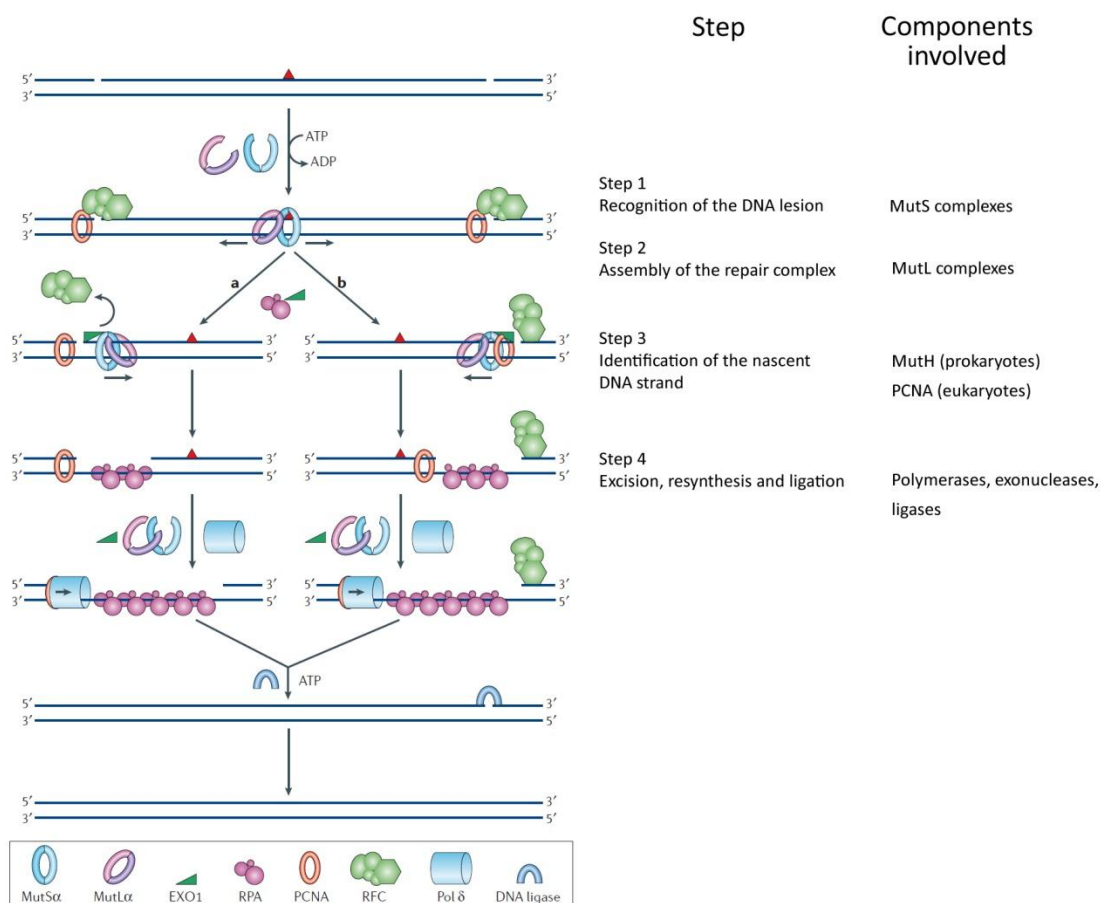


**Figure 1.2 | Schematic representing an overview of the mismatch repair pathway based on the reconstituted human MMR *in vitro*.** Two scenarios are depicted. a: MutS and MutL clamps diffuse upstream and encounter the Replication Fork Complex RFC first. b: MutS and MutL clamps diffuse downstream and encounter a PCNA molecule first. Following excision, resynthesis and ligation steps are shared between the two scenarios. Adapted from Jiricny, 2006.

the DNA (evidence reviewed in Jiricny, 2006), the dynamics of this assembly is still obscure. The mechanism of identification of the nascent strand in human MMR is still a matter of debate. Several lines of evidence suggest that the determinant may be provided by strand discontinuities arising from DNA replication (Spampinato et al., 2009). It has been suggested that PCNA (Proliferating Cell Nuclear Antigen) may be involved in this process, as in yeast MutSα and MutSβ were shown to associate with PCNA and then be transferred to the mismatch (Lau and Kolodner, 2003). However, more recently it has been shown that the binding affinity and specificity of human MutSα are in fact not dependent on PCNA (Iyer et al., 2008). The final steps of MMR are aimed at the restoration of the original strand by excision, resynthesis and final ligation of the affected molecule. Given that mismatches can be either at 5' or 3' to the MutS/MutL assembly point, both 5'-3' and 3'-5' exonucleases should be implicated in the excision step, similarly to what has been shown in *E. coli* (Burdett et al., 2001; Spampinato et al., 2009). However, to date only EXO1 has been associated with mammalian MMR, albeit only with some and not all the subsets of events (Wei et al., 2003). The reconstitution of the MMR system *in vitro* led to the additional identification of RPA (single-stranded binding-factor replication protein A) and the non-histone chromatin component high-mobility group box 1 (HMGB1) as MMR factors (Jiricny, 2006).

### 1.10.4  Mismatch repair in *S. pombe*

An intermediate situation is present in the fission yeast *S. pombe*. Three MutS and two MutL homologs have been found to date: Swi4[Sp], Msh2[Sp] and Msh6[Sp] correspond to MSH3[Hs], MSH2[Hs] and MSH6[Hs] in human cells; Mlh1[Sp] and Pms1[Sp] are MutL homologs of MLH1[Hs] and PMS2[Hs] (Marti et al., 2002). Msh2[Sp] is a central component of MMR-mediated repair, as deletion mutants show increased rate of mutation in mitotic growth (Rudolph et al., 1999). Furthermore, this protein has been implicated in mating-type switching, chromosome organization during meiosis and control of GT repeat stability (Rudolph et al., 1999; Mansour et al., 2001). Msh6[Sp] appears to play the same crucial role in MMR as Msh2[Sp]: these

components showed comparable increase of mutation rates in both mitotic and meiotic mismatch repair (Tornier et al., 2001; Rudolph et al., 1999). In contrast, Swi4$^{Sp}$ is only marginally involved in the MMR pathway and may be more important in processes such as mating-type switching (Rudolph et al., 1999; Mansour et al., 2001). The MutL homolog Pms1$^{Sp}$ is required both in mitotic MMR and in mismatches arising during meiotic recombination (Schär et al., 1997; Fleck et al., 1999). Little is known about the second MutL homolog, Mlh1$^{Sp}$. Downstream, Exo1$^{Sp}$ endonuclease has been shown to be involved in the same MMR pathway as Pms1$^{Sp}$ and Msh2$^{Sp}$, although its role is likely to be redundant with other yet unidentified endonucleases (Rudolph et al., 1998; Mansour et al., 2001).

Detailed analyses of mismatches on a molecular level have suggested that in S. *pombe* two independent repair systems operate: a major long-patch pathway, dealing with all base mismatches except C/C, and a minor short-patch system, which repairs all mismatches including C/C with low efficiency (Schär and Kohli, 1993; Schär et al., 1993; Rudolph et al., 1998). Components of other pathways such as Nucleotide Excision Repair have been found to be involved in the minor system (Fleck et al., 1999).

## 1.11 Removal of bulky DNA adducts: Nucleotide Excision Repair

### 1.11.1 Overview of the nucleotide excision repair system

Nucleotide excision repair (NER) is a versatile DNA repair system which deals with a wide range of bulky DNA lesions caused by agents such as nitrosamines, benzo[a]pyrenes, cross-linking agents and UV light (Nouspikel, 2009). The basis for this flexibility lies in the signal for NER response being distortions in the DNA double helix and not specific DNA lesions (Nouspikel, 2009). NER is commonly divided into two sub-pathways: global genome repair (GGR), acting on nontranscribed or unexpressed regions of the genome; transcription-coupled repair (TCR), specialised in the removal of lesions from actively transcribed genomic sequences (fig. 1.3). The sequential steps involved in NER are well characterised and they can be grouped into four

stages. The first stage is the recognition of the DNA lesion. It has been shown that in order to act as a signal for NER, a distorsion in the DNA helix and the presence of a chemical modification are required (Hess et al., 1997; Sugasawa et al., 2001). The second step is the denaturation of the DNA double strand around the lesion. Following a double incision step 5' and 3' to the lesion and the removal of the affected DNA oligonucleotide, the final stage is the gap filling and the ligation to restore the original DNA sequence.

The importance of NER for the maintenance of genomic stability is proven by the number of diseases associated with mutations in NER components: Xeroderma pigmentosum (XP), Cockayne syndrome (CS), Cerebro-occulofacio-skeletal syndrome (COFS), UV-sensitive syndrome (UVSS), Trichothiodystrophy (TTD) (Lehmann, 2003).

### 1.11.2 Mechanism of human global genome repair

The complex which senses the DNA distortion in human cells is composed of three subunits: XPC, HR23B and centrin 2. XPC$^{Hs}$ has been shown to bind preferentially to the DNA strand opposite the lesion, so it is thought to recognise DNA distortions and not the lesion *per se* (Maillard et al., 2007). HR23B$^{Hs}$ interacts with XPC but its precise role is still unclear (Sugasawa et al., 1997). Data from the *S. cerevisiae* ortholog Rad23$^{Sc}$ suggest that HR23B$^{Hs}$ may control the ubiquitylation status of XPC (Watkins et al., 1993). The association of centrin 2 with XPC-HR23B stabilises the complex and stimulates NER (Araki et al., 2001).

The recognition of mildly distorting lesions such as cyclobutane pyrimidine dimers (CPDs) is problematic for the XPC complex. The DDB (Damage DNA Binding) complex, composed of DDB1$^{Hs}$ and DDB2$^{Hs}$/XPE$^{Hs}$, has been proposed to favour the recruitment of the XPC complex by exacerbating the DNA distortion (Nouspikel, 2009). Furthermore, the DDB2-associated E3 enzyme ubiquitylates XPC$^{Hs}$, increasing its affinity for DNA while inducing degradation of the DDB complex itself (Sugasawa et al., 2005). These concerted mechanisms are thought to underlie a handover mechanism whereby XPC persists at the heart of the recognition stage of NER (Nouspikel, 2009).

**Figure 1.3 | Schematic representing the current model for human nucleotide excision repair.** Global genome repair (GGR) is involved in removing bulky adducts from non-transcribed regions of the genome, whereas transcription-coupled repair (TCR) acts on actively transcribed sequences. The four repair stages (recognition, denaturation, double incision and gap filling/ligation) appear to be shared by the two pathways. In global genome repair, the lesion is recognised primarily by the XPC-HR23B-centrin 2 complex. For mildly distorting lesions such as cyclobutane pyrimidine dimers (CPDs), the recognition step by the XPC complex may be aided by the DDB (Damage DNA Binding) complex, which has been suggested to exacerbate the distortion. At this stage, ubiquitylation appears to play an important role, increasing the affinity of the XPC complex for DNA and inducing degradation of the DDB complex. The denaturation stage of GGR is performed by the transcription factor TFIIH in concert with the XPD and XPB helicases (not shown). The double endonucleolytic incision is performed by XPF-ERCC1 and XPG, respectively 5' and 3' of the lesion. The consequent gap is filled in by the replicative polymerases Polδ and Polε in association with PCNA. Finally, the integrity of the DNA is restored by Lig III-XRCC1 and possibly Lig I. Mechanistic details for TCR are still unclear. CSA and CSB have been implicated in the initial recognition stage, although the exact meaning of their recruitment to lesion-stalled RNA polymerases II is still obscure. Diagram adapted from Nouspikel, 2009.

The denaturation of the double helix around the lesion is carried out by the transcription factor TFIIH, composed of multiple subunits and involved in transcription (Nouspikel, 2009). The switchover between the transcriptional and the NER role appears to depend on the subunit MAT1[Hs] (Busso et al., 2000). The helicases XPD[Hs] and XPB[Hs], of opposite polarities, are involved in opening the bubble around the lesion (Winkler et al., 2000; Coin et al., 2007). However, the role of the other subunits of the complex in NER is still unclear.

Despite being essential for NER, the precise role played by XPA[Hs] has not been elucidated yet. It has been proposed that XPA[Hs], in association with RPA[Hs], may function to recognise the strand carrying the lesion, or to verify the lesion itself (Nouspikel, 2009).

The endonucleolytic incision 5' and 3' of the lesion is performed by XPF[Hs]-ERCC1[Hs] and XPG[Hs], respectively (Evans et al., 1997; O'Donovan et al., 1994). Interestingly, the heterodimer XPF[Hs]-ERCC1[Hs] has been linked to other biological processes such as recombination and telomere maintenance (Nouspikel, 2009). A role in early steps of interstrand cross-link repair has also been proposed for this complex (see below).

The last stage of NER is the refill of the gap and the ligation of the nicked strand. DNA resynthesis is performed by the replicative DNA polymerases $\delta$ and $\varepsilon$ in association with PCNA (Popanda and Thielmann, 1992; Shivji et al., 1992; Nichols and Sancar, 1992). Recent work has indicated that ligation is executed by XRCC1[Hs] and DNA ligase III (Moser et al., 2007).

### 1.11.3 Transcription-coupled repair

The existence of transcription-coupled repair (TCR) was proposed following the observation of selective and more efficient removal of UV-induced damage from actively transcribed genes and transcribed strands from active genes (Mellon, 2005). TCR has been shown to be a sub-pathway of NER in both prokaryotes and eukaryotes, as many proteins are shared between TCR and GGR (Nouspikel, 2009). The main difference between the two pathways appears to be at the recognition step, where the lesion is thought to be sensed by RNAPII during transcription. This has been directly inferred by the finding that lesions that do not affect

RNAPII are not able to elicit a TCR response (Donahue et al., 1996). However, the subsequent connection between the recognition step and the involvement of NER factors is still a matter of debate. In *E. coli*, mutations in the *mfd*[Ec] gene negatively affect TCR (Mellon and Champe, 1996; Mellon, 2005). Supported with further biochemical and genetic evidence, a model has been proposed where Mfd plays a role in promoting and coordinating the recruitment of NER factors at the site of stalled RNA polymerase complex (Mellon, 2005). A similar situation may occur in higher eukaryotes, although mechanistic details are so far lacking. In human cells, CSA[Hs] and CSB[Hs] have been implicated in the recruitment of NER factors to lesion-stalled RNA polymerase II (Fousteri et al., 2006). TCR components and mechanisms appear to be conserved in yeast (Tornaletti, 2009).

### 1.11.4  Yeast NER

Early genetic characterisation led to the classification of yeast NER genes into two groups, according to the severity of the sensitivity shown by the respective single mutants to UV light and other DNA damaging agents, including DNA cross-linking agents (Prakash and Prakash, 2000). NER components and mechanisms are mainly conserved between yeast and higher eukaryotes, with the exception of two proteins that have not been identified in human cells: Rad7 and Rad16 (table 1.3). In *S. cerevisiae* these proteins appear to be specifically involved in the repair of nontranscribed DNA, suggesting that Rad7[Sc]-Rad16[Sc] and not Rad4[Sc] are in fact functional homologs of XPC[Hs] (Verhage et al., 1994; Mueller and Smerdon, 1995).

### 1.11.5  Translesion synthesis polymerases in lower and higher eukaryotes

Upon encountering a block impeding its progress, a replication fork can replicate the DNA past the damage in a process called translesion synthesis (TLS). This process depends on the switch between standard, hi-fidelity replicative DNA polymerases and specialised, low-fidelity polymerases (Lehmann et al., 2007). A brief description of these low-fidelity polymerases will be given below.

Human DNA polymerase η (Polη) is capable of efficient bypass of CPDs such as cyclobutane thymine dimers (McCulloch et al., 2004). Although this was shown *in vitro*, clinical data from patients defective in the gene coding for Polη indicate that this enzyme is indeed the main one responsible for replicating past CPDs in human cells (Lehmann et al., 2007). The role for this protein is thought to be the reduction of *in vivo* mutagenesis, although data from human, mouse and budding yeast cells in this respect are controversial and partially argue against the mutagenic potential of the polymerase itself (Waters et al., 2009).

It has been demonstrated both *in vitro* and *in vivo* that DNA polymerase κ (Polκ) is able to replicate DNA past a variety of lesions such as benzo[a]pyrene-guanine (Lehmann *et al.*, 2007). Interestingly, an unexpected function for this polymerase has been shown in mammalian NER, where this enzyme was required for efficient removal of pyrimidine(6-4)pyrimidine (6-4 PP) photoproducts (Ogi and Lehmann, 2006).

DNA polymerase ζ belongs to the B-family of polymerases and is a heterodimer composed of two subunits, the catalytic subunit Rev3 and the regulatory subunit Rev7 (Nelson et al., 1996). However, in contrast with the other members of the B-family, Polζ lacks the 3'-5' proofreading exonuclease activity, possesses low processivity and is mutagenic on undamaged DNA (McCulloch and Kunkel, 2008).

| *H. sapiens* | *S. pombe* | *S. cerevisiae* |
|---|---|---|
| Not known | Rhp7 | Rad7 |
| Not known | Rhp16 | Rad16 |
| XPA | Rhp14 | Rad14 |
| XPC | Rhp41/Rhp42 | Rad4 |
| HR23B | Rhp23 | Rad23 |
| XPD | Rhp3/Rad15 | Rad3 |
| XPB | Ercc3sp | Rad25 |
| XPF | Rad16 | Rad1 |
| ERCC1 | Rad16 | Rad10 |
| XPG | Rad13 | Rad2 |
| CSB | Rhp26 | Rad26 |
| CSA | ?Ckn1 | Rad28 |

**Table 1.3 | NER components in *H. sapiens*, *S. pombe* and *S. cerevisiae*.**

In both human and *S. cerevisiae,* REV3 mutants have been shown to be defective for spontaneous as well as for induced *in vivo* mutagenesis (Waters et al., 2009). The involvement of another Rev protein in TLS, Rev1, is more atypical. Rev1 is in fact not a polymerase but a deoxycytidyl transferase, although its activity has been shown to be similarly required for spontaneous mutagenesis or mutagenesis induced by DNA-damaging agents. Polζ and REV1 are considered to be the main proteins responsible for the mutagenic repair of DNA lesions in lower and higher eukaryotes (Waters et al., 2009).

Little is known about the function of the Y-polymerase DNA polymerase ι (Polι). It is characterised by very poor processivity and high error rates (Tissier at al., 2000), but details of its function *in vivo* are still obscure. Rather than being directly involved in TLS (or in addition to this role), the multiple interactions associated with this protein have suggested a role in the coordination of TLS at the replication fork (Lehmann 2007).

### 1.11.6  PCNA as a DNA polymerase switchboard

Work in *S. cerevisiae* has shown that the initiation step in TLS is the mono-ubiquitination of the homotrimeric complex PCNA. Mono-ubiquitination is performed by Rad6 and Rad18 on Lys-164 in response to DNA damage. In a second step, mono-ubiquitinated PCNA is poly-ubiquitinated on Lys-63 in a reaction dependent on Mms2-Ubc13 and Rad5 (Hoege et al., 2002). Interestingly, the polyubiquitination rather than the monoubiquitination on Lys-164 appears to channel DNA repair into a still uncharacterised error-free pathway (Stelter and Ulrich, 2003). A similar regulation occurs in *S. pombe* although, in contrast with the budding yeast, mutants defective in the ubiquitination of PCNA are also sensitive to IR (Frampton et al., 2006). Similarly, in mammalian cells PCNA is mono-ubiquitinated in response to UV, MMS, mitomycin C, cisplatin and a variety of other DNA damaging agents (Lehmann et al., 2007). In the budding yeast and humans, the mono-ubiquitination of PCNA recruits the Y-family polymerases and provides a likely mechanism for the polymerase switch (Kannouche et al., 2004; Watanabe et al., 2004; Bi et al., 2006; Guo et al., 2006). It has been proposed that the

stalling of the replicative polymerase generates single-stranded DNA which activates Rad18 (Bi et al., 2006). The binding of Rad6 to Rad18 establishes an E2-E3 complex that mono-ubiquitinates PCNA. The consequent recruitment of Y-family polymerases to mono-ubiquitinated PCNA leads to replication past the lesion and following dissociation and replication restart (Lehmann et al., 2007). Intriguingly, PCNA appears also to provide a flexible switchboard for other biological processes through post-translational SUMO modifications (reviewed in Bergink and Jentsch, 2009).

## 1.12 Repair of DNA interstrand cross-links: ICL repair and Fanconi anemia pathway

### 1.12.1 DNA interstrand cross-link inducers in clinic and research

Amongst all the lesions occurring on the DNA double helix, interstrand cross-links (ICLs) represent a particularly insidious threat to genomic stability. Interstrand cross-links create covalent bonds linking the two DNA strands in a duplex, generating an abnormal structure that poses an insurmountable obstacle to the progression of cellular machinery like DNA replisomes. ICL-inducing agents have been used in clinical treatment of a diverse range of cancers since the second half of the nineteenth century. DNA interstrand cross-linkers are still commonly used nowadays, alone or in combination with other therapies, against many types of tumours such as haematological malignancies and those affecting lung, bladder, testicles, ovaries and pancreas (Lehoczký et al., 2007). Cross-linking agents can also be found in naturally occurring products such as medicinal and edible plants (Smith et al., 2004; Manderfeld et al., 1997). In addition, evidence has been found of ICLs generated by exogenous environmental factors such as UV light (Love et al., 1986) as well as by metabolites of endogenous cellular metabolism (Niedernhofer et al., 2003). Although a detailed discussion of ICL-forming agents is beyond the scope of this introduction, a brief overview of the main classes of cross-linkers will

be given below. Further molecular details underlying their cytotoxicity are given in 4.1.2, with focus on the three compounds used in this study (cisplatin, mitomycin C, mechloretamine).

The family of furocumarins comprises psolarens such as 8-methoxypsolaren (8-MOP), widely used in research as well as in dermatology for treatment of inflammatory skin diseases like psoriasis, vitiligo and eczema (Lehoczký et al., 2007).

Cisplatin (*cis*-platinum diamminedichloride, or CDDP) is widely used in chemotherapy and research. Despite its high cytotoxic burden, cisplatin is routinely used for treatment of a broad range of tumours, in particular testicular and ovarian (Boulikas and Vougiouka, 2004). The majority of lesions caused by cisplatin are intrastrand (IaCL) cross-links between two adjacent purine bases, whereas interstrand cross-links account for only a minority of the lesions (Brabec and Kasparkova, 2002).

Nitrogen mustards are commonly used in clinic for treatment of tumours including multiple myeloma, lymphoma, leukemia and ovarian carcinoma (Lehoczký et al., 2007). Mechlorethamine (bis(2-chloroethyl)methylamine, or HN2) is the nitrogen mustard most widely used in research, although the generation of ICL accounts for only a small proportion of a wide range of lesions (Lehoczký et al., 2007).

Mitomycin C (MMC) is a naturally occurring antibiotic employed in the treatment of gastric, pancreatic and non-small cell lung cancers (Verweij and Pinedo, 1990). Following enzymatic activation by physiological reductases, MMC is capable of generating a higher load of ICLs (approximately 13%) compared to other ICL-inducing agents (Lehoczký et al., 2007).

Another class of interstrand cross-linking agents is represented by nitrosoureas like carmustine (Bis(2-chloroethyl)nitrosurea, or BCNU), used in the treatment of intracranial tumours and malignant melanomas (Lehoczký et al., 2007).

### 1.12.2 The multifaceted DNA interstrand cross-link repair

The mechanisms for the response to ICLs in unicellular organisms depend on components involved in the major DNA repair pathways: nucleotide excision repair, base excision repair,

mismatch repair, translesion synthesis and homologous recombination (Lehoczký et al., 2007).

A similar situation is present in multicellular organisms, although the existence of the specialised Fanconi anemia (FA) pathway (McCabe et al., 2009) marks a significant difference. The evolution of this additional repair pathway may reflect the increased susceptibility of multi-cellular organisms to the exposure to endogenous and exogenous DNA interstrand cross-linking agents.

Due to the unique structure of this multifaceted DNA repair pathway, the precise identification of its components and their precise roles has proven to be an elusive task. Furthermore, it is important to notice that a general complication with the use of ICL-inducing agents in research is the generation of a variety of DNA lesions of which interstrand cross-links are in fact the minority. For instance, in cisplatin treatment 1,2-intrastrand cross-links between adjacent purines account for the majority of lesions caused; in psolaren treatment, 8-methoxypsolaren monoadducts persist even following photoactivation (Brabec, 2002). Available evidence indicates that ICLs are indeed the main lesions responsible for the cytotoxicity of the commonly used cross-linkers (Lehoczký et al., 2007). These considerations should be taken into account when assessing the contribution of the different repair pathways specifically to the resolution of DNA interstrand cross-links. This issue is further discussed in 4.1.2. In the next sections, the eukaryotic interstrand cross-link repair pathway will be dissected in its constitutive sub-components, with a final overview of the specialised Fanconi anemia pathway in mammalian cells and the recently discovered role of FAN1 in higher eukaryotes. The emphasis will be primarily given to functional details emerged from the literature so far, with the aim of providing a global picture for ICL repair in lower and higher eukaryotes.

### 1.12.3 Recombination-dependent and –independent ICL repair

The ICL repair is commonly divided into two sub-pathways. In one pathway, referred to as recombination-independent or mutagenic, following ICL removal the gap is filled by translesion polymerases. This pathway relies on NER and TLS and occurs normally in G1 phase, when a

homologous template is not available to act as a template. Well characterised in *E. coli*, the mutagenic ICL repair appears to be a minor and more elusive mechanism in lower and higher eukaryotes (Legerski, 2010). The second pathway depends on the homologous recombination machinery and is the prominent system for ICL repair in cycling mammalian cells (Legerski, 2010). Thus, ICL repair in the S phase of the cell cycle appears to the preferable option, probably reflecting the fact that error-free ICL repair would be unfeasible without the presence of an undamaged homologous template, as both the DNA strands are compromised by the cross-link. Indeed, it has been suggested that ICLs can be tolerated until the S phase is reached, and that passage through S phase is required to elicit efficient repair (Akkari et al., 2000; Zheng et al., 2003). Although different models have been proposed for this recombination-dependent pathway, their common feature is the initial collapse of a replication fork encountering the ICL and the consequent generation of a single-sided DSB (Legerski, 2010). These aspects of HR-dependent ICL repair will be discussed in 1.12.7.

### 1.12.4 NER proteins and ICL repair

Given the DNA-distorting lesions created by interstrand cross-linkers, it is not surprising that proteins involved in nucleotide excision repair have been shown to be centrally involved in ICL repair in both prokaryotes and eukaryotes (Lehoczky et al., 2007; McCabe, 2009). However, the exact role for these proteins is still unclear. It should be noted that ICLs represent a type of bulky lesion which is structurally distinct from the canonical NER substrates, as the two DNA strands are covalently linked and a complete opening of the bubble around the lesion is not achievable. However, this does not appear to constitute a limiting step for the reaction (see below).

Using a cross-linked reporter plasmid assay, the core set of human NER components (XPC, XPA, TFIIH, XPG and XPF-ERCC1) was shown to be required for repair of ICLs induced by mitomycin C or photo-activated psolaren (Wang et al., 2001; Zheng et al., 2003).

Work in lower and higher eukaryotes indicates that NER is involved in the initial recognition step. In *S. cerevisiae,* deletion of *rad4* (XPC[Hs]) caused hypersensitivity to treatment with HN2, cisplatin and mitomycin C (McHugh et al., 1999; Wu et al., 2004). Human XPC was shown to have affinity for ICLs *in vitro* (Zhao et al., 2009). The requirement for XPC was also demonstrated using a cross-linked reporter plasmid (Zheng et al., 2003). More direct evidence has been shown using a system capable of inducing laser-localised psolaren cross-links, to which XPC is rapidly recruited, along with other NER factors (Muniandy *et al.*, 2009).

Evidence has been found for the involvement of the elusive NER component XPA[Hs]/Rad14[Sc] in ICL repair. In the budding yeast, *rad14*-deleted cells showed similar hypersensitivity to HN2 compared to *rad4*-d strains (McHugh et al., 1999). Consistently, primary human XPA-deficient fibroblasts showed hypersensitivity to MMC (Niedernhofer et al., 2006). Kaye et al. (1980) showed that cells deficient in XPA were unable to remove ICLs formed by photoactivated 8-methoxypsolaren. More recently, Clingen et al. (2007) reported in a comet assay system that XPA (along with XPF) is required for an efficient reaction of ICL unhooking.

Further downstream in the NER cascade, work in the budding and the fission yeast has affirmed the crucial involvement of the nuclease Rad2[Sc]/Rad13[Sp] (homologs of mammalian XPG) in the response to cross-linking agents. In *S. cerevisiae*, deletion of *RAD2* leads to increased sensitivity to cisplatin, HN2, MMC and 8-MOP (Chanet et al., 1985; Wilborn and Brendel, 1989; Wu et al., 2004). Following induction of 8-MOP ICLs at the mating-type locus MATα, *rad2*-d showed impaired repair attributed to defective incision of the substrate (Meniel et al., 1995). In *S. pombe*, *rad13*-d strains are hypersensitive to exposure to HN2, cisplatin and mitomycin C (Lambert et al., 2003 and this study). The human ortholog XPG has also been directly associated with ICL repair (Wang et al., 2001; Zheng et al., 2003). XPG-deficient chinese hamster cell lines showed not only sensitivity to cisplatin, but also defects in ICL uncoupling, the first double incision which leads to release of the ICL from one of the two DNA strands (De Silva et al., 2002).

However, the most remarkable evidence of involvement of NER components in ICL repair is represented by the mammalian XPF-ERCC1 complex. Whereas in *S. cerevisiae* the deletion of the XPF ortholog *RAD1* leads to a significant but not dramatic sensitivity to HN2 (Barber et al., 2005), data from mammalian cells indicates a fundamental role in response to ICLs (see below). This component will be further discussed in section 1.12.8.

1.12.5 **Translesion synthesis in HR-independent ICL repair**

Numerous lines of evidence suggest that the eukaryotic recombination-independent ICL repair pathway, occurring mainly in G0/G1, is dependent on translesion polymerases. Indirect evidence has been found in both yeast and mammalian cells, where it has been demonstrated that repair of ICLs is mutagenic (Ruhland and Brendel, 1979; McHugh et al., 1999; Sarkar et al., 2006; Wang et al., 2001; Zheng et al., 2003). A summary of the most relevant direct evidence of the involvement of TLS polymerases in recombination-independent ICL will be presented below.

Early work in *S. cerevisiae* pointed at a crucial role for Rev3, the catalytic subunit of the B-family polymerase Polζ (Nelson et al., 1996). Also known as Pso1, Rev3 has been implicated in ICL repair based on sensitivity of the deletion mutant to psolaren (Henriques and Moustacchi, 1980; Cassier-Chauvat and Moustacchi, 1988). Sensitivity has been subsequently demonstrated for cisplatin, HN2 and MMC (Grossmann et al., 1999; Grossmann et al., 2000; McHugh et al., 2000; Wu et al., 2004). Polζ-null yeast mutants are more sensitive to HN2 treatment in G0/G1 than in S phase, pointing at a role for this polymerase in recombination-independent ICL repair (McHugh et al., 2000; Sarkar et al., 2006). In this context, NER-dependent incision is shown to be required prior to TLS-dependent gap filling (McHugh and Sarkar, 2006; Sarkar et al., 2006). A role for Polζ in the HR-independent ICL repair pathway has also been shown in avian, mouse and human cells (Shen et al., 2006; Zhang et al., 2007). Direct biochemical evidence has been found for Polζ activity in HR-dependent ICL repair using cell-

free *X. laevis* extracts. In this system, the regulatory subunit REV7 appears to be required for the extension step past the ICL (Räschle et al., 2008).

Rev1[Sc] possesses a deoxycytidyl-transferase rather than a standard polymerase activity (Waters et al., 2009) and it has been shown to be epistatic to Polζ in *S. cerevisiae* ICL repair (Sarkar et al., 2006). However, work in *S. cerevisiae* and mammalian cells have failed so far to identify a precise role for this protein. Thus, it is possible that the proposed role for Rev1[Sc] (REV1[Hs]) in coordinating TLS at the replication fork (Lehmann, 2007) holds true for ICL repair as well.

The involvement of other TLS factors in the budding yeast ICL repair is still unclear. Genetic evidence excludes a role for Rad30, the second major Y-polymerase in yeast (Grossmann et al., 2001; Wu et al., 2004; Sarkar et al., 2006). In contrast, data from host-cell reactivation assays are consistent with a role for the human ortholog Polη in the HR-independent ICL repair, as repair of MMC and psolaren ICLs is affected in XPV (Polη-deficient) cells (Wang et al., 2001; Zheng et al., 2003).

The requirement for other factors of the TLS machinery is still unclear. However, the participation of ubiquitinated PCNA and/or other posttranslational modifications has been proposed (Sarkar et al., 2006).

### 1.12.6  MMR and BER in ICL repair

Genetic data indicate that in *S. cerevisiae* the deletion of MMR proteins Msh2, Msh6 and Pms1 does not affect the response to cisplatin and HN2 (Beljanski et al., 2004). However, based on epistasis analysis, Msh2 has been implicated in ICL processing in S phase (Barber et al., 2005).

Human clinical data in this respect are controversial, as MMR-deficient cells have been reported to be more resistant to cisplatin treatment (Johnson et al., 1998). Discrepancies have been found in MMR- cells treated with MMC, where response has been reported to be either uninfluenced or negatively affected by the absence of MMR (Papouli et al., 2004; Fiumicino et al., 2000). Several hypotheses have been proposed for the involvement of MMR in ICL repair. It

has been proposed that resistance to cisplatin may be simply due to the mutator phenotype conferred by the absence of MMR, and this would explain the degree of variable resistance observed in different studies (Papouli et al., 2004; Pani et al., 2007). Alternatively, it has been suggested that MMR may be involved in the resolution of mismatches generated following the activity of TLS polymerases (Moggs et al., 1997). In contrast, recent data suggest that MMR in human cells participates in the homologous recombination-dependent ICL repair pathway and not in the error-prone pathway (Wu et al., 2005). Using psolaren-modified triplex-forming oligonucleotides, Zhao et al. (2009) demonstrated the participation of MutSβ in the XPA/XPC-dependent recognition of ICLs *in vitro* and *in vivo*, confirming previous *in vitro* data (Zhang et al., 2002). Taken together, the evidence on MMR implication in response to ICL-inducing agents suggests the existence of a diversified scenario, where MMR components may act on intermediates of ICL repair only in specific circumstances. However, a direct role for the MMR pathway in ICL repair seems to be excluded. In fact, it has been proposed that direct action by MMR on cisplatin adducts may trigger a futile repair cycle that would finally lead to apoptosis (Brabec et al., 2002). This hypothesis would provide another possible explanation for the increased resistance in cisplatin-treated cell cultures.

The role for base excision repair in the resolution of ICLs is still unclear. In *S. cerevisiae*, the lack of 3-methyladenine glycosylase (Mag1) leads to hypersensitivity to HN2 (McHugh et al., 1999). In this study, *mag1* (and no other BER component) is shown to be epistatic to *rad4* for HN2 sensitivity. However, the lower sensitivity of *mag1*-d compared to *rad4*-d suggests potential overlapping roles in the repair of less toxic HN2 lesions such as monoadducts.

Studies in human cells indicate that psolaren-induced DNA monoadducts are firstly excised by the DNA glycosylase NEIL1 and secondly processed by the apurinic/apyrimidinic endonuclease 1 (APE1) (Couvé-Privat et al., 2007). Recent work highlights a crosstalk between FA proteins and NEIL1 where the Fanconi anemia pathway would act in the stabilisation of the BER

component at ICL sites (Macé-Aimé et al., 2010). However, the details of this interaction are still unclear and further investigations are needed.

### 1.12.7 Homologous recombination-dependent ICL repair

Homologous recombination (HR) is crucially involved in the repair of interstrand cross-links in eukaryotes (Legerski, 2010). Studies in *S. cerevisiae* clearly indicate that this yeast relies on homologous recombination for ICL repair, as *RAD51* and *RAD52* null mutants are hypersensitive to ICL-inducing agents, especially in exponentially growing cells (Henriques and Moustacchi, 1980; McHugh *et al.*, 2000; Grossmann *et al.*, 2001). A similar importance has been demonstrated for the fission yeast ortholog Rhp51 (Lambert *et al.*, 2003 and this study). Consistently, sensitivity to interstrand cross-linkers has been demonstrated for other mutants defective in components of the budding yeast HR machinery such as the MRX complex, Rad54, Rad55 and Rad57 (Henriques and Moustacchi, 1980; McHugh *et al.*, 2000; Wu *et al.*, 2004). Interestingly, the sensitivity of *RAD55*-deleted mutants in stationary phase suggested an additional role for this protein aside from the HR-dependent ICL repair (Wu et al., 2004).

Likewise, siRNA depletion of RAD51 and RAD52 in human fibroblasts led to increased sensitivity to MMC (Hanlon Newell et al., 2008). Other *in vivo* studies in rodent and chicken cells have confirmed the requirement of the HR machinery for wild-type resistance to cross-linking agents, although differences appear to exist in the involvement of Rad52-dependent events (Hinz, 2010).

As discussed above, the involvement of the HR machinery is confined to S phase of the cell cycle, when a homologous sequence is available as a template for the repair. In both yeast and mammals, it has been shown that DSB formation after exposure to ICL-inducing agents requires passage through S phase (McHugh et al., 2000; Akkari et al., 2000; De Silva et al., 2000; Räschle et al., 2008). One-ended DSBs can be generated in either of two scenarios: the replication fork proceeds past the end of a single-stranded region of DNA previously processed by endonucleolytic cleavage; or, the replication fork collapses following direct collision with

the ICL (Legerski, 2010). However, a third scenario has been proposed where the collapse of two converging replication forks generates a two-ended DSB (Räschle et al., 2008). In any of these situations, it is important to note that homologous recombination could not operate directly on a template containing an ICL, as the covalent bond would prevent the necessary separation of the two complementary strands. Thus, the interplay between HR and other repair mechanisms is crucial for the HR-dependent ICL repair pathway. This section will present a brief summary of the evidence implicating homologous recombination in ICL repair.

One of the mechanisms postulated for the formation of one-ended breaks is mediated by the structure-specific endonuclease Mus81-Eme1 (Mus81$^{Sc}$-Mms4$^{Sc}$). Work in mouse ES cells has implicated this complex in the ICL resolution, as Mus81-Eme1- dependent cleavage is required for DSB formation in cells treated with cisplatin and MMC (Hanada et al., 2006). Based also on the preceding characterisation of this endonuclease *in vivo* and *in vitro* (see Rahn et al., 2010 for reviewed evidence), it has been proposed that the endonucleolytic cleavage occurs on one of the affected strands, 3' to the lesion (Hanada et al., 2006). The second incision, 5' to the cross-link, appears to be performed by XPF-ERCC1 (see 1.12.8.). This double incision (unhooking) is thought to be necessary in order to provide a suitable substrate for recombination-mediated replication restart (see 1.12.8.). Further downstream, mounting evidence suggest that the recruitment of translesion synthesis polymerases after the unhooking reaction is dependent in mammals on the Fanconi anemia pathway (Shen et al., 2009). In this context, this pathway would provide a recruitment mechanism for TLS polymerases, given the absence of stretches of single-stranded DNA which would serve as an activator for RAD18 (Bi et al., 2006).

Thus, a role for recombination-dependent replication restart in ICL repair has been repeatedly indicated by the available data, and models have been proposed for the re-establishment of a replication fork at the site of nucleotide incorporation. However, it should be also noted that the models for replicational fork restart presented so far (reviewed in Lambert et al., 2007)

may not directly be applicable to an ICL-stalled replication fork, as in this case the damage involves both, and not only one, of the two complementary DNA strands.

## 1.12.8 Mammalian XPF-ERCC1 and ICL response

In mammalian NER, the XPF-ERCC1 endonuclease functions by cleaving the denatured bubble 5' to the adduct (Evans et al., 1997). Human and CHO cells defective in XPF-ERCC1 are dramatically more sensitive to ICL-inducing agents compared to other NER mutants (evidence reviewed in (Wood, 2010). This may suggest that the activity of this complex in ICL repair is in fact distinct from the standard role played in NER and that XPF-ERCC1 would be involved in different stages of ICL repair.

It has been proposed that XPF-ERCC1 is involved in the initial reaction of ICL unhooking from the DNA duplex. In the first model proposed, a 3'-5'exonucleolytic activity has been invoked for this complex in the presence of RPA (Bessho et al., 1997). Together with other components of the NER pathway, this nuclease would remove a short stretch of ssDNA 5' to the ICL, event which would initiate a futile repair reaction that would terminate with either an unligated cross-linked product or a ligated product resembling the original cross-link (Bessho et al., 1997; Mu et al., 2000). Alternatively, dual incisions would be executed by XPF-ERCC1 in the canonical context of the NER pathway (Wang et al., 2001; Zheng et al., 2003).

In dividing cells, the process of ICL unhooking is thought to be a necessary step for the generation of the one-ended and two-ended DSBs (Räschle et al., 2008; Hinz, 2010). Importantly, a recent study has demonstrated the requirement for ERCC1-XPF-dependent ICL unhooking for localisation of FANCD2 to chromatin (Bhagwat et al., 2009). Although it has been proposed that at this stage XPF-ERCC1 may be the only endonuclease responsible for the cleavage of one of the two DNA strands, 5' and 3' to the ICL (Kuraoka et al., 2000; Fisher et al., 2008), the most commonly accepted model proposes a combined two-step incision of Mus81-Eme1 (3' to the ICL) first, followed by XPF-ERCC1 (5' to the ICL) (Hanada et al., 2006). This scenario would be compatible with SLX4 acting as a scaffold for both the endonucleases

(Fekairi et al., 2009; Muñoz et al., 2009). However, some controversy exists in this respect, as the endonucleolytic activity of XPF/ERCC1 5' of the ICL has been shown only *in vitro* on an artificial structure with the cross-link adjacent to a single-stranded 3' flap (Kuraoka et al., 2000).

### 1.12.9  Models for replication-initiated ICL repair

Based on studies in bacteria, lower and higher eukaryotes, different models have been proposed for replication-initiated ICL repair. The models proposed by McHugh et al. (2001) and Niedernhofer et al. (2004) envisage that following the encounter of a replication fork with the ICL, a one-ended DSB is created (fig. 1.4). Although the mechanism for DSB formation in this context is still unclear, it can be postulated that one-ended DSBs are created as a consequence of a 3' endonucleolytic cleavage or of a replication fork run-off. It is thought that the subsequent cleavage 5' to the ICL releases the adduct (ICL unhooking). According to Niedernhofer et al. (2004), TLS polymerases would be then responsible for filling in the single-stranded gap and excisional repair for removing the ICL from the DNA duplex. Finally, gap filling and recombinational repair would restore the integrity of the double strand (Niedernhofer et al., 2004). This model differs from the one proposed by McHugh et al. (2001), where homologous recombination is thought to rescue DNA replication and it would not act as a final repair mechanism *per se*. In the light of the data reviewed in this chapter, the adapted model shown in fig. 1.4 has been based on Niedernhofer et al., 2004. The most accepted endonucleolytic mechanism for the release of the adduct (Hanada et al., 2006) is shown here, a two-step incision where Mus81-Eme1 would be responsible for the cleavage 3' to the ICL and XPF-ERCC1 for the 5' cut, although this aspect is still subject of controversy (see 1.12.8).

The above models are based on a single replication fork encountering the ICL adduct. However, recently a model has been proposed which postulate a scenario where two replication forks would converge at the ICL (fig. 1.5; Räschle et al., 2008). After an initial fork pausing 20-40 nt from the lesion, one of the leading strands would be extended to 1 nt from

the adduct. Following incision, translesion synthesis would occur as hypothesised in Niedernhofer et al., 2004. Finally, the repair of the top strand would be carried out by NER mechanisms, whereas the bottom strand would be restored by recombinational repair. The adapted model proposed by Räschle et al. (2008) is shown in fig. 1.5. One important difference between the single and the double replication fork model is the extension past the ICL: whereas with a single replication fork TLS polymerases would be required for the filling of a single stranded gap, in the double fork model translesion synthesis would be implicated in the extension of one of the newly replicated strands. It should be noted that questions still exist whether the double replication fork model is relevant *in vivo*. One of the issues that might pose a conceptual obstacle to this model is the fact that the activation of DNA damage checkpoints would act to prevent the firing of late origins (Lambert et al., 2007), thereby significantly reducing the possibility of two forks converging at the ICL. However, it is still possible that a combination of the two scenarios occur in vivo, although further studies are needed to support any further hypothesis.

1.12.10 **The role of Pso2/Snm1 in ICL repair**

Screens in *S. cerevisiae* for mutants sensitive to ICL-inducing treatments revealed the existence of two genes, *snm1* (Sensitivity to Nitrogen Mustard) and *pso2* (sensitive to PSOlaren), required for wild-type resistance (Henriques and Moustacchi, 1980; Ruhland et al., 1981). Cassier-Chauvat and Moustacchi (1988) later demonstrated that *snm1* and *pso2* are in fact allelic. Widely conserved across eukaryotes, Pso2/SNM1 belong to the $\beta$-CASP subfamily of the metallo-$\beta$-lactamase (MBL) super-family of proteins and mounting evidence suggest conserved important roles in response to ICLs (Cattell et al., 2010). In *S. cerevisiae*, Snm1 has been shown to be a DNA 5'exonuclease, and this activity is required for its function in ICL repair (Li et al., 2005). Interestingly, *snm1*-d mutants show defects in repair of DSBs induced by ICL treatment, implicating this gene in processing intermediates generated after the incision step (Li and Moses, 2003; Barber et al., 2005).
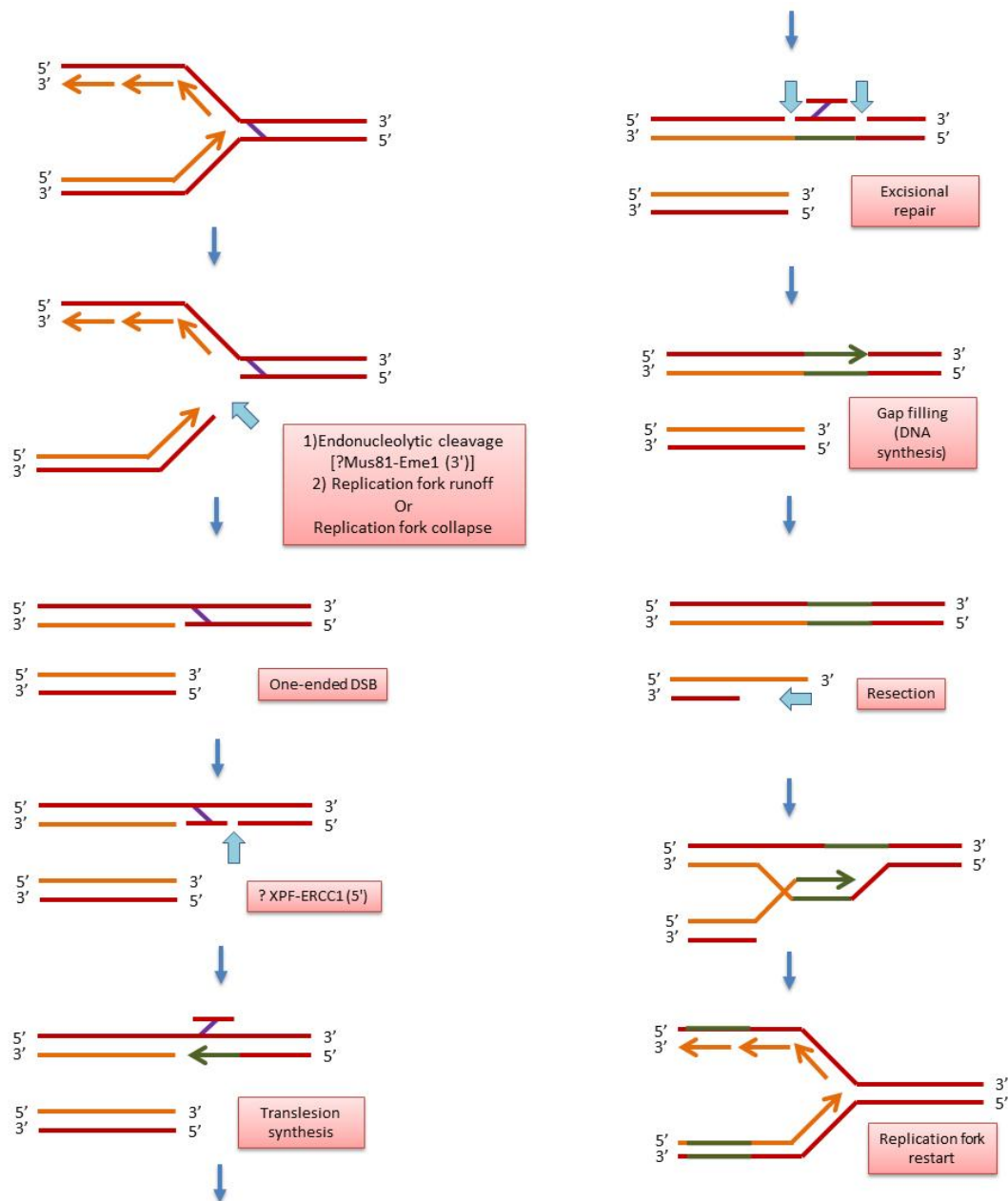
**Figure 1.4 | Model for single replication fork-initiated ICL repair (adapted from Niedernhofer et al., 2004 and Hanada et al., 2006).** This model proposes that either a 3' endonucleolytic cleavage or a replication fork run-off generates a one-ended DSB. Translesion synthesis is thought to fill in the gap created by the ICL unhooking and final excisional and recombinational repair would finally restore the integrity of the genetic information. Mus81-Eme1 and XPF-ERCC1 would be responsible for the cleavage 3' and 5' to the ICL, respectively, as proposed in Hanada et al., 2006.
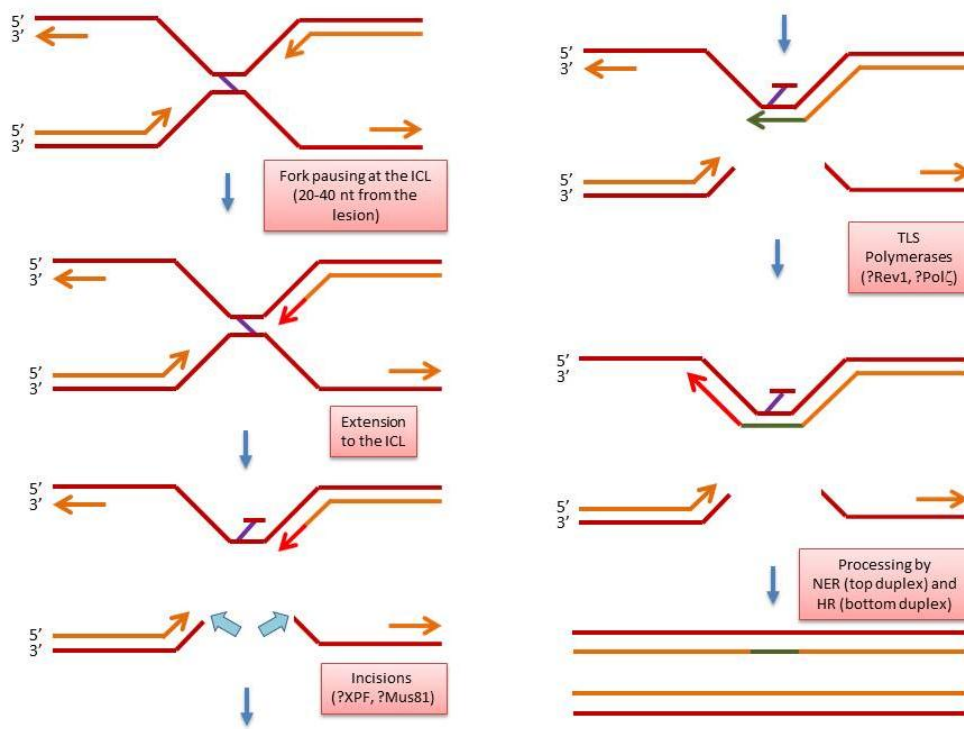
**Figure 1.5 | Model for double replication fork-initiated ICL repair (adapted from Räschle et al., 2008).** In this model, two converging replication forks stall 20-40 nucleotides from the ICL. Extension to 1 nt from the adduct is followed by translesion synthesis, required for the further extension of one of the two nascent strands past the lesion. Finally, the top and the bottom duplex would be restored by NER and HR processing, respectively.

Based on the available data, a role for Snm1/Pso2 has been postulated where its nuclease activity would resect the DNA flanking the ICL to facilitate TLS or homologous recombination (Li et al., 2005; McHugh and Sarkar, 2006). However, epistatic analyses suggest that in *S. cerevisiae* the role of Snm1/Pso2 in DNA repair may in reality be broader and more complex. In S phase, overlapping roles in ICL damage processing have been found for Pso2, Exo1 and Msh2 (Barber et al., 2005). Furthermore, in response to ionizing radiation (IR), overlapping functions have been suggested for Pso2, Exo1 and Mre11 (Lam et al., 2008). These data indicate that Pso2 function in *S. cerevisiae* may not be confined exclusively to ICL resolution, and a complex interplay with other repair factors may occur, partly dependently on the cell cycle phase. Of the three human paralogs, the most similar in structure to yeast Pso2 is SNM1A (Dronkert et al., 2000). The finding that only SNM1A and not SNM1B or SNM1C can suppress the sensitivity

of *pso2*-d yeast null mutants to ICL-inducing agents strongly indicates that SNM1A is a functional homolog of yeast Pso2 (Hazrati et al., 2008). Human fibroblasts depleted in SNM1A are more sensitive than wild-type cells to MMC treatment (Hemphill et al., 2008). Following treatment with the interstrand cross-linking agent 4HC (4-Hydroperoxycyclophosphamide), SNM1A showed increased localisation to damage-induced foci (Richie et al., 2002). Interestingly, in this study SNM1A foci formation was augmented also upon IR treatment and in colocalisation with MRE11 and 53BP1, which could indicate a wider role for this protein in DNA repair (Richie et al., 2002). An additional similarity to the yeast ortholog is the finding that the increase in foci formation is cell-cycle dependent (Richie et al., 2002). The existence of a SNM1A ICL repair pathway partly independent of the canonical FA pathway has been indicated by epistasis analysis (Ishiai et al., 2004; Hemphill et al., 2008). An additional level of regulation has also been suggested by the physical interaction and the nuclear colocalisation of SNM1 with the SUMO E3 ligase PIAS1 (Ishiai et al., 2004). The importance of post-translational modifications in this scenario has been highlighted by recent work showing that SNM1A is recruited to damage-induced nuclear foci through its UBZ domain and dependently on RAD18-monoubiquitination of PCNA (Yang et al., 2010).

The specificity in sensitivity to MMC and no other DNA interstrand cross-linking agents has hinted at the existence of overlapping functions between SNM1A and the other human paralogs. However, despite the defective response to ICL-inducing agents which has been shown for mammalian SNM1B in some circumstances (evidence reviewed in Cattell et al., 2010), the data suggest that SNM1A is the only human paralog clearly involved in ICL repair.

### 1.12.11 The Fanconi anemia pathway in ICL repair

The Fanconi anemia (FA) pathway is a DNA damage response cascade present in higher eukaryotes defined by at least 13 genes found mutated in the corresponding genetic disease: FANCA, FANCB, FANCC, FANCD1, FANCD2, FANCE, FANCF, FANCG, FANCI, FANCJ, FANCL, FANCM and FANCN. The FA pathway is normally divided into three units: upstream

components (FANCA, FANCB, FANCC, FANCE, FANCF, FANCG, FANCL and FANCM), which assemble into an E3 ubiquitin ligase complex called the "FA core complex"; the central complex FANCD2-FANCI (termed "ID complex"), which is ubiquitinated by the FA core complex in response to DNA damage; and the downstream components, including FANCD1/BRCA2, FANCN, FANCJ (Kee and D'Andrea, 2010). Additional associated downstream components such as FAAP24, FAAP100, MHF1, MHF2 and the newly discovered FAN1 are not part of the FA pathway as described above, but are required for its functionality (Kee and D'Andrea, 2010). Finally, deubiquitination mediated by the USP1/UAF1 complex has been shown to be required for the completion of the pathway (Nijman et al., 2005; Cohn et al., 2007). Although multiple functions are being increasingly associated with the FA pathway, its primary role is in response to interstrand cross-links.

The helicase/translocase FANCM is a crucial component of the FA pathway with several identified biochemical activities (Whitby, 2010). FANCM appears to be required, in complex with FAAP24, for the recruitment of the FA core complex to chromatin in response to DNA damage (Kim et al., 2008). Taken together, complementation and biochemical studies indicate that FANCM-FAAP24 acts as a sensor for the DNA lesion and recruits the FA core complex to facilitate the monoubiquitination of FANCD2 (Whitby, 2010). However, the finding that defects in FANCM[Hs] ATP-binding capabilities lead to deficiency in resistance to MMC but not in the monoubiquitination of FANCD2 and FANCI suggest that the role of FANCM in DNA repair is broader and partially independent of the main FA pathway (Xue et al., 2008; Singh et al., 2009). The ATP-dependent translocational activity on synthetic four-way junctions and DNA forks may indicate a role for FANCM in remodelling stalled forks at sites of damage, possibly to facilitate ICL repair (Xue et al., 2008). Other important activities proposed for FANCM in response to DNA damage are the activation of the S-phase checkpoint, the stabilisation of stalled replication forks and avoidance of sister chromatid exchanges (evidence reviewed in Whitby, 2010). These roles have been proposed also in the light of work done with FANCM

orthologs in the budding and fission yeast (Mph1$^{Sc}$ and Fml1$^{Sp}$ respectively), which appear to be the only FA components in lower eukaryotes (Whitby, 2010). Interestingly, further support to the proposal of FA-independent ICL repair functions for FANCM derives from work in *S. pombe*, which showed that *fml1* deletion mutants are hypersensitive to cisplatin (Sun et al., 2008).

The monoubiquitination of the central mediators FANCD2-FANCI is a crucial step for the downstream events in the FA pathway, although detailed mechanisms of how this event coordinates ICL repair are still enigmatic (Alpi and Patel, 2009). A role has been shown in *Xenopus* for the FA pathway in supporting HR-dependent ICL repair. In this study, it has been demonstrated that monoubiquitinated FANCD2-FANCI would promote incisions near the ICL and translesion synthesis (Knipscheer et al., 2009). Although numerous studies have indicated that the FA pathway acts to support recombinational ICL repair (Kee and D'Andrea, 2010), the most direct connection found was the identification of biallelic mutations in the HR factor BRCA2 from FA patients (Howlett et al., 2002).

The current model for the involvement of the FA pathway in ICL repair is as follows: the ICL is recognised by FANCM-FAAP24 bound to the recently discovered MHF complex (Singh et al., 2010; Yan et al., 2010; Kee and D'Andrea, 2010). FANCM-FAAP24-MHF recruits the FA core complex, which in turn monoubiquitinates FANCD2 and FANCI on chromatin (Alpi and Patel, 2009; Kee and D'Andrea, 2010). FANCD2-FANCI then recruits downstream factors such as the newly identified FAN1 nuclease and interacts with HR and TLS factors, finally facilitating HR-dependent ICL repair (Kee and D'Andrea, 2010). Furthermore, it is thought that a parallel crosstalk with S-phase checkpoint proteins mediates and coordinates the ICL repair with other DNA damage response mechanisms (Kee and D'Andrea, 2010).

### 1.12.12 FAN1, a novel component associated with the FA pathway

Recent work from independent laboratories identified and characterised FAN1 (Fanconi anemia-associated nuclease 1, or FANCD2/FANCI-associated nuclease 1), a novel component

associated with the FA pathway in higher eukaryotes (Smogorzewska et al., 2010; MacKay et al., 2010; Kratz et al., 2010; Yoshikiyo et al., 2010; Liu et al., 2010; Shereda et al., 2010).

FAN1 (previously named MTMR15/KIAA1018) was originally identified from a set of size-fractionated human brain cDNA libraries coding for large proteins *in vitro* (Nagase et al., 1999). Interestingly, FAN1 appears to be the only eukaryotic protein with a VRR_nuc (virus-type replication-repair nuclease) domain. This domain was found in bacteriophage and prophage proteins involved in DNA metabolism processes including replication and recombination (Kinch et al., 2005; Iyer et al., 2006). Successive protein alignments established that human FAN1 possesses three conserved domains: a UBZ-type ubiquitin-binding domain, a SAP-type DNA binding motif and the VRR_nuc domain. FAN1 is widely conserved across eukaryotes, with the notable exception of *S. cerevisiae* (Smogorzewska et al., 2010; MacKay et al., 2010; Kratz et al., 2010; Liu et al., 2010; Shereda et al., 2010).

A first indication that FAN1 is involved in genome maintenance processes came from the finding that human FAN1 strongly interacts with MLH1 and PMS2, involved in the mismatch repair pathway (Cannavo et al., 2007). However, a possible role for FAN1[Hs] in canonical MMR was ruled out by the finding that FAN1-depleted cells show wild-type resistance to 6-thioguanine, a marker drug for MMR (MacKay et al., 2010). Evidence for human, worm and chicken FAN1 involvement in the response to ICL-inducing agents was found in all the independent studies (Smogorzewska et al., 2010; MacKay et al., 2010; Kratz et al., 2010; Liu et al., 2010; Shereda et al., 2010). A mild sensitivity was shown to CPT and MMS for Fan1[Hs] – depleted cells by Smogorzewska et al., 2010, but this was not confirmed in three other studies (MacKay et al., 2010; Kratz et al., 2010; Liu et al., 2010). FAN1 localises to ICL-, IR- and HU-induced foci, and its UBZ domain is necessary and sufficient for this localisation (Smogorzewska et al., 2010; MacKay et al., 2010; Kratz et al., 2010; Liu et al., 2010; Shereda et al., 2010). Upon damage induction FAN1[Hs] colocalises to ICL-induced foci with and dependently on monoubiquitinated FANCD2[Hs], suggesting a role with the FA pathway. FANCD2[Hs]

monoubiquitination is not impaired in the absence of FAN1, indicating that FAN1[Hs] acts downstream of FANCD2[Hs] (Smogorzewska et al., 2010; MacKay et al., 2010; Kratz et al., 2010; Liu et al., 2010). Defects in homologous recombination suggest that FAN1[Hs] may be involved in the HR processes linked to ICL repair. As DSB resection is not impaired in the absence of FAN1[Hs] and RAD51 foci persist in FAN1[Hs]-depleted cells, it has been proposed that FAN1[Hs] may be required for late stages of HR-dependent repair (MacKay et al., 2010; Kratz et al., 2010). Biochemical analyses show that FAN1[Hs] possesses a robust endonuclease activity toward 5'-flap structures, specifically on dsDNA 1-5 nucleotides from the branchpoint. Additionally, FAN1[Hs] is a 5'-3' exonuclease acting on the double stranded portion of 5'- and 3'-flap structures and nicked structures (Smogorzewska et al., 2010; MacKay et al., 2010; Kratz et al., 2010). Both exo- and endonucleolytic activities are absent when the key residues in the VRR_nuc domain D960, E975, K977 are mutated in Fan1[Hs] (Smogorzewska et al., 2010; Kratz et al., 2010; Liu et al., 2010). Additional mutations found to impair Fan1[Hs] nuclease activity are Q864A (Smogorzewska et al., 2010) and the double mutations D981A R982A (MacKay et al., 2010). Interestingly, whereas mutations in the nuclease domain do not affect FAN1 localisation to laser-induced damage, mutations or total ablation of the SAP domain in human FAN1 reduce the GFP-FAN1 recruitment signal (Smogorzewska et al., 2010). Moreover, deletion of the SAP domain in *C. elegans* FAN1 causes embryonic hypersensitivity to MMC and HN2 (Smogorzewska et al., 2010).

Epistasis analyses showed an intriguing difference between human and avian FAN1, as in the latter model organism FANCC^{-/-} FAN1^{-/-} and FANCJ^{-/-} FAN1^{-/-} combined deletions led to increased sensitivity to cisplatin compared to the single mutants, in contrast with FAN1[Hs]-depleted cells, which showed epistatic relationship with FANCD2 or FANCA in response to ICL-inducing agents (Yoshikiyo et al., 2010; Kratz et al., 2010; Liu et al., 2010). It has been proposed that this data might indicate a role more independent of the FA pathway in avian cells than in human cells (Yoshikiyo et al., 2010).

Taken together, the data on FAN1 in higher eukaryotes strongly supports a role for this nuclease in the resolution of ICLs, in parallel with the FA pathway. In particular, a role in the ICL unhooking would be consistent with the biochemical activity. However, questions have been raised regarding a substantial functional redundancy with MUS81/EME1 and possibly XPF/ERCC1 which would render FAN1 activity superfluous at this stage of ICL repair (MacKay et al., 2010; Kratz et al., 2010). Consistently with the defects showed at late stages of recombinational repair, a more plausible role for FAN1 appears to be in processing recombination intermediates generated by ICL treatment (MacKay et al., 2010; Kratz et al., 2010). Furthermore, the strong interactions showed with MMR factors suggest that they may indeed be functional. In particular, it has been proposed that MMR factors would act independently of the canonical MMR pathway for the recruitment of FAN1, which would perform incisions at the site of ICL, possibly in combination with other nucleases (Smogorzewska et al., 2010). Alternatively, or in addition to this role, FAN1 might serve as a recruiting component for MMR factors, which would promote the correction of translesion synthesis-induced mismatches during ICL repair (MacKay et al., 2010).

Further studies are needed to elucidate these aspects. However, it is interesting to note that the appearance of FAN1 earlier than the FA pathway on an evolutionary scale suggests that the role for this component is distinct from the canonical FA pathway in higher eukaryotes. For this reason, the study of FAN1 in the lower eukaryote *S. pombe* will provide unique functional insights that may be relevant to FAN1 in higher eukaryotes. The investigation of *S. pombe* FAN1 (named Fan1[Sp] following the work discussed in this section) is the focus of the present study.

## 1.13   Aim of this work

The aim of this work is to characterise Fan1[Sp], the ortholog of FAN1 in the fission yeast *S. pombe*. This study profits from the amenability of the genetic tools available for this model

organism, in particular the possible use of high-throughput approaches to explore genetic interactions between the protein and other components of the DNA repair machinery. Given the absence of a yeast FA pathway, the study of this protein in *S. pombe* provides a unique opportunity to investigate the existence of alternative pathways of ICL repair in higher eukaryotes.

Chapter Two

MATERIALS AND METHODS

## 2.1 General media and reagents used in this study

| Yeast Extract Media (YE) | For 5 litres |
|---|---|
| Yeast Extract | 25 g |
| Glucose | 150 g |
| Adenine | 500 mg |
| Leucine | 500 mg |
| Uracil | 500 mg |
| Lysine | 500 mg |
| Histidine | 500 mg |
| For YEP, add Bactopeptone | 100 g |

| EMM2 Minimal Medium | For 1 litre |
|---|---|
| 1X EMM2 salt | 50 ml 20X EMM2 salt (see below) |
| 0.5% NH4Cl | 25 ml 20% $NH_4Cl$ |
| 0.01M $Na_2HPO_4$ | 25 ml 0.4M $Na_2HPO_4$ |
| 0.5% Glucose | 12.5 ml 40% Glucose |
| 1X vitamins (see below ) | 1 ml 1000X vitamins |
| 1X trace elements (see below) | 100 ul 10000X trace elements |

| 20 X  EEM2 salts | For 1 litre |
|---|---|
| Potassium Hydrogen Phthalate | 61.2 g |
| KCl | 20.0 g |
| $MgCl_2 \cdot 6H_2O$ | 21.4 g |
| $Na_2SO_4$ | 0.20 g |
| $CaCl_2 \cdot 2H_2O$ | 0.26 g |
| | to 1 litre and FILTER STERILIZE |

| 1000 X  Vitamins | For 100 ml |
|---|---|
| Pantotenic Acid calcium salt | 100 mg |
| Nicotinic Acid | 1 g |
| myo-Inositol | 1 g |
| Biotin (kept at 4°C) | 1 mg |
| | KEPT IN THE FRIDGE AND PROTECTED FROM LIGHT |

| 10000 X  Trace Elements | For 100 ml |
|---|---|
| $H_3BO_3$ | 500 mg |
| $MnSO_4$ | 400 mg |
| $ZnSO_4 \cdot 7H_2O$ | 400 mg |
| $Fe_2(SO_4)_3$ | 300 mg |
| $Na_2MoO_4$ | 150 mg |
| KI | 100 mg |
| $CuSO_4 \cdot 5H_2O$ | 40 mg |

| | |
|---|---|
| Citric Acid | *1000 mg* |
| | |
| **Leu 100 X\*** | *For 1 litre* |
| 7.5 mg/ml | *7.5 g in 1 litre distilled water* |
| | *Autoclave sterilization* |
| | |
| **Ade 100 X\*** | *For 1 litre* |
| 7.5 mg/ml | *7.5 g in 1 litre distilled water* |
| | *Autoclave sterilization* |
| | |
| **His 100 X\*** | *For 1 litre* |
| 7.5 mg/ml | *7.5 g in 1 litre distilled water* |
| | *Autoclave sterilization* |
| | |
| **Ura 50 X** | *For 1 litre* |
| 3.75 mg/ml | *3.75 g in 1 litre distilled water* |
| | *Autoclave sterilization* |
| | |
| **CSE** | *For 1 litre* |
| 28 mM $Na_2HPO_4$ | *70 ml 0.4M $Na_2HPO_4$* |
| 8.8 mM citric acid | *44 ml 0.2M citric acid* |
| 40 mM EDTA | *14.9 g $Na_2EDTA.2H_2O$* |
| 1.2 M sorbitol | *218.6 g sorbitol* |
| | *to 1 litre with distilled water and filter sterilise* |
| | |
| **10/50 Tris-EDTA (pH 7.4)** | *For 1 litre* |
| 10 mM Tris-HCl, pH 7.4 | *5 ml 2 M Tris-HCl pH 7.4* |
| 50 mM EDTA, pH 8.0 | *100 ml 0.5 M EDTA, pH 8.0* |
| | *to 1 litre with distilled water and filter* |
| | |
| **5 X TBE** | *For 2 litres* |
| 445 mM Tris Base | *108.0 g Tris base* |
| 445 mM Boric Acid | *55 g Boric acid* |
| 10 mM EDTA | *7.44 g $Na_2EDTA • 2H_2O$* |
| | *to 2 litres with distilled water* |
| | |
| **0.5 M EDTA pH 9.5** | *For 1 litre* |
| | *186.12 g $Na_2EDTA • 2H_2O$ (MW=372.24)* |
| | *Bring volume to 800 ml with distilled water* |
| | *Mix* |
| | *Adjust to pH 9.5 with NaOH pellets* |
| | *Adjust volume to 1 litre with distilled water* |
| | |
| **0.5 M EDTA pH 8** | *For 1 litre* |
| | *186.1 g $Na_2EDTA • 2HO$ (MW=372.24)* |

| | |
|---|---|
| | *Bring volume to 800 ml with distilled water* |
| | *Mix* |
| | *Adjust to pH 8.0 with NaOH pellets* |
| | *Adjust volume to 1 litre with distilled water* |
| | |
| **1000 X Ampicillin (50 mg/ml)** | *For 10 ml* |
| | *Dissolve 500 mg in 10 ml water* |
| | |
| **G-418** | |
| 100 mg/ml in $H_2O$, filter sterilised | |
| | |
| **NAT (Nourseothricin)** | |
| 100 mg/ml in $H_2O$, filter sterilised | |
| | |
| **1 M Tris-HCl** | *For 1 litre* |
| | *121.1 g Tris-base to 800 ml of distilled water* |
| | *Adjust to desired pH with concentrated HCl* |
| | *Adjust volume to 1 litre with distilled water* |
| | |
| **TE, pH 7.4** | *For 1 litre* |
| (10 mM Tris-HCl, pH 7.4 | *10 ml 1 M Tris-HCl* |
| 1 mM EDTA, pH 8.0) | *2 ml 0.5 M EDTA, pH 8.0* |
| | *Adjust volume to 1 litre with distilled water* |
| | |
| **TBE-Tris-borate, EDTA buffer 5 X** | *For 1 litre* |
| 445 mM Tris base | *54.0 g Tris base* |
| 445 mM Boric acid | *27.5 g Boric acid* |
| 10 mM EDTA | *3.72 g NaEDTA • $2H_2O$ (MW=372.24)* |
| | *Adjust to 1 litre with distilled water* |
| | |
| **TAE-Tris-acetate, EDTA buffer 50X** | *For 1 litre* |
| 2 M Tris base | *242.2 g Tris base* |
| 2 M Glacial acetic acid | *57.1 ml Glacial acetic acid* |
| 50 mM EDTA | *18.61 g $Na_2EDTA$ • $2H_2O$ (MW=372.24)* |
| | *Adjust to 1 litre with distilled water* |
| | |
| **3 M Sodium acetate** | *For 1 litre* |
| | *408.3 g Sodium acetate (3HO) in 800 ml* |
| | *Adjust to pH 4.8 or 5.2 with 3 M acetic acid* |
| | *Adjust volume to 1 litre with distilled water* |
| | |
| **SSC 20X** | *For 1 litre* |
| 3 M NaCl | *175.3 g NaCl* |
| 0.3 M sodium citrate | *88.2 g tri-Nacitrate •$2H_2O$* |
| | *Adjust to pH 7.0 with 1 M HCl* |

| | |
|---|---|
| | *Adjust volume to 1 litre with distilled water* |
| | |
| **0.1 M Sodium phosphate buffer, pH 7.0** | *For 1 litre* |
| | *57.7 ml of 1 M NaHPO* |
| | *42.3 ml of 1 M NaHPO* |
| | *Adjust volume to 1 litre with distilled water* |
| | |
| **1 M NaHPO (Sodium phosphate-dibasic)** | *For 1 litre* |
| | *142.0 g NaHPO in 800 ml distilled water* |
| | *Adjust volume to 1 litre with distilled water* |
| | |
| **1 M NaHPO (Sodium phosphate-monobasic)** | *For 1 litre* |
| | *120.0 g NaHPO in 800 ml distilled water* |
| | *Adjust volume to 1 litre with distilled water* |
| | |
| **YNB minimal media (liquid)** | *For 1 litre* |
| Formendium® YNB | *1.9 g* |
| Ammonium sulphate | *5 g* |
| Glucose | *20 g* |
| | |
| **YNB plates** | *For a 400 ml bottle* |
| YNB minimal media (liquid) – see above | |
| 10 M Sodium hydroxide | *0.08 ml* |
| DIFCO® Bacto agar | *10 g* |
| | |
| **ELN media** | *For 1 litre* |
| Formendium® EMM broth (no nitrogen) | *27.3 g* |
| Ammonium chloride | *0.05 g* |
| Uracil | *0.1 g* |
| Leucine | *0.1 g* |
| Histidine | *0.1 g* |
| Arginine | *0.1 g* |
| Adenine | *0.2 g* |
| ( for plates: add 10 g BACTO® agar per 400 ml bottle) | |

G418: Melford® G-418 disulphate (product code G0175)

NAT: Nourseothricin-dihydrogen sulfate ClonNAT 2000mg cat.no. 502000.

## 2.2 General techniques used in this study

### 2.2.1 Crosses and random spore analysis

Fresh strain patches from YE plates were streaked on ELN plates and mixed together with a loopful of sterile water. ELN plates were incubated for 2-3 days at 25°C.

For random spore analysis, a loopful from crossed patches was resuspended in 1 ml sterile water added with 20 ul helicase (1:10 dilution; Biosepra® S.H.P. / H.P.J. helix pomatia juice). After o/n incubation at room temperature, between 100 and 1000 spores were plated on YE plates and incubated at 30°C until colonies reached a satisfactory size. Colonies were then replicated on selective plates and grown at 30°C.

## 2.3 Methods used in chapter three (biochemical characterisation of Fan1$^{Sp}$)

### 2.3.1 DNA digest – restriction site analysis (*HindIII*, *SalI*)

*HindIII*: NEB R0104.

*SalI*: NEB R0138.

Digests carried out overnight at 37°C.

### 2.3.2 DNA gel electrophoresis

Invitrogen® L.M.P. (Low Melting Point) Agarose [Cat. no. 15517-022] was melted in 300ml 1X TBE (final concentration 1%). The apparatus used was the Biorad® SubCell GT®. DNA marker used: Fermentas® GeneRuler® DNA Ladder Mix. Gel was run at 20V overnight and for further 6 hrs at 80V.

### 2.3.3 Southern blot analysis

DNA from agarose gels was transferred onto GeneScreen™ Hybridization Transfer Membrane (cat. n. NEF983001PK) using an Amersham® Biosciences Vacugene® XL apparatus. Gels were

treated as follows: depurination (0.25 M HCl for 15 minutes each), denaturation (1.5 M NaCl + 0.5 M NaOH for 15 minutes each), neutralization (1 M Tris pH 8 + 1.5 M NaCl for minutes each). The membrane was quickly rinsed in in 4 X SSC and dried on Whatman® 3MM paper. The DNA was cross-linked on the membrane by using a Stratagene® Stratalinker® (2 cycles at 1200 J/m$^2$). The membrane was incubated at 65°C in 80 ml hybridisation solution added with 266 ul 30% BSA (SIGMA A8327-50ml) for at least 30 minutes. The probe was prepared with 150 ng DNA for each membrane in a total volume of 45 ul and boiled for 5 minutes. The DNA probe was added to the labelling mix GE Healthcare® Ready-To-Go™ DNA Labeling Beads (-dCTP) (product code: 27-9240-01). 5 ul $\alpha$-$^{32}$P - dCTP (GE Healthcare® REDIVUE™ DEOXYCYTIDINE 5'-[$\alpha$-$^{32}$P]TRIPHOSPHATE, TRIETHYLAMMONIUM SALT (product code: AA0005-250UCI) were added to the labelling mix and incubated at 37°C for 30 minutes. The labelling mix was filtered with GE Healthcare® G50 columns. The filtered probe was boiled and added to 20 ml hybridisation solution, together with boiled salmon sperm (Invitrogen® cat. no. 15632-011, 200 ul each membrane from a 10 mg/ml stock solution). The membrane was incubated with the 20 ml hybridisation solution at 65°C overnight. Membrane was washed with gentle shaking as follows: wash solution I at 65°C for 15 minutes; wash solution II at 42°C for 15 minutes. The signal from the membrane was detected by using Amersham storage phosphor-screen cassettes on a Molecular Dynamics® Storm 840 phosphorimager apparatus.

Hybridization solution (in 100 ml): 30 ml 20 X SSC, 1 ml Denhardt solution 100 X, 3.33 ml 30 % Sarcosyl. Wash solution I (in 500 ml): 50 ml 20 X SSC, 50 ml 10% SDS. Wash solution II (in 1 litre): 5 ml 20 X SSC, 10 ml 10% SDS. 100X Denhardt's reagent: 2% (w/v) Ficoll 400, 2% (w/v) polyvinylpyrrolidone, 2% (w/v) bovine serum albumin (Sigma® Cat. No. A3059).

### 2.3.4 Whole cell extracts (TCA extraction)

Cells were grown in 5ml YE overnight. About 5 ODs of cells were harvested and washed. The pellet was resuspended in 1 ml 20% TCA (Trichloroacetic Acid) and transferred to ribolyser tubes. Cells were centrifuged again, resuspended in 200 ul 30% TCA and ribolysed by using

glass beads (Sigma® G8772-500G) for at least 4 cycles (15 sec each) at speed 6.5, or until lysis of approximately 90% of cells was accomplished. The contents of the ribolyser tubes were filtered and centrifuged at 4000 rpm for 5 minutes at 4°C into fresh centrifuge tubes. These were then centrifuged again at 14000 rpm for 5 minutes at 4°C. The supernatant was discarded and the pellet resuspended in 200 ul 1X sample buffer. Samples were finally boiled for about 3 minutes prior to storage at -20°C.

4X Sample buffer (100ml): 250mM Tris pH 6.8, 8% SDS, 20% glycerol, 20% β-mercaptoethanol, bromophenol blue (final concentration 0.4%).

**2.3.5 Western blot analysis**

All protein gels were run by using a Biometra® Minigel® apparatus. Running gels were prepared at a concentration of 8% (see below). Stacking gels were prepared as described below. Voltage was increased from 80V to 120V upon migration of the samples from stacking to running gel. Transfer was performed by using a Biorad® Miniprotean® II apparatus onto a GE® Healthcare® ECL membrane and carried out overnight at 15V at 4°C. Membrane was stained with Ponceau dye and washed with PBS added with Tween, final concentration 0.1% (SIGMA® Cat. No. P7949). Blocking was performed for 2 hours in PBS-Tween® (PBST) added with final 3% milk (Marvel® dried skimmed milk). Primary antibodies were added to PBST + milk in a 1:3000 dilution and incubated for 2 hours at room temperature (r.t.) under slow agitation. Secondary antibodies were added to PBST + milk in a 1:5000 dilution and incubated for 45 minutes at r.t. under slow agitation. Washes were performed three times for 15 minutes each at r.t. with medium-fast agitation. Chemoluminescence was induced and detected by GE® Healthcare® ECL Plus® (Product No. RPN2132) and GE® Healthcare® ECL Hybond® film (Product No. RPN3032D) .

Primary antibodies used in this study: anti-myc (Santa Cruz® mouse anti-myc, 9E10 – sc-40); anti-HA (Santa Cruz® HA probe, F7 – sc-7392); anti-FLAG (SIGMA® F1804). Secondary antibody: Dako® anti-mouse HRP (P0260).

10X running gel was prepared as follows: 75g Tris base, 470g glycine, 25g SDS in 2.5 litres milliQ water. Transfer buffer: 12.1 g tris base, 56.3 g glycine, 1 litre methanol, 10 ml 10% SDS in 5 litres milliQ water. Buffer A (PBS): 8 g  NaCl, 0.2 g KCl, 1.44 g $Na_2HPO_4$, 0.24 g $KH_2PO_4$, 800 ml milliQ water.

Running gel (8%) prepared as follows (recipe for one minigel) : 2.3 ml $H_2O$, 1.3 ml 30% acrylamide mix, 1.3 ml 1.5M Tris (pH 8.8), 0.05 ml 10% SDS, 0.05 ml 10% ammonium persulfate, 0.003 ml TEMED.

Stacking gel (recipe for one minigel): 3.7 ml $H_2O$, 0.650 ml 30% acrylamide mix, 0.6 ml 1 M Tris (pH 6.8), 0.05 ml 10% SDS, 0.05 ml 10% ammonium persulfate, 0.010 ml TEMED.

Protein marker: NEB® Prestained Protein Marker, Broad Range (7-175 kDa) (Cat. No. P7708).

### 2.3.6 Co-immunoprecipitation

Approximately 50-100 ODs of cells were centrifuged at 3,000 g at 4°C for 5 mins. Pellets were resuspended in 1 ml sterile water, transferred to ribolyser tubes and centrifuged at 13,000g at 4°C for 5 minutes. After discarding the supernatants, pellets were kept at -20°C for 10 minutes. Samples were transferred on ice and added with 400 ul Miltenyi Biotec® (MB) lysis buffer supplemented with Roche® protease inhibitors and PMSF (Phenyl-MethylSulphonyl Fluoride). 1 centrifuge tube cap of SIGMA glass beads (Sigma® G8772-500G) was added to each sample. Cells were lysed using a ribolyser (Fastprep® FP120 BIO101 Thermo-savant®: 4-8 cycles for 15 seconds, speed 6.5; 30 seconds of cooling on ice between cycles). Satisfactory lysis was confirmed by visual inspection by microscope. The glass beads were removed from the samples and the supernatants were transferred to fresh centrifuge tubes. 90 ul from each lysate was added to 40 ul 4x sample buffer (final concentration 1x) supplemented with 26 ul β-mercaptoethanol (final concentration 20%), boiled for 5 minutes and stored at -20°C (input samples). 600 ul of MB lysis buffer were finally added to the lysates before proceeding with the purification. 50 ul MB lysis anti-tag MB microbeads were added to each sample and incubated on ice for 30 minutes (note: FLAG-tagged microbeads were prepared by adding 1 ug

SIGMA flag Ab (SIGMA® F1804) to unlabelled MB microbeads). MB µMACS$^{TM}$ columns were placed in a magnetic separator and prepared by addition of 200 ul MB lysis buffer supplemented with Roche® protease inhibitors and PMSF. After the labelling reaction was finished, the cell lysate was loaded on the columns. These were then washed with 200 ul MB wash buffer 1 for 4 times and finally with 100 ul MB wash buffer 2. 20 ul of MB elution buffer pre-heated at 95°C was applied to the columns and incubated at room temperature for 5 minutes. The immunoprecipitates were eluted with additional 50 ul of pre-heated MB elution buffer. Between 25 and 35 ul of lysate/immunoprecipitate per sample were loaded on SDS-PAGE gel for western blot analysis (see 2.3.5).

Miltenyi Biotec® buffers used: MB Lysis buffer (150 mM NaCl, 1% Triton® X-100, 50 mM Tris HCl pH 8.0); MB wash buffer 1 (150 mM NaCl, 1% Igepal CA-630, 0.5% sodium deoxycholate, 0.1% SDS, 50 mM Tris HCl pH 8.0); MB wash buffer 2 (20 mM Tris HCl pH 7.5); elution buffer for SDS-PAGE (50 mM Tris HCl pH 6.8, 50 mM DTT, 1% SDS, 1 mM EDTA, 0.005% bromphenol blue, 10% glycerol).

Roche® protease inhibitors complete, EDTA-free (Product No. 05 056 489 001)

PMSF (Phenyl-MethylSulphonyl Fluoride): SIGMA® P7626.

## 2.3.7 Recombinase-Mediated Cassette Exchange to construct tagged strains

Recombinase-Mediated Cassette Exchange (RMCE) was employed in this study for gene tagging as described in Watson *et al.*, 2008. A schematic on the use of this system for gene tagging is shown in figure 3.1. The base strains Fan1-loxP-ura4+-loxM3, Mlh1-loxP-ura4+-loxM3 and Pms1-loxP-ura4+-loxM3 were constructed by standard homologous recombination techniques. The base strains were transformed with the following plasmids to allow the Recombinase-Mediated Cassette Exchange: pAW8_13myc, pAW8_3HA, pAW8_6FLAG (see Watson *et al.*, 2008). Transformants were plated on YNB + adenine. Three to five colonies were grown in 5 ml YE and approximately 10000 cells were plated on 5-FOA. Three to five colonies

were checked by sequencing. Two positive isolates were frozen in 60% YE + 40 % glycerol at -

80°C.

### 2.3.8 Transformation of *S. pombe* cells

Transformation of *S. pombe* cells was carried out in sterile conditions. The optimal pH of LiOAc

stock solution was pH 4.9 for transformation of plasmids and pH 7.5 for transformation of

linear DNA. Cells were grown overnight o/n in 100 ml YEP. Approximately $1*10^8$ cells were

centrifuged, washed in water and LiOAc-TE and transferred to centrifuge tubes. Cells were

centrifuged again and resuspended in LiOAc-TE (100 ul each tube). Tubes were incubated at

30°C for approximately 60 minutes. The following reagents were added to each tube: 5 ul

boiled salmon sperm; DNA to transform (about 0.1-1 ug for plasmid DNA; 1-10 ug for linear

DNA); DMSO (SIGMA® D2650; 10% final concentration); 700 ul pre-warmed 40% PEG-LiOAc-TE.

Tubes were incubated at 30°C for 30 mins-1 hour. Cells were heat-shocked at 42°C for 5

minutes and left at r.t. for 10 minutes. Cells were centrifuged, resuspended in 100 ul TE and

plated onto appropriate selective plates. Plates were incubated for at least 2-3 days at 30°C.

5X LiOAc stock solution: 0.5 M LiOAc (pH 4.9 for transformation of plasmids / pH 7.5 for

transformation of linear DNA); LiOAc-TE : 1 mM EDTA, 100 mM LiOAc, 10 mM Tris-HCl pH 7.5;

40% PEG-LiOAc-TE (for 5 ml ca.): 4 ml 50 % PEG, 1 ml 5 X LiOAC, 10 ul 0.5 M EDTA, 25 ul 2M

Tris-HCl pH 7.5.

### 2.3.9 Genomic DNA extraction

Cells were grown o/n in 10 ml YEP at 30°C to approximately OD 5. Approximately 50 ODs of

cells were centrifuged at 3,000 g for 5 minutes. Pellets were resuspended in 1 ml CSE added

with zymolyase 20T (Seikagaku®, product code 12049) (1 mg/ml final concentration). Pellet

was resuspended in 1 ml CSE and incubated for 30-60 minutes at 37°C. After 30 minutes,

satisfactory lysis was checked under microscope. Cells were centrifuged at 3,000 g for 5

minutes. Pellet was resuspended in 450 ul of 5X TE and transferred to 1.5 ml centrifuge tubes.

50 ul 10% SDS was added to each tube, then incubated for 5 minutes at r.t. 150 ul 5M KAc was

added to each tube, then incubated 10 minutes on ice. Tubes were centrifuged for 10 minutes at 20,000 g. The supernatant from each tube was transferred to fresh tubes. 1 volume of isopropanol was added. Samples were centrifuged at 20,000 g at 4 °C for 10 minutes and the supernatant was discarded. The pellet was washed with 500 ul 70% ethanol and centrifuged for 5 minutes at 20,000 g. The supernatant was discarded and the pellet was resuspended in 250 ul 5XTE added with RNAse A (5 ul of a 10 mg/ml solution). Samples were incubated at 37°C for 20 minutes. 2ul 10% SDS and proteinase K (SIGMA® P2308) 10 ul of a 10 mg/ml solution) were added to each sample. Tubes were incubated for 60 minutes at 55°C. Genomic DNA was purified by phenol chloroform extraction twice as follows: 1 volume of phenol chloroform-isoamyl alcohol (SIGMA® product no. 77617), vortexing, spinning at 13000 g for 5 minutes, upper phase transferred to fresh tubes. DNA was further purified by isopropanol precipitation (1 volume isopropanol, 1/10 volume 3M Sodium Acetate, wash with 70% ethanol). Pellet was finally resuspended in 30 ul 1XTE.

## 2.3.10 Spontaneous mutation rate assay

Single colonies were isolated on YEA from individual streaks. 11 colonies from each strain were grown in 5ml YE in individual tubes. Samples were incubated at 30°C for 48 hours to stationary phase. Cultures were serially diluted as follows: 10 ul saturated culture in 1 ml $H_2O$; 10 ul of this dilution into 1 ml $H_2O$. 50 ul of this dilution were plated on YE-Agar (YEA) plates. 50 ul of saturated culture were plated on YE-5-FOA (*5-Fluoroorotic acid*; Melford® F5001) plates (0.1% final concentration). Plates were incubated for 3-4 days at 30°C. Spontaneous mutation rates were calculated by the Lea-Coulson method of the median (Rosche and Foster, 2000; Foster, 2006).

## 2.4 Methods used in chapter four (genetic characterisation of Fan1$^{Sp}$ by *in vivo* survival assays)

### 2.4.1 In vivo survival assays: spot tests

Strains were inoculated in 5 ml YE and grown at 30°C o/n. $10^7$ cells from each logarithmically growing culture were harvested and resuspended in 1 ml water. Four serial 1/10 dilutions were prepared from each culture. 10 ul were spotted onto YEA plates added with increasing doses of DNA damaging agents. All the spots were deposited in duplicates on the same plate to guarantee an internal control. Plates were incubated at 30°C for three days. Images were acquired by a Syngene® Ingenius® apparatus.

DNA damaging agents used:

- UV irradiation: performed with a Stratagene® Stratalinker®

- Methyl methanesulfonate (MMS): SIGMA® (cat. no. 129925)

- Camptothecin (CPT) (98%): Acros Organics® (cat. no. 27672)

- Hydroxyurea (HU) (98%): SIGMA® (cat. no. H8627)

- Cisplatin (Cis-platinum(II)diammine dichloride): SIGMA® (product no. P4394)

- Mitomycin C (MMC): Sigma® Mitomycin C - 2mg (cat. no. M0503).

### 2.4.2 In vivo survival assays: survival curves

$2x10^8$ cells grown to exponential phase were centrifuged and washed with PBS. Pellets were resuspended in 10 ml and split into five 2 ml aliquots in 15 ml tubes. Stock solutions of the drugs were made at this stage; subsequent serial dilutions and inoculations were made quickly in order to minimise the loss of efficacy of unstable drugs. Each dilution was inoculated into the 2 ml aliquoted cultures and tubes incubated at 30°C with shaking for 1 hour. 1 ml ($2x10^7$ cells) from each aliquot was washed and resuspend in 10 ml PBS. Each aliquot was diluted 100-fold (100 ul into 10 ml PBS). 10 ul of these dilutions (approximately 200 cells) were plated onto YEA and grown at 30°C for 3-4 days. Standard error of the mean was calculated as standard deviation divided by the square root of the number of independent experiment repeats.

DNA damaging agents used:

- HN1 (2-Chloro-N,N-dimethylethylamine hydrochloride): SIGMA® (product no. 24362)

- HN2 (Mechlorethamine hydrochloride, 98%): SIGMA® (product no. 122564)

- MMC (Mitomycin C): Sigma® Mitomycin C - 2mg (product no. M0503).

## 2.5 Methods used in chapter six (synthetic genetic arrays)

### 2.5.1 Automated Screening of the Bioneer deletion library

A loopful of query mutant (Q) was inoculated from a fresh patch into 15 ml YE+NAT and grown

for at least 6 hours. The above culture was poured into an empty Singer® PlusPlate® ("Q bath")

Once thawed, library plates were replicated onto YEA PlusPlates®: four liquid 96-well plates

combined onto one YEA PlusPlate® (384 spots) [PROGRAM 1, TWICE PER ARRAY]. A 384 agar

plate was build using the Q bath as a source ("Q YEA PlusPlates®") [PROGRAM 2, TWICE PER

ARRAY]. Cells were grown for 2-3 days at 30°C (or until colonies are grown to satisfactory size).

Each library was replicated to fresh YEA PlusPlates® ("L YEA PlusPlates®") [PROGRAM 3].

Mating: colonies were combined from the L and Q YEA PlusPlates® onto ELN PlusPlates®

[PROGRAM 4, RUN TWICE PER ARRAY]. ELN PlusPlates® were incubated at 25°C for 4 days.

YEA PlusPlates® were incubated at 30°C for 3 days: pictures were taken approximately every

12 hours to monitor the fitness of the single mutants. Spore germination: colonies were

replicated from ELN PlusPlates® to YEA PlusPlates® [PROGRAM 5] and incubated at 30°C for 3

days. Selection 1: colonies were replicated from YEA PlusPlates® to YE+GC PlusPlates®

[PROGRAM 5] and incubated at 30°C for 2-3 days (or until colonies have grown to satisfactory

size). Selection 2: cells were replicated from YE+GC PlusPlates® to YE+GNC PlusPlates®

[PROGRAM 3] and incubate at 30°C for 1-3 days. Pictures to assess the fitness of double

mutants were taken at this stage every approximately 12 hours.

For the assessment of resistance to DNA damaging agents, cells were replicated from YE+GNC

PlusPlates® to YE PlusPlates® added with different concentrations of chosen DNA damaging

agents [PROGRAM 3]. Plates were incubated at 30°C for 2-4 days and pictures taken approximately every 12 hours.

Pictures were taken by using a Syngene® Ingenius® apparatus.

Software used for colony size analysis: HT Colony Grid Analyser 1.1.0/1.1.7, Adobe® Photoshop® CS5 Extended, Microsoft® Excel® 2007/2010.

Additional reagent used: Cycloheximide, SIGMA® (product no. C7698) (100 mg/l from a 100 mg/ml stock in DMSO)

**2.5.2 RoTor® PROGRAMS**

(the section follows on the next page)

## PROGRAM 0 (Library replicas; automatically run twice)

### Use: to create replicas of the frozen gene deletion library (96 well plates)

- WET 96 -> WET 96

- Long pads 96

- Program: "Library replicate" (personalised program), X# number of copies to perform

Selected options:

- Recycle mode: OFF

- Revisit mode: OFF

- Liquid mix source: ON

- Liquid mix target: ON

**SOURCE:**

**Pinning tab:**

- speed = 15 mm/sec

- backoff = - 0.1 mm

**Wet mix tab**:

- diameter = 0.5 mm

- speed = 25 mm/sec

- cycles = 10

- travel = 3D (0.25)

**TARGET**:

**Pinning tab**:

- speed = 15 mm/sec

- backoff = 0.3 mm

**Wet mix tab**:

- diameter = 1 mm

- speed = 25 mm/se

- cycles = 6

- travel = 3D (3).

## PROGRAM 1 (Replica WET 96 -> DRY 384)

**Use: to combine deletion library 96 well plates onto agar plates (4 wet plates to 1 dry plate)**

- WET 96 -> DRY 384

- Long pads 96

- Program: "1 to 4 array"

Selected options:

- Liquid mix source: ON

- Agar mix target: OFF

**SOURCE**:

**Pinning tab**:

- speed = 15 mm/sec

- backoff = - 0.1 mm

**Wet mix tab**:

- diameter = 1.3 mm

- speed = 25 mm/sec

- cycles = 10

- travel = 3D (1)

**TARGET**:

**Pinning tab**:
- pin pressure = 32 %

- speed = 9mm/sec

- overshoot = 2 mm

**This program was run twice per array to ensure that enough cells are transferred.**

# PROGRAM 2 (BATH 96 -> DRY 384)

**Use: to transfer cells from a query strain culture onto agar plates (384)**

- BATH 96 -> DRY 384
- Long pads 96
- Program: "1 to 4 array single source"

Selected options:
- Recycle mode: ON
- Revisit mode: ON
- Liquid mix source: ON
- Agar mix target: OFF

<u>**SOURCE**</u>**:**

**Pinning tab**:
- speed = 15 mm/sec
- backoff = 0.4 mm

**Wet mix tab**:
- diameter = 1.3 mm
- speed = 25 mm/sec
- cycles = 5
- travel = 3D (1)

<u>**TARGET**</u>:

**Pinning tab**:
- pin pressure = 32 %
- speed = 9mm/sec
- overshoot = 2 mm

**This program was run twice per array to ensure that enough cells are transferred.**

# PROGRAM 3 (DRY 384 -> DRY 384)

**Use: to replicate colonies from agar (384) to agar plates (384), single replicas.**

- DRY 384 -> DRY 384
- short pads 384
- Program: "Replicate"

Selected options:
- Recycle mode: OFF
- Revisit mode: OFF
- Agar mix source: OFF (Optional: ON – see below*)
- Agar mix target: OFF

**<u>SOURCE</u>:**

**Pinning tab:**
- pin pressure = 32 %
- speed = 9mm/sec
- overshoot = 2.5 mm

**[Dry mix tab:]**

This mode is optional, but it might be needed to make sure to replicate also smaller, scattered colonies.

- clearance = 2.5 mm
- diameter = 1 mm
- cycles = 1

**<u>TARGET</u>:**

**Pinning tab:**
- pin pressure = 32 %
- speed = 9mm/sec
- overshoot = 2.5 mm

# PROGRAM 4 (MATING, DRY 384 -> DRY 384)

**Use: to mate colonies from agar (384) to agar plates (384).**

- DRY 384 -> DRY 384
- short pads 384
- Program: "mate"

Selected options:
- No offset
- Agar mix source: OFF (Optional: ON – see below*)
- Agar mix target: OFF

<u>**SOURCE**</u>:

**Pinning tab**:
- pin pressure = 32 %
- speed = 9mm/sec
- overshoot = 2 mm

**[Dry mix tab:]**

This mode is optional, but it might be needed to make sure to replicate also smaller, scattered colonies.

- clearance = 2.5 mm
- diameter = 1 mm
- cycles = 1

<u>**TARGET**</u>:

**Pinning tab**:
- pin pressure = 32 %
- speed = 9mm/sec
- overshoot = 2 mm

**This program was run twice.**

# PROGRAM 5 (Dry 384 -> Dry 384, automatically run twice)

## Use: to create replicas of the 384 agar plates (intermediate steps of the screening, double replicas)

- Dry 384 -> Dry 384
- Short pads 384
- Program: "Library replicate X1" (personalised program)

Selected options:

- Recycle mode: ON
- Revisit mode: ON (See **IMPORTANT NOTE** below)
- Agar mix source: OFF (Optional: ON – see below)
- Agar mix target: OFF

<u>SOURCE</u>:

**Pinning tab**:

- pin pressure = 32 %
- speed = 9mm/sec
- overshoot = 2.5 mm

**[Dry mix tab:]**

This mode is optional, but it might be needed to make sure to replicate also smaller, scattered colonies.

- clearance = 2.5 mm
- diameter = 1 mm
- cycles = 1

<u>TARGET</u>:

**Pinning tab**:
- pin pressure = 32 %
- speed = 9mm/sec
- overshoot = 2.5 mm

## 2.6 Chapter seven: phenotypic analysis of point mutants

### 2.6.1 Site-directed mutagenesis PCR

Primers to construct the loxP-Fan1-loxM3 base strain:

> *mtmr15(upstream)-loxP*

AGCAACTTTCGCTAAACTTGCATTATAGACAACACTGTAACTTACGAATGCAGTTAAATTTTCAAAAGCA

TTTATTTAAACGGATCCCCGGGGTTAATTAA

> *mtmr15(downstream)-loxM3*

GCAAAACGATGGTAATTCAGCAAGCAAAGTGTAATTTACATAAGCTATGCATTTAATGAAAAGATTAAC

AATCACGTTTTgaattcgagctcgtttaaac.

Primers to construct the point mutants:

> *MTMR15_D651N_F*

ATAGTTCTAGCGGGATACCTaacTTATGTTTGTGGAATCCGTC

> *MTMR15_D651N_R*

GACGGATTCCACAAACATAAgttAGGTATCCCGCTAGAACTAT

> *MTMR15_D651A_F*

CTAGCGGGATACCTGcaTTATGTTTGTGGAATC

> *MTMR15_D651A_R*

GATTCCACAAACATAATGCAGGTATCCCGCTAG

> *MTMR15_E666Q_K668A_F*

AAAAAATTTATGTTTTCAcAAGTTgctAGCGATAATGATAGGCTCTCAGAA

> *MTMR15_E666Q_K668A_R*

TTCTGAGAGCCTATCATTATCGCTAGCAACTTGTGAAAACATAAATTTTTT

> *MTMR15_K668A_F*

AAAAAATTTATGTTTTCAGAAGTTgctAGCGATAATGATAGGCTCTCAGAA

> *MTMR15_K668A_R*

TTCTGAGAGCCTATCATTATCGCTAGCAACTTCTGAAAACATAAATTTTTT

>*MTMR15_L159A_F_new*

CGATGAAgcGCGTTCGTTAGCTAGACAAACGAAGGTGTGTGG

>*MTMR15_L159A_R_new*

CTAGCTAACGAACGCGCTTCATCGAGAGATAGAATTTCAATTATTTCTTCAGTTG

>*MTMR15_E666Q_F_new*

GTTTTCAcAAGTTAAAAGCGATAATGATAGGCTCTCAGAAGCGCAAAAATTCTGG

> *MTMR15_E666Q_R_new*

ATCATTATCGCTTTTAACTTGTGAAAACATAAATTTTTTTTTAGACGGATTCCACAAAC.


PCR program: 1) 94°C, 3 mins; 2) 94°, 30 sec; 3) 58°C, 1 min; 4) 68°C 20 mins (or: 2 minutes/kb); 5) repeat steps 1)-4) for 20 times; 6) 4°C (stop).

Polymerase used: Stratagene® Pfu Turbo (Cat. No. 600250).


## 2.7 Methods used in appendix 1 (Ch16 DSB repair system)

### 2.7.1 Ch16 DSB repair system (thiamine promoter-regulated HO)

Strains were grown from frozen stocks in selective EMM2 minimal media (+thiamine 8 uM +selection for HO plasmid) and streaked on G418 plates. Cells were inoculated directly from G418 plate into 10 ml selective media (EMM2 minimal media +thiamine 8 uM +selection for HO plasmid) and grown o/n at 30°C in 50 ml tubes. The cell concentration of the cultures (optical density, OD) was measured and diluted to OD 0.1 in 10 ml (minimal +thiamine 8 uM +selection for plasmid). Cultures were grown for 3 hours at 30°C. The equivalent of 20 ul OD 0.2 was inoculated into 10 ml YE, and 100 ul of this culture were plated on YEA (3 plates/culture) (0 minutes timepoint). The remainder of the cultures were split in half. Half of

the cultures (- thiamine samples) were washed 2 times in PBS (20 ml each wash) to remove the thiamine from the medium. Pellets were resuspend in 10 ml selective media (+ / - thiamine +selection for plasmid + adenine to avoid selection against rearrangements or minichromosome loss). Cultures were grown for 48 hrs at 30°C (concentration was kept below OD 1 throughout the experiment). After 48 hours growth, OD was checked and the equivalent of 20 ul OD 0.2 was inoculated into 10 ml YE. 100ul of this dilution were plated on YEA plates (three plates per samples). After 2-3 days of growth, plates were replicated on YEA-G418; EMM +ULHT; EMM +ULAT (U, uracil; L, leucine; H, histidine; A, adenine; T, thiamine). Colonies were scored using a manual colony counter.

**2.7.2 Pulse-field gel electrophoresis**

Cells were grown overnight in 10 ml YEP at 30°C. Cultures were transferred to 15 ml tubes and centrifuged at 2500 g at room temperature (r.t.) for 3 minutes. Cells were washed twice in 10 ml distilled water. Cells were counted by hemocytometer and diluted in fresh minimal EMM medium (+ / - thiamine as appropriate, final concentration 30 uM) (cell density was kept below $2*10^7$ cells/ml throughout the experiment). The agarose for plugs was melted in TSE (0.8% final concentration) and kept at 55°C. $3*10^8$ cells were harvested from each samples and transferred to 50 ml tubes. 1/100 volume of 10% $NaN_3$ and 1/10 volume of 0.5 M pH 8 EDTA were added to each sample and incubated on ice for 5 minutes. Cultures were centrifuged at 2500 g at 4°C for 3 minutes and the pellets washed in CSE and then resuspended in 2 ml CSE by using sterile loops.  0.5 ml lyticase solution in CSE (1.5 mg/ml) were added to each culture and incubated at 37°C for 15-30 minutes (or up to 80-90 % of cells lysis). Cultures were centrifuged at 1000 g at r.t. for 3 minutes, the supernatant removed by aspiration and the cell pellet resuspended in 300 ul TSE by sterile loops. Plugs were prepared for each sample with 400 ul of pre-melt agarose and incubated on ice for 5 minutes. Plugs were resuspended in 10 ml TES and incubated at 55°C for 90 minutes. Plugs were transferred to 10 ml lauryl sarcosine solution (1% lauryl sarcosine in 0.5 M EDTA pH 9.5; SIGMA® Biochemika® 61747) added with proteinase K

(final concentration 0.5 mg/ml) and incubated at 55°C for 24 hours. After 24 hours, 250 ul of fresh proteinase K (final amount 5 mg) was added to the tubes and the plugs incubated for further 24 hours. For the electrophoretic run, half a plug from each sample was equilibrated in 1 ml TAE for three times. Plugs were incorporated in the melted agarose and samples run as indicated below.

PFGE apparatus: Biorad PFGE CHEF-DR® III. Agarose: Certified Megabase® Agarose for PFGE (Biorad® 161-3109). Gel: final concentration 8%. Program used: initial sw. time = 1.8 k sec (30 mins); final sw. time = 1.8 k sec (30 mins); run time = 68 hours; Volts / cm = 2.0; angle = 106°. Recipes: TSE (10 mM Tris-HCl pH 7.5; 45 mM 0.5 M pH 8 EDTA; 0.9 M sorbitol); TES (50 mM Tris-HCl pH 7.5; 250 mM EDTA pH 8; 1 % SDS).

### 2.7.3 Ch16 DSB repair system (estradiol receptor-hormone binding domain-regulated HO)

Two single colonies per strain (ER-HBD-HO, N-terminal and C-terminal constructs) were inoculated and grown overnight in 10 ml EMM2 added with adenine, leucine, thiamine, histidine. Cultures were washed four times with distilled water and split into two cultures. Only one of the two cultures was added with thiamine (60 uM final concentration). Each culture was again split into two subcultures, only one of which was added with β-estradiol (0.3 uM final concentration). Approximately 500 cells were plated on YEA after 24 and 48 hours from induction. After 2-3 days of growth on YEA, colonies were replica-plated on YEA-G418 and EMM2 ade-. After 1-2 days of growth, marker loss was scored as the number of G418-sensitive and adenine-auxotroph colonies.

β-Estradiol: SIGMA® Cat. No. E2758.

### 2.7.4 Ch16 DSB repair system (invertase promoter-regulated HO)

Protocol was based on the standard protocol presented in 2.6.1, with the below modifications. Strains were woken up on selective plates and restreaked onto G418 plates o/n. A starter culture was inoculated from these streaks. After o/n growth, cultures were diluted to 0.2 OD in 100 ml YE containing 6.25mg G418 and grown for 4 hours. Cells were harvested, washed with

PBS, resuspended in the 100 ml of selective medium and grown overnight. Cultures were divided into two and diluted to 0.1 OD in EMM containing either glucose or sucrose. Cultures were grown at 30˚C under agitation (200 rpm).

EMM for repression state: EMM dry mix (Potassium Hydrogen Phthalate, 75 g; $Na_2HPO_4$, 55g; $NH_4Cl$, 125 g; glucose, 500 g). EMM media (dry EMM stock 30.2 g/l; 50X Salts 20ml/l; 1000X vitamins 1.0ml/l; 10000X minerals 0.1ml/l). For agar plates, EMM media + 2% agar. 8% glucose (final concentration) added per litre after autoclaving. Salts for EMM solution ($MgCl_2 \cdot 2H_2O$ 0.26 M; $CaCl_2 \cdot 2H_2O$ 5.0 mM; KCl 0.67 M; $Na_2SO_4$ 14.1 mM). Vitamins for EMM solution (pantothenic acid 4.2 mM; nicotinic acid 8.12 mM; inositol 55.5 mM; biotin 40.8 uM). Minerals for EMM solution (boric acid 80.9 mM; $MnSO_4$ 23.7 mM; $ZnSO_4 \cdot 7H_2O$ 13.9 mM; $FeCl_3 \cdot 6H_2O$ 7.4 mM; molybdic acid 2.5 mM; KI 6.0 mM; $CuSO_4 \cdot 5H_2O$ 1.6 mM; citric acid 47.6 mM).

EMM for induced state: EMM media (potassium hydrogen pthalate 0.3% w/v; $Na_2HPO_4$ 0.22%; ammonium chloride 0.5%; sucrose 4%; 50X Salts 2mls/ 100ml; 1000X Vitamins 0.1ml/100ml; 10000X Minerals 0.01 ml/100ml).

YE, supplement mix: 10 g each of adenine, histidine, leucine, lysine, and uracil.

YE5S liquid/agar: 1.125 g supplements/litre; 30 g glucose/l; 5 g yeast extract/l. For plates, add agar at 2%. 8% glucose (final concentration) added after autoclaving.

## 2.8    List of strains used

| Strain code | Name | Genotype | Phenot. | M.t. | Notes |
|---|---|---|---|---|---|
| AMC1 | 501 | leu1-32 ura4-D18 ade6-704 | leu- ura4- ade- | h- | Standard "wild-type" strain, h- |
| AMC3 | 503 | leu1-32 ura4-D18 ade6-704 | leu- ura4- ade- | h+ | Standard "wild-type" strain, h+ |

| YFS2 | 501-cdc13nd | leu1-32 ura4-D18 ade6-704 | leu- ade- | h- | 501 transformed with ER_cdc13nd plasmid (YFP3) |
|---|---|---|---|---|---|
| YFS3 | TH1230 | ade6-M210 Ch16-MG | ura- leu- | h- | Minichromosome strain (see Prudden et al. 2003); Ch16-MG genotype: ade6-M216 rad21::MATa-kanMX6 cid2::his3 |
| YFS4 | TH1293 | ade6-M210 Ch16-MG | ura- leu- | h+ | Minichromosome strain (see Prudden et al. 2003); Ch16-MG genotype: ade6-M216 rad21::MATa-kanMX6 cid2::his3 |
| YFS5 | TH1230-HO | ade6-M210 Ch16-MG | ura- | h- | Minichromosome strain (see Prudden et al. 2003); Ch16-MG genotype: ade6-M216 rad21::MATa-kanMX6 cid2::his3 HO endonuclease in pREP81X (PW25, or YFP5) |
| YFS6 | TH1230-HOER | ade6-M210 Ch16-MG | leu- | h- | Minichromosome strain (see Prudden et al. 2003); Ch16-MG genotype: ade6-M216 rad21::MATa-kanMX6 cid2::his3 ER-HBD_HO (YFP2) |
| YFS11 | TH2158 + p86 | MGH wt + p86 | ura- | | From A. Dave: MGH wt transformed with p86(leu), plasmid carrying the HO endonuclease under invertase promoter |
| YFS12 | TH2368 + p86 | MGH crb2-d rqh1-d + p86 | ura- | | From A. Dave: MGH wt transformed with p86(leu), plasmid carrying the HO endonuclease under invertase promoter |
| YFS13 | TH2369 + p86 | MGH crb2-d rqh1-d + p86 | ura- | | From A. Dave: MGH wt transformed with p86(leu), plasmid carrying the HO endonuclease under invertase promoter |
| YFS14 | TH2370 + p86 | MGH crb2-d rqh1-d + p86 | ura- | | From A. Dave: MGH wt transformed with p86(leu), plasmid carrying the HO endonuclease under invertase promoter |

| | | | | |
|---|---|---|---|---|
| YFS15 | TH2368 + p96 | MGH crb2-d rqh1-d + p96 | ura- | | From A. Dave: MGH wt transformed with p96(leu), plasmid -empty vector with the invertase promoter |
| YFS16 | fan1-d strain, or 14152 | ade6-M216 "MTMR::kanR" | G418r, ura-, ade-, leu- | h+ | strain # 14152 from Bioneer library |
| YFS17 | fan1-d strain ("PN"3909), or 3909 | leu1-32 ura4-D18 ade6-M? SPBC146.06c::kanR | G418r, ura-, ade-, leu- | h+ | Strain 3909 from Paul Nurse's lab |
| YFS19 | msh2Δ (SAS364) | msh2::kanMX6 leu1-32 ade6-704 ura4-D18 | G418r | h- | Strain SAS34 from Stephanie Schalbetter's collection |
| YFS20 | 3909x IMS461 | leu1-32 ?ura4-D18? ?ade6-M? SPBC146.06c::kanR cdc6-wt ura4+ | G418r ura+ | h+ | crossed isolate n.5 - checked by PCR |
| YFS21 | 3909x IMS463 | leu1-32 ?ura4-D18? ?ade6-M? SPBC146.06c::kanR cdc6-L591M ura4+ | G418r ura+ | h- | crossed isolate n. 8 - checked by PCR |
| YFS22 | 14152x IMS461 | ade6-M216 "MTMR::kanR" cdc6-wt ura4+ | G418r ura+ | h+ | crossed isolate n.3 - checked by PCR |
| YFS23 | 14152x IMS463 | ade6-M216 "MTMR::kanR" cdc6-L591M ura4+ | G418r ura+ | h- | crossed isolate n. 2 - checked by PCR |
| YFS24 | pms1-P-ura4-M | pms1-loxP-ura4-loxM | ura4+ | h- | Base strain, first step RMCE to tag pms1; 501 transformed with linear fragment, see details on separate files; sequenced. |
| YFS25 | fan1-P-ura4-M | fan1-loxP-ura4-loxM | ura4+ | h- | Base strain, first step RMCE to tag fan1; colony M20. 501 transformed with linear fragment, see details on separate files; sequenced. |

| YFS26 | mlh1-P-ura4-M | mlh1-loxP-ura4-loxM | ura4+ | h- | Base strain, first step RMCE to tag mlh1; colony m1. 501 transformed with linear fragment, see details on separate files; sequenced. |
|---|---|---|---|---|---|
| YFS27 | pms1-P-6xFLAG-M | pms1-loxP-6xFLAG-loxM | G418r | h- | Final step RMCE, see YFS24; colony frozen: P4-3 (see 7.22) |
| YFS31 | mlh1-3HA | 501 mlh1-3HA | G418r | h- | isolate 1; checked by Western (see7.37) |
| YFS32 | mlh1-3HA | 501 mlh1-3HA | G418r | h- | isolate 2; checked by Western (see 7.37) |
| YFS33 | 3909x IMS534 | fan1::kanMX, cdc20wt ura+ | ura+, G418r | h- | colony 1; checked by colony PCR |
| YFS34 | 3909x IMS534 | fan1::kanMX, cdc20wt ura+ | ura+, G418r | h+ | colony 14; checked by colony PCR |
| YFS35 | 3909x IMS536 | fan1::kanMX, cdc20M630F ura+ | ura+, G418r | h- | colony 8; checked by colony PCR |
| YFS36 | 3909x IMS536 | fan1::kanMX, cdc20M630F ura+ | ura+, G418r | h+ | colony 1; checked by colony PCR |
| YFS41 | 14152x IMS534 | fan1::kanMX, cdc20wt ura+ | ura+, G418r | h- | colony 1; checked by colony PCR |
| YFS42 | 14152x IMS534 | fan1::kanMX, cdc20wt ura+ | ura+, G418r | h- | colony 7; checked by colony PCR |

| | | | | | |
|---|---|---|---|---|---|
| YFS43 | 14152x IMS536 | fan1::kanMX, cdc20M630F ura+ | ura+, G418r | h+ | colony 7; checked by colony PCR |
| YFS44 | 14152x IMS536 | fan1::kanMX, cdc20M630F ura+ | ura+, G418r | h- | colony 12; checked by colony PCR |
| YFS49 | fan1-13myc | 501 fan1-13myc | G418r | h- | isolate A, Western blot see logbook 7.44 |
| YFS50 | fan1-13myc | 501 fan1-13myc | G418r | h- | isolate D; fewer myc repeats: Western blot see logbook 7.44 |
| YFS55 | pREP4N no HO strain (-ve control) | 501 pREP4N empty | NATr | | |
| YFS56 | Nt pREP4N ERHBD-HO | 501 Nt pREP4N ERHBD-HO | NATr | | |
| YFS57 | Ct pREP4N ERHBD-HO | 501 Ct pREP4N ERHBD-HO | NATr | | |
| YFS59 | fan1:: NAT (3909N) | leu1-32 ura4-D18 ade6-M? SPBC146.06c::NAT | NATr, ura-, ade-, leu- | h+ | isolate 2; checked G418s; checked by PCR (see 7.48, 7.52) and Southern (see 7.64) |
| YFS60 | fan1:: NAT (14152N) | ade6-M216 "MTMR::NAT" | NATr, ura-, ade-, leu- | h+ | isolate 1; checked G418s; checked by PCR (see 7.48, 7.52) and Southern (see 7.64) |
| ETS12 | chk1::kanMX6 | Chk1::KanMX6 Ade6-704 Leu1-32 Ura4D18 | G418r, ura-, ade-, leu- | h- | |

| | | | | | |
|---|---|---|---|---|---|
| YFS64 | fan1:: NAT (14152) chk1::kan | ade6-M216 "MTMR::NAT" chk1::kanMX | NATr, G418r | h- | YFS60XETS12, isolate B1 |
| YFS65 | fan1:: NAT (14152) chk1::kan | ade6-M216 "MTMR::NAT" chk1::kanMX | NATr, G418r | h+ | YFS60XETS12, isolate C1 |
| SAL181 | pso2-d | ade6-704, leu1-32, pso2::kanMX6, ura4-D18 | KANr, ura-, ade-, leu- | h- | |
| YFS68 | fan1:: NAT (14152) pso2::kan | ade6-M216 "MTMR::NAT" pso2::kanMX | NATr, G418r | h- | YFS60XSAL181, isolate A2 |
| YFS69 | fan1:: NAT (14152) pso2::kan | ade6-M216 "MTMR::NAT" pso2::kanMX | NATr, G418r | h+ | YFS60XSAL181, isolate A4 |
| YFS70 | mlh1-3HA | mlh1-loxP-3HA-loxM | G418r | h+ | derived from YFS31 (x 503) col.A4 (see Western 7.59) |
| YFS71 | pms1-P-6xFLAG-M | pms1-loxP-6xFLAG-loxM | G418r | h+ | Derived from YFS27; col. A2 (see Western 7.46) |
| YFS72 | pms1-P-6xFLAG-M | pms1-loxP-6xFLAG-loxM | G418r | h+ | Derived from YFS27; col. A4 (see Western 7.46) |
| YFS73 | fan1:: NAT msh2:: kan | ade6-M216 "MTMR::NAT" msh2::kanMX6 leu1-32 ade6-704 ura4-D18 | NATr, G418r | h- | YFS19 crossed with YFS60 |
| YFS74 | fan1:: NAT msh2:: kan | ade6-M216 "MTMR::NAT" msh2::kanMX6 leu1-32 ade6-704 ura4-D18 | NATr, G418r | h+ | YFS19 crossed with YFS60 |

| | | | | | |
|---|---|---|---|---|---|
| YFS75 | fan1::NAT (3909) chk1::kan | leu1-32 ura4-D18 ade6-M? SPBC146.06c::NAT chk1::kanMX | NATr, G418r | h+ | YFS59XETS12, isolate 3 |
| YFS76 | fan1::NAT (3909) chk1::kan | leu1-32 ura4-D18 ade6-M? SPBC146.06c::NAT chk1::kanMX | NATr, G418r | h- | YFS59XETS12, isolate 4 |
| YFS77 | fan1::NAT (3909) pso2::kan | leu1-32 ura4-D18 ade6-M? SPBC146.06c::NAT pso2::kanMX | NATr, G418r | h- | YFS59XSAL181, isolate 1 |
| YFS78 | fan1::NAT (3909) pso2::kan | leu1-32 ura4-D18 ade6-M? SPBC146.06c::NAT pso2::kanMX | NATr, G418r | h+ | YFS59XSAL181, isolate 2 |
| YFS79 | fan1::NAT QUERY STRAIN Q1 (derived from 3909) | ade6-M210; leu1-32; ura4-D18; mat1_m-cyhS, smt0; rpl42::cyhR (sP56Q) fan1::NATMX (derived from YFS59) | NATr, CyhS | h- | YFS59 x AMC400; from tetrad analysis (spore 1) 2 checked NATr, CyhS + segregation of rpl42::cyhR locus by tetrad analysis |
| YFS80 | fan1::NAT QUERY STRAIN Q2 (derived from 3909) | ade6-M210; leu1-32; ura4-D18; mat1_m-cyhS, smt0; rpl42::cyhR (sP56Q) fan1::NATMX (derived from YFS59) | NATr, CyhS | h- | YFS59 x AMC400; isolate 3; checked NATr, CyhS. Random spores, but rpl42::cyhR locus checked by test crosses |
| YFS81 | fan1::NAT QUERY STRAIN Q3 (derived from 14152) | ade6-M210; leu1-32; ura4-D18; mat1_m-cyhS, smt0; rpl42::cyhR (sP56Q) fan1::NATMX (derived from YFS60) | NATr, CyhS | h- | YFS60 x AMC400; isolate 5; checked NATr, CyhS. Random spores, but rpl42::cyhR locus checked by test crosses |
| YFS82 | fan1::NAT QUERY STRAIN Q4 (derived from 14152) | ade6-M210; leu1-32; ura4-D18; mat1_m-cyhS, smt0; rpl42::cyhR (sP56Q) fan1::NATMX (derived from YFS60) | NATr, CyhS | h- | YFS60 x AMC400; from tetrad analysis (spore 3) 2 checked NATr, CyhS + segregation of rpl42::cyhR locus by tetrad analysis |

| YFS83 | Query base strain (AMC400) | ade6-M210; leu1-32; ura4-D18; mat1_m-cyhS, smt0; rpl42::cyhR (sP56Q) | CyhS | h- | AMC400 = P392 = THS3181 (strain received from Tim Humphrey) (see Roguev et al., 2007) |
|---|---|---|---|---|---|
| YFS84 | fan1D msh2D (derived from 3909) | leu1-32 ura4-D18 ade6-M? SPBC146.06c::NAT msh2::kanMX | NATr, G418r | h- | YFS59XYFS19; isolate 5 |
| YFS89 | fan1-d msh2-d (derived from 3909) | leu1-32 ura4-D18 ade6-M? SPBC146.06c::NAT msh2::kanMX | NATr, G418r | h- | YFS59XYFS19; isolate 3 |
| YFS90 | mlh1-3HA | mlh1-loxP-3HA-loxM | G418r | h+ | derived from YFS31 (x 503) col.C1 (see Western 7.59) |
| YFS91 | fan1-13myc pms1-6xFLAG | 501 fan1-loxP-13myc-loxM pms1-loxP-6xFLAG-loxM | G418r | ? | YFS49 X YFS71, col. D1 (see Western blot 7.60) |
| YFS92 | fan1-13myc pms1-6xFLAG | 501 fan1-loxP-13myc-loxM pms1-loxP-6xFLAG-loxM | G418r | ? | YFS49 X YFS71, col. D3 (see Western blot 7.60) |
| JMM21 | fen1-d | ade6-704, leu1-32, rad2::ura4, ura4-D18 | ura+, ade-, leu- | h- | |
| YFS93 | fan1-d (3909) fen1-d | leu1-32 ura4-D18 ade6-M? SPBC146.06c::NAT fen1::ura+ | NATr ura+ | h+ | YFS59 X JMM21, isolate 2 |
| YFS94 | fan1-d (3909) fen1-d | leu1-32 ura4-D18 ade6-M? SPBC146.06c::NAT fen1::ura+ | NATr ura+ | h- | YFS59 X JMM21, isolate 6 |
| YFS95 | fan1-d (14152) fen1-d | ade6-M216 "MTMR::NAT" fen1::ura+ | NATr ura+ | h+ | YFS60 X JMM21, isolate 2 |

| JMM38 | exo1-d | exo1::ura4, leu1-32, ura4-D18 | ura+, leu- | h+ | |
|---|---|---|---|---|---|
| YFS96 | exo1-d (h-version derived from JMM38) | exo1::ura4+; leu1-32; ura4-D18 | ura4+ | h- | JMM38 X 501 (isolate 2); see JMM38; from GP1055, strain from P. Sgankasi |
| YFS97 | exo1-d (h+ version derived from JMM38) | exo1::ura4+; leu1-32; ura4-D18 | ura4+ | h+ | JMM38 X 501 (isolate 4); see JMM38; from GP1055, strain from P. Sgankasi; ### BACKUP STRAIN, USE JMM38 INSTEAD) ### |
| YFS101 | msh6-d (h-version derived from Izumi Miyabe's IMS480) | | G418r; ade-; ura- | h- | IMS480 X 501 (col.6) |
| YFS102 | msh6Δ (h-version derived from Izumi Miyabe's IMS480) | | G418r; ade-; ura- | h- | IMS480 X 501 (col.3) |
| YFS103 | mlh1-d (h-version from Izumi Miyabe's IMS482) | | G418r; ade-; ura- | h- | IMS482 X 501 (col.3) |
| YFS104 | mlh1-d (h-version from Izumi Miyabe's IMS482) | | G418r; ade-; ura- | h- | IMS482 X 501 (col.4) |
| YFS105 | pms1-d (h-version from Izumi Miyabe's IMS483) | | G418r; ade-; ura- | h- | IMS483 X 501 (col.2) |

| | | | | | |
|---|---|---|---|---|---|
| YFS106 | pms1-d (h-version from Izumi Miyabe's IMS483) | | G418r; ade-; ura- | h- | IMS483 X 501 (col.1) |
| YFS107 | msh3-d (h-version derived from Izumi Miyabe's IMS481) | | G418r; ade-; ura- | h- | IMS481 X 501 (col. 1) |
| YFS108 | msh3-d (h-version derived from Izumi Miyabe's IMS481) | | G418r; ade-; ura- | h- | IMS481 X 501 (col. 5) |
| AMC77 | rad13-d | ade6-704, leu1-32, rad13::ura4, ura4-D18 | ura+, ade-, leu- | h- | |
| YFS109 | fan1-d (3909) rad13-d | leu1-32 ura4-D18 ade6-M? SPBC146.06c::NAT rad13::ura4+ | NATr, ura+ | h+ | YFS59XAMC77; col. 1 |
| YFS110 | fan1D (3909) rad13-d | leu1-32 ura4-D18 ade6-M? SPBC146.06c::NAT rad13::ura4+ | NATr, ura+ | h- | YFS59XAMC77; col. 4 |
| YFS111 | fan1-d (14152) rad13-d | ade6-M216 "MTMR::NAT" rad13::ura4+ | NATr, ura+ | h- | YFS60XAMC77; col. 2 |
| YFS112 | fan1-d (14152) rad13-d | ade6-M216 "MTMR::NAT" rad13::ura4+ | NATr, ura+ | h+ | YFS60XAMC77; col. 5 |
| YFS115 | fan1-d (3909) mlh1-d | leu1-32 ura4-D18 ade6-M? SPBC146.06c::NAT mlh1::kanMX | NATr, G418r | h- | YFS59 X YFS103; col. 3 |

| YFS116 | fan1-d (3909) mlh1-d | leu1-32 ura4-D18 ade6-M? SPBC146.06c::NAT mlh1::kanMX | NATr, G418r | h- | YFS59 X YFS103; col. 8 |
|---|---|---|---|---|---|
| YFS117 | fan1-d (14152) mlh1-d | ade6-M216 "MTMR::NAT" mlh1::kanMX | NATr, G418r | h+ | YFS59 X YFS103; col. 6 |
| YFS118 | fan1-d (14152) mlh1-d | ade6-M216 "MTMR::NAT" mlh1::kanMX | NATr, G418r | h+ | YFS59 X YFS103; col. 8 |
| YFS119 | fan1-d (3909) pms1-d | leu1-32 ura4-D18 ade6-M? SPBC146.06c::NAT pms1::kanMX | NATr, G418r | h- | YFS59 X YFS105; col. 3 |
| YFS120 | fan1-d (3909) pms1-d | leu1-32 ura4-D18 ade6-M? SPBC146.06c::NAT pms1::kanMX | NATr, G418r | h+ | YFS59 X YFS105; col. 4 |
| YFS121 | fan1-d (14152) pms1-d | ade6-M216 "MTMR::NAT" pms1::kanMX | NATr, G418r | h+ | YFS59 X YFS105; col. 5 |
| YFS122 | fan1-d (14152) pms1-d | ade6-M216 "MTMR::NAT" pms1::kanMX | NATr, G418r | h- | YFS59 X YFS105; col. 6 |
| YFS123 | fan1-d (3909) exo1-d | leu1-32 ura4-D18 ade6-M? SPBC146.06c::NAT exo1::ura4+ | NATr; ura+ | h+ | YFS59 X YFS96; col.3 |
| YFS124 | fan1-d (3909) exo1-d | leu1-32 ura4-D18 ade6-M? SPBC146.06c::NAT exo1::ura4+ | NATr; ura+ | h- | YFS59 X YFS96; col.8 |
| YFS125 | fan1-d (14152) exo1-d | ade6-M216 "MTMR::NAT"exo1 ::ura4+ | NATr; ura+ | h- | YFS60 X YFS96; col.5 |

| YFS126 | fan1-d (14152) exo1-d | ade6-M216 "MTMR::NAT"exo1 ::ura4+ | NATr; ura+ | h- | YFS60 X YFS96; col.7 |
|---|---|---|---|---|---|
| JMM1814 | rhp18-d | ade6-704, leu1-32, rhp18::ura4, ura4-D18 | ura+, leu-, ade- | h- | |
| YFS127 | fan1-d (3909) rhp18-d | leu1-32 ura4-D18 ade6-M? SPBC146.06c::NAT rhp18::ura4+ | NATr; ura+ | h+ | YFS59 X JMM1814; col.1 |
| YFS128 | fan1-d (3909) rhp18-d | leu1-32 ura4-D18 ade6-M? SPBC146.06c::NAT rhp18::ura4+ | NATr; ura+ | h- | YFS59 X JMM1814; col.2 |
| YFS129 | fan1-d (14152) rhp18-d | ade6-M216 "MTMR::NAT"rhp18::ura4+ | NATr; ura+ | h+ | YFS60 X JMM1814; col.1 |
| YFS130 | fan1-d (14152) rhp18-d | ade6-M216 "MTMR::NAT"rhp18::ura4+ | NATr; ura+ | h- | YFS60 X JMM1814; col.3 |
| YFS131 | pso2-d exo1-d | pso2::kanMX exo1::ura+ | G418r, ura+ | h+ | SAL181 X JMM38; col. 1 |
| YFS132 | pso2-d exo1-d | pso2::kanMX exo1::ura+ | G418r, ura+ | h- | SAL181 X JMM38; col. 2 |
| YFS135 | fan1-13myc mlh1-3HA | 501 fan1-loxP-13myc-loxM mlh1-loxP-3xHA-loxM | G418r | ? | YFS49 X YFS70, spore E2 (see Western blot 7.68) |
| YFS139 | fan1D strain ("PN"3909) pso2D | leu1-32 ura4-D18 ade6-M? SPBC146.06c::kanR pso2::kanR | G418r | h+ | YFS17XSAL181; spore C2 |

| YFS140 | fan1-d strain ("PN"3909) pso2-d | leu1-32 ura4-D18 ade6-M? SPBC146.06c::kanR pso2::kanR | G418r | h+ | YFS17XSAL181; spore C3 |
|---|---|---|---|---|---|
| YFS141 | fan1-d strain ("PN"3909) pso2-d | leu1-32 ura4-D18 ade6-M? SPBC146.06c::kanR pso2::kanR | G418r | h+ | YFS17XSAL181; spore H1 |
| YFS142 | pso2-d msh2-d | 501 pso2::kanMX msh2::kanMX | G418r | h+ | SAL182XYFS19; spore C2 |
| YFS143 | pso2-d msh2-d | 501 pso2::kanMX msh2::kanMX | G418r | h+ | SAL182XYFS19; spore C3 |
| YFS144 | fan1-d (derived from 3909) pso2-d msh2-d | leu1-32 ura4-D18 ade6-M? SPBC146.06c::NATr pso2::kanR msh2::kanR | G418r NATr | ? | YFS59XYFS143; spore B3 |
| YFS145 | fan1-d (derived from 14152) pso2-d msh2-d | ade6-M216 "MTMR::NAT" pso2::kanR msh2::kanR | G418r NATr | ? | YFS60 X YFS143; spore D1 |
| YFS146 | fan1-d (derived from 14152) pso2-d msh2-d | ade6-M216 "MTMR::NAT" pso2::kanR msh2::kanR | G418r NATr | ? | YFS60 X YFS143; spore E3 |
| YFS147 | fan1-d (derived from 3909) pso2-d exo1-d | leu1-32 ura4-D18 ade6-M? SPBC146.06c::NATr pso2::kanR exo1::ura+ | G418r Natr ura+ | ? | YFS123 X SAL181; col. 3 |
| YFS148 | fan1-d (derived from 3909) pso2-d exo1-d | leu1-32 ura4-D18 ade6-M? SPBC146.06c::NATr pso2::kanR exo1::ura+ | G418r Natr ura+ | ? | YFS123 X SAL181; col. 1 |
| YFS149 | fan1-d (derived from 14152) pso2-d exo1-d | ade6-M216 "MTMR::NAT" pso2::kanR exo1::ura+ | G418r Natr ura+ | ? | YFS125 X SAL182; col.1 |

| | | | | | |
|---|---|---|---|---|---|
| YFS150 | fan1-d (derived from 14152) pso2-d exo1-d | ade6-M216 "MTMR::NAT" pso2::kanR exo1::ura+ | G418r Natr ura+ | ? | YFS125 X SAL182; col.3 |
| SAL261 | rhp51-d | ade6-704, leu1-32, rhp51::kanMX6, smt-0, ura4-D18 | G418r, ade-, leu-, ura- | h- | |
| YFS155 | fan1-d (derived from 3909) rhp51-d | leu1-32 ura4-D18 ade6-M? SPBC146.06c::NATr rhp51::kanR | NATr G418r | h+ | YFS59 X SAL261; col. 2 |
| YFS156 | fan1-d (derived from 3909) rhp51-d | leu1-32 ura4-D18 ade6-M? SPBC146.06c::NATr rhp51::kanR | NATr G418r | h- | YFS59 X SAL261; col. 7 |
| YFS157 | exo1-d msh2-d | exo1::ura4+; msh2::kanMX6 leu1-32; ura4-D18 | ura4+; G418r | h- | YFS96 X YFS19; col.1 |
| YFS158 | exo1-d msh2-d | exo1::ura4+; msh2::kanMX6 leu1-32; ura4-D18 | ura4+; G418r | h+ | YFS96 X YFS19; col.3 |
| YFS159 | fan1-d (derived from 3909) pso2-d rad13-d | leu1-32 ura4-D18 ade6-M? SPBC146.06c::NATr pso2::kanR rad13::ura+ | G418r NATr ura+ | ? | YFS78 X AMC77; col.2 |
| YFS160 | fan1-d (derived from 3909) pso2-d rad13-d | leu1-32 ura4-D18 ade6-M? SPBC146.06c::NATr pso2::kanR rad13::ura+ | G418r NATr ura+ | ? | YFS78 X AMC77; col.3 |
| YFS161 | fan1-d (derived from 14152) pso2-d rad13-d | ade6-M216 "MTMR::NAT" pso2::kanR rad13::ura+ | G418r NATr ura+ | ? | YFS69 X AMC77; col. 2 |
| YFS162 | fan1-d (derived from 14152) pso2-d rad13-d | ade6-M216 "MTMR::NAT" pso2::kanR rad13::ura+ | G418r NATr ura+ | ? | YFS69 X AMC77; col. 6 |

| | | | | | |
|---|---|---|---|---|---|
| YFS163 | fan1-d (derived from 3909) pso2-d rhp18-d | leu1-32 ura4-D18 ade6-M? SPBC146.06c::NATr pso2::kanR rhp18::ura+ | G418r NATr ura+ | ? | YFS127 X SAL181; col.1 |
| YFS164 | fan1-d (derived from 3909) pso2-d rhp18-d | leu1-32 ura4-D18 ade6-M? SPBC146.06c::NATr pso2::kanR rhp18::ura+ | G418r NATr ura+ | ? | YFS127 X SAL181; col 7 |
| YFS165 | fan1-d (derived from 14152) pso2-d rhp18-d | ade6-M216 "MTMR::NAT" pso2::kanR rhp18::ura+ | G418r NATr ura+ | ? | YFS129 X SAL181; col. 1 |
| YFS166 | fan1-d (derived from 14152) pso2-d rhp18-d | ade6-M216 "MTMR::NAT" pso2::kanR rhp18::ura+ | G418r NATr ura+ | ? | YFS129 X SAL181; col. 5 |
| SAL161 | rad3-d | ade6-704, leu1-32, rad3::kanMX6, ura4-D18 | G418r, ura-, ade-, leu- | h- | |
| YFS171 | fan1-d (derived from 3909) rad3-d | leu1-32 ura4-D18 ade6-M? SPBC146.06c::NAT rad3::kanMX | NATr, G418r | h- | YFS59 X SAL161; col. 3 |
| YFS172 | fan1-d (derived from 3909) rad3-d | leu1-32 ura4-D18 ade6-M? SPBC146.06c::NAT rad3::kanMX | NATr, G418r | h+ | YFS59 X SAL161; col. 1 |
| YFS173 | fan1-d (derived from 14152) rad3-d | ade6-M216 "MTMR::NAT" rad3::kanMX | NATr, G418r | h+ | YFS60 X SAL161; col. 3 |
| YFS174 | fan1-d (derived from 14152) rad3-d | ade6-M216 "MTMR::NAT" rad3::kanMX | NATr, G418r | h+ | YFS60 X SAL161; col. 4 |
| AMC293 | cds1-d | cds1::ura4, leu1-32, ura4-D18 | ura+, leu-, ura- | h- | |

| YFS175 | fan1-d (derived from 3909) cds1-d | leu1-32 ura4-D18 ade6-M? SPBC146.06c::NAT cds1::ura+ | NATr, ura+ | h- | YFS59 X AMC293; col. 2 |
|---|---|---|---|---|---|
| YFS176 | fan1-d (derived from 3909) cds1-d | leu1-32 ura4-D18 ade6-M? SPBC146.06c::NAT cds1::ura+ | NATr, ura+ | h+ | YFS59 X AMC293; col. 3 |
| YFS177 | fan1-d (derived from 14152) cds1-d | ade6-M216 "MTMR::NAT" cds1::ura+ | NATr, ura+ | h+ | YFS60 X AMC293; col. 4 |
| YFS178 | fan1-d (derived from 14152) cds1-d | ade6-M216 "MTMR::NAT" cds1::ura+ | NATr, ura+ | h- | YFS60 X AMC293; col. 5 |
| YFS179 | fan1-d (derived from 14152) rhp51-d | ade6-M216 "MTMR::NAT" rad51::kanR | NATr, G418r | h- | YFS60 X SAL261; col. 1 |
| YFS180 | fan1-d (derived from 14152) rhp51-d | ade6-M216 "MTMR::NAT" rad51::kanR | NATr, G418r | h+ | YFS60 X SAL261; col. 8 |
| YFS181 | fan1:: NAT (14152) pso2-d rhp51-d | ade6-M216 "MTMR::NAT" pso2::kanMX rhp51::kanMX | NATr, G418r | ? | YFS69XSAL261, tetrads 2:2, spore D4 |
| YFS182 | fan1:: NAT (14152) pso2-d rhp51-d | ade6-M216 "MTMR::NAT" pso2::kanMX rhp51::kanMX | NATr, G418r | ? | YFS69XSAL261, tetrads 2:2, spore I2 |
| YFS183 | fan1-d (derived from 3909) pso2-d rhp51-d | leu1-32 ura4-D18 ade6-M? SPBC146.06c::NAT pso2::kanMX rhp51::ura+ | NATr, G418r, ura+ | ? | YFS78xIMS22; col.5 |
| YFS184 | fan1-d (derived from 3909) pso2-d rhp51-d | leu1-32 ura4-D18 ade6-M? SPBC146.06c::NAT pso2::kanMX rhp51::ura+ | NATr, G418r, ura+ | ? | YFS78xIMS22; col.1 |

| | | | | | |
|---|---|---|---|---|---|
| YFS185 | fan1-d (derived from 3909) pso2-d rhp51-d | leu1-32 ura4-D18 ade6-M? SPBC146.06c::NAT pso2::kanMX rhp51::ura+ | NATr, G418r, ura+ | ? | YFS78xIMS22; col.7 |
| YFS186 | pso2-d rhp51-d | pso2::kanMX6 rhp51::ura4+ | G418r, ura+ | ? | SAL182xIMS22; col.1 |
| YFS187 | pso2-d rhp51-d | pso2::kanMX6 rhp51::ura4+ | G418r, ura+ | ? | SAL182xIMS22; col.4 |
| YFS188 | pso2-d rhp51-d | pso2::kanMX6 rhp51::ura4+ | G418r, ura+ | ? | SAL182xIMS23; col.3 |
| YFS189 | rad13-d pso2-d | rad13::ura4+ pso2::kanMX6 | ura4+, G418r | ? | AMC77xSAL182; col.1 |
| YFS190 | rad13-d pso2-d | rad13::ura4+ pso2::kanMX6 | ura4+, G418r | ? | AMC77xSAL182; col.4 |
| YFS191 | rhp18-d pso2-d | rhp18::ura+ pso2::kanMX6 | ura4+, G418r | ? | JMM1814xSAL182; col. 1 |
| YFS192 | rhp18-d pso2-d | rhp18::ura+ pso2::kanMX6 | ura4+, G418r | ? | JMM1814xSAL182; col. 5 |
| YFS193 | fan1 base strain | loxP-ura4+-loxM3 fan1 base strain | ura4+ | h+ | 503 transformed with linear fragment (1st step RMCE); col. 5. Sequenced ok (loxP and loxM3 sites) |
| YFS194 | fan1 base strain | loxP-ura4+-loxM3 fan1 base strain | ura4+ | h+ | 503 transformed with linear fragment (1st step RMCE); col. 5. NOT sequenced |

| | | | | | |
|---|---|---|---|---|---|
| KAF1177 | rhp18::kanMX6 | ade6-704, leu1-32, rhp18::kanMX6, ura4-D18 | G418r, ura-, leu-, ade- | h+ | |
| YFS197 | fan1D (3909) rhp18D | leu1-32 ura4-D18 ade6-M? SPBC146.06c::NAT rhp18::kanMX | NATr, G418r | ? | YFS59xKAF1177; col.1 |
| YFS198 | fan1-d (14152) rhp18-d | ade6-M216 "MTMR::NAT" rhp18::kanMX | NATr, G418r | ? | YFS60xKAF1177; col.2 |
| YFS199 | fan1-d (14152) rhp18-d | ade6-M216 "MTMR::NAT" rhp18::kanMX | NATr, G418r | ? | YFS60xKAF1177; col.3 |
| YFS200 | fan1-d (14152) rhp18-d | ade6-M216 "MTMR::NAT" rhp18::kanMX | NATr, G418r | ? | YFS60xKAF1177; col.4 |
| AMC75 | rad17-d | ade6-704, leu1-32, rad17::ura4, ura4-D18 | ura+, ade-, leu- | h- | |
| YFS207 | fan1-d (3909) rad17-d | leu1-32 ura4-D18 ade6-M? SPBC146.06c::NAT rad17::ura4+ | NATr, ura+ | ? | YFS59xAMC75; col.2 |
| YFS208 | fan1-d (3909) rad17-d | leu1-32 ura4-D18 ade6-M? SPBC146.06c::NAT rad17::ura4+ | NATr, ura+ | ? | YFS59xAMC75; col.3 |
| YFS209 | fan1-d (14152) rhp18-d | ade6-M216 "MTMR::NAT" rhp18::kanMX | NATr, G418r | ? | YFS60xAMC75; col. 2 |
| YFS210 | fan1-d (14152) rhp18-d | ade6-M216 "MTMR::NAT" rhp18::kanMX | NATr, G418r | ? | YFS60xAMC75; col. 3 |

MATERIALS AND METHODS

| | | | | | |
|---|---|---|---|---|---|
| AMC79 | rad9-d | ade6-704, leu1-32, rad9::ura4, ura4-D18 | ura+, ade-, leu- | h- | |
| YFS211 | fan1-d (3909) rad9-d | leu1-32 ura4-D18 ade6-M? SPBC146.06c::NAT rad9::ura4+ | NATr, ura+ | ? | YFS59xAMC79; col.1 |
| YFS212 | fan1-d (3909) rad9-d | leu1-32 ura4-D18 ade6-M? SPBC146.06c::NAT rad9::ura4+ | NATr, ura+ | ? | YFS59xAMC79; col.3 |
| YFS213 | fan1-d (14152) rad9-d | ade6-M216 "MTMR::NAT" rad9::ura4+ | NATr, ura+ | ? | YFS60xAMC79; col. 2 |
| YFS214 | fan1-d (14152) rad9-d | ade6-M216 "MTMR::NAT" rad9::ura4+ | NATr, ura+ | ? | YFS60xAMC79; col. 3 |
| YFS215 | rad1-d | rad1::ura4+ | ura+ | h- | JMM319x501; col., 3 |
| YFS216 | pli1-d | pli1::natMX6 | NATr | h- | FZW1981x501; col. 2 |
| YFS217 | pli1-d | pli1::natMX6 | NATr | h- | FZW1981x501; col. 6 |
| YFS221 | pli1-d pso2-d | pli1::natMX6 pso2::kanMX6 | NATr G418r | ? | SAL181xFWZ1981; col. 1 |
| YFS222 | pli1-d pso2-d | pli1::natMX6 pso2::kanMX6 | NATr G418r | ? | SAL181xFWZ1981; col. 5 |

| | | | | | |
|---|---|---|---|---|---|
| YFS223 | fan1-d (3909) rad1-d | leu1-32 ura4-D18 ade6-M? SPBC146.06c::NAT rad1::ura4+ | NATr ura4+ | ? | YFS59xYFS215; col. 1 |
| YFS224 | fan1-d (3909) rad1-d | leu1-32 ura4-D18 ade6-M? SPBC146.06c::NAT rad1::ura4+ | NATr ura4+ | ? | YFS59xYFS215; col. 2 |
| YFS225 | fan1-d (14152) rad1-d | ade6-M216 "MTMR::NAT" rad1::ura4+ | NATr ura4+ | ? | YFS60xYFS215; col. 1 |
| YFS226 | fan1-d (14152) rad1-d | ade6-M216 "MTMR::NAT" rad1::ura4+ | NATr ura4+ | ? | YFS60xYFS215; col. 4 |
| YFS228 | fan1 base strain pso2-d | loxP-ura4+-loxM3 fan1 base strain pso2::kanMX6 | G418r ura+ | h+ | YFS193xSAL181; col. 1 |
| YFS229 | fan1 base strain pso2-d | loxP-ura4+-loxM3 fan1 base strain pso2::kanMX6 | G418r ura+ | h+ | YFS193xSAL181; col. 5 |
| YFS230 | fan1-d (3909) pli1-d | leu1-32 ura4-D18 ade6-M? SPBC146.06c::kanMX6 pli1::natMX6 | G418r NATr | ? | YFS17xYFS216; col. 1 |
| YFS231 | fan1-d (3909) pli1-d | leu1-32 ura4-D18 ade6-M? SPBC146.06c::kanMX6 pli1::natMX6 | G418r NATr | ? | YFS17xYFS216; col. 4 |
| YFS232 | fan1-d (14152) pli1-d | ade6-M216 "MTMR::kan" pli1::natMX6 | G418r NATr | ? | YFS16xYFS216; col. 2 |
| YFS233 | fan1-d (14152) pli1-d | ade6-M216 "MTMR::kan" pli1::natMX6 | G418r NATr | ? | YFS16xYFS216; col. 5 |

| YFS237 | fan1-D651A | 501 loxP_fan1-D651A_loxM | ade-ura-leu- | ? | RMCE: colony DA2A. Vector sequenced: ok (top + bottom strand); genome sequenced: ok but unsequenced gaps (see separate file). |
|---|---|---|---|---|---|
| YFS240 | fan1-D651N | 501 loxP_fan1-D651N_loxM | ade-ura-leu- | ? | RMCE: colony DN1D. Vector sequenced: ok (top + bottom strand); genome sequenced: ok but unsequenced gaps (see separate file). |
| YFS241 | fan1-K668A | 501 loxP_fan1-K668A_loxM | ade-ura-leu- | ? | RMCE: colony KA1A. Vector sequenced: ok (top + bottom strand); genome sequenced: ok but unsequenced gaps (see separate file). |
| YFS242 | fan1-K668A | 501 loxP_fan1-K668A_loxM | ade-ura-leu- | ? | RMCE: colony KA1B. Vector sequenced: ok (top + bottom strand). |
| YFS243 | fan1-E666Q K668A | 501 loxP_fan1-E666Q K668A_loxM | ade-ura-leu- | ? | RMCE: colony dm1A. Vector sequenced: ok (top + bottom strand); genome sequenced: ok but unsequenced gaps (see separate file). |
| YFS247 | fan1-D651A pso2D | 501 loxP_fan1-D651A_loxM pso2::kanMX6 | ade-ura-leu-G418r | ? | YFS77xYFS237; col 1 (checked G418r NATs) |
| YFS248 | fan1--d651A pso2-d | 501 loxP_fan1-D651A_loxM pso2::kanMX6 | ade-ura-leu-G418r | ? | YFS77xYFS237; col 2 (checked G418r NATs) |
| YFS249 | fan1--d651N pso2-d | 501 loxP_fan1-D651N_loxM pso2::kanMX6 | ade-ura-leu-G418r | ? | YFS77xYFS239; col 1 (checked G418r NATs) |
| YFS250 | fan1--d651N pso2-d | 501 loxP_fan1-D651N_loxM pso2::kanMX6 | ade-ura-leu-G418r | ? | YFS77xYFS239; col 2 (checked G418r NATs) |
| YFS251 | fan1-K668A pso2-d | 501 loxP_fan1-K668A_loxM pso2::kanMX6 | ade-ura-leu-G418r | ? | YFS77xYFS241; col 1 (checked G418r NATs) |

| YFS252 | fan1-K668A pso2-d | 501 loxP_fan1-K668A_loxM pso2::kanMX6 | ade-ura-leu-G418r | ? | YFS77xYFS241; col 2 (checked G418r NATs) |
| --- | --- | --- | --- | --- | --- |
| YFS253 | fan1-E666Q K668A pso2-d | 501 loxP_fan1-E666Q K668A_loxM pso2::kanMX6 | ade-ura-leu-G418r | ? | YFS77xYFS243; col 1 (checked G418r NATs) |
| YFS254 | fan1-E666Q K668A pso2-d | 501 loxP_fan1-E666Q K668A_loxM pso2::kanMX6 | ade-ura-leu-G418r | ? | YFS77xYFS243; col 2 (checked G418r NATs) |

| Strains used in APPENDIX 1 | Strains used in Chapter 3 | Strains used in Chapter 4 | Strains used in Chapter 5 | Strains used in Chapter 6 | Strains used in more than one chapter |
| --- | --- | --- | --- | --- | --- |

Note: in this table Δ, D or –d are used interchangeably to indicate a deletion mutant.

Chapter Three

BIOCHEMICAL CHARACTERISATION OF FAN1 IN
SCHIZOSACCHAROMYCES POMBE

## 3.1    Introduction

### 3.1.1    Spontaneous mutation rate as a readout for MMR pathway dysfunctions

The mismatch repair (MMR) pathway deals with deviations from the standard G/C and A/T DNA base pairing (Kunz et al., 2009).  The study of MMR activity has led to the development of several *in vivo* and *in vitro* systems to detect hallmarks of genomic instability such as single-base substitutions and microsatellite instability (Spampinato et al., 2009). A widely used methodology is based on the detection of phenotypic changes consequent to mutations incurred in a genetic marker (mutator phenotype). In yeast, such methods comprise forward or reverse mutation assays. In the first case, a diversified spectrum of mutations can lead to a mutator phenotype such as acquired resistance to a specific toxic compound or loss of prototrophy. Reverse mutation assays usually detect a specific type of mutations that needs to be reverted in order to generate a viable cell (Spampinato et al., 2009).

In this study, a forward mutation assay is used to detect the rate of spontaneous mutation in *fan1*-deleted fission yeast cells. The readout in this system is the switch from uracil prototrophy to uracil auxotrophy. Studies indicate that the estimated mutation rate during DNA replication in eukaryotic cells is lower than 1 mutation every $10^9$ bases (McCulloch and Kunkel, 2008). This level of mutation rate would be undetectable by current mutation assays. In *S. cerevisiae*, a mutation in the Polδ DNA polymerase catalytic subunit (Pol3-L615M) leads to a 7-fold increased spontaneous mutation rate with no measurable changes in other phenotypes monitored (Venkatesan et al., 2006). In this study, the spontaneous mutation rate was increased to detectable levels by using a strain harbouring the corresponding mutation in the polymerase Cdc6 (Cdc6-L591M). To determine mutation rates in *fan1*-d wild-type and mutator backgrounds, fluctuation analysis as described in Foster (2006) was used. The analysis of the results was performed by using the Lea-Coulson median estimator method (Rosche and Foster, 2000; Foster, 2006).

### 3.1.2    Use of recombinase-mediated cassette exchange to construct tagged strains

The recombinase-mediated cassette exchange (RMCE) method developed by Watson et al., (2008) was used to generate epitope-tagged strains. This cre/lox recombination system provides a rapid and efficient way to tag or replace target genes in *S. pombe.* The first step is the construction of a base strain by insertion of a loxP-*ura4$^+$*-loxM3 cassette at the site of interest. The second step is the transformation of the base strain with a plasmid carrying the tag or the replacement gene inserted within the loxP and loxM3 cassettes. The final step is the recombinational exchange between the sequences flanked by loxP and loxM3. A schematic of the procedure is shown in fig. 3.1.
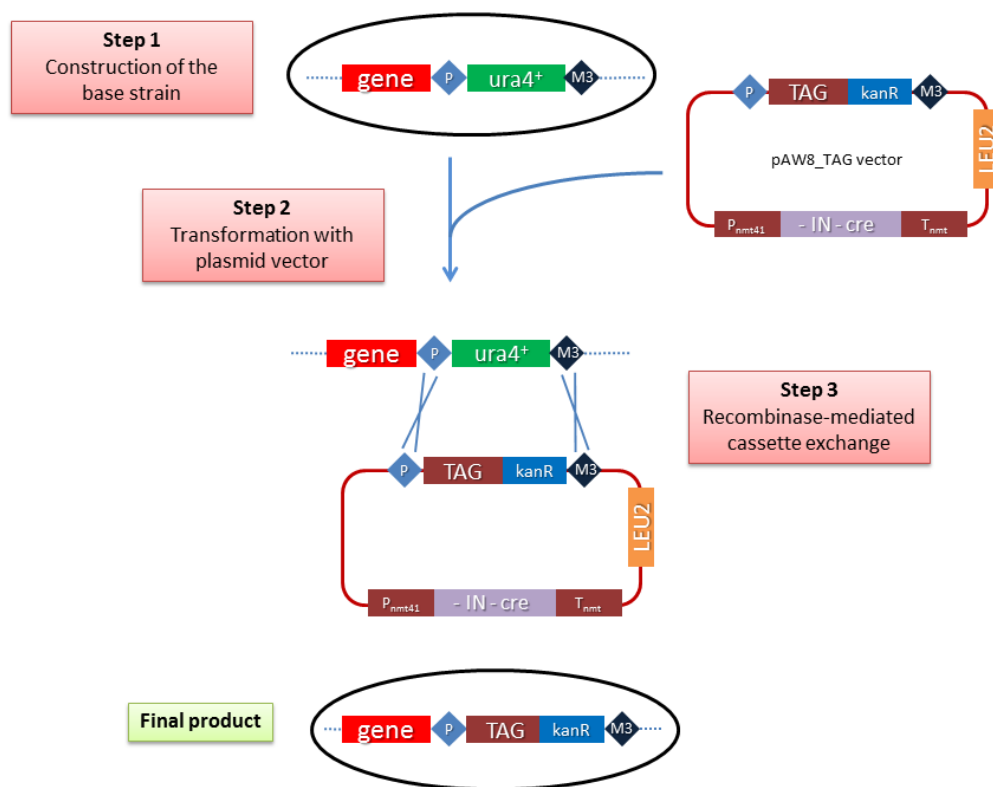


**Figure 3.1 | Schematic representation of Recombinase-Mediated Cassette Exchange (RMCE) to tag proteins of interest.** The base strain was constructed by standard molecular biology techniques. Dotted lines indicate cassettes located on a *S. pombe* chromosome. Crosses represent homologous recombination between loxP and loxM3 cassettes  Abbreviations: *ura4+*, *S. pombe* uracil marker; *LEU2*, *S. cerevisiae* leucine marker; gene, gene of interested to be tagged; P, loxP site; M3, mutant loxM3 site; P$_{nmt41}$, *S. pombe* nmt41 promoter; T$_{nmt}$, nmt terminator sequence; IN, *S. pombe rad50* intron 1; cre, gene coding for the recombinase Cre. Adapted from Watson et al., 2008.

## 3.2    Aim of this chapter

FAN1[Hs] (also known as KIAA1018) has been shown to interact with components of the mismatch repair (MMR) pathway such as MLH1, PMS1 and PMS2 (Cannavo et al., 2007; MacKay et al., 2010; Smogorzewska et al., 2010). The aim of this chapter is to investigate whether Fan1 plays a role in the MMR pathway in *S. pombe* by assessing physical protein-protein interactions and alterations in the spontaneous mutation rates in *fan1*-d strains.

## 3.3    Results

### 3.3.1    Southern blot analysis of Fan1[Sp] deletion mutants

Two independently-derived *fan1*-d mutants (*fan1*::*kanMX*; kanMX confers resistance to the drug geneticin, or G418) have been analysed in parallel in this study. The first mutant (3909) was kindly donated by Professor Paul Nurse; the second mutant (14152) is derived from the Bioneer® *S. pombe* deletion mutant library (http://pombe.bioneer.co.kr/). To test the correct disruption of the *fan1* cassette, genomic DNA from the two strains was extracted and analysed by Southern blot analysis following diagnostic digests by restriction endonucleases. Both the two mutant strains showed the expected size for *SalI*-digested genomic DNA (approximately 9880 bp) (fig. 3.2). However, 3909 in the *HindIII* digests showed a probed fragment approximately 300 bp shorter than expected (approximately 2500 bp compared to the expected 2818 bp). This apparent discrepancy is due to the *kanMX* cassette in the 3909 strain being inverted compared to the 14152 strain, as confirmed by sequencing of the two mutants. Thus, it can be concluded that the size of the fragments showed by Southern blot analysis confirmed the identity of the two independently derived *fan1* disruptants.

## a.
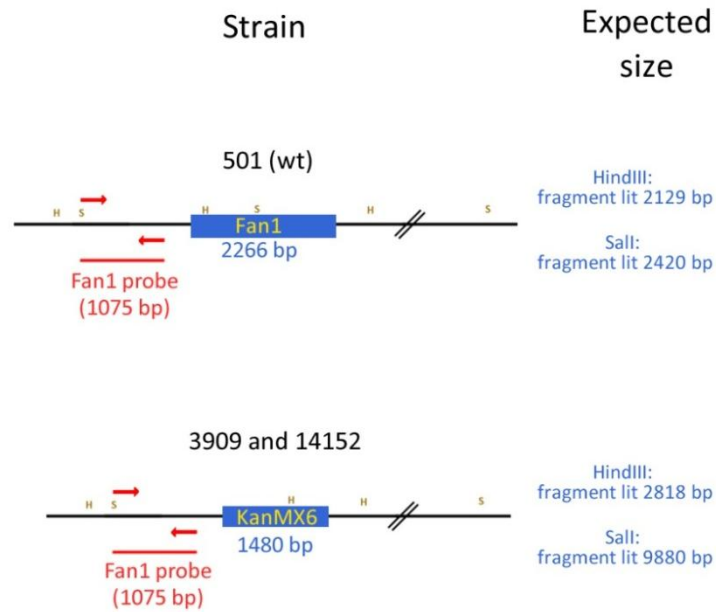


## b.
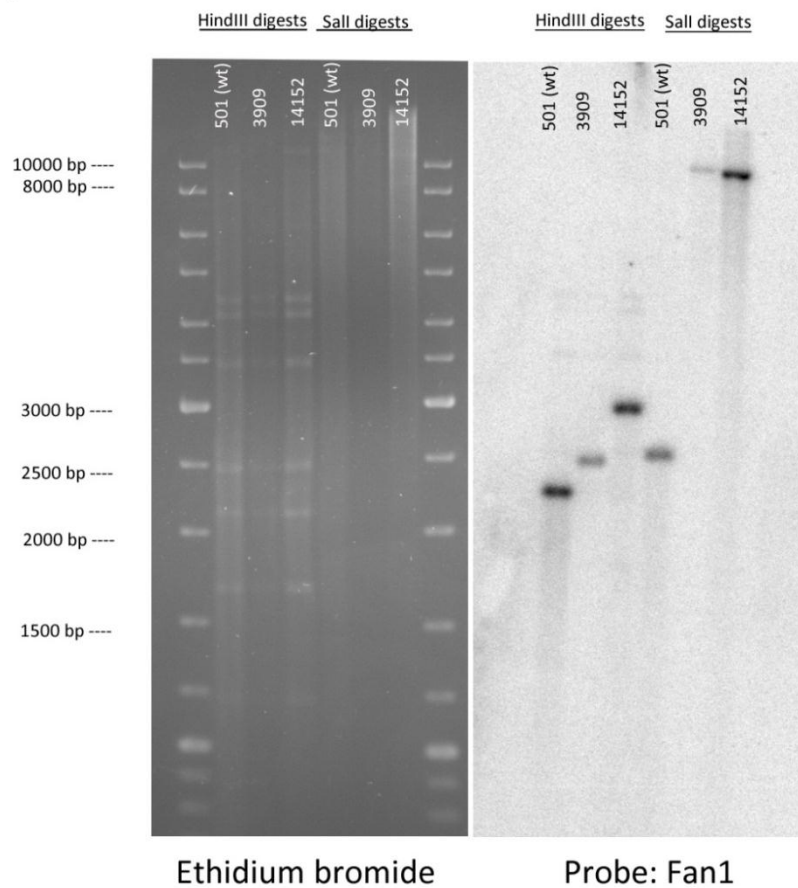


**Figure 3.2 | Southern blot analysis of the two independently-derived *fan1*-deleted strains, 3909 and 14152.** a. Schematic showing the expected size for the digests in the Southern analysis (Fan1 probe). b. The Southern blot analysis confirmed the identity of the two deleted strains. The slight size differences in the *HindIII* fragment are due to the inverted position of the kanMX6 cassette. H, *HindIII*; S, *SalI*.

### 3.3.2    **Western blot analysis of Fan1$^{Sp}$ double-tagged strains**

Three single tagged strains (Fan1-13myc, Mlh1-3HA, Pms1-6FLAG) were constructed using the RMCE method illustrated in fig. 3.1. The choice of these two components of the MMR pathway was based on parallel work showing that human FAN1 interacts *in vivo* with MLH1, PMS1 and PMS2 (Cannavo et al., 2007; MacKay et al., 2010; Smogorzewska et al., 2010). In *S. pombe*, Mlh1 (Mlh1$^{Sc}$, MLH1$^{Hs}$) and Pms1 (Pms1$^{Sc}$, PMS2$^{Hs}$) are part of the MutL$\alpha$ heterodimer, involved in the DNA repair complex assembly step of MMR (Marti et al., 2002; Marti et al., 2003). Whole cell (TCA) extracts of the two double tagged strains (Fan1-13myc Mlh1-3HA and Fan1-13myc Pms1-6FLAG) were analysed by Western blot. Single and double tagged proteins migrated with electrophoretic mobility lower than the expected based on their calculated protein mass (fig. 3.3, panels a and b). This could be due to technical factors such as running conditions and buffer composition of the SDS-PAGE performed. However, the relative electrophoretic mobility for the tagged proteins and the antibody specificity shown in this analysis reveal an acceptable consistency. Thus, it can be concluded that the Western blot analysis confirms the identity of the single and double tagged proteins constructed.

### 3.3.3    *S. pombe* **Fan1 does not associate with the mismatch repair proteins Mlh1 and Pms1**

To test whether Fan1 interacts with Mlh1 and Pms1 *in vivo*, cell extracts of Fan1-13myc Mlh1-3HA and Fan1-13myc Pms1-6FLAG double tagged strains were subjected to immuno-precipitation and western blot analysis. The western blot analysis of Fan1-13myc, Mlh1-3HA and the double tagged Fan1-13myc Mlh1-3HA immuno-precipitates confirmed the correct $\alpha$-myc immuno-purification of Fan1 in both Fan1-13myc and Fan1-13myc Mlh1-3HA (fig. 3.4, top gel, IP lanes). When the same samples were subjected to western blot analysis using the $\alpha$-HA antibody, a faint band corresponding to Mlh1-3HA was visible in the Fan1-13myc Mlh1-3HA IP lane, suggesting that Fan1 and Mlh1 co-immunoprecipitate (fig. 3.4, bottom gel, IP lanes).
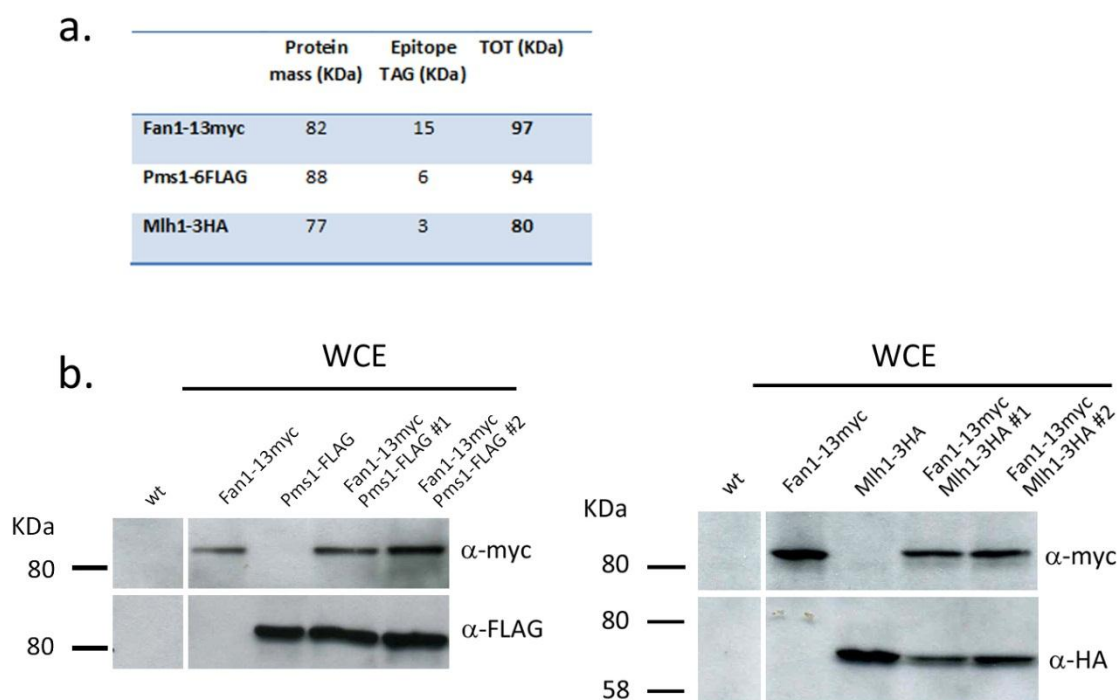
**Figure 3.3 | Western blot analysis of the Fan1$^{Sp}$ double tagged strains Fan1-13myc Pms1-6FLAG and Fan1-13myc Mlh1-3HA.** a. Calculated mass for the tagged proteins used in this study (source for proteins: http://old.genedb.org/genedb/pombe/; tag size estimated based on their sequence). b. Whole cell extracts of wild-type and tagged strains. Western blot analysis performed using the indicated antibodies on four separate 8% SDS-PAGE gels. Band sizes are estimated based on NEB® Prestained Protein Marker, Broad Range (not shown). The tagged proteins migrate with mobility lower than expected, but consistently with their relative calculated mass. WCE, whole cell extract (TCA extraction).

However, a similar faint band is visible also in the Mlh1-3HA (single tagged strain) IP lane. The simplest explanation for this result is that the immuno-purification with the α-myc antibody cross-reacts with other proteins, such as Mlh1-3HA. This explanation is consistent with the immuno-purification using the reciprocal antibody against HA (fig. 3.5). The western blot analysis with the α-HA antibody confirmed the correct immuno-precipitation of the single and the double tagged strains (Mlh1-3HA and Fan1-13myc Mlh1-3HA, respectively; fig. 3.5, top gel, IP lanes). However, no bands corresponding to the Fan1-13myc were identified in the immuno-precipitates subjected to western blot analysis with the α-myc antibody (fig. 3.5, bottom gel, IP

lanes). Thus, the immunoprecipitation with the α-HA antibody appears to be more specific than the immunoprecipitation performed with a α-myc antibody. This shows that the two proteins do not co-immunoprecipitate. Taken together, the western blot analysis on Fan1-13myc and Mlh1-3HA α-myc and α-HA immunoprecipitates excludes a strong interaction between the two proteins.

A similar result was obtained with the Fan1-13myc and Pms1-6FLAG immuno-precipitates. The α-myc western analysis on the α-myc pulldown confirmed the presence of Fan1 in the Fan1-13myc and Fan1-13myc Pms1-FLAG IP lanes (fig. 3.6, top gel, IP lanes). A faint band corresponding to the size expected for Pms1-FLAG was visible also in the Fan1-13myc Pms1-FLAG lane in the α-FLAG western blot (fig. 3.6, bottom gel, IP lanes). However, as a band of similar size was also visible in the Pms1-FLAG IP lane, this result demands some caution. In the reciprocal immuno-precipitation with the α-FLAG antibody, a strong band of the size expected for Fan1-13myc was shown in the α-myc western blot (fig. 3.7, bottom gel, IP lanes). This would suggest that Fan1-13myc co-immunoprecipitates with Pms1-FLAG in the α-FLAG pulldown. However, it cannot be excluded that Fan1-13myc is identified in this western blot due to non-specific precipitation of proteins and not due to specific protein-protein interactions.

### 3.3.4 *fan1*-d mutants do not exhibit an increase in spontaneous mutation rate

To further test a possible involvement of Fan1$^{Sp}$ in the mismatch repair system, a series of *fan1* deletion mutants were tested for increase in their spontaneous mutation rate. Forward mutation assays are routinely used as standard methods to determine increases in spontaneous mutation rate, strongly correlated with defects in the mismatch repair pathway (Spampinato et al., 2009). To further investigate a possible involvement of Fan1$^{Sp}$ in the resolution of base-base mismatches, a forward mutation assay was employed where the loss of uracil prototrophy was monitored in standard growing conditions.
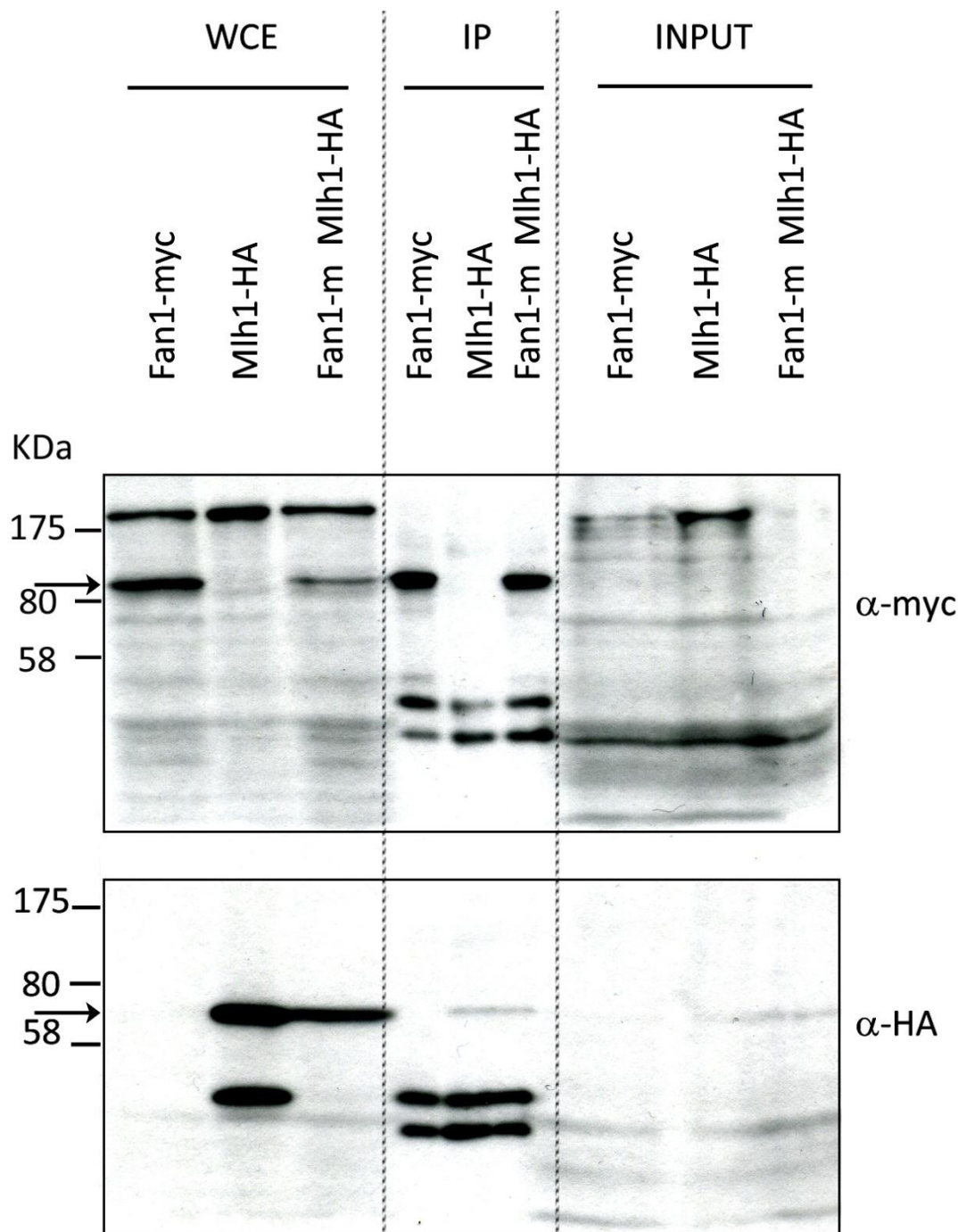
**Figure 3.4 | Western blot analysis of Fan1-13myc, Mlh1-3HA and Fan1-13myc Mlh1-3HA immunoprecipitates, α-myc pulldown.** Fan1-13myc and Mlh1-3HA do not co-immunoprecipitate in the α-myc pulldown. Top gel: western blot analysis with antibody against the myc epitope. The arrow indicates the size of the band expected for Fan1-13myc. Bottom gel: western blot analysis with antibody against the HA epitope. The arrow indicates the size of the band expected for Mlh1-3HA. The two 8% SDS-PAGE gels were loaded with the same samples and subjected to two independent western blot analyses. Band sizes are estimated based on NEB® Prestained Protein Marker, Broad Range. WCE, whole cell extract (TCA extraction); IP, immunoprecipitate: INPUT, 45% of the total lysate.
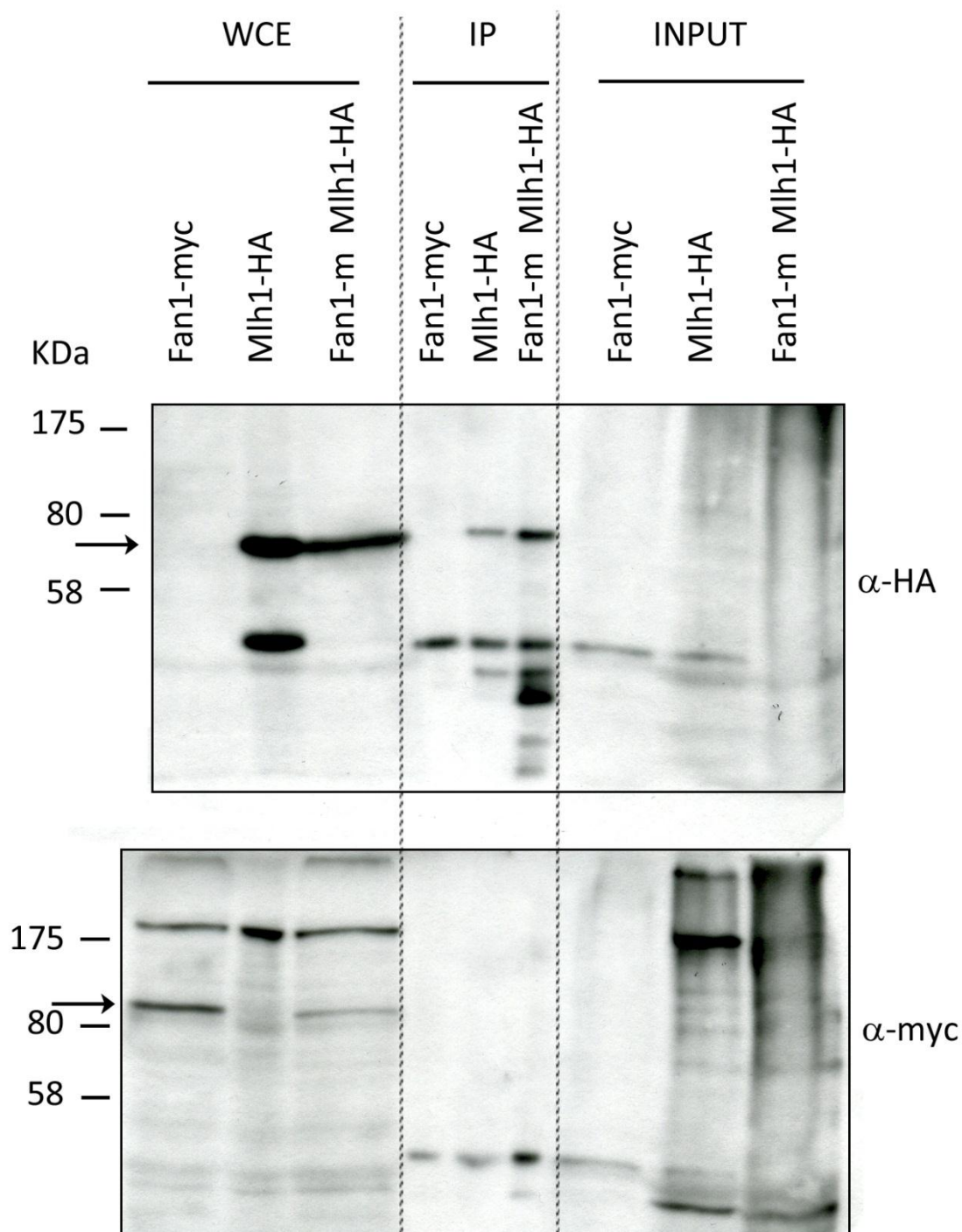
**Figure 3.5 | Western blot analysis of Fan1-13myc, Mlh1-3HA and Fan1-13myc Mlh1-3HA immunoprecipitates, α-HA pulldown.** Fan1-13myc and Mlh1-3HA do not co-immunoprecipitate in the α-HA pulldown. Top gel: western blot analysis with antibody against the HA epitope. The arrow indicates the size of the band expected for Mlh1-3HA. Bottom gel: western blot analysis with antibody against the myc epitope. The arrow indicates the size of the band expected for Fan1-13myc. The two 8% SDS-PAGE gels were loaded with the same samples and subjected to two independent western blot analyses. Band sizes are estimated based on NEB® Prestained Protein Marker, Broad Range. WCE, whole cell extract (TCA extraction); IP, immunoprecipitate: INPUT, 45% of the total lysate.
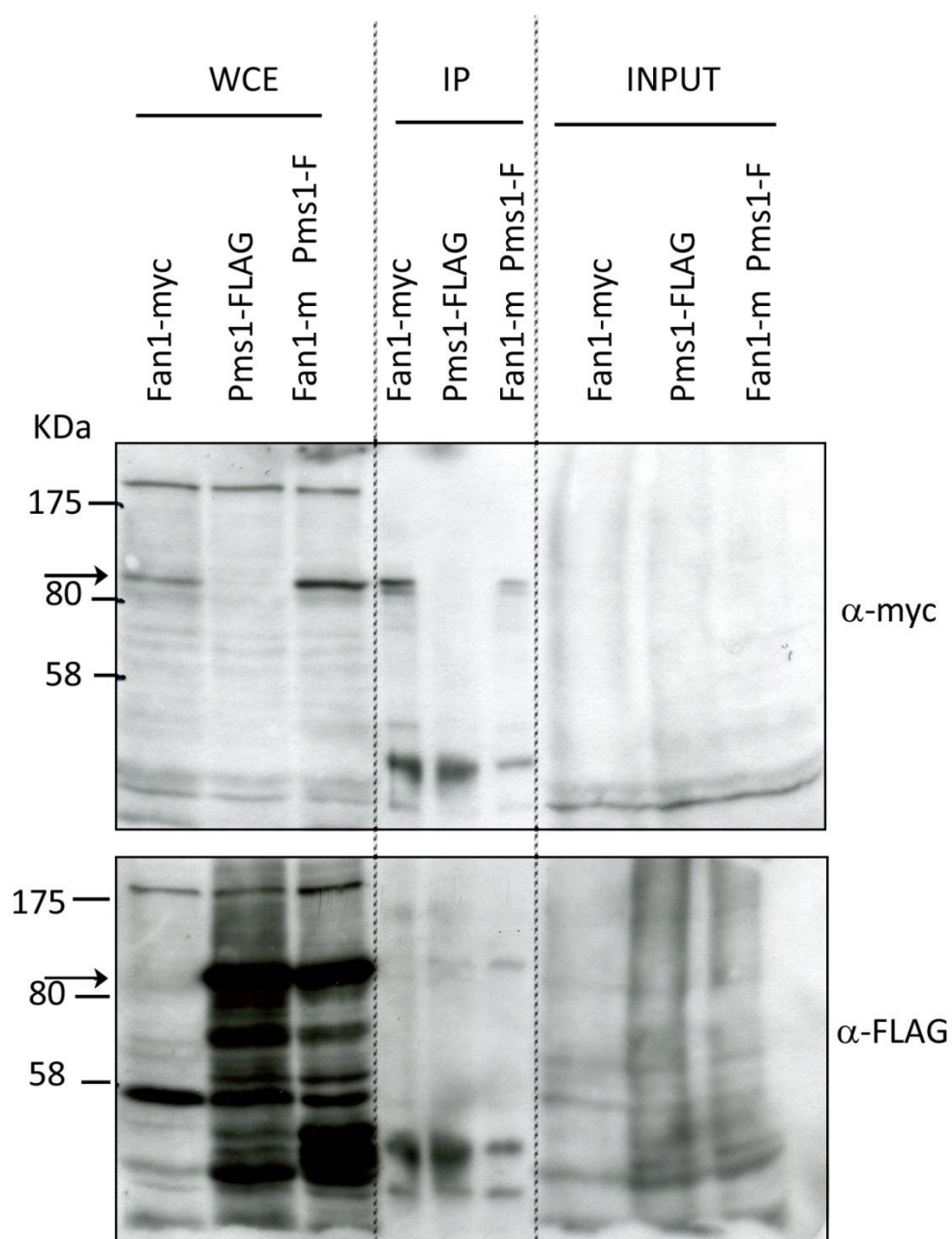
**Figure 3.6 | Western blot analysis of Fan1-13myc, Pms1-6FLAG and Fan1-13myc Pms1-6FLAG immunoprecipitates, α-myc pulldown.** Fan1-13myc and Pms1-6FLAG do not co-immunoprecipitate in the α-myc pulldown. Top gel: western blot analysis with antibody against the myc epitope. The arrow indicates the size of the band expected for Fan1-13myc. Bottom gel: western blot analysis with antibody against the FLAG epitope. The arrow indicates the size of the band expected for Pms1-FLAG. The two 8% SDS-PAGE gels were loaded with the same samples and subjected to two independent western blot analyses. Band sizes are estimated based on NEB® Prestained Protein Marker, Broad Range. WCE, whole cell extract (TCA extraction); IP, immunoprecipitate: INPUT, 45% of the total lysate.
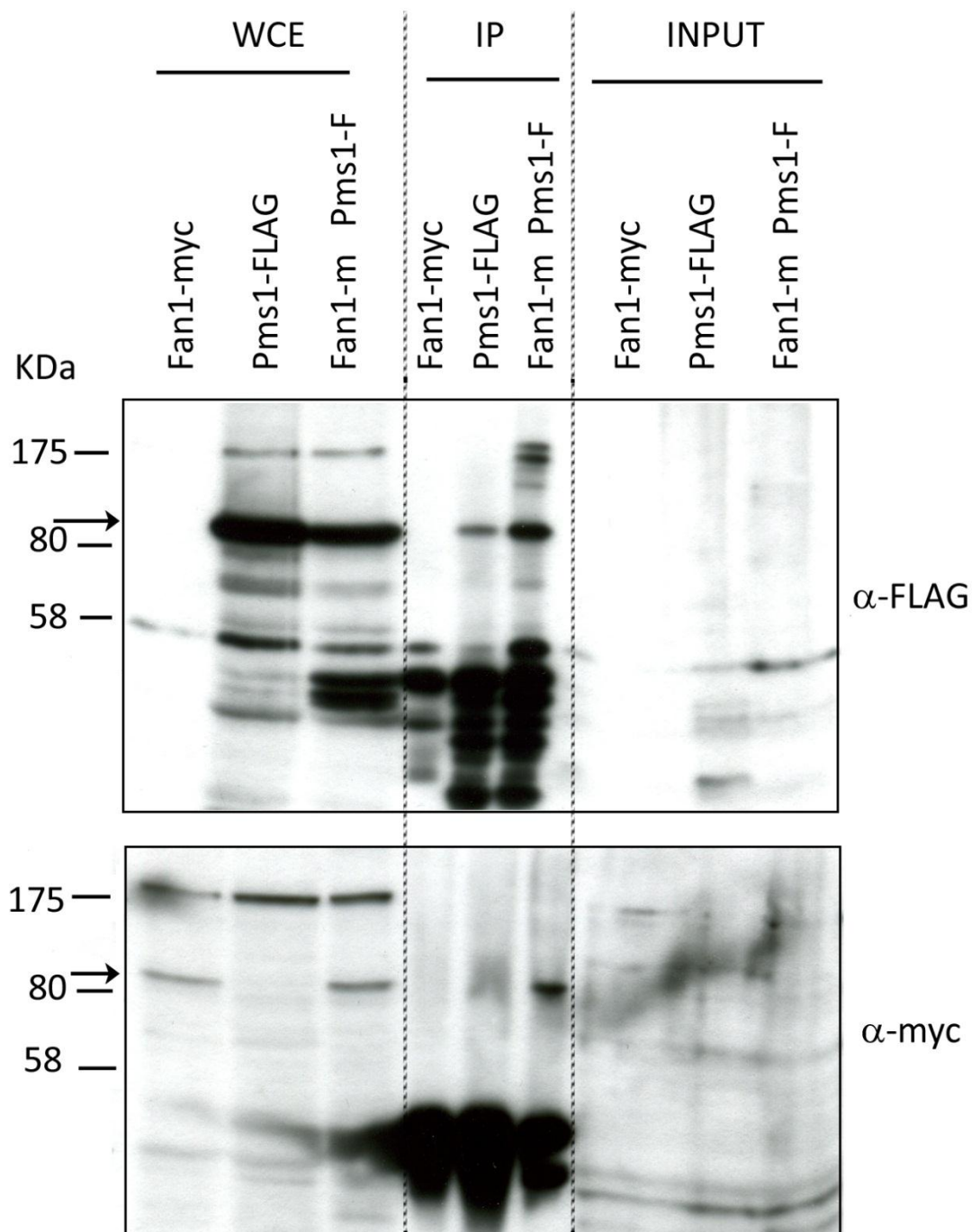
**Figure 3.7 | Western blot analysis of Fan1-13myc, Pms1-6FLAG and Fan1-13myc Pms1-6FLAG immunoprecipitates, α-FLAG pulldown.** A strong band corresponding to Fan1-13myc is shown in the α-FLAG pulldown, α-myc western blot. Top gel: western blot analysis with antibody against the FLAG epitope. The arrow indicates the size of the band expected for Pms1-FLAG. Bottom gel: western blot analysis with antibody against the myc epitope. The arrow indicates the size of the band expected for Fan1-13myc. The two 8% SDS-PAGE gels were loaded with the same samples and subjected to two independent western blot analyses. Band sizes are estimated based on NEB® Prestained Protein Marker, Broad Range. WCE, whole cell extract (TCA extraction); IP, immunoprecipitate: INPUT, 45% of the total lysate.

The *S. pombe* mutant *cdc6* -L591M was used as a background to increase the basal mutation rate to detectable levels, as the spontaneous mutation rate in a *cdc6*[+] background is in the order of 1 mutation every $10^9$ bases copied (table 3.1 and fig. 3.8). In a *cdc6* -L591M background, the mutation rate is increased by three orders of magnitude every $10^6$ bases copied. However, no significant increase in the spontaneous mutation rate was observed following deletion of *fan1* (table 3.1 and fig. 3.8). This data argued against a direct involvement of Fan1[Sp] in the MMR pathway. The deletion of Msh2[Sp] (central component of the MMR pathway) in a *cdc6*-L591M background would prove to be a good validation for the use of this assay to detect increased levels of mismatches. However, *msh2*-d *cdc6* -L591M is not viable (I. Miyabe, personal communication). For this reason, an alternative version of the system was used where a point mutation in the catalytic subunit of Polε (*cdc20*-M630F) leads to a milder mutator phenotype. In *S. cerevisiae,* the corresponding mutation *pol2*-M644F leads to a significant increase in the spontaneous mutation rate only when combined with an *msh6* deletion (Pursell et al., 2007). In a wt background, the deletion of *msh2* led to an increase in mutation rate up to $2.9*10^{-7}$ from undetectable levels in *msh2*[+] (table 3.1 and fig. 3.9, blue

| | Mutation rate/cell division | | | | | |
|---|---|---|---|---|---|---|
| | Experiment 1 | Experiment 2 | Experiment 3 | Average | Standard error | Fold elev. |
| *cdc6+* | 8.09E-10 | 5.27E-10 | 5.65E-10 | 6.33E-10 | 8.85E-11 | 1 |
| *cdc6+ fan1*-d (3909) | 9.98E-10 | 8.45E-10 | 9.17E-10 | 9.20E-10 | 4.42E-11 | 1 |
| *cdc6+ fan1*-d (14152) | 6.49E-10 | 5.74E-10 | 5.02E-10 | 5.75E-10 | 4.24E-11 | 1 |
| *cdc6*-L591M | 2.08E-06 | 1.08E-05 | 2.82E-06 | 5.25E-06 | 2.81E-06 | 1 |
| *cdc6*-L591M *fan1*-d (3909) | 2.55E-06 | 6.35E-06 | 3.37E-06 | 4.09E-06 | 1.16E-06 | 1 |
| *cdc6*-L591M *fan1*-d (14152) | 1.90E-06 | 2.93E-06 | 2.99E-06 | 2.61E-06 | 3.54E-07 | 0 |

**Table 3.1 | Spontaneous forward mutation rate of *fan1*-d mutants in cdc6+ and cdc6-L591M backgrounds.** Data from three independent experiments. For each strain, 11 colonies were grown to saturation at 30°C for 48 hours. Fluctuation analysis was performed as described in chapter 2. Spontaneous mutation rates were calculated by the Lea-Coulson method of the median (Rosche and Foster, 2000; Foster, 2006). Standard error: standard deviation divided by $\sqrt{3}$. Fold elevation calculated as ratio between the average of the mutant and the average of the corresponding background of reference (cdc6+ or cdc6-L591M). Fold elevation of value 0 reflects the reduction in spontaneous mutation rate displayed by Cdc6-L591M *fan1*-d (14152).
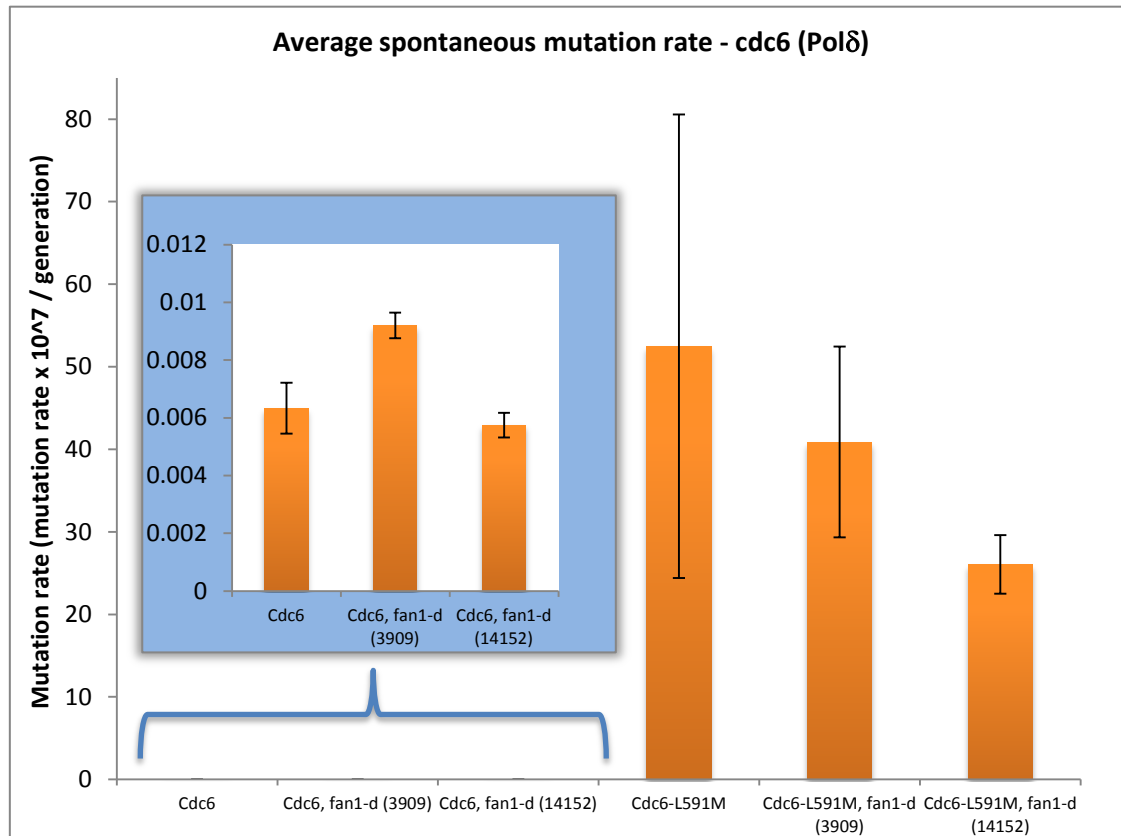
**Figure 3.8 | Spontaneous mutation rate of *fan1*-d mutants in *cdc6+* and *cdc6*-L591M backgrounds.** Bars represent the average of the three independent experiments in table 3.1. The spontaneous mutation rate is not increased in a *cdc6*-L591M background when *fan1* is deleted. Error bars represent the standard error of the mean, calculated as standard deviation divided by $\sqrt{3}$. Blue inset: expanded values on the Y axis for *cdc6+*, *cdc6+ fan1*-d (3909) and *cdc6+ fan1*-d (14152), which would not be visible with the main Y axis scale (left of the graph).

bars). When *msh2* is deleted in a *cdc20*-M630F background, the relative increase in mutation rate is approximately five fold, up to $1.5*10^{-6}$ (fig. 3.9, blue bars). As this experiment was only performed once, this data was compared to the data from a similar experiment performed in our laboratory by Dr I. Miyabe. The fold increase between the *cdc20+* and the *cdc20*-M630F strains in an *msh2*-deleted background was approximately four-fold, from $1*10^{-6}$ to $4.2*10^{-6}$ (fig. 3.9, red bars), consistent with the experiment performed for this study. This data confirms that the spontaneous mutation rate assay used in this study is an appropriate indicator of defects in the MMR pathway. A further confirmation that Fan1[Sp] is not directly involved in the resolution of base-base mismatches is the fact that when combined with the *cdc20*-M630F

mutation, the spontaneous mutation rate again did not fall within the detection limit of the assay (supplementary fig. 9.21). Taken together, these data indicate that Fan1[Sp] is not directly involved in the resolution of DNA base-base mismatches through the MMR pathway.

## 3.4    Discussion

### 3.4.1    Fan1[Sp] does not associate *in vivo* with MMR components and is not involved in the MMR pathway

In mammalian cells, FAN1[Hs] interacts *in vivo* with MLH1[Hs] and PMS2[Hs], ortholog of Pms1[Sp]



**Spontaneous Mutation Rate Assay - *cdc20 msh2*-d**

| | cdc20+, msh2-d | cdc20-M630F, msh2-d |
|---|---|---|
| This study | 2.90E-07 | 1.46E-06 |
| I. Miyabe | 1.03E-06 | 4.21E-06 |
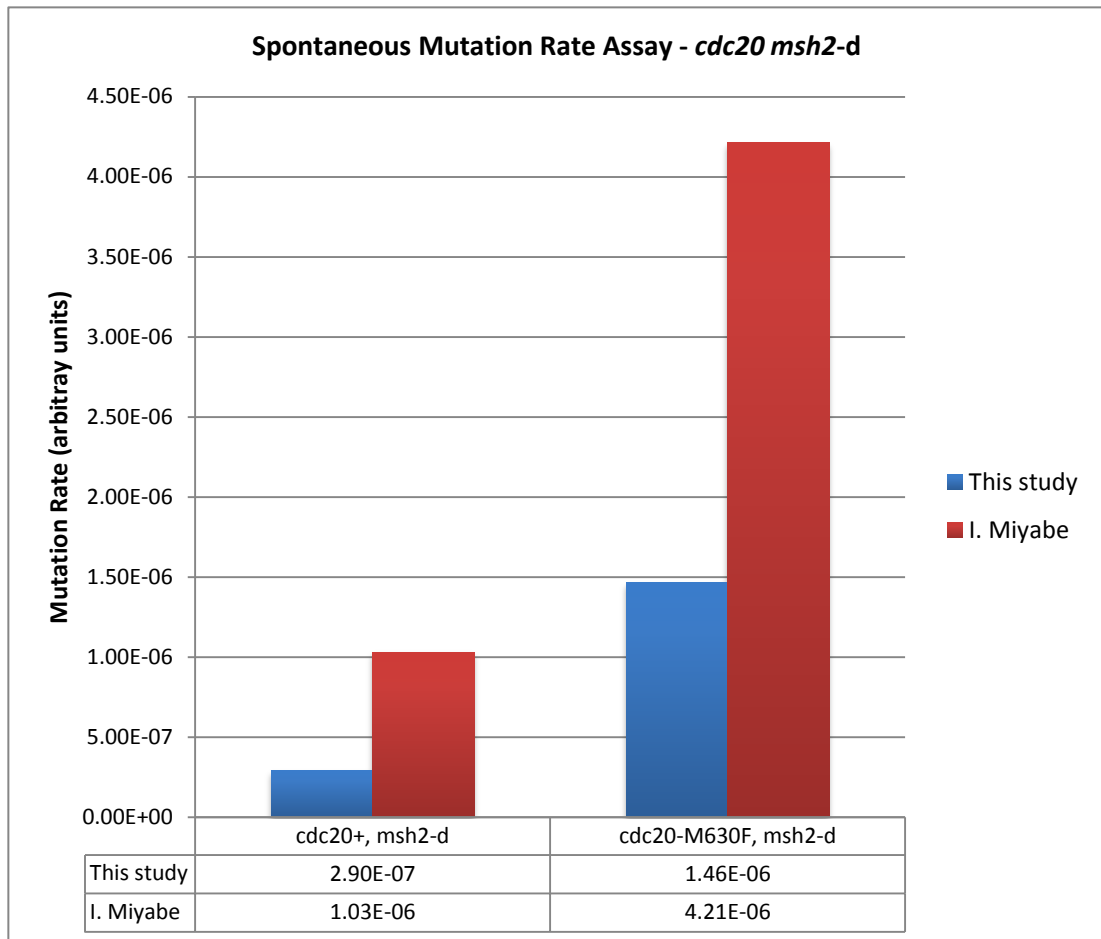
**Figure 3.9 | Spontaneous mutation rate of *msh2*-d mutants in a *cdc20* wt and *cdc20*-M630F backgrounds.** For each strain, 11 colonies were grown to saturation at 30°C for 48 hours. Fluctuation analysis was performed as described in chapter 2. Spontaneous mutation rates were calculated by the Lea-Coulson method of the median (Rosche and Foster, 2000; Foster, 2006). As the experiment in this study (blue bars) was performed only once, the result was compared with the result of a similar experiment obtained by Dr I. Miyabe (red bars). In both the experiments, a similar significant increase in the spontaneous mutation rate is shown in the *cdc20*-M630F compared to *cdc20+*.

(Cannavo et al., 2007; Smogorzewska et al., 2010; MacKay et al., 2010; Kratz et al., 2010). Despite this physical *in vivo* interaction, two lines of evidence suggest that in fact FAN1[Hs] is not directly involved in mismatch resolution. Firstly, it was shown that siRNA depletion of FAN1[Hs] in a MLH1-mutated background still induces sensitivity to ICL-inducing agents, indicating that FAN1[Hs] role is independent of the MMR status (Smogorzewska et al., 2010). Secondly, FAN1[Hs]-depleted cells are not sensitive to 6-thioguanine, a marker drug for the MMR pathway (MacKay et al., 2010). Despite the evidence excluding a direct role in the MMR pathway, the physical association found in mammalian cells still suggests a functional significance for the FAN1[Hs]-MMR interaction. Indeed, it has been proposed that human FAN1 might serve as a recruitment factor for MMR components to act at the ICL, possibly to correct mismatches arising as a consequence of the activity of error-prone translesion polymerases (Smogorzewska et al., 2010; MacKay et al., 2010).

The situation in *S. pombe* appears to differ. As presented above, in the western blot analysis of co-immunoprecipitation experiments no physical interaction between Fan1[Sp] and the homologous *S. pombe* MMR components Mlh1[Sp] and Pms1[Sp] were detected (figures 3.4 - 3.7). To further investigate the involvement of Fan1[Sp] in the MMR pathway, spontaneous mutation rate was calculated in *fan1*-deleted cells in *cdc6+* wild-type and *cdc6*-L591M mutated backgrounds. As *fan1*-d cells failed to show an increase in the spontaneous mutation rate compared to the control strains (fig. 3.8), a direct role for Fan1[Sp] in the MMR pathway could be ruled out. Taken together, the data presented here rules out a direct role for Fan1[Sp] in the repair of base-base mismatches.

## 3.5   Conclusions

A basic biochemical characterisation was presented in this chapter where a myc-tagged Fan1[Sp] was analysed by western blot for prospective interactions with components of the mismatch repair pathway. Furthermore, the direct involvement in the MMR pathway was tested by

spontaneous mutation rate in the absence of Fan1. Both the approaches gave negative results, indicating that Fan1 is not a novel member of the mismatch repair pathway. In the next chapter, an extensive genetic characterisation is presented, the aim of which is the integration of Fan1$^{Sp}$ into the *S. pombe* DNA damage responses.

Chapter Four

GENETIC CHARACTERISATION OF SCHIZOSACCHAROMYCES
POMBE FAN1: ASSESSMENT OF EPISTATIC INTERACTIONS BY
IN VIVO SURVIVAL ASSAYS

## 4.1    Introduction

### 4.1.1    Use of epistasis analysis to infer protein functions

In this chapter, *in vivo* survival assays are used to assign genetic interactions between Fan1[Sp] and known proteins involved in previously characterized pathways of DNA metabolism. In particular, this section presents an extensive use of the serial-dilution colony spotting assay, a highly standardized technique widely used to assess synergistic interactions between genes of interest. Profiting from the amenable genetics of the fission yeast, a series of double and triple null mutants can be rapidly created and exposed to increasing doses of a range of chemical agents known to induce specific subsets of lesions on the DNA molecule. Thus, the function of a protein can be deduced on the basis of the observed sensitivity of combinations of mutants to specific agents. According to the classical interpretation of genetic interactions, a gene is defined as epistatic to a second non-allelic gene if the phenotype of the deletion of the first gene is masked by the deletion of the second gene (Roth et al., 2009). In the case of exposure to DNA damaging agents, it is generally assumed that two genes involved in the same repair pathway show a similar phenotype (namely, augmented sensitivity compared to the wild-type gene) when either gene, or both, are deleted. Conversely, a non-epistatic interaction is assumed when the deletion of the second gene aggravates the sensitivity due to the deletion of the first gene. In this latter scenario, it can be deduced that the two genes code for proteins that act in distinct, compensatory pathways of DNA repair. Although these interpretations represent an oversimplification of interactions between gene products, they provide a simple logical framework to help infer the role of uncharacterized proteins.

### 4.1.2    DNA cross-linking agents used in this study

In order to understand the rationale behind the use of cross-linking agents in this study, it is useful to consider the molecular mechanisms underlying their cytotoxicity.

Cisplatin is commonly used in research as an inducer of DNA interstrand cross-links. However,

the majority of the lesions created by this agent are intrastrand cross-links (IaCL) between two adjacent purine bases (1,2-intrastrand cross-links), whereas 1,3-intrastrand cross-links and interstrand cross-links (ICLs) account for a more limited proportion of the total lesions (Brabec, 2002). The specific response of the DNA repair machinery to the different lesions caused by cisplatin is still unclear. It has been shown that 1,2- and 1,3-intrastrand cross-links are recognised by the mammalian NER apparatus. However, 1,2-intrastrand adducts are poor substrates for this repair pathway and they may represent the lesions responsible for cisplatin cytotoxicity (Zamble et al., 1996; Moggs et al., 1997).

The most commonly used agent belonging to the nitrogen mustard family of DNA interstrand cross-linking agents is bis(2-chloroethyl)methylamine (HN2, mechloretamine). The vast majority of lesions formed by this bi-functional alkylating agent are of mono-adducts, with a small proportion of ICLs that total 1-5% of the lesion burden (Lehoczký et al., 2007). However, in budding and fission yeast, HN2 ICLs have been shown to be the lesions responsible for the resulting cytotoxicity (McHugh et al., 1999; Lambert et al., 2003).

Mitomycin C is a naturally-derived antibiotic used experimentally for its capacity to form a significant proportion (approximately 13%) of non-distorting ICLs on the DNA molecule (Lehoczký et al., 2007).

The chemical structures and the degree of distortion induced by these agents on two opposing DNA bases in a duplex are illustrated in fig. 4.1. In this study, cisplatin has been widely used as an interstrand cross-linking agent. Despite the mixed proportion of adducts generated, following considerations of cost-effectiveness, chemical stability and data from pre-existing literature, this drug was thought to be the best choice for the current work. However, comparisons with MMC and HN2 are also reported and considered, where appropriate.
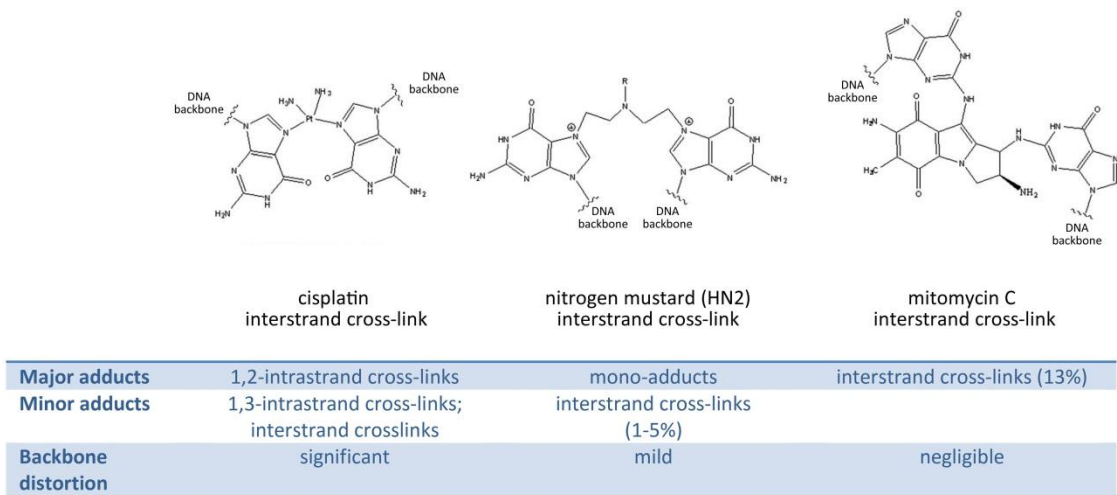
**Figure 4.1 |Structures and adducts created by the interstrand cross-linking agents used in this study.** The three chemical compounds used create a diversified range of adducts on the DNA molecule. The chemical structures illustrated here refer to distortions created by the interstrand cross-links portion of adducts. Chemical structures adapted from Hlavin et al., 2010; data from Brabec et al., 2002; Lehoczký et al., 2007.

## 4.2    Aim

The aim of this chapter is to define epistatic interactions of Fan1$^{Sp}$ with a selection of candidate genes by use of *in vivo* survival assays such as spot tests and survival curves. By exposing several combinations of null mutants to a range of DNA damaging agents, it is possible to identify synergistic effects leading to increased or decreased cell viability to specific subsets of DNA damage. The results from these assays lead to the assignment of genetic interactions between Fan1$^{Sp}$ and other known components participating in common and compensatory pathways of DNA metabolism.

## 4.3    Results

### 4.3.1    Fan1$^{Sp}$ is a novel component of the DNA damage response

To assess the response of *fan1*-d mutants to a variety of DNA lesions, the two Fan1$^{Sp}$ deletion mutants 3909 and 14152 were initially back-crossed twice to a wild-type strain and five independent G418-resistant colonies were isolated and tested under increasing concentrations of a selection of DNA damaging agents. All the *fan1* deletion isolates showed wild-type sensitivity to UV, camptothecin (CPT), methyl methanesulfonate (MMS) and hydroxyurea (HU)

(fig. 4.2). However, a subtle but reproducible sensitivity was shown when cells were exposed to cis-platinum diammine-dichloride (cisplatin, CDDP) and mitomycin C (MMC). These drugs belong to a family of DNA damaging agents that induce covalent cross-links between the two strands of a DNA molecule [interstrand cross-links, ICLs; reviewed in Lehoczký et al. (2007)]. The same pattern of sensitivity was observed for the five independent colonies derived from the second mutant 14152 (fig. 4.3). It should be noted that the independent deletion isolates
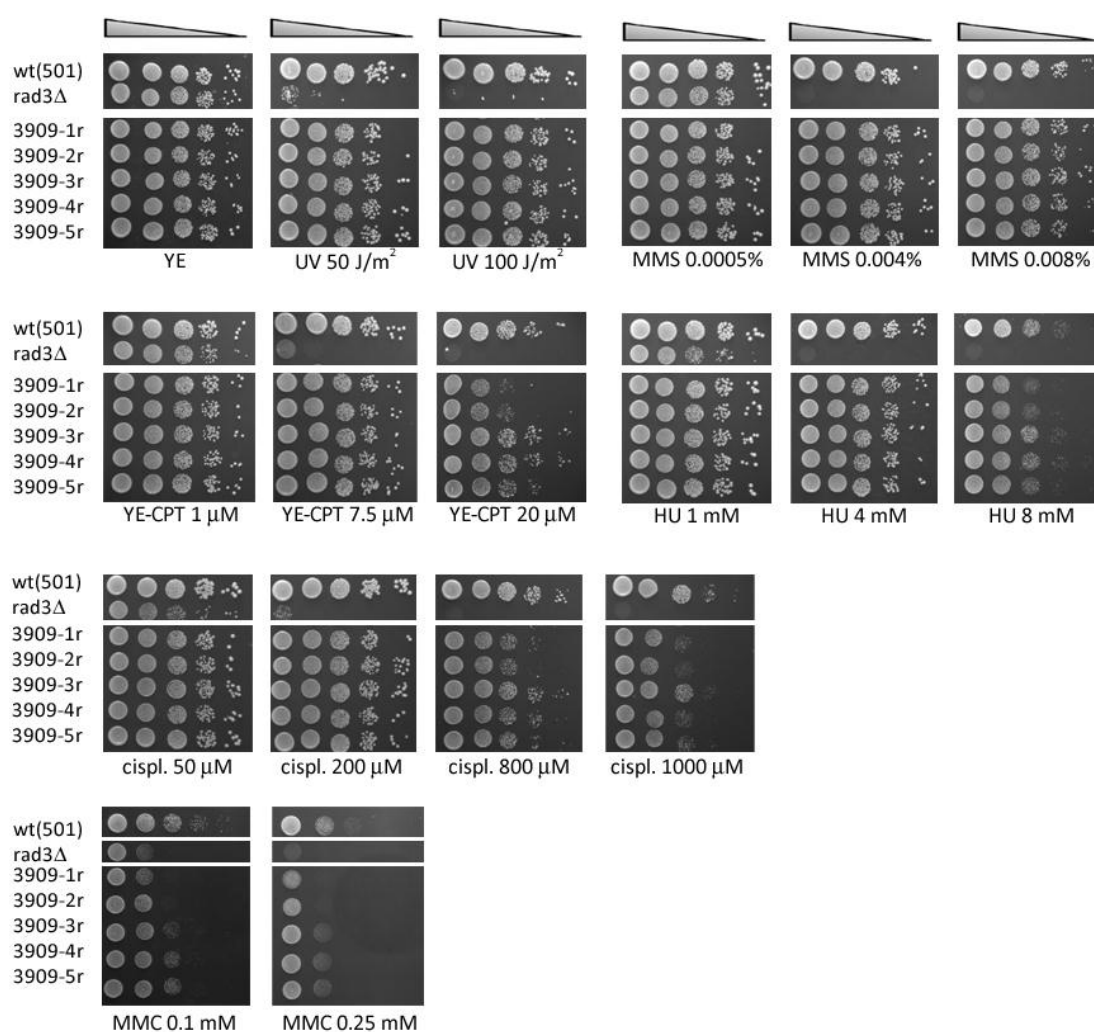


**Figure 4.2 | Sensitivity of Fan1$^{Sp}$ deletion isolates of mutant 1 (3909) to a variety of DNA damaging agents.** Logarithmically grown cultures were spotted in four 1:10 serial dilutions starting from $10^7$ cells (first spot on the left) on YEA plates containing the agents in the amount indicated. *rad3*-d is used as a standard hypersensitive control for the efficacy of the agents used. *fan1*-d isolates from mutant 3909 (3909-1r/5r) display a subtle but reproducible sensitivity to ICL-inducing agents. Abbreviations used: UV, Ultra-Violet irradiation; CPT, camptothecin; MMS, methyl methanesulfonate; HU, Hydroxyurea; cispl, cisplatin; MMC, mitomycin C.
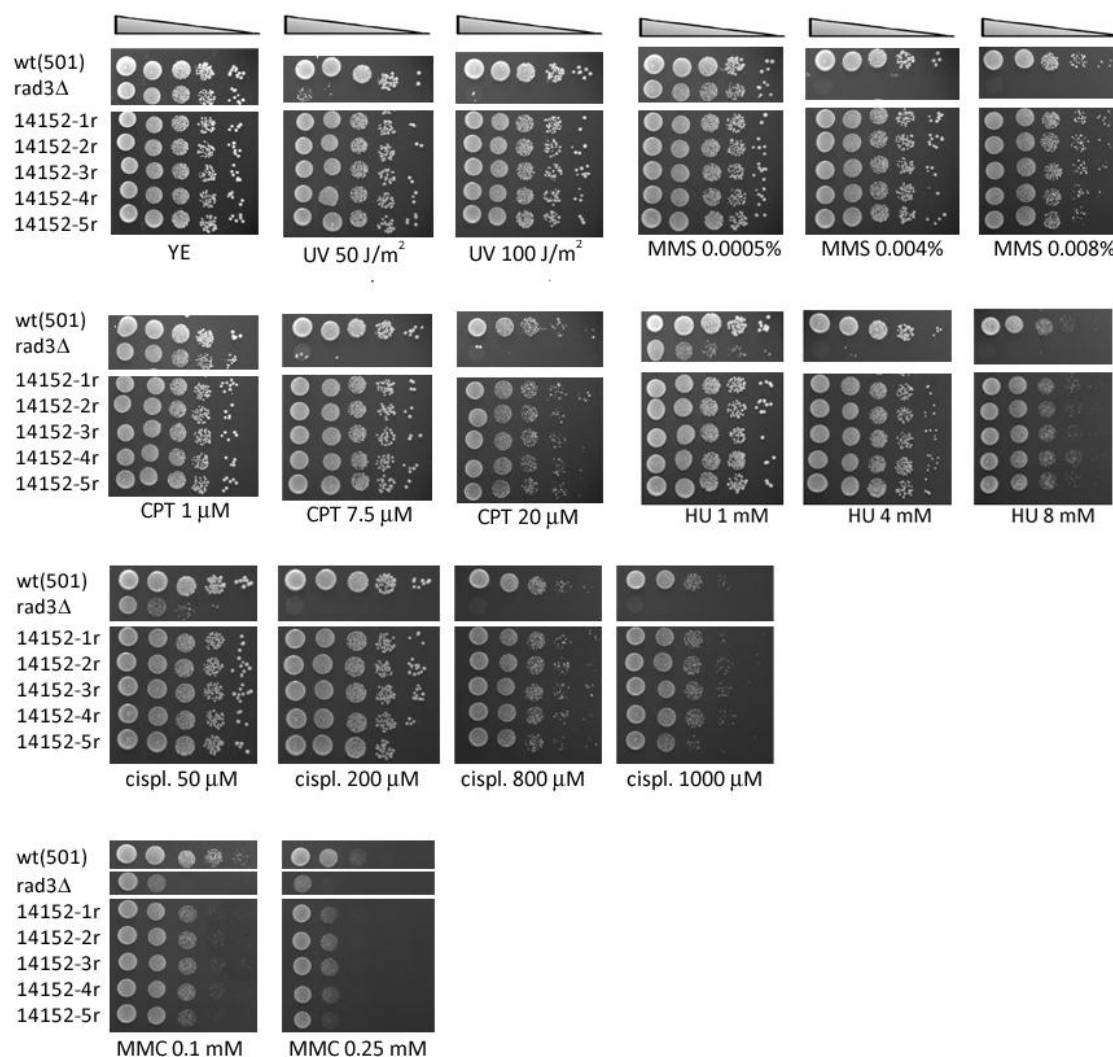
**Figure 4.3 | Sensitivity of Fan1$^{Sp}$ deletion isolates of mutant 1 (14152) to a variety of DNA damaging agents.** Logarithmically grown cultures were spotted in four 1:10 serial dilutions starting from $10^7$ cells (first spot on the left) on YEA plates containing the agents in the amount indicated. *rad3*-d is used as a standard hypersensitive control for the efficacy of the agents used. *fan1*-d isolates from mutant 14152 (14152-1r/5r) display a subtle but reproducible sensitivity to ICL-inducing agents. Abbreviations used: UV, Ultra-Violet irradiation; CPT, camptothecin; MMS, methyl methanesulfonate; HU, Hydroxyurea; cispl, cisplatin; MMC, mitomycin C.

display a variable degree of sensitivity to the drugs tested. It can be hypothesized that this is due to the effects of unknown suppressors in different isolates. However, albeit subtle, the sensitivity to DNA interstrand cross-linkers was reproducible for all the isolates. Thus, it could be concluded that this phenotype pointed towards a role for Fan1[Sp] in the repair of DNA interstrand cross-links.

### 4.3.2 Fan1[Sp] shows a non-epistatic interaction with Pso2[Sp] in response to cisplatin and mitomycin C

The mild sensitivity towards ICL-inducing agents suggested that Fan1[Sp] was implicated in ICL repair but its role overlapped with the function of other components of the DNA repair machinery. Thus, in the absence of Fan1[Sp], the repair of ICLs appears to be carried out through alternative pathways. To test this, the original 3909 and 14152 mutants were crossed with a series of deletion mutants of genes reported to be involved in the ICL resolution pathway, either in *S. pombe* or in the budding yeast *S. cerevisiae.* Although little is known about the resolution of DNA ICLs in *S. pombe*, the nuclease Pso2[Sp] (Snm1[Sc]) has been clearly shown to be specifically required for normal resistance to ICL-inducing agents (Lambert et al., 2003). To allow a flexible and rapid series of genetic crosses between different deletion mutants, the original *kanMX* deletion cassettes in the 3909 and 14152 strains were replaced with a *natMX6* deletion cassette, which confers resistance to nourseothricin (Hentges et al., 2005). The *natMX6* null mutants derived from 3909 and 14152 were named 3909N and 14152N, respectively. The two strains were shown to be G418s and were further checked by Southern blot analysis (see supplementary fig. 9.22).

When exposed to increasing doses of cisplatin and MMC, the *fan1 pso2* double mutant showed a dramatic reduction in viability compared to the single mutants and the wt strain (fig. 4.4). A slight increase in sensitivity was also shown following irradiation with UV. This observation is consistent with the finding that UV light induces a small amount of DNA interstrand cross-links (Love et al., 1986). No synergistic hypersensitivity was shown for MMS, CPT or HU (fig. 4.4). To rule out any possible effect due to the replaced *natMX6* deletion cassette, the assay was repeated with a *fan1 pso2* mutant generated by using the original 3909
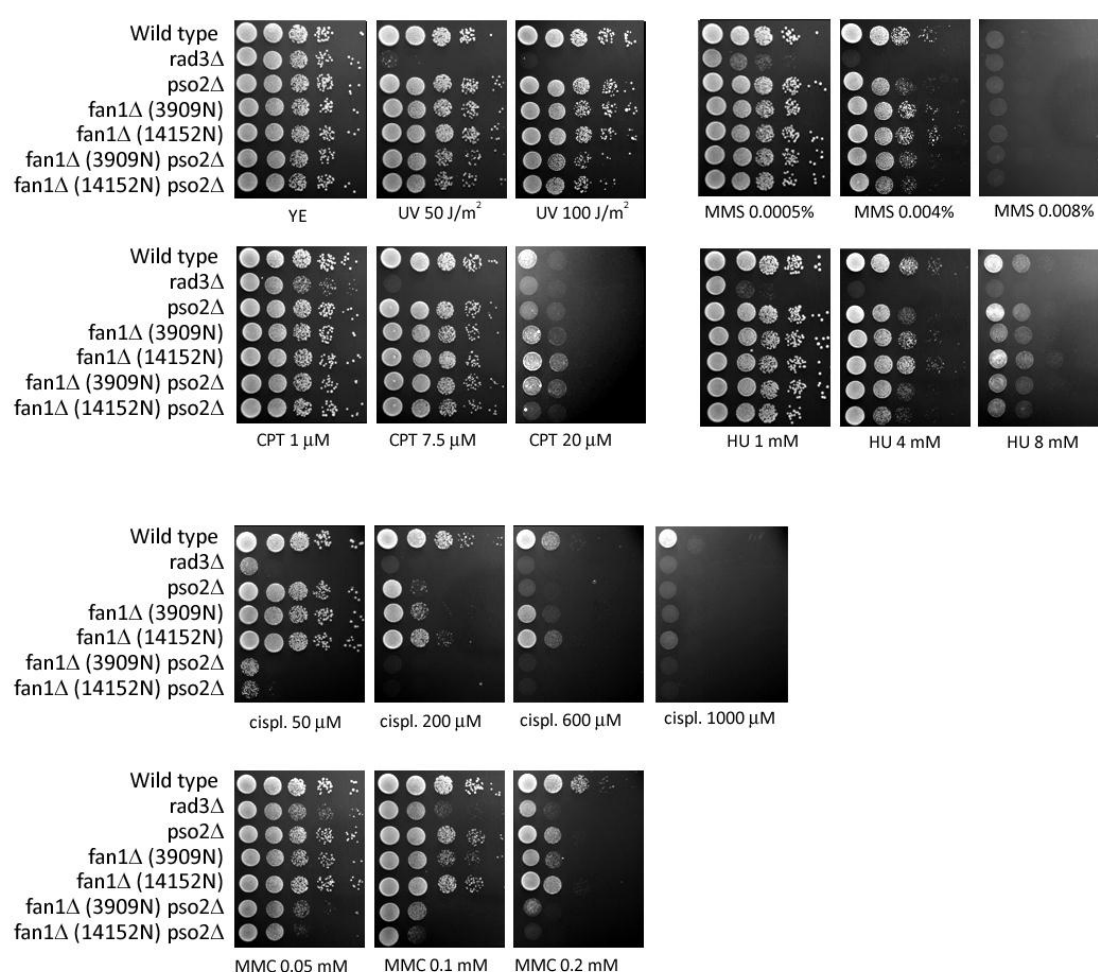


**Figure 4.4 | Sensitivity of fan1-d pso2-d double mutant to a variety of DNA damaging agents.** Logarithmically grown cultures were spotted in four 1:10 serial dilutions starting from $10^7$ cells (first spot on the left) on YEA plates containing the agents in the amount indicated. *rad3*-d is used as a standard hypersensitive control for the efficacy of the agents used. The combined deletion of *fan1* and *pso2* aggravates the sensitivity to cisplatin and MMC. Abbreviations used: UV, Ultra-Violet irradiation; CPT, camptothecin; MMS, methyl methanesulfonate; HU, Hydroxyurea; cispl, cisplatin; MMC, mitomycin C.

*kanMX* mutant as a parental strain. The two combined *kanMX* mutations (*fan1::kanMX pso2::kanMX*) resulted in the same sensitivity to UV and cisplatin compared to the *fan1*::*natMX6 pso2*::*kanMX* combined mutations (supplementary fig. 9.5). Thus, any possible artefact due to the *natMX6* cassette can be confidently ruled out. Taken together, these data indicate that Fan1[Sp] is a novel DNA repair component acting in a pathway that is parallel and distinct from the one involving Pso2[Sp].

### 4.3.3 Fan1[Sp] is specifically involved in the response to DNA interstrand cross-links

In order to confirm that Fan1[Sp] is specifically involved in the resolution of covalent bonds between the two strands of a DNA molecule, cell survival assays were repeated for *fan1*-d and *pso2*-d using bis(2-chloroethyl)methylamine (HN2, mechloretamine), agents shown to generate a cleaner proportion of DNA interstrand cross-links compared to cisplatin (Lehoczký et al., 2007).

When exposed to increasing concentrations of HN2, *fan1*-d cells showed a marked decrease in viability only when combined with the deletion of the gene coding for *Pso2*[Sp] (fig. 4.5). A similar experiment with MMC confirmed the results obtained in the spot tests (fig. 4.4), as again the double mutant *fan1*-d *pso2*-d was the most sensitive strain (supplementary fig. 9.6, top panel). As a further control, the same experiment was conducted in the presence of HN1 (2-dimethylaminoethylchloride hydrochloride), a mono-functional nitrogen mustard which does not form ICLs (McHugh et al., 2000). None of the strains treated with this agent, including the double mutant *pso2*-d *fan1*-d, showed any sensitivity to this agent to doses up to 100 times higher than HN2 (supplementary fig. 9.6, bottom panel).

Taken together, these data confirm that Fan1[Sp] is a novel component of the DNA repair pathway that specifically acts in *S. pombe* to repair cross-links linking covalently the two strands of a DNA molecule, and that Fan1[Sp] and Pso2[Sp] act in two separate pathways.
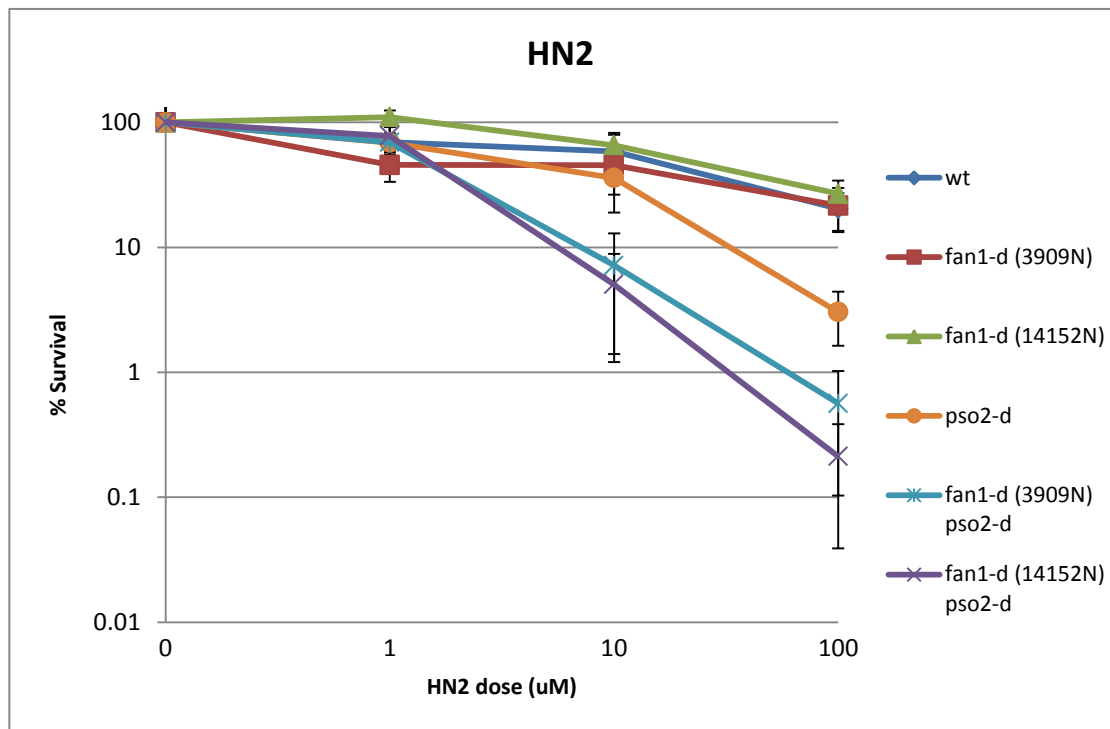
**Figure 4.5 | Sensitivity of *fan1*-d mutants, alone and in combination with *pso2*-d, to HN2.** $4 \times 10^7$ cells from logarithmically growing cultures were exposed to each indicated dose of damaging agents. Approximately 200 cells were plated on YEA and grown for 3-4 days at 30°C. Lines represent the average of three independent experiments. Error bars represent the standard error of the mean. The combination of the deletions of *fan1* and *pso2* causes the most marked sensitivity among the mutants tested. HN2, bis(2-chloroethyl) methylamine.

## 4.3.4 Fan1[Sp] is epistatic with the effector kinase Chk1[Sp]

The protein kinase Chk1, the main effector of the DNA damage checkpoint pathway in *S. pombe* (reviewed in Carr, 2002), has been shown to be involved in the response to ICLs (Lambert et al., 2003). To assess whether the deletion of *fan1* aggravates the sensitivity to ICL-inducing agents, the double mutant *fan1*-d *chk1*-d was exposed to increasing doses of cisplatin and MMC. Both the double disruptants showed sensitivity to cisplatin comparable to the *chk1* null mutant (fig. 4.6). When exposed to high doses of mitomycin C, the double mutant appeared to be slightly more sensitive than the cognate mutants. The sensitivity of the *chk1*-null background was marked, as previously reported (Lambert et al., 2003). This result suggests that Fan1[Sp] and Chk1[Sp] functions overlap, although not entirely, in the resolution of adducts created by DNA cross-linkers.

The effector kinase Cds1$^{Sp}$ (Rad53$^{Sc}$) is the central component of the DNA replication checkpoint in *S. pombe* (Carr, 2002). To assess the requirement for an intact DNA replication checkpoint in the absence of *fan1*-d, the double mutant *fan1*-d *cds1*-d was tested. No sensitivity was shown for either the single deletion mutant or the combination *fan1*-d *cds1*-d (fig. 4.7), indicating that the replication checkpoint is not required for the viability of wt cells or *fan1*-d cells when these are challenged by agents inducing interstrand cross-links.
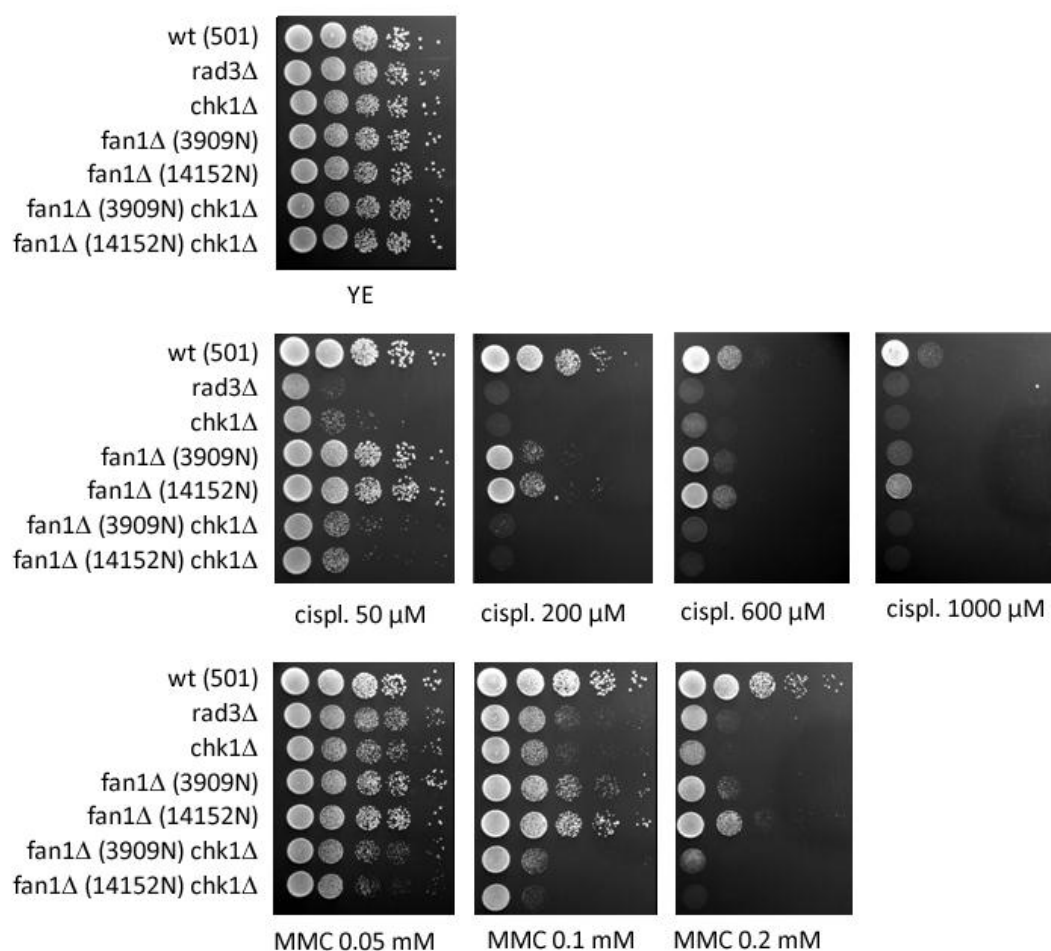


**Figure 4.6 | Sensitivity of *chk1* mutants to interstrand cross-linking agents.** Logarithmically grown cultures were spotted in four 1:10 serial dilutions starting from $10^7$ cells (first spot on the left) on YEA plates containing the agents in the amount indicated. *rad3*-d is used as a standard hypersensitive control for the efficacy of the agents used. The combined deletion of *fan1* and *chk1* leads to a slight increased sensitivity only in cells exposed to MMC but not cisplatin. Abbreviations used: cispl, cisplatin; MMC, mitomycin C.

### 4.3.5 Core MMR factors are not involved in the resolution of ICLs with Fan1$^{Sp}$

Although it has been demonstrated that the mismatch repair (MMR) pathway is not crucially involved in the resolution of ICLs in *S. cerevisiae* (Beljanski et al., 2004; Barber et al., 2005), In this organism, Pso2 has shown overlapping functions with Msh2 in response to nitrogen mustard (HN2) (Barber et al., 2005). Furthermore, human MutSβ has been reported to be involved in the recognition and uncoupling of ICLs induced by psolaren (Zhang et al., 2002; Zhao et al., 2009). Nevertheless, the study of the role of the MMR pathway in resistance to interstrand cross-linking agents has led to contrasting results (see 1.12.6). To investigate the requirement for MMR factors in the ICL-repair in *S. pombe*, a series of double and triple disruptants were tested for sensitivity to cisplatin and UV.

The deletion of *msh2*, alone or in combination with *fan1*-d, did not lead to increased sensitivity to either agent compared to wt cells (fig. 4.8). The same result was confirmed for two other components of the MMR pathway, Pms1$^{Sp}$ and Mlh1$^{Sp}$ (supplementary fig. 9.7). This result
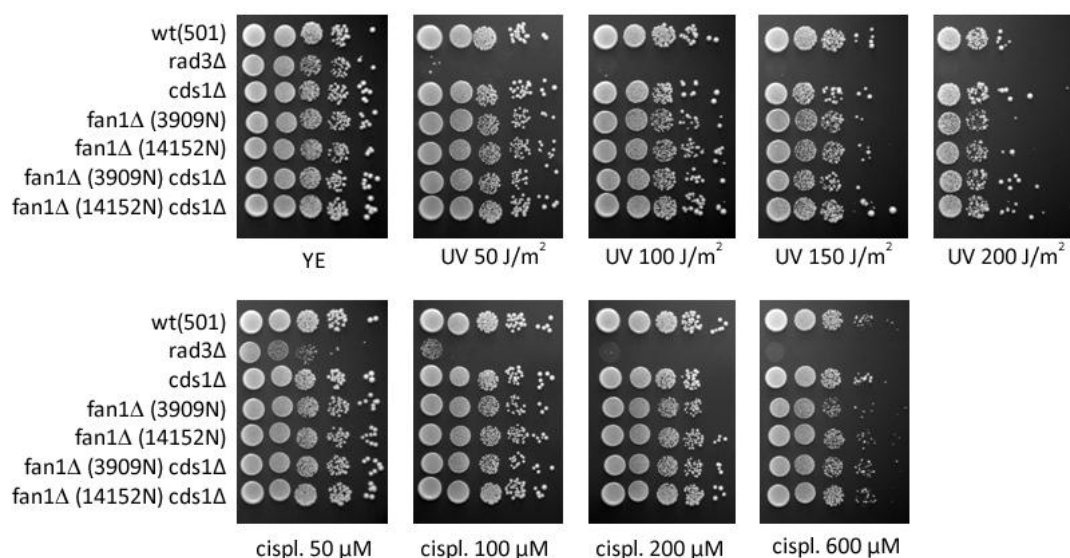


**Figure 4.7 | Sensitivity to UV and cisplatin of replication checkpoint mutants *cds1*-d.** Logarithmically grown cultures were spotted in four 1:10 serial dilutions starting from $10^7$ cells (first spot on the left) on YEA plates containing the agents in the amount indicated. *rad3*-d is used as a standard hypersensitive control for the efficacy of the agents used. The combined deletion of *fan1* and *cds1* phenocopies the cognate deletion mutants. Abbreviations used: UV, Ultra-Violet irradiation; cispl, cisplatin.

suggests that the central components of MMR are not involved in the resolution of interstrand cross-links in *S. pombe*. The concomitant disruption of *pso2* and *msh2* did not result in a synergistic sensitivity to cisplatin, ruling out possible overlapping roles for the two enzymes (fig. 4.9). Interestingly, the additional deletion of *fan1* (*fan1*-d *pso2*-d *msh2*-d) led to a subtle increase in sensitivity in the 3909N background compared to the *fan1* (3909N) *pso2* strain (fig. 4.9) in cells exposed to UV. Although this phenotype was reproducible also for the second mutant (14152N, supplementary fig. 9.8), its extreme subtlety indicates that there is no clear overlap in the functions of these three components and any additional role for Msh2$^{Sp}$ in a *fan1*-d *pso2*-d background might be confined exclusively to a limited subset of lesions.

### 4.3.6 Exo1$^{Sp}$ is not involved in the efficient resolution of ICLs

Despite showing redundant activities with Pso2 in response to HN2 treatment in *S. cerevisiae* (Barber et al., 2005; Lam et al., 2008), the precise role of the Exo1 exonuclease in the ICL repair is still being debated. To assess whether a clear function can be assigned to Exo1 in the ICL repair in *S. pombe*, several combinations of mutants were generated and tested. The *exo1*-d mutant showed wild-type sensitivity to UV and a subtle augmented sensitivity to cisplatin,
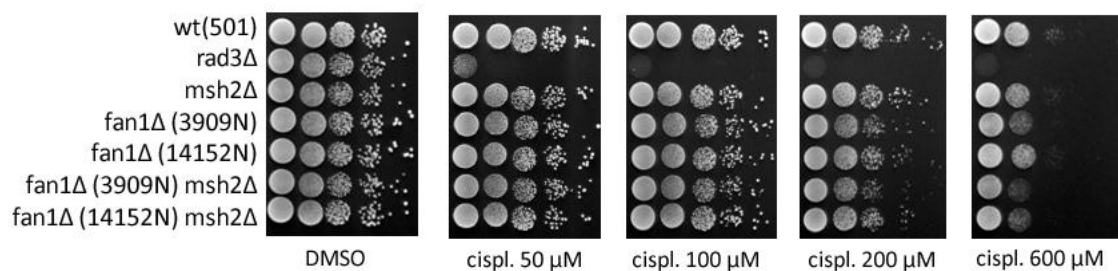


**Figure 4.8 | Sensitivity of *msh2*-d mutants, alone or in combination with *fan1*-d.** Logarithmically grown cultures were spotted in four 1:10 serial dilutions starting from $10^7$ cells (first spot on the left) on YEA plates containing the agents in the amount indicated. *rad3*-d is used as a standard hypersensitive control for the efficacy of the agents used. The combined deletion of *fan1* and *msh2* does not affect the sensitivity to UV and cisplatin compared to the single mutants. Abbreviations used: cispl, cisplatin.
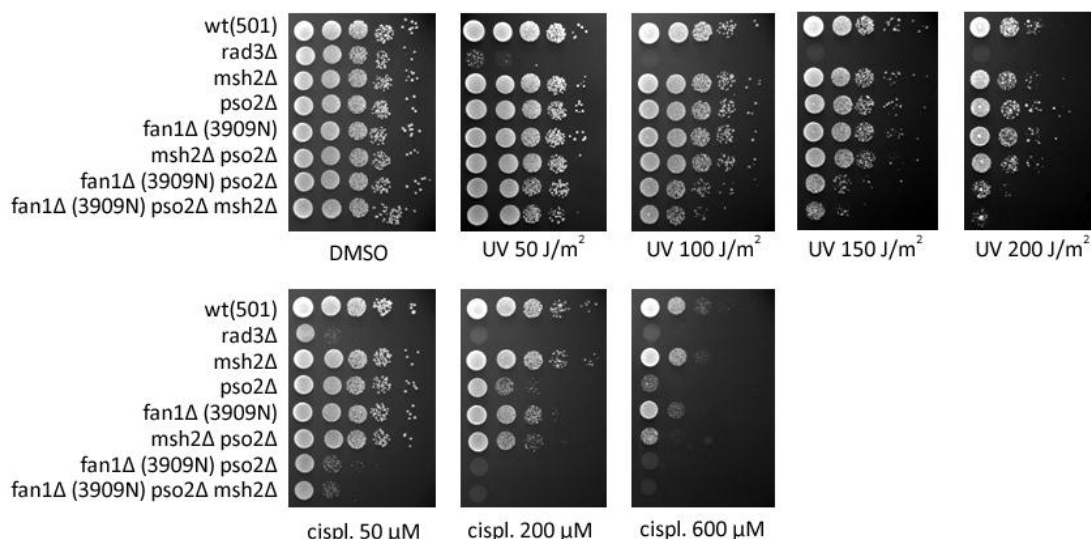
**Figure 4.9 | Sensitivity of _fan1_-d (3909N) _pso2_-d _msh2_-d triple mutant to UV and cisplatin.** Logarithmically grown cultures were spotted in four 1:10 serial dilutions starting from $10^7$ cells (first spot on the left) on YEA plates containing the agents in the amount indicated. _rad3_-d is used as a standard hypersensitive control for the efficacy of the agents used. A subtle increased sensitivity to cisplatin is noticed only for the combined triple mutant _fan1_-d _pso2_-d _msh2_-d when exposed to UV. Abbreviations used: UV, Ultra-Violet irradiation; cispl, cisplatin.

indicating a possible minor role in the resolution of lesions generated by cisplatin (fig. 4.10). The combined deletion _fan1_-d _exo1_-d led to a slight increased sensitivity compared to the parental single mutants (fig. 4.10, top panel). The _pso2 exo1_ double mutant was also more sensitive to cisplatin than the corresponding single mutants, suggesting independent roles for Pso2 and Exo1 in ICL repair in _S. pombe_ (fig. 4.10, bottom panel). However, when directly compared with the _pso2_-d _fan1_-d mutant, the synergistic sensitivity of _pso2_-d _exo1_-d was considerably milder, showing that Exo1^Sp involvement in the ICL pathway is only marginal (fig. 4.11 and supplementary fig. 9.9). This observation is further confirmed by the absence of any significant additional sensitivity of the _fan1 exo1 pso2_ triple mutant compared to _pso2 fan1_ following exposure to cisplatin (fig. 4.11 and supplementary fig. 9.9). Taken together, these data suggest that Exo1^Sp is overall involved but not crucially required for the efficient resolution of interstrand cross-links in _S. pombe._
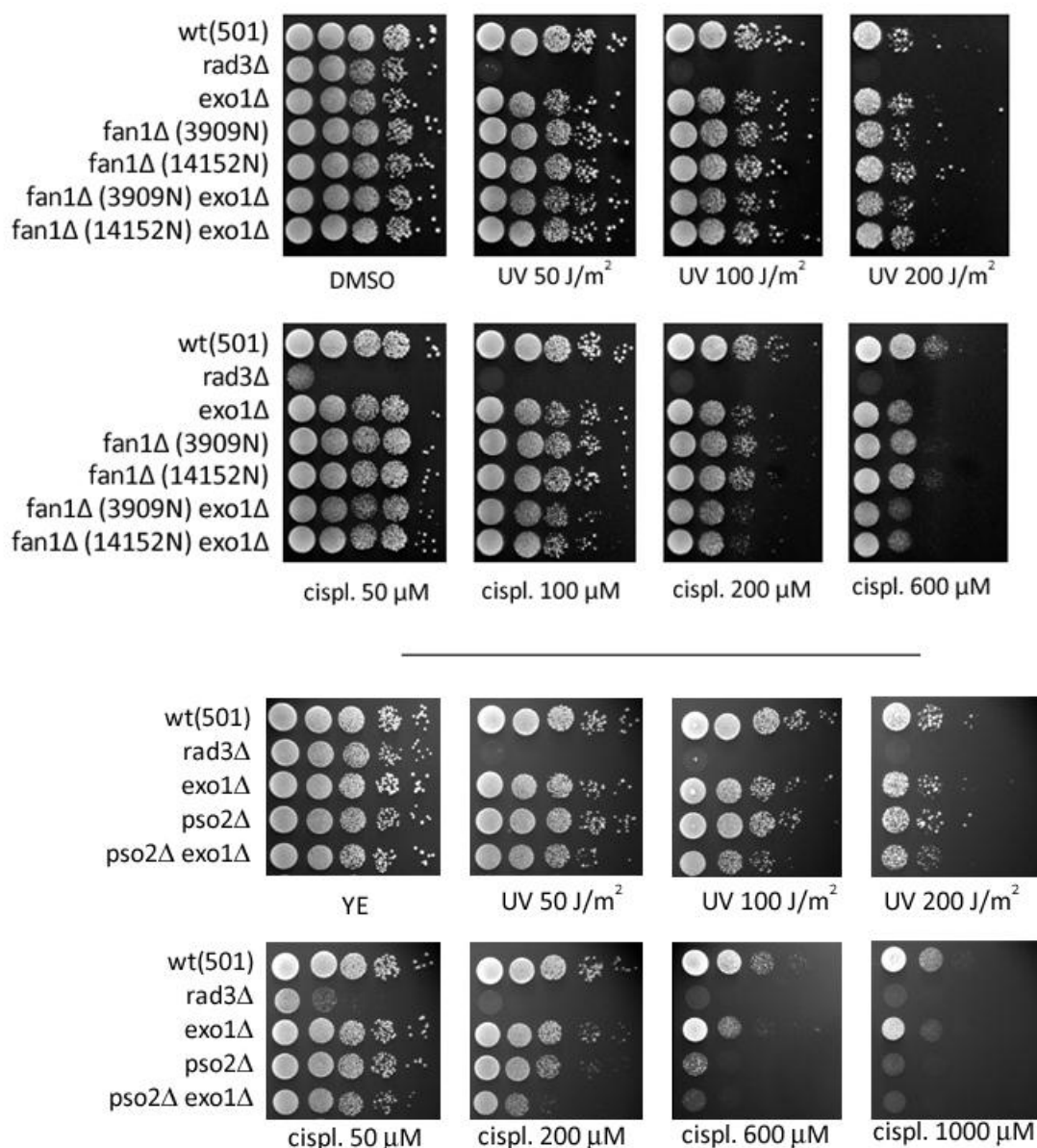
**Figure 4.10 | Sensitivity to UV and cisplatin of the *exo1*-d mutant in combination with either *fan1*-d (top panel) or *pso2*-d (bottom panel).** Logarithmically grown cultures were spotted in four 1:10 serial dilutions starting from $10^7$ cells (first spot on the left) on YEA plates containing the agents in the amount indicated. *rad3*-d is used as a standard hypersensitive control for the efficacy of the agents used. The concomitant deletion of *fan1* or *pso2* in an *exo1*-d background (top and bottom panels respectively) causes increased sensitivity to cisplatin. Abbreviations used: UV, Ultra-Violet irradiation; cispl, cisplatin.
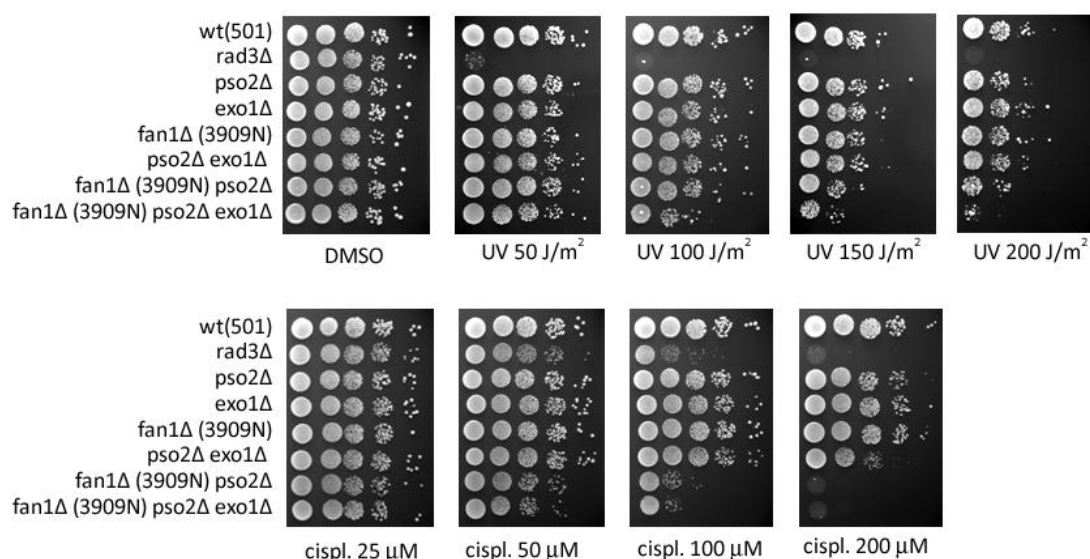
**Figure 4.11 | Sensitivity of different combinations of *fan1*-d (3909N background), *exo1*-d and *pso2*-d mutants to UV and cisplatin.** Logarithmically grown cultures were spotted in four 1:10 serial dilutions starting from $10^7$ cells (first spot on the left) on YEA plates containing the agents in the amount indicated. *rad3*-d is used as a standard hypersensitive control for the efficacy of the agents used. The triple deletion of *fan1*, *pso2* and *exo1* does not aggravate the sensitivity of the cognate double mutant *fan1 pso2*. Abbreviations used: UV, Ultra-Violet irradiation; cispl, cisplatin.

### 4.3.7 Rad13$^{Sp}$ shows a non-epistatic relationship with Fan1$^{Sp}$

ICL repair in lower and higher eukaryotes has proved to be elusive due to the intersection of different DNA repair pathways competing for the same intermediate substrates. In *S. cerevisiae*, components of the nucleotide excision repair (NER), post-replication repair (PRR) and homologous recombination (HR) pathways have all been implicated in the resolution of interstrand cross-links (Lehoczký et al., 2007). To test whether a similar involvement can be identified for the Fan1$^{Sp}$ ICL repair pathway in *S. pombe*, a series of double and triple mutants were created and tested for sensitivity to UV and cisplatin.

Rad13$^{Sp}$ (XPG$^{Hs}$, Rad2$^{Sc}$) is a nuclease centrally involved in NER, pathway that is required for the initial incision at early steps of ICL repair in *S.* cerevisiae (Lehoczký et al., 2007). A *rad13*-d strain showed a dramatic reduction in viability, compared to wt, when exposed to cisplatin (fig. 4.12). Interestingly, *rad13*-d sensitivity was significantly increased when combined with a deletion of the gene coding for Fan1$^{Sp}$, but not with *pso2*-d (fig. 4.12, bottom panel). However,

the triple mutant *fan1*-d *pso2*-d *rad13*-d (14152N background) phenocopied the *fan1*-d *pso2*-d

strain (fig. 4.12, top panel). The same pattern of sensitivity was observed for the 3909N

background (supplementary fig. 9.10). These data suggest that in *S. pombe* Rad13 is involved in

the resolution of DNA interstrand cross-links in the Pso2 but not in the Fan1 pathway.

### 4.3.8  Rhp18 is epistatic with Fan1$^{Sp}$ and Pso2$^{Sp}$

In *S. cerevisiae*, the post-replication repair (PRR) complex Rad6-Rad18 has been shown to have

a role in the regulation of DNA synthesis following endonucleolytic cleavage of ICL
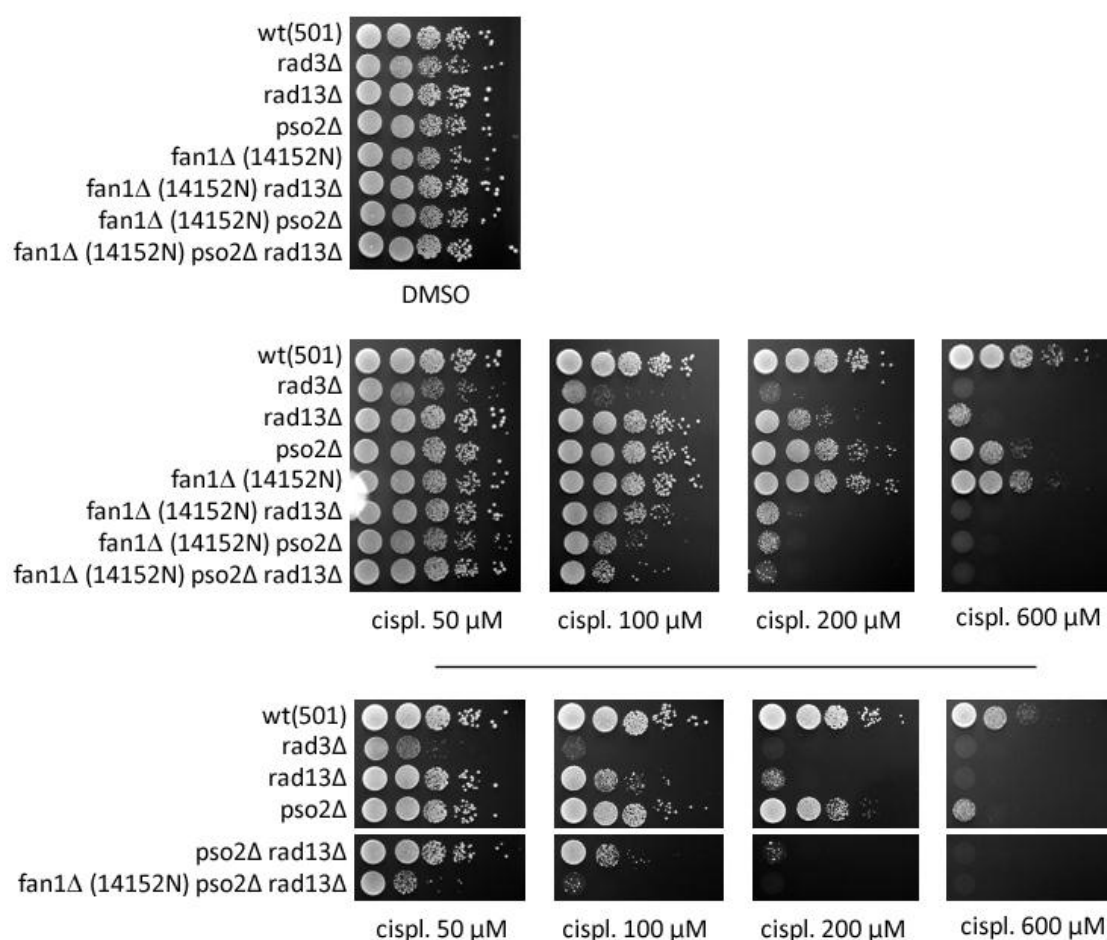


**Figure 4.12 | Sensitivity of *rad13* mutants exposed to increasing doses of cisplatin (*fan1*-d: 14152N background).** Logarithmically grown cultures were spotted in four 1:10 serial dilutions starting from $10^7$ cells (first spot on the left) on YEA plates containing the agents in the amount indicated. *rad3*-d is used as a standard hypersensitive control for the efficacy of the agents used. The deletion of both *fan1* and *rad13* causes a marked hypersensitivity to cisplatin. Bottom panel: independent experiment showing the compared sensitivity of *pso2*-d *rad13*-d and the respective single mutants. Abbreviations used: cispl, cisplatin.

intermediates (Lehoczký et al., 2007). The fission yeast homolog of Rad18 is the E3 ubiquitin ligase Rhp18. Following exposure to cisplatin, *rhp18*-d was markedly more sensitive than wt at doses as low as 50 μM (fig. 4.13 and 4.14). In an *rhp18*-d background, deletion of either *fan1* or *pso2*, or both (*fan1*-d *pso2*-d *rhp18*-d) did not lead to increased sensitivity compared to *rhp18*-d (fig. 4.14). The same result was shown for the 14512N background (supplementary fig. 9.11). This result suggests that Rhp18 is involved in the resolution of ICL repair in a step that is common to the Pso2$^{Sp}$ and Fan1$^{Sp}$ pathways.

### 4.3.9 Rhp51 is non-epistatic with Pso2$^{Sp}$ and Fan1$^{Sp}$

Homologous recombination has been shown to be involved in the repair of ICLs in the budding and fission yeast (Lehoczký et al., 2007; Lambert et al., 2003). This was confirmed in the present study by the increased sensitivity to UV and cisplatin of the strain deleted for Rhp51 (homolog of RAD51), required for most recombination events in the fission yeast (fig. 4.15). The deletion of both *fan1* and *rhp51* led to a marked drop in viability compared to wild-type and single mutants when cells were exposed to cisplatin (fig. 4.15) Interestingly, the triple deletion of the genes coding for Fan1$^{Sp}$, Rhp51 and Pso2$^{Sp}$ resulted in the most dramatic decrease in viability compared to all the combinations of mutants tested (fig. 4.15 and supplementary fig. 9.12). These data suggest a crucial role for Rhp51 in the resolution of ICLs outside the Pso2$^{Sp}$ and Fan1$^{Sp}$ pathways. Moreover, the notable differences in sensitivity between the combinations *fan1*-d *rhp51*-d and *pso2*-d *rhp51*-d (fig. 4.15 and supplementary fig. 9.12) highlight the differential extent of involvement for Rhp51 in the Pso2$^{Sp}$ and Fan1$^{Sp}$ pathways.
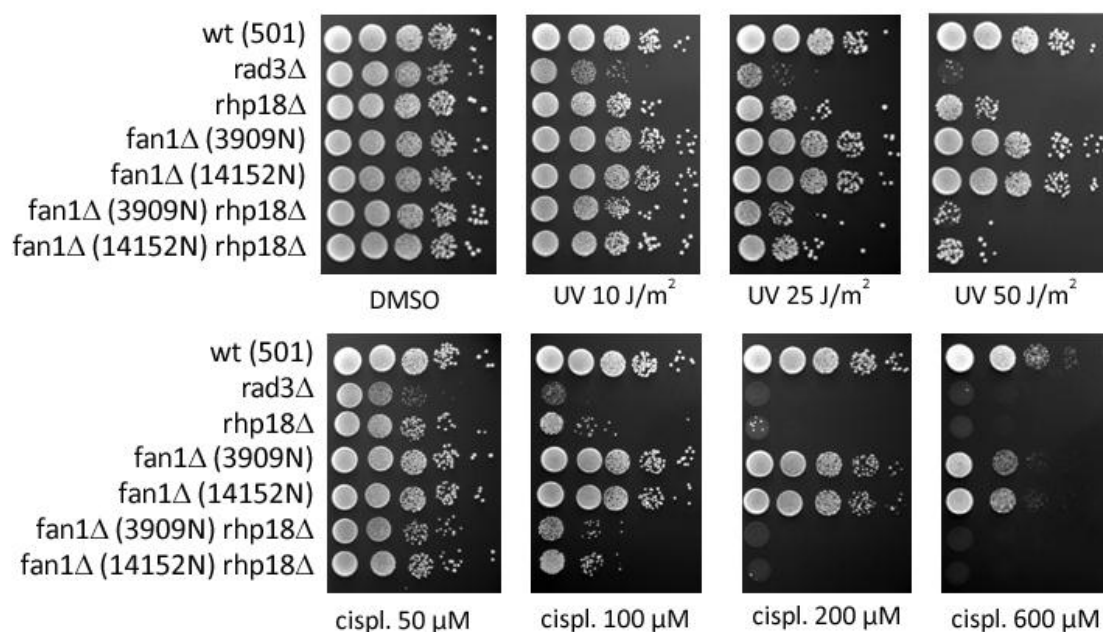
**Figure 4.13 | Sensitivity of combinations of single and double *rhp18* mutants to UV and cisplatin.** Logarithmically grown cultures were spotted in four 1:10 serial dilutions starting from $10^7$ cells (first spot on the left) on YEA plates containing the agents in the amount indicated. *rad3*-d is used as a standard hypersensitive control for the efficacy of the agents used. The additional deletion of *rhp18* does not affect the sensitivity of *fan1*-d to cisplatin. Abbreviations used: UV, Ultra-Violet irradiation; cispl, cisplatin.
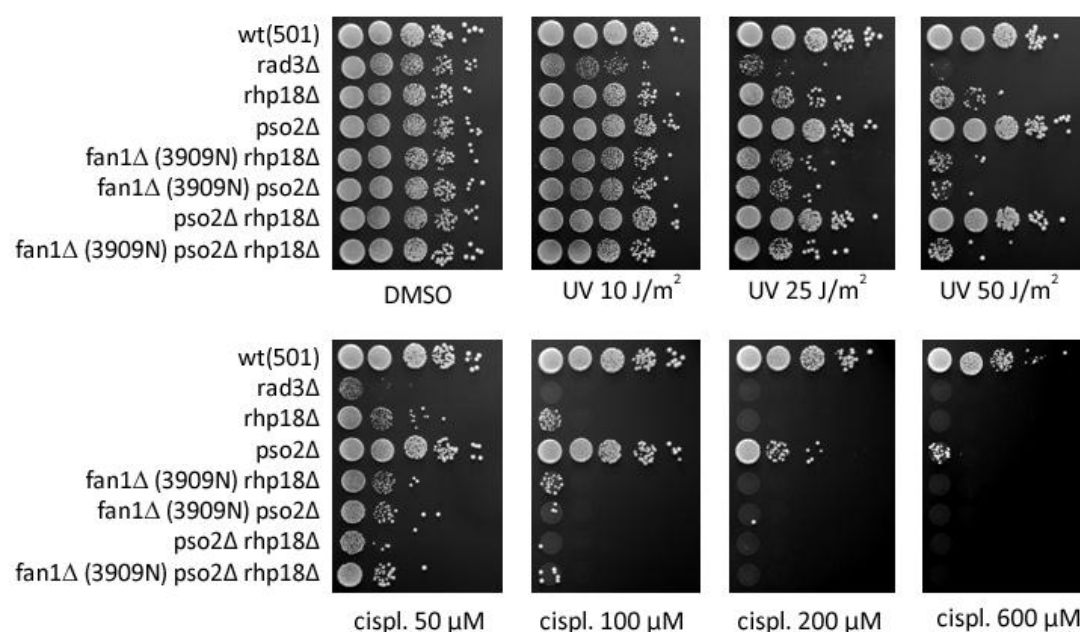


**Figure 4.14 | Sensitivity of combinations of *rhp18* mutants to UV and cisplatin (*fan1*-d: 3909N background).** Logarithmically grown cultures were spotted in four 1:10 serial dilutions starting from $10^7$ cells (first spot on the left) on YEA plates containing the agents in the amount indicated. *rad3*-d is used as a standard hypersensitive control for the efficacy of the agents used. The additional deletion of *rhp18* does not affect the sensitivity of *pso2*-d to cisplatin. Abbreviations used: UV, Ultra-Violet irradiation; cispl, cisplatin.
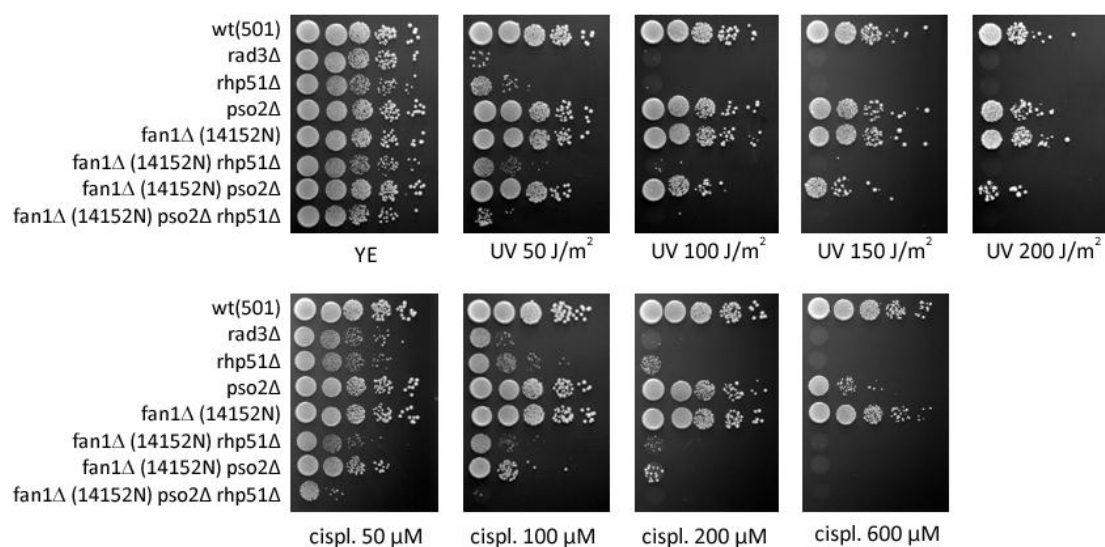
**Figure 4.15 | Sensitivity to cisplatin of various combinations of *rhp51* mutants (*fan1*-d: 14152N background).** Logarithmically grown cultures were spotted in four 1:10 serial dilutions starting from $10^7$ cells (first spot on the left) on YEA plates containing the agents in the amount indicated. *rad3*-d is used as a standard hypersensitive control for the efficacy of the agents used. The deletion of *rhp51* aggravates the sensitivity of the *fan1*-d and *fan1*-d *pso2*-d mutants. Abbreviations used: UV, Ultra-Violet irradiation; cispl, cisplatin.

## 4.4 Discussion

### 4.4.1 Overlapping activity for Fan1$^{Sp}$ and Pso2$^{Sp}$ in the resolution of DNA ICLs

The genetic characterisation in this chapter is based on the assessment of sensitivity of a combination of *fan1*-d mutants to a variety of DNA damaging agents. The initial observation that all the isolates from two independently-derived *fan1*-d mutants are specifically sensitive to cisplatin and mitomycin C (fig. 4.2 and fig. 4.3) pointed towards a role for Fan1$^{Sp}$ in the resolution of covalent cross-links between the two strands of the DNA molecule. In fission yeast, the only component implicated specifically in the resolution of ICLs in fission yeast is the nuclease Pso2$^{Sp}$ (Lambert et al., 2003). When combined with the deletion of *fan1*, *pso2*-d cells showed a dramatic increased sensitivity to cisplatin and MMC (fig. 4.4), consistent with a possible overlapping activity of the two enzymes in the repair of lesions created by cross-linking agents. This conclusion was further supported as the same pattern of sensitivity was

shown following exposure to the nitrogen mustard HN2 (fig. 4.5). Pso2$^{Sp}$ belongs to the β-CASP

metallo- β -lactamase (MBL) family of DNA nucleases. The best characterised protein in the

family is the *S. cerevisiae* Pso2, a 5'-exonuclease involved in response to all ICL-inducing

treatments (Li et al., 2005; Henriques et al., 1997). Although it has recently been recently

suggested that the role of Pso2$^{Sc}$ may be extended to the processing of ionizing radiation (IR)-

induced DSBs in conjunction with Mre11$^{Sc}$ and Exo1$^{Sc}$ (Lam et al., 2008), the role of this family

of nucleases remains more closely associated with ICL repair (Cattell et al., 2010). Thus, this

initial characterisation strongly indicates the existence of two distinct pathways for the

resolution of ICLs in *S. pombe.*

### 4.4.2 The DNA checkpoint control of the ICL pathway

The importance of the DNA damage checkpoint in response to ICLs is highlighted by the

extreme hypersensitivity displayed by *chk1*-d (fig. 4.6). Interestingly, the combination of *fan1*-d

and *chk1*-d appeared to lead to increased combined hypersensitivity only in cells treated with

MMC, but not in cells treated with cisplatin (fig. 4.6). The most plausible explanation for this

result is that the Fan1 pathway in *S. pombe* acts within the Chk1-dependent damage response.

However, for a subset of lesions enriched in interstrand cross-links as those generated by

MMC, Fan1$^{Sp}$ may additionally have Chk1–independent roles.

### 4.4.3 MMR factors are not involved in the efficient resolution of ICLs in *S. pombe*

The involvement of components of the mismatch repair pathway in the ICL resolution has

proven to be elusive. Although the core MMR components are not required for an efficient

response to ICL in *S. cerevisiae* (Beljanski et al., 2004), Msh2$^{Sc}$ and Pso2$^{Sc}$ seem to play

overlapping roles in response to HN2 treatment (Barber et al., 2005). The situation in *S. pombe*

appears to differ. Neither the single deletion of *msh2* nor the combined deletion with *pso2* led

to any detectable increased sensitivity to cisplatin treatment (fig. 4.8 and 4.9), arguing against

a role for MMR in the ICL response in *S. pombe*. This observation is further confirmed by the

lack of any synergistic sensitivity shown for *pso2*-d in combination with the deletion of either

*pms1* or *mlh1*, downstream effectors of the MMR cascade (supplementary fig. 9.7). This is in contrast with *S. cerevisiae*, where the sensitivity of a *pso2*-d mutant is aggravated by the additional deletion of *pms1* (Barber et al., 2005). Thus, two possibilities can be envisaged: the first possibility is that *S. pombe* differs from *S. cerevisiae* as MMR core factors may not play any role in the resolution of interstrand adducts. Alternatively, the role for MMR factors might be confined to a specific phase of the cell cycle that would be masked in experiments where the cell population grows asynchronously prior to treatment with DNA damaging agents. In *S. cerevisiae*, the overlap between the activity of Pso2 and Msh2 seems to be confined to the S phase of the cell cycle, where the collision of replication forks with ICLs will precipitate DSB formation (Barber et al., 2005). Although the synergistic sensitivity in *pso2-d msh2*-d is still detectable following acute treatment with HN2 in an asynchronous population (Barber et al., 2005), the result might differ when cells are treated chronically with cisplatin, as in the present study (fig. 4.8 and fig. 4.9). Further experiments with a synchronous population could rule out or confirm the latter possibility.

Interestingly, a subtle but reproducible increase in sensitivity could be observed for the triple mutant *fan1 pso2 msh2* compared to the cognate strains when exposed to UV light and not to cisplatin (fig. 4.9 and supplementary fig. 9.8). It could be speculated that in *S. pombe* Msh2 would deal with a subset of lesions generated by UV light towards which Fan1 and Pso2 are inert. However, the extreme subtlety of this synergistic effect demands additional work to support any further conclusion.

Studies of the Exo1 nuclease in eukaryotes have revealed a multitude of roles in several aspects of DNA metabolism (Tran et al., 2004). In the repair of ICLs, overlapping functions have been shown in *S. cerevisiae* for Pso2[Sc] and Exo1[Sc] (Barber et al., 2005; Lam et al., 2008). The data presented in this study suggests that the same is true in the fission yeast, as *pso2* shows an increased sensitivity with *exo1* when cells are exposed to cisplatin (fig. 4.10 and fig. 4.11). Interestingly, this possible overlap in the roles of the two enzymes in ICL repair does not

appear to extend to Fan1 in *S. pombe*, as the sensitivity of *fan1*-d *exo1*-d is very subtle (fig. 4.10). However, it is important to notice that the overlapping role between Pso2[Sp] and Exo1[Sp] seems to be marginal and less pronounced than in *S. cerevisiae* (Barber et al., 2005; Lam et al., 2008). Intriguingly, the triple mutant *fan1*-d *pso2*-d *exo1*-d shows a very subtle increased sensitivity confined to UV exposure rather than cisplatin treatment (fig. 4.11 and supplementary fig. 9.9). It could be speculated that Exo1[Sp] is required to repair a subset of lesions generated by UV normally repaired by Fan1[Sp] and Pso2[Sp]. This role might echo the situation in *S. cerevisiae*, where Exo1[Sc] has been shown to play a role in the response to UV damage (Qiu et al., 1998). However, the subtlety of the phenotype found in this study demands further analysis to support this hypothesis.

### 4.4.4 Rad13[Sp] is involved in the Pso2[Sp] pathway of ICL response

The observation that the deletion of Rad13[Sp] (XPG[Hs], Rad2[Sc]), a core component of the nucleotide excision repair (NER) pathway, results in a strong sensitivity to ICLs (fig. 4.12) confirms previous data in fission yeast (Lambert et al., 2003). The crucial role of the NER in the ICL repair has been shown to be conserved across lower and higher eukaryotes (Lehoczký et al., 2007; Wood, 2010). In *S. cerevisiae*, genes belonging to the NER complementation group have been found to be critically required for resistance to cisplatin (Wu et al., 2004). In the light of the present study, it is possible to suggest that in *S. pombe* the involvement of NER is confined to the Pso2[Sp] pathway of ICL response, as the synergistic sensitivity to cisplatin is shown only for the combination *fan1*-d *rad13*-d and not for *pso2*-d *rad13*-d or for the triple mutant *fan1*-d *pso2*-d *rad13*-d (fig. 4.12). However, as the epistasis analysis presented here is limited to Rad13[Sp], it cannot be excluded that other NER components may be required at different stages of the ICL repair. In the budding yeast, Rad2[Sc] (Rad13[Sp]) is required for wild-type resistance to cisplatin, HN2, MMC and 8-Methoxypsoralen (8-MOP) (Wilborn and Brendel, 1989; Wu et al., 2004). The observation that the DNA incision is inhibited in *rad2*-d cells in budding yeast following treatment with 8-MOP (Chanet et al., 1985; Meniel et al., 1995)

suggests that this nuclease is involved at early stages of the ICL repair. With the analysis presented in this chapter it is not possible to assess whether this is also the case for the fission yeast. It is tempting to speculate that if Rad13$^{Sp}$ plays a similar role at the incision step of the ICL removal, another nuclease should be involved for a similar activity in the Fan1$^{Sp}$ pathway. This component could either be Fan1$^{Sp}$ itself or a yet unidentified nuclease.

### 4.4.5 **Rhp18 is overall required for the ICL response**

The requirement for RAD18 for wild-type resistance to cisplatin has been previously observed in *S. pombe*, *S. cerevisiae* and higher eukaryotes (Lambert et al., 2003; Wu et al., 2004; Tateishi et al., 2003; Nojima et al., 2005). Interestingly, the data presented here showed no increased sensitivity for either *fan1*-d *rhp18*-d or *pso2*-d *rhp18*-d (fig. 4.13 and fig. 4.14). This would indicate that the role for Rhp18$^{Sp}$ in the ICL response is required for both the Fan1$^{Sp}$ and Pso2$^{Sp}$ pathways. Rhp18$^{Sp}$ is an E3 ubiquitin ligase homologous to Rad18$^{Sc}$ and belongs to the Rad6-Rad18 post-replication repair epistasis group in budding and fission yeast. Although the role for this protein in the DNA repair of ICLs has not yet been fully elucidated, work in *S. cerevisiae* has shown that this protein would act in conjunction with Rad6 in controlling the DNA synthesis at late stages of the ICL processing (Lehoczký et al., 2007). Recent work in mammalian cells has shown that RAD18$^{Hs}$ is required for the recruitment of SNM1A$^{Hs}$ (Pso2$^{Sp,Sc}$) to DNA repair complexes following exposure to UV and MMC. The UBZ (ubiquitin-binding zinc finger) domain of SNM1A$^{Hs}$ is essential for this localisation (Yang et al., 2010). As neither Fan1$^{Sp}$ nor Pso2$^{Sp}$ possess UBZ domains, in the fission yeast the scenario might be different and ubiquitylation might not be required for the activity of Fan1$^{Sp}$. The RAD18-dependent monoubiquitination of PCNA is a pre-requisite for the recruitment of SNM1A to the site of damage (Yang et al., 2010). The epistasis analysis presented here does not exclude a similar role in the fission yeast, although no further details can be deduced from the data presented in this chapter.

### 4.4.6    Rhp51 shows a differential involvement in the Fan1[Sp] and Pso2[Sp] pathways

Several studies highlight the importance of homologous recombination (HR) processes in the ICL resolution. In *S. pombe*, the deletion of *rhp51* leads to hypersensitivity to HN2 (Lambert et al., 2005). In *S. cerevisiae*, HR-deficient cells in exponential phase are sensitive to cisplatin and HN2 (McHugh et al., 2000; Beljanski et al., 2004). Data show that homologous recombination processes are required to repair DSBs generated by treatment with cisplatin or HN2 in replicating budding yeast cells (McHugh et al., 2000; Frankenberg-Schwager et al., 2005).

It has been suggested that homologous recombination might be required only for an ICL repair pathway that is functional in replicating cells (Frankenberg-Schwager et al., 2005). However, there is no clear indication about the proportion of DSBs that are generated as repair intermediates or as a result of the collision of replication forks with ICLs, so it is difficult to establish how and in which scenarios HR processes are required in the ICL repair. The data presented in this chapter confirms the importance of the *S. pombe* Rad51 homolog Rhp51 in the response to ICLs. The deletion of *rhp51* leads to a significant decrease in viability when cells are exposed to cisplatin (fig. 4.15). This decrease is aggravated by the deletion of *pso2*, but interestingly this effect is even more dramatic in combination with a deletion of *fan1* (supplementary fig. 9.12 and fig. 4.15). This finding suggests that Rhp51-dependent HR processes would be involved in greater extent in the absence of the Fan1[Sp] pathway. However, it is also important to notice that HR appears to play a crucial role in a yet unknown contribution to the ICL response, as the triple mutant *fan1*-d *pso2*-d *rhp51*-d shows a further reduction in viability compared to all the cognate mutants (fig. 4.15 and supplementary fig. 9.12). Epistasis analysis in *S. cerevisiae* has suggested the existence of three separate pathways for ICL response, defined by Pso2[Sc], Rev3[Sc] and Rad51[Sc] (Grossmann et al., 2001). Rev3 is part of the translesion synthesis (TLS) polymerase Polζ, recognized for its crucial role in ICL response in *S. cerevisiae* and vertebrates (evidence reviewed in Ho and Schärer, 2010).  It

would be interesting to further extend the epistasis analysis presented in this chapter to Rev3$^{Sp}$ mutants, in order to assess whether the same situation occurs in the fission yeast.

## 4.5    Conclusions

Taken together, the epistasis analysis presented in this chapter demonstrates an important role for Fan1 in the resolution of DNA interstrand cross-links in *S. pombe*. All the data presented here was obtained by testing double and triple combinations of null mutants for survival to a range of DNA damaging agents. As these null mutants were created on a rational basis of existing data from published literature, it could not be excluded that other genetic interactions might exist with still uncharacterised components of the DNA repair machinery. For this reason, an automated screen of a deletion library was set up to expand the investigation into further genetic interactions.

Chapter Five

ASSESSMENT OF GENETIC INTERACTIONS THROUGH
HIGH-DENSITY SYNTHETIC GENETIC ARRAYS

## 5.1    Introduction

### 5.1.1    Genetic interactions and genetic networks

Genetic interactions examine how the mutation in one gene alters the phenotype due to the deletion of a second one. As seen in the previous chapter, the classic definition of epistasis dictates that a gene is epistatic to a second non-allelic one when the phenotype consequent to the deletion of the second gene is masked by the phenotype caused by the deletion of the first one (Roth et al., 2009). On a wider scale, genetic interactions can be classified into negative or positive. Negative interactions occur when the deletion of a second gene leads to a reduction in the fitness of a single mutant (synthetic sickness). An extreme case of negative interaction occurs when the deletion of the second gene leads to loss of viability (synthetic lethality). Positive (alleviating) interactions occur when the fitness of the double mutant is higher than the healthiest single mutant.

A series of high-throughput approaches have been recently developed in the budding and fission yeast to allow for extensive screens of genetic interactions. In the diploid-based synthetic lethality analysis on microarrays (dSLAM), a series of haploid-convertible heterozygous diploid knock-outs were profiled by DNA microarrays for gene-compound and gene-gene interactions in *S. cerevisiae* (Pan et al., 2004; Pan et al., 2006). In the synthetic genetic array (SGA) approach, a series of automated pinning procedures are employed to construct arrays of haploid double mutants to be analysed for gene-gene interactions (Tong et al., 2001; Tong et al., 2004; Roguev et al., 2007). Based on the SGA method, epistatic miniarray profiles (E-MAPs) were generated where the quantitative analysis of genetic interactions could be used to link subsets of genes to specific biological processes (Schuldiner et al., 2005; Schuldiner et al., 2006; Collins et al., 2006; Collins et al., 2007). In less than a decade since their introduction, these high-throughput approaches have proved to be useful tools in defining genetic interaction networks in fission and budding yeast (Dixon et al., 2009).

## 5.2 Aim

The analysis presented in the previous chapter was based on a rational selection of known components of DNA metabolism that were thought to potentially result in genetic interactions with *fan1*. The work presented in this chapter aims at exploring the genetic landscape of *S. pombe* in order to detect further genetic interactions between *fan1* and other components of DNA metabolism. The genetic interactions between *fan1* and a series of null mutants from the Bioneer® V2 deletion library were assessed by construction of high-throughput synthetic genetic arrays (SGAs). The first phase of the screen focused on genetic interactions in standard conditions of growth. The second phase of the screen assessed the phenotypes of double deletion mutants derived from phase one for hypersensitivity to the interstrand cross-linking agent cisplatin.

## 5.3 Results

### 5.3.1 Construction of synthetic genetic arrays in *S. pombe*: the PEM-2 strategy

In the present work, the assessment of genetic interactions between *fan1* and other genes in *S. pombe* was carried out by applying the SGA method as described in Roguev et al., 2007. This method employs a series of pinning procedures in order to generate arrays of haploid double mutants. Of the two strategies presented in Roguev et al., 2007, the PEM-2 (pombe epistatic mapper 2) system was used. This approach is based on recessive resistance to cycloheximide, an inhibitor of protein synthesis, which allows for selection against diploid cells. Initially, the strains 3909N and 14152N (see 4.3.2) were crossed with a query base mutant strain (kind donation of Dr Tim Humphrey) bearing two alleles of the large ribosomal subunit 60S, the target of cycloheximide. One allele, $cyh^S$, confers sensitivity to cycloheximide and is inserted within the H1 and H2 homology boxes of the mating-type locus *mat-1* (fig. 5.1). The second allele, $cyh^R$, confers resistance to cycloheximide and is placed at the endogenous 60s subunit locus (*rpl42*).
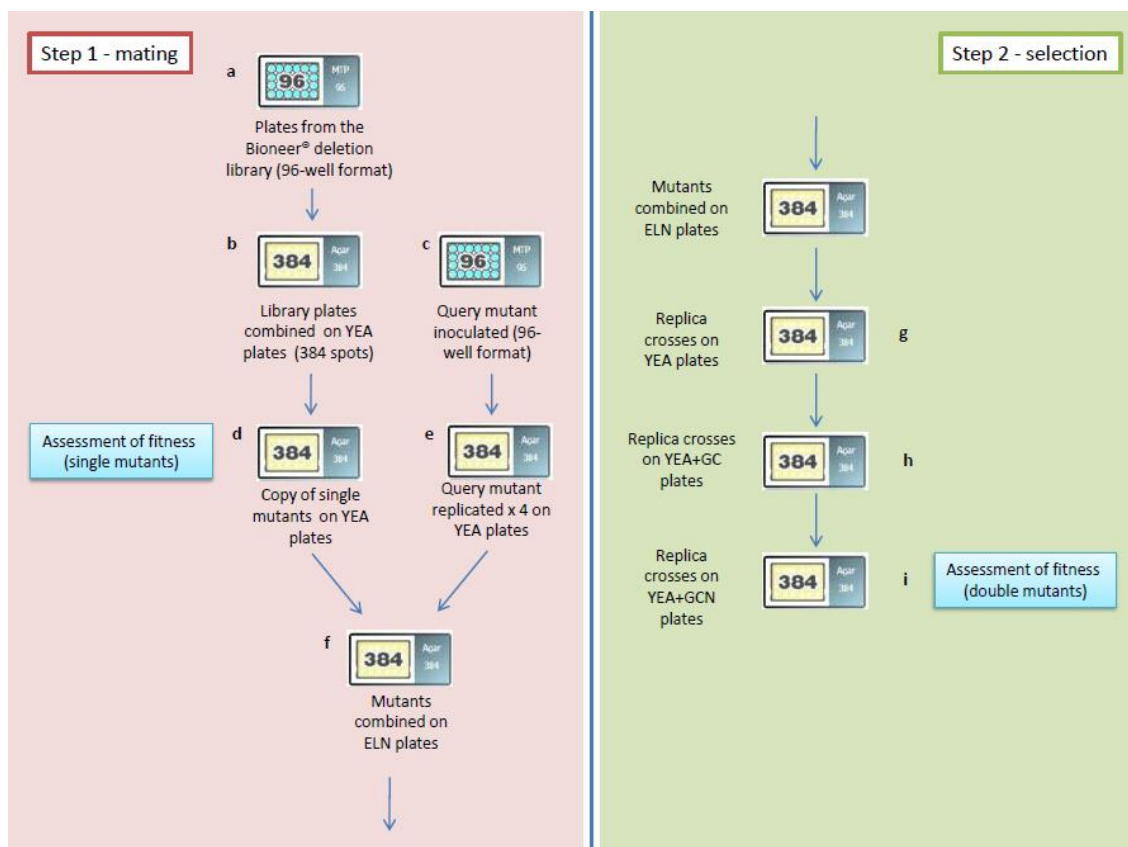
**Figure 5.1 | Schematic overview of the pinning procedures to construct the synthetic genetic arrays used in the present work.** The screen was performed in a 384-pin format. Four 96-well plates from the Bioneer® library were combined on one YEA 384-spot agar plate (a-b). Likewise, the query mutant was inoculated from a 96-well to a 384-spot format (c-e). The screen was repeated for at least three times from independent query mutant isolates. All the replicas were carried out by using the Singer® RoToR© HDA station by use of short 384 pins.

However, due to the recessive nature of the mutation, this strain is sensitive to cycloheximide. Following mating, h- cyh-sensitive spores carrying both the cyhS and cyhR alleles and the *fan1* deletion were selected by tetrad dissection. This genetic background defines the strain called *fan1*::natMX6 query mutant (fig. 5.1). The *fan1*-d query mutant was then crossed with a series of deletion mutants from the Bioneer® collection following the procedure shown in fig. 5.2. Pictures were taken at different timepoints at steps *d* and *i* and used to assess the fitness of single and double mutants, respectively.
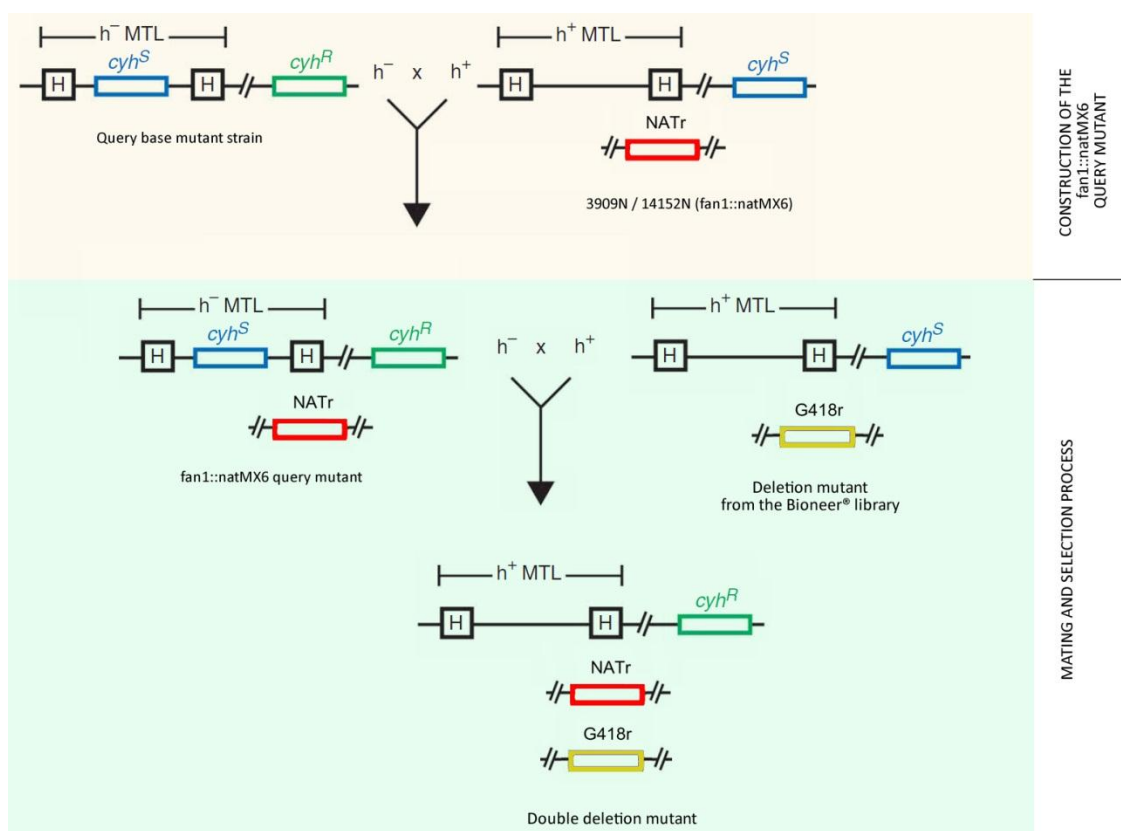
**Figure 5.2 | Schematic representing the marker selection process throughout the PEM-2 screen.** The PEM-2 (Pombe Epistatic Mapper - 2) approach is based on recessive resistance to the drug cycloheximide. Step1 (pink panel): construction of the *fan1*::*natMX6* query mutant. Tetrad analysis is necessary to ensure the maintenance of both the $cyh^S$ allele within the mating-type locus and the $cyh^R$ allele at the native locus. Step 2 (green panel): screen of the deletion mutant library. Mating and selection procedures ensure the maintenance of the three markers $NAT^R$, $G418^R$ and $cyh^R$ (at the native locus), conferring to the final double deletion mutant resistance to nourseothricin, geneticin and cycloheximide, respectively. MTL, mating-type locus mat1. Schematic adapted from Roguev *et al.*, 2007.

### 5.3.2    Computational analysis of colony size

In order to refine the detection of phenotypic changes in the double mutant colonies showing a decrease (synthetic sickness) or increase (alleviating interaction) in colony size, a computational procedure has been employed which relies on the use of digital imaging analysis. Previous work has shown that colony size can be used as a phenotypic readout to assess epistatic interactions (Schuldiner et al., 2005; Schuldiner et al., 2006; Collins et al., 2006; Collins et al., 2007). The approach presented in this chapter is based on the method presented

in Collins et al., 2006. Since interactions between two unrelated genes in living organisms are rare (Pan et al., 2004; Tong et al., 2004; Schuldiner et al., 2005), the median colony size expected for double mutant colonies can be used as a reference to determine significant deviations that can reflect aggravating or alleviating interactions between pair or genes (Collins et al., 2006). However, due to the nature of the present analysis, which is limited to a single query mutant strain, comprehensive and statistically robust approaches such as E-MAP would not be feasible. For this reason, the imaging software HT Colony Grid Analyser presented in Collins et al., 2006 was used to build only a semi-quantitative dataset of categories of genetic interaction between *fan1* and a series of null mutant from the Bioneer® library. This procedure was applied further to the construction of SGAs (see 5.3.1).

The first step was to extract raw colony size from digital images of single and double mutant arrays (fig. 5.1, *d* and *l* respectively). For each array, the median colony size was calculated and compared to the size of every colony on the same plate. To exclude biases due to differential growth of colonies dependent on their location on the plates, separate medians were calculated for the two outermost and for the innermost rows and columns of the plate. However, when the values were compared with each other, the difference in pixels was never significantly high enough to justify a separate analysis. Thus, a single value of median colony size was used for each plate. An example of a spreadsheet created for one synthetic genetic array is shown in supplementary fig. 9.16. Five colour-coded categories of deviation from the median colony size ($\Delta F = F$ value $-$ median) were assigned according to the criteria shown in fig. 5.3. A separate category was assigned to synthetic lethality, where F=-median.

The second step in this analysis was to collect together the data from all the independent screens on a single spreadsheet for each genetic array. An example of the spreadsheets generated is shown in supplementary fig. 9.17. Finally, double mutants were assigned to categories of genetic interactions with a high or low degree of confidence, depending on criteria of consistency across different screens and healthiness of the single mutants.
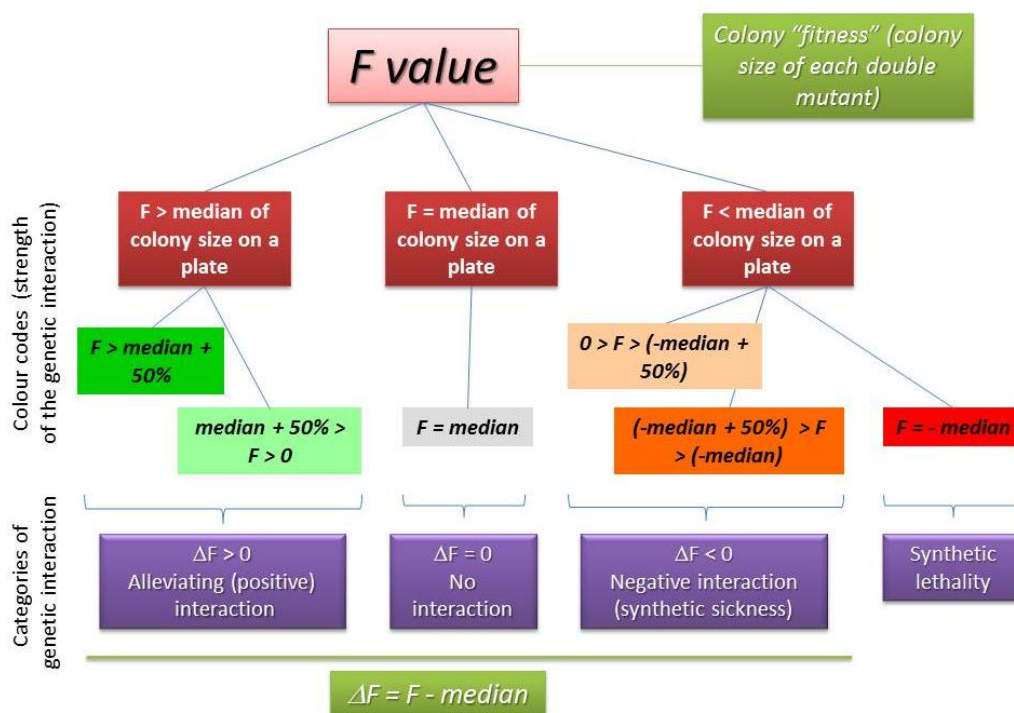
**Figure 5.3 | Criteria for the assignment of colour codes to categories of genetic interaction according to the degree of deviation from the median colony size on each array.** The size of every double mutant colony ("F value") on each array was compared to the median colony size on that array. Five colour-coded categories of deviation from the median colony size ($\Delta$F) were assigned to each double mutant: two green categories for $\Delta$F>0; two orange categories for $\Delta$F<0; one category for $\Delta$F=0. A separate red category was assigned to synthetic lethality (no double mutant colony, F=-median).

### 5.3.3 The visual assessment of genetic interactions leads to a first series of prospective

### *fan1* interacting partners

The synthetic genetic arrays were constructed following the procedure described in Roguev et al., 2007 (PEM-2 strategy). The pictures of the GNC plates obtained at the end of the automated selection process (fig. 5.2, step *l*) were compared with the pictures of the YEA plates carrying the single mutants from the Bioneer® deletion library (fig. 5.2, step *d*). Categories of synthetic sickness, synthetic lethality or alleviating interactions were assigned according to the logical framework shown in fig. 5.4. The results of the analysis are shown in tables 5.1a and 5.1b. Genes that are physically close to the *fan1* ORF could be potentially scored as synthetic lethal, as the recombination efficiency in this case is dramatically reduced due to linkage effects. To identify false positive entries due to genetic linkage biases, a further level of control was introduced by intersecting the results in table 5.1a and 5.1b with a list of

genes 50 kb upstream and downstream the *fan1* ORF ("Linkage" column in tables 5.1a and 5.1b; the complete list of genes is shown in supplementary fig. 9.13). Due to the limitations of this type of analysis, most of the interactions scored resulted in the synthetic lethal category, as synthetic sickness and alleviating interactions were more difficult to assess with good confidence. When matched with gene ontology (GO) *S. pombe* annotations, a few entries resulted in categories of biological processes associated with DNA metabolism (supplementary fig. 9.14). In particular, three genes associated with DNA repair appeared to be synthetic sick (*rhp18*) or synthetic lethal (*rhp54*, *rhp55*) when combined with the *fan1* deletion. As the *fan1*-d *rhp18*-d strain had already been tested by *in vivo* survival assays (see 4.3.8) and no defect in growth had been clearly noticed in the double mutant, this occurrence was further considered in the second stage of the screen analysis and later dismissed as an artefact of the visual
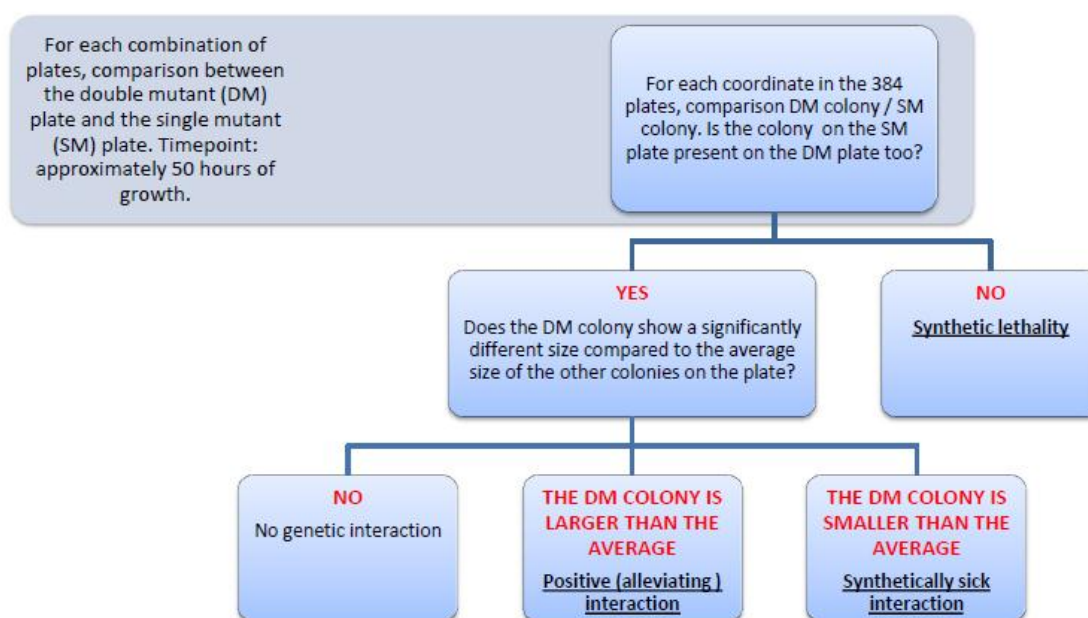


**Figure 5.4 | Logical framework used to assign categories of genetic interactions to the double mutants generated by the automated screen.** Note: if a colony was present in the double mutant plate but not in the single mutant plate, this case has been treated as a defect in the pinning procedure, rather than an extreme case of alleviating interaction.

inspection (see below). Rhp55 (Rad55[Sc]) and Rhp54 (Rad54[Sc]) have been associated with homologous recombination processes in *S. pombe* (Muris et al., 1996; Khasanov et al., 1999). To validate the apparent synthetic lethality of the *rhp54*-d *fan1*-d and *rhp55*-d *fan1*-d combinations, these strains were re-constructed with independently derived mutants and checked by tetrad analysis. Neither combination resulted in consistent synthetic lethal interactions (supplementary fig. 9.15). This data suggests that the apparent synthetic lethality shown for these two double mutants is in fact due to defects in biological processes which hamper the progression through successive stages of the screen, such as cell cycle defects. In particular, it should be noted that deletions of *rhp54* and *rhp55* significantly affect the growth of the corresponding mutants. Thus, it cannot be excluded that the poor survival of the mutant strains through the selection process may be the reason underlying the apparent synthetic lethality.

### 5.3.4 The computational analysis of colony size leads to a more accurate assignment to categories of genetic interactions

In order to overcome the limitations intrinsic to the visual inspection of colony size, a digital analysis was applied where the size of the double and single mutant colonies was calculated via computational software. The results of this analysis are shown in tables 5.2, 5.3 and 5.4. Compared to the visual approach, the dataset was overall expanded, predominantly in the compartment of positive interactions. 13 entries were excluded compared to the visual dataset due to either low consistency across different screens or poor viability of the corresponding single mutants. One example of the latter case is *rhp54*. All the other entries in the visual dataset were consistently confirmed in the computational dataset, although some interactions were classified under a low degree of confidence. One such case is *rhp18*, which resulted in an unclear synthetic lethal / synthetic sick interaction with *fan1* which was not confirmed by the analysis presented in the previous chapter (see 4.3.8). Tetrad dissection may prove to be helpful in clarifying whether the interaction between these two genes leads to a

| Gene ID | Gene name | Description | Synthetic sickness (black, blue, brown) | | | Synthetic lethality (black, blue, brown) | | | Alleviating (black, blue, brown) | | | Linkage (ORF ± 50 kb) |
|---|---|---|---|---|---|---|---|---|---|---|---|---|
| SPAC11D3.18c | | nicotinic acid plasma membrane transporter | | | | black | blue | brown | | | | |
| SPAC15A10.16 | bud6 | actin interacting protein 3 homolog Bud6 | blue | | | black | blue | brown | | | | |
| SPCC16C4.11 | pef1 | Pho85/PhoA-like cyclin-dependent kinase Pef1 | black | | | | blue | brown | | | | |
| SPAC1D4.13 | byr1 | MAP kinase kinase Byr1 | | | | black | blue | | | | | |
| SPAC11G7.02 | pub1 | ubiquitin-protein ligase E3 | | | | black | blue | brown | | | | |
| SPBC1709.18 | tif452 | translation initiation factor eIF4E 4F complex subunit | black | blue | | | | | | | | |
| SPBC13E7.04 | atp16 | F1-ATPase delta subunit | | | | black | blue | brown | | | | |
| SPAC13C5.03 | tht1 | nuclear membrane protein involved in karyogamy | | | | black | blue | brown | | | | |
| | | | | | | | | | | | | |
| SPBP35G2.06c | nup131 | nucleoporin Nup131 | black | blue | | | | brown | | | | purple |
| SPBC1734.12c | alg12 | dolichyl pyrophosphate Man7GlcNAc2 alpha-1,3-glucosyltransferase Alg12 | | | | black | blue | | | | | |
| SPBC19C7.02 | ubr1 | N-end-recognizing protein Ubr1 | | | | black | | | | blue | | |
| SPAC3H5.07 | rpl702 | 60S ribosomal protein L7 | | | | | | | black | blue | | |
| SPBC12C2.02c | ste20 | sterility protein Ste20 | | | | | blue | brown | | | | |
| SPBC646.13 | sds23 | inducer of sexual development Sds23/Moc1 | black | blue | brown | | | | | | | |
| SPBC1734.06 | rhp18 | Rad18 homolog Rhp18 | | | | black | blue | brown | | | | |
| SPBC651.02 | | nitrilase | | | | black | blue | brown | | | | |
| | | | | | | | | | | | | |
| SPBC1734.07c | | TRAPP complex subunit Trs85 | | blue | | black | | brown | | | | |
| SPBC646.17c | dic1 | dynein intermediate chain Dic1 | | blue | | black | | brown | | | | |
| SPBC18H10.06c | swd2 | COMPASS complex subunit Swd2 | | | | | blue | brown | | | | |
| SPBP35G2.14 | | RNA-binding protein | | | | | | | | | | purple |
| SPBC146.06c | | human MTMR15 homolog | | | | | | | | | | purple MTMR15 |
| SPBC146.04 | | sulfhydryl oxidase | black | blue | | | | brown | | | | purple |
| SPBC1921.05 | ape2 | aminopeptidase Ape1 | | | | black | blue | | | | | |
| | | | | | | | | | | | | |
| SPBC24C6.06 | gpa1 | G-protein alpha subunit | | | | black | blue | | | | | |
| SPBC1D7.05 | byr2 | MAP kinase kinase kinase Byr2 | | | | black | blue | brown | | | | |
| SPBC21.05c | ral2 | Ras guanyl-nucleotide exchange factor Ral2 | | | | black | blue | | | | | |
| SPCC1223.02 | nmt1 | no message in thiamine Nmt1 | | | | | | | black | blue | | |
| SPAC17A2.13c | rad25 | 14-3-3 protein Rad25 | | | | | | | black | blue | | |
| SPACUNK4.12c | mug138 | metallopeptidase | | | | black | blue | | | | | |
| SPCC1827.04 | | ankyrin repeat protein, unknown biological role | | | | | | | black | blue | | purple |
| SPBC337.07c | | carboxypeptidase | | | | | blue | | | | | purple |
| SPAC15A10.03c | rhp54 | Rad54 homolog Rhp54 | | | | | blue | brown | | | | |
| SPAC23E2.03c | ste7 | meiotic suppressor protein Ste7 | | | | black | blue | brown | | | | |
| SPBC3B8.02 | php5 | CCAAT-binding factor complex subunit Php5 | black | | | | blue | brown | | | | |
| SPAC15E1.05c | | ethanolamine-phosphate cytidylyltransferase | | | | black | blue | brown | | | | |

**Table 5.1a | Genes in the Bioneer® library that resulted in a significant genetic interaction with *fan1* following visual inspection of synthetic genetic arrays.** The result of three independent screens is shown. Only genetic interactions scored for both screen 1 (black) and 3 (blue) are shown. Screen 2 (brown) was additionally compared with the screens 1 and 3 as a further quality control. Gene IDs, gene names and descriptions are extracted from the strain list provided with the Bioneer® deletion mutant haploid set. Linkage (ORF ± 50 kb): purple boxes indicate genes within ± 50 kb from the *fan1* ORF.

| Gene ID | Gene name | Description | Synthetic sickness | | | Synthetic lethality | | | Alleviating | | | Linkage (ORF ± 50 kb) |
|---|---|---|---|---|---|---|---|---|---|---|---|---|
| SPAC1D4.06c | csk1 | cyclin-dependent kinase activating kinase Csk1 | | | | black | blue | brown | | | | |
| SPAP7G5.04c | lys1 | aminoadipate-semialdehyde dehydrogenase | | | | black | blue | brown | | | | |
| SPAC15E1.10 | | PI31 proteasome regulator related | | | | black | blue | brown | | | | |
| SPBP35G2.07 | ilv1 | acetolactate synthase catalytic subunit | | | | black | blue | brown | | | | purple |
| SPCC1442.01 | ste6 | guanyl-nucleotide exchange factor Ste6 | | | | black | blue | brown | | | | |
| SPAC3C7.03c | rhp55 | RecA family ATPase Rhp55 | | | | black | blue | brown | | | | |
| | | | | | | | | | | | | |
| SPAC11G7.04 | ubi1 | ribosomal-ubiquitin fusion protein Ubi1 | black | blue | | | | | | | | |
| SPAC1002.06c | bqt2 | bouquet formation protein Bqt2 | | | | black | blue | | | | | |
| SPBC8E4.05c | | fumarate lyase superfamily | | | | | blue | | | | | |
| SPAC10F6.12c | mam4 | protein-S isoprenylcysteine O-methyltransferase Mam4 | | | | | blue | brown | | | | |
| SPBC3B8.03 | | saccharopine dehydrogenase | | | | | blue | | | | | |
| SPAC15E1.02c | | DUF1761 family protein | | | | | blue | | | | | |
| SPAC25B8.18 | | mitochondrial electron carrier | | blue | | | blue | brown | | | | |
| SPCP1E11.04c | pal1 | membrane associated protein Pal1 | | | | | blue | | | | | |
| SPBC337.15c | coq7 | ubiquinone biosynthesis protein Coq7 | | blue | | black | | brown | | | | purple |
| SPAC1F12.04c | | conserved fungal protein | | | | | blue | | | | | |
| SPBC13E7.03c | | RNA hairpin binding protein | | | | | blue | | | | | |
| | | | | | | | | | | | | |
| SPAC22E12.03c | | THIJ/PFPI family peptidase | | blue | | black | | | | | | |
| SPAP7G5.05 | rpl1002 | 60S ribosomal protein L10 | | | | black | blue | brown | | | | |
| SPBC27B12.10c | tom7 | mitochondrial TOM complex subunit Tom7 | | | | | | | | blue | | |
| | | | | | | | | | | | | |
| SPCC553.12c | | conserved fungal protein | | | | black | blue | | | | | |
| SPAC1F12.02c | p23fy | translationally controlled tumor protein homolog | | | | black | blue | | | | | |
| SPBC2G2.10c | mug110 | sequence orphan | | | | black | blue | brown | | | | |
| SPAC15A10.15 | sgo2 | shugoshin Sgo2 | | | | black | blue | brown | | | | |
| SPAC15A10.08 | ain1 | alpha-actinin | | | | black | blue | | | | | |
| SPCC1235.09 | | histone deacetylase complex subunit | | | | black | | | | | | |
| SPCC1672.04c | | mitochondrial copper ion transport protein | | | | | | | black | blue | | |
| SPAC644.08 | | haloacid dehalogenase-like hydrolase | | | | black | | | | blue | brown | |
| SPAC17G8.13c | mst2 | histone acetyltransferase Mst2 | | | | black | blue | brown | | | | |
| SPAC144.06 | apl5 | AP-3 adaptor complex subunit Apl5 | | | | black | | | | blue | | |
| SPBC146.11c | mug97 | meiotically upregulated gene Mug97 | black | | brown | | blue | | | | | purple |

**Table 5.1b | Genes in the Bioneer® library that resulted in a significant genetic interaction with *fan1* following visual inspection of synthetic genetic arrays.** The result of three independent screens is shown. Only genetic interactions scored for both screen 1 (black) and 3 (blue) are shown. Screen 2 (brown) was additionally compared with the screens 1 and 3 as a further quality control. Gene IDs, gene names and descriptions are extracted from the strain list provided with the Bioneer® deletion mutant haploid set. Linkage (ORF ± 50 kb): purple boxes indicate genes within ± 50 kb from the *fan1* ORF.

truly severe genetic interaction. However, tetrad analysis with this pair of genes is hampered by the proximity of the two ORFs, separated by approximately 57 kb. Thus, a different approach and further work would be required to address this issue.

Surprisingly, *rhp55*-d appeared to be again synthetic lethal with *fan1*-d, despite the fact that this possibility was ruled out by tetrad analysis (supplementary fig. 9.15). This particular case is further discussed in 5.4.1.

Consistently with the visual approach, no other severe genetic interactions were shown between *fan1* and known components of DNA repair pathways in standard conditions of growth.

In an attempt to validate the method used, four additional mutant strains (*byr1*-d, *byr2*-d, *pub1*-d, *csk1*-d) were freshly streaked from the synthetic lethality set (high confidence) and independently crossed with wt strains 501 (h-) and 503 (h+). After three days on ELN plates at 25°C, no spores were visible for the any of the three crosses following iodine staining, whereas 501 and 503 turned dark red, indicating efficient processes of mating and sporulation for this control strains (supplementary figure 9.20). The absence of spores was confirmed by visual inspection by microscope. Thus, this test cross indicate that the four mutants from the Bioneer® library are pulled out in the final synthetic lethality set because of a general dysfunction in the mating and/or sporulation process and not because of synthetic lethal genetic interaction with *fan1*.

### 5.3.5   The cisplatin sensitivity screen reveals new genetic interactions with DNA repair components

As shown in the previous chapter, epistasis analysis has proven to be a useful tool to define the role of proteins acting in pathways of DNA repair that are alternative to the one where Fan1$^{Sp}$ is involved. However, the epistasis analysis presented in the previous chapter was based on a rational selection of components of DNA repair pathways known from previous published work. In order to extend the investigation to yet uncharacterised genetic interactions, the

| Colour code | | | Gene ID | Bioneer® plate ref. | Gene name | Description | Linkage? (ORF ± 50 kb) |
|---|---|---|---|---|---|---|---|
| | 🟥 | | **Synthetic Lethality (SL)** | | | | |
| | | | High confidence | | | | |
| | | | SPAC11D3.18c | V2-04-B09 | | nicotinic acid plasma membrane transporter | |
| | | | SPAC15A10.16 | V2-04-C12 | bud6 | actin interacting protein 3 homolog Bud6 | |
| | | | SPAC1D4.13 | V2-05-F06 | byr1 | MAP kinase kinase Byr1 | |
| | | | SPAC11G7.02 | V2-04-F09 | pub1 | ubiquitin-protein ligase E3 | |
| | | | SPBC13E7.04 | V2-03-G09 | atp16 | F1-ATPase delta subunit | |
| | | | SPAC13C5.03 | V2-04-G10 | tht1 | nuclear membrane protein involved in karyogamy | |
| | | | SPBC651.02 | V2-08-H05 | | nitrilase | |
| | | | SPBC18H10.06c | V2-11-F03 | swd2 | COMPASS complex subunit Swd2 | |
| | | | SPBP35G2.14 | V2-10-F10 | | RNA-binding protein | |
| | | | SPBC146.06c | V2-12-F06 | | human MTMR15 homolog | MTMR15 |
| | | | SPBC1921.05 | V2-12-G07 | ape2 | aminopeptidase Ape1 | |
| | | | SPBC24C6.06 | V2-15-A03 | gpa1 | G-protein alpha subunit | |
| | | | SPBC1D7.05 | V2-15-B02 | byr2 | MAP kinase kinase kinase Byr2 | |
| | | | SPBC21.05c | V2-15-C02 | ral2 | Ras guanyl-nucleotide exchange factor Ral2 | |
| | | | SPACUNK4.12c | V2-17-E12 | mug138 | metallopeptidase | |
| | | | SPAC23E2.03c | V2-14-H06 | ste7 | meiotic suppressor protein Ste7 | |
| | | | SPBC3B8.02 | V2-16-H07 | php5 | CCAAT-binding factor complex subunit Php5 | |
| | | | SPAC15E1.05c | V2-16-H11 | | ethanolamine-phosphate cytidylyltransferase | |
| | | | SPAC1D4.06c | V2-19-A02 | csk1 | cyclin-dependent kinase activating kinase Csk1 | |
| | | | SPCC1795.06 | V2-25-A05 | map2 | P-factor | |
| | | | SPAP7G5.04c | V2-22-B02 | lys1 | aminoadipate-semialdehyde dehydrogenase | |
| | | | SPAC15E1.10 | V2-22-B05 | | PI31 proteasome regulator related | |
| | | | SPAC3C7.03c | V2-19-G03 | rhp55 | RecA family ATPase Rhp55 | |
| | | | SPCC1393.10 | V2-25-G06 | ctr4 | copper transporter complex subunit Ctr4 | |
| | | | SPBP35G2.13c | V2-19-H11 | swc2 | chromatin remodeling complex subunit Swc2 | 🟪 |
| | | | SPAC1565.04c | V2-20-A11 | ste4 | adaptor protein Ste4 | |
| | | | SPAC10F6.12c | V2-24-B08 | mam4 | protein-S isoprenylcysteine O-methyltransferase Mam4 | |
| | | | SPAC25B8.18 | V2-23-E10 | | mitochondrial electron carrier | |
| | | | SPBC13E7.03c | V2-23-H04 | | RNA hairpin binding protein | |
| | | | SPAC1F12.02c | V2-33-A10 | p23fy | translationally controlled tumor protein homolog | |
| | | | SPBC2G2.10c | V2-29-B08 | mug110 | sequence orphan | |
| | | | SPAC15A10.15 | V2-30-B03 | sgo2 | shugoshin Sgo2 | |
| | | | SPAC15A10.08 | V2-30-D03 | ain1 | alpha-actinin | |
| | | | SPCC1235.09 | V2-30-D08 | | histone deacetylase complex subunit | |
| | | | SPAC17G8.13c | V2-28-H04 | mst2 | histone acetyltransferase Mst2 | |
| | | | Low confidence | | | | |
| | | | SPAC1556.03 | V2-04-H11 | azr1 | serine/threonine protein phosphatase Azr1 | |
| | | | SPAC8C9.12c | V2-06-C11 | | iron ion transporter | |
| | | | SPBC337.04 | V2-08-D02 | ppk27 | serine/threonine protein kinase Ppk27 | 🟪 |
| | | | SPBC1734.07c | V2-10-A02 | | TRAPP complex subunit Trs85 | |
| | | | SPCC1442.01 | V2-19-D12 | ste6 | guanyl-nucleotide exchange factor Ste6 | |
| | | | SPAC11G7.04 | V2-23-A09 | ubi1 | ribosomal-ubiquitin fusion protein Ubi1 | |
| | | | SPBC337.15c | V2-24-F03 | coq7 | ubiquinone biosynthesis protein Coq7 | 🟪 |

**Table 5.2 | Interactions between *fan1* and a series of deletion mutants from the Bioneer®library showed as synthetically lethal, as determined by the computational analysis of colony size.** High confidence is defined by: 1) high consistency of results across the screens and 2) higher degree of size deviation of the double mutant from the median compared to the size deviation of the corresponding single mutant. In cases where the single mutant showed poor viability, any apparent synthetic lethality with *fan1* was removed from the dataset. Gene IDs, Bioneer® plate reference, gene names and descriptions are extracted from the strain list provided with the Bioneer® deletion mutant haploid set. Linkage (ORF ± 50 kb): purple boxes indicate genes within ± 50 kb from the *fan1* ORF.

| Colour code | Gene ID | Bioneer® plate ref. | Gene name | Description | Linkage? (ORF ± 50 kb) |
|---|---|---|---|---|---|
| | **Synthetic Sickness (SS)** | | | | |
| | *High confidence* | | | | |
| | SPBC83.04 | V2-02-D11 | apc15 | anaphase-promoting complex subunit Apc15 | |
| | SPBC336.14c | V2-08-B02 | ppk26 | serine/threonine protein kinase Ppk26 | |
| | SPBC530.14c | V2-17-H08 | dsk1 | SR protein-specific kinase Dsk1 | |
| | SPBP4H10.05c | V2-26-G01 | spe2 | S-adenosylmethionine decarboxylase proenzyme Spe2 | |
| | SPBC20F10.03 | V2-24-G02 | | conserved eukaryotic protein | |
| | *Low confidence* | | | | |
| | SPBC354.13 | V2-08-G02 | rga6 | GTPase activating protein Rga6 | |
| | SPAC4H3.07c | V2-11-H01 | | protein phosphatase Fmp31 | |
| | SPBC1709.04c | V2-22-D10 | cyp3 | cyclophilin family peptidyl-prolyl cis-trans isomerase Cyp3 | |
| | SPCC576.12c | V2-25-E05 | | conserved eukaryotic protein | |
| | SPBC651.03c | V2-19-G10 | gyp10 | GTPase activating protein Gyp10 | |
| | SPAC630.04c | V2-23-B12 | | sequence orphan | |
| | **Synthetic Sickness / Synthetic Lethality (SS/SL)** | | | | |
| | *High confidence* | | | | |
| | SPAC17A2.06c | V2-05-C02 | vps8 | WD repeat protein Vps8 | |
| | SPCC16C4.11 | V2-03-F02 | pef1 | Pho85/PhoA-like cyclin-dependent kinase Pef1 | |
| | SPBC19G7.04 | V2-07-A08 | | HMG box protein | |
| | SPBC1734.12c | V2-09-B12 | alg12 | glucosyltransferase Alg12 | |
| | SPAC24H6.03 | V2-12-G02 | cul3 | cullin 3 | |
| | SPBC1709.13c | V2-15-A01 | | lysine methyltransferase | |
| | SPCC584.13 | V2-15-A12 | | amino acid permease, unknown 14 | |
| | SPBC337.07c | V2-16-G07 | | carboxypeptidase | ▰ |
| | SPAC6B12.12 | V2-22-A01 | tom70 | mitochondrial TOM complex subunit Tom70 | |
| | SPBC1734.05c | V2-23-A05 | spf31 | DNAJ protein Spf31 | |
| | SPAP7G5.05 | V2-27-A08 | rpl1002 | 60S ribosomal protein L10 | |
| | SPBC1734.15 | V2-30-E11 | rsc4 | RSC complex subunit Rsc4 | |
| | *Low confidence* | | | | |
| | SPBC146.10 | V2-02-A06 | mug57 | meiotically upregulated gene Mug57 | ▰ |
| | SPCC1223.15c | V2-03-B02 | spc19 | DASH complex subunit Spc19 | |
| | SPBC1539.06 | V2-02-C06 | | acyl-coenzyme A binding protein | |
| | SPBC1709.18 | V2-02-G07 | tif452 | translation initiation factor eIF4E 4F complex subunit | |
| | SPBC216.05 | V2-03-G10 | rad3 | ATR checkpoint kinase | |
| | SPBP35G2.06c | V2-08-B09 | nup131 | nucleoporin Nup131 | ▰ |
| | SPBC36.07 | V2-08-C03 | iki3 | RNA polymerase II elongator subunit Iki3 | |
| | SPBC3H7.13 | V2-08-G03 | | FHA domain protein Far10 | |
| | SPBC646.13 | V2-08-G05 | sds23 | inducer of sexual development Sds23/Moc1 | |
| | SPBC1734.06 | V2-09-G09 | rhp18 | Rad18 homolog Rhp18 | |
| | SPBC216.04c | V2-07-H08 | | methionine sulfoxide | |
| | SPBC1105.04c | V2-12-C06 | cbp1 | CENP-B homolog | |
| | SPBC646.17c | V2-11-E08 | dic1 | dynein intermediate chain Dic1 | |
| | SPCC622.16c | V2-12-F11 | epe1 | transcription factor Epe1 | |
| | SPBP35G2.11c | V2-10-G02 | | transcription related zf-ZZ type zinc finger protein | ▰ |
| | SPBC146.04 | V2-10-G08 | | sulfhydryl oxidase | |
| | SPBC1711.05 | V2-15-B01 | | nucleocytoplasmic transport chaperone Srp40 | |
| | SPBC409.11 | V2-17-E08 | meu18 | sequence orphan | |
| | SPAC8F11.10c | V2-22-B09 | pvg1 | pyruvyltransferase | |
| | SPBC1709.11c | V2-21-H04 | png2 | ING family homolog Png2 | |
| | SPCC970.05 | V2-21-H11 | rpl3601 | 60S ribosomal protein L36 | |
| | SPBP35G2.04c | V2-26-A04 | | sequence orphan | ▰ |
| | SPBC8E4.05c | V2-23-B01 | | fumarate lyase superfamily | |
| | SPAC3A12.13c | V2-26-B10 | | translation initiation factor eIF3 complex subunit | |
| | SPBC1709.16c | V2-24-E02 | | conserved protein (fungal bacterial plant) | |
| | SPCP1E11.04c | V2-20-F03 | pal1 | membrane associated protein Pal1 | |
| | SPAC4F10.14c | V2-24-G08 | btf3 | nascent polypeptide-associated complex subunit | |
| | SPAC1F12.04c | V2-26-G12 | | conserved fungal protein | |
| | SPBC409.03 | V2-33-E11 | swi5 | Swi5 protein | |
| | SPBC146.11c | V2-28-H05 | mug97 | meiotically upregulated gene Mug97 | ▰ |

**Table 5.3 | Interactions between *fan1* and a series of deletion mutants from the Bioneer®library showed as synthetic sick and synthetic sick / lethal (SS/SL), as determined by the computational analysis of colony size.** SS/SL represents varied but consistent negative interactions across different screens. High confidence is defined by: 1) high consistency of results across the screens and 2) higher degree of size deviation of the double mutant from the median compared to the size deviation of the corresponding single mutant. Gene IDs, Bioneer® plate reference, gene names and descriptions are extracted from the strain list provided with the Bioneer® deletion mutant haploid set. Linkage (ORF ± 50 kb): purple boxes indicate genes within ± 50 kb from the fan1 ORF.

| Colour code | | Gene ID | Bioneer® plate ref. | Gene name | Description | Linkage? (ORF ± 50 kb) |
|---|---|---|---|---|---|---|
| | | **Alleviating (positive interactions)** | | | | |
| | | High confidence | | | | |
| | | SPAC25A8.01c | V2-03-E06 | | fun thirty related protein Fft3 | |
| | | SPBC29A3.21 | V2-02-E09 | | sequence orphan | |
| | | SPCC126.11c | V2-04-F02 | | RNA-binding protein | |
| | | SPAC24C9.14 | V2-05-F11 | otu1 | ubiquitin-specific protease | |
| | | SPBPB2B2.10c | V2-08-B10 | | galactose-1-phosphate uridylyltransferase | |
| | | SPAC12B10.05 | V2-09-B11 | | metallopeptidase | |
| | | SPAC3H5.07 | V2-06-E05 | rpl702 | 60S ribosomal protein L7 | |
| | | SPAC13G7.05 | V2-16-C11 | | acyl-coA-sterol acyltransferase | |
| | | SPBC3E7.11c | V2-15-D05 | | DNAJ protein Caj1/Djp1-type | |
| | | SPBP4G3.02 | V2-15-D07 | pho1 | acid phosphatase Pho1 | |
| | | SPCC1223.02 | V2-15-D08 | nmt1 | no message in thiamine Nmt1 | |
| | | SPCC18.17c | V2-15-D10 | | sequence orphan | |
| | | SPAC18B11.10 | V2-16-E02 | tup11 | transcriptional corepressor Tup11 | |
| | | SPAC17A2.13c | V2-16-E12 | rad25 | 14-3-3 protein Rad25 | |
| | | SPBC428.14 | V2-15-F05 | | 1-acylglycerol-3-phosphate acyltransferase | |
| | | SPAC323.01c | V2-22-B08 | | mitochondrial NADH kinase | |
| | | Low confidence | | | | |
| | | SPAC23G3.08c | V2-05-A11 | ubp7 | ubiquitin C-terminal hydrolase Ubp7 | |
| | | SPAC23H4.17c | V2-03-B06 | srb10 | cyclin-dependent protein kinase Srb10 | |
| | | SPAC24H6.11c | V2-03-C06 | | sulfate transporter | |
| | | SPAC24C9.08 | V2-05-E11 | | vacuolar carboxypeptidase | |
| | | SPAPB17E12.02 | V2-02-G03 | yip12 | SMN family protein Yip12 | |
| | | SPBC725.10 | V2-04-G01 | | tspO homolog | |
| | | SPAC57A7.12 | V2-06-E07 | | heat shock protein Pdr13 | |
| | | SPAC630.05 | V2-06-G07 | gyp7 | GTPase activating protein Gyp7 | |
| | | SPBC1348.02 | V2-13-B11 | | S. pombe specific 5Tm protein family | |
| | | SPAC8F11.08c | V2-14-B10 | | esterase/lipase | |
| | | SPBC582.10c | V2-15-C06 | | ATP-dependent DNA helicase Rhp16b | |
| | | SPBC713.07c | V2-15-D06 | | vacuolar polyphosphatase | |
| | | SPBC3E7.16c | V2-15-E05 | leu3 | 2-isopropylmalate synthase | |
| | | SPCC1235.12c | V2-15-E08 | mug146 | meiotically upregulated gene Mug46 | |
| | | SPCC63.14 | V2-17-E11 | | conserved fungal protein | |
| | | SPBC2F12.03c | V2-15-F03 | | EST1 family protein | |
| | | SPBC776.15c | V2-15-F06 | | e2 component of oxoglutarate dehydrogenase complex | |
| | | SPCC1259.11c | V2-15-F08 | gyp2 | GTPase activating protein Gyp2 | |
| | | SPCC16A11.04 | V2-15-F09 | snx12 | sorting nexin Snx12 | |
| | | SPBC16A3.19 | V2-14-F12 | | histone acetyltransferase complex subunit Eaf7 | |
| | | SPCC16C4.06c | V2-15-G09 | | tRNA pseudouridylate synthase (predicted) | |
| | | SPBC16G5.07c | V2-14-G12 | | prohibitin | |
| | | SPAC30D11.11 | V2-14-H07 | | Haemolysin-III family protein | |
| | | SPBC12C2.08 | V2-14-H11 | dnm1 | dynamin Dnm1 | |
| | | SPAC343.15 | V2-16-H05 | tit1 | tRNA isopentenyltransferase | |
| | | SPCC663.12 | V2-24-G06 | cid12 | poly(A) polymerase Cid12 | |
| | | SPAC644.08 | V2-33-E06 | | haloacid dehalogenase-like hydrolase | |

**Table 5.4 | Interactions between *fan1* and a series of deletion mutants from the Bioneer®library showed as positive interactions, as determined by the computational analysis of colony size.** High confidence is defined by: 1) high consistency of results across the screens and 2) higher degree of size deviation of the double mutant from the median compared to the size deviation of the corresponding single mutant. Gene IDs, Bioneer® plate reference, gene names and descriptions are extracted from the strain list provided with the Bioneer® deletion mutant haploid set.

| Gene ID | Bioneer® plate ref. | Gene name | Description |
|---|---|---|---|
| SPAC1687.05 | V2-05-A01 | pli1 | SUMO E3 ligase Pli1 |
| SPAC1952.07 | V2-05-B05 | rad1 | checkpoint clamp complex protein Rad1 |
| SPBC3E7.08c | V2-13-C04 | rad13 | DNA repair nuclease Rad13 |
| SPAC20G4.04c | V2-19-C02 | hus1 | checkpoint clamp complex protein Hus1 |
| SPAC9E9.14 | V2-28-D07 | vps24 | vacuolar sorting protein Vps24 |
| SPAC14C4.13 | V2-30-G05 | rad17 | RFC related checkpoint protein Rad17 |

**Table 5.5| Double mutants that showed progressive increased sensitivity to cisplatin in all the three independent screens.** Gene IDs, Bioneer® plate reference, gene names and descriptions are extracted from the strain list provided with the Bioneer® deletion mutant haploid set.

computational approach presented above was applied to a screen for synthetic hypersensitivity to the DNA damaging agent cisplatin. Plates carrying double mutant strains from the automated replicas (fig. 5.1, step *l*) were replicated onto plates containing increasing concentrations of cisplatin (0 μM, 50μM, 200 μM, 600 μM). The size of the colonies arising after 24 hours and 39 hours of growth was calculated and analysed, in search for consistent and progressive reduction in colony size with increasing concentrations of cisplatin. An example of Excel® spreadsheet build for this analysis is shown in supplementary fig. 9.18. By intersecting the data from three independent screens, six candidates showed a progressive and consistent reduction in colony size upon increasing concentrations of cisplatin (table 5.5). The presence of the DNA repair nuclease Rad13 in the list proved to be an important initial validation of the methodology, as the deletion of this gene already showed synergistic hypersensitivity to cisplatin when combined with *fan1*-d (see 4.3.7). However, as this analysis was performed only on double mutants, it could not be excluded that the hypersensitivity to cisplatin was in fact due to the sole single mutant in the deletion library, and not to the combination with *fan1*-d. To assess whether the hypersensitivity shown in the screen is a true synergistic hypersensitivity and to provide a further validation to the methodology, double disruptants were recreated from independently derived mutants and then tested by employing standard *in vivo* survival assays.

Rad1[Sp] and Hus1[Sp] are part of the 9-1-1 clamp complex, which play crucial roles in checkpoint activation following DNA damage (Caspari et al., 2000; Parrilla-Castellar et al., 2004). Rad17[Sp] acts as a clamp loader for the trimeric complex (Parilla-Castellar et al., 2004). Interestingly, all these three highly correlated factors were pulled out in the screen. Rad9[Sp], third component of the 9-1-1 complex, could not be in the final list because it was missing in the series of deletion mutants tested.

When tested for sensitivity to cisplatin, both the *fan1*-d mutants 3909N and 14152N showed a strong hypersensitivity when combined with *rad1*-d, *hus1*-d or *rad17*-d (fig. 5.5). This data proved to be a good validation for the methodology used in the screen. However, the single mutants were similarly highly sensitive, indicating an epistatic interaction between these
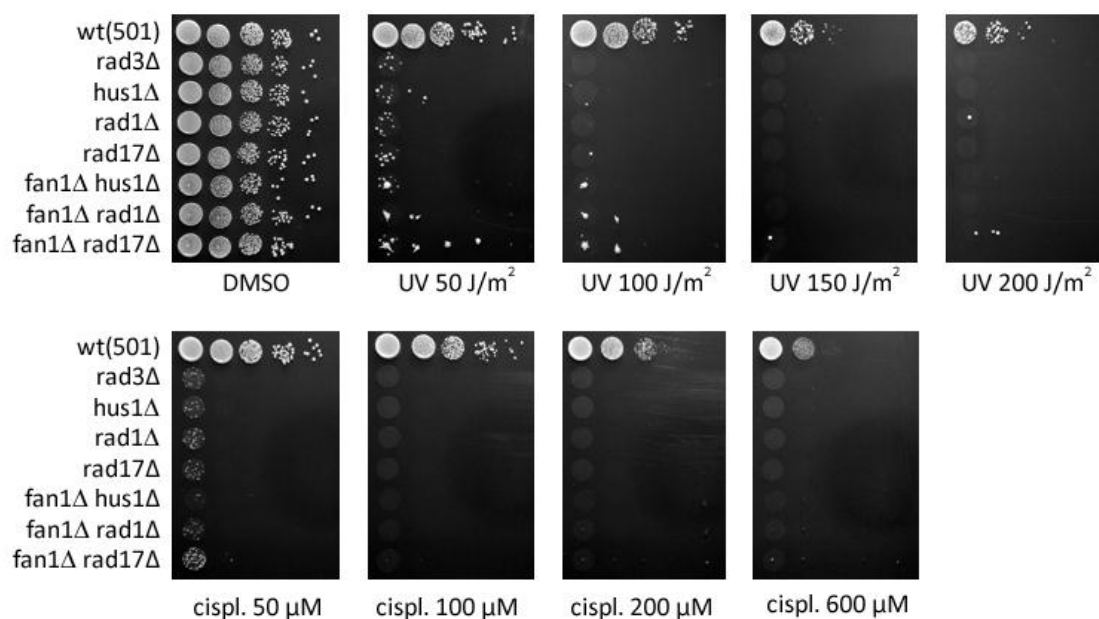


**Figure 5.5| Sensitivity of *hus1*, *rad1* and *rad17* mutants to UV cisplatin.** Logarithmically grown cultures were spotted in four 1:10 serial dilutions starting from $10^7$ cells (first spot on the left) on YEA plates containing the agents in the amount indicated. *rad3*-d is used as a standard hypersensitive control for the efficacy of the agents used. The double mutants tested in this experiment are derived from independently constructed single deletion mutants. All the mutants shown, alone or in combination with *fan1*-d, display a dramatic hypersensitivity to both UV and cisplatin. Abbreviations used: UV, Ultra-Violet irradiation; cispl, cisplatin.

components and *fan1*. To determine whether the same occurs for the third component of the 9-1-1 complex Rad9[Sp], independently derived double mutants *fan1*-d *rad9*-d were constructed and tested by *in vivo* survival assays. Consistently with a common role as part of the 9-1-1 heterotrimer, *rad9*-d phenocopied *hus1*-d and *rad1*-d, either as a single mutant or in combination with *fan1*-d (supplementary fig. 9.19).

Intriguingly, *fan1*-d *pli1*-d was also pulled out as a hypersensitive double deletion mutant. Pli1 is a SUMO (small ubiquitin-related modifier) E3 ligase that has been associated with DNA repair, although its role has not been elucidated yet (Beratgink and Jentsch, 2009). When tested by *in vivo* survival assays, independently constructed *fan1*-d *pli1*-d mutants (3909 or 14152 background) showed hypersensitivity to cisplatin compared to the wild-type, *fan1*-d and *pli1*-d strains (fig. 5.6). This increased sensitivity is dramatic following exposure to cisplatin and
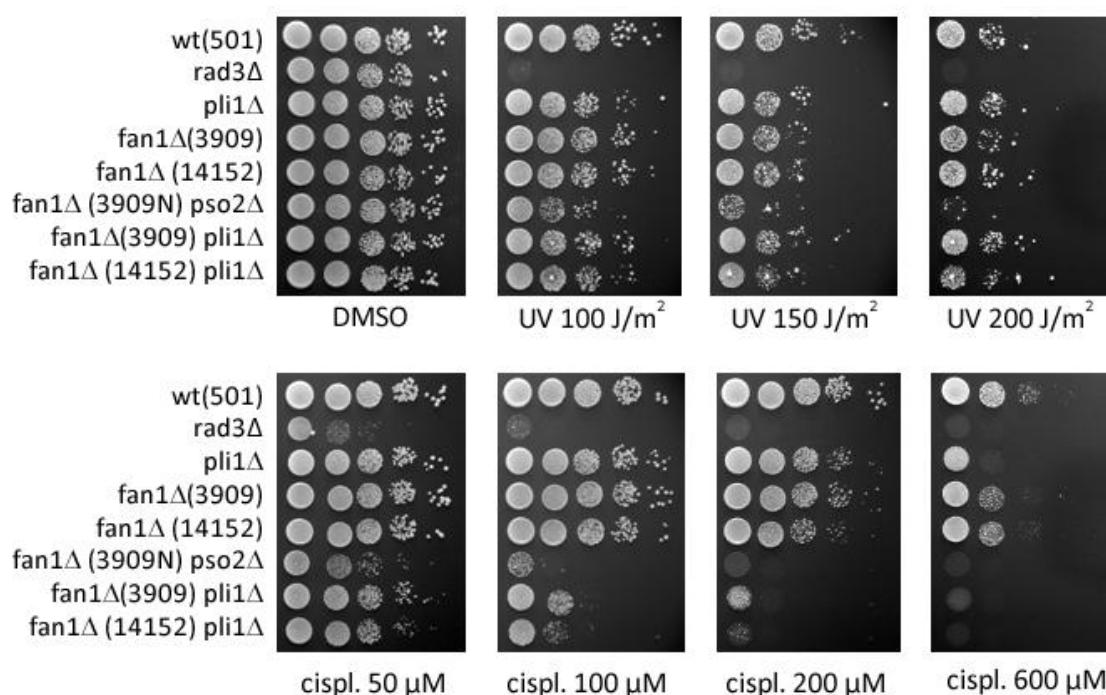


**Figure 5.6 | Sensitivity of *pli1*-d mutants to UV and cisplatin. *fan1*-d: 3909 and 14152 backgrounds.** Logarithmically grown cultures were spotted in four 1:10 serial dilutions starting from $10^7$ cells (first spot on the left) on YEA plates containing the agents in the amount indicated. *rad3*-d is used as a standard hypersensitive control for the efficacy of the agents used. The double mutants tested in this experiment are derived from independently constructed single deletion mutants. The combination of *fan1*-d and *pli1*-d leads to a strong hypersensitivity to cisplatin. Abbreviations used: UV, Ultra-Violet irradiation; cispl, cisplatin.

absent upon UV irradiation, indicating that the two proteins are required in response to the formation of DNA interstrand cross-links.

Taken together, these findings confirm that the application of the computational analysis of colony size to the high-throughput screen for sensitivity to cisplatin is an effective methodology that allowed the discovery of a novel genetic connection in the repair of DNA interstrand cross-links.

## 5.4    Discussion

### 5.4.1    Use of high-throughput approaches to explore novel genetic interactions in standard conditions of growth

The analysis presented in this chapter makes use of high-throughput approaches to rapidly generate and analyse an extensive number of double haploid mutants. The visual inspection provided only an initial indication of genetic interactions and was used primarily to assess apparent synthetic lethal combinations. Following the computational analysis of colony size, the subdivision of the entries into high and low degree of confidence allowed for the maintenance of potentially interesting but ambiguous candidates while creating a list of high-confidence interacting genes. Overall, the correspondence between the lists of candidate genetic interactions derived from the visual and the computational approach was satisfactory. The focus of this study is centred on potential pathways of DNA repair alternative to the one where Fan1$^{Sp}$ is involved. Thus, only candidates that had been previously associated with DNA repair were considered from the high-confidence list. All the ORFs identified with this initial approach were clustered in categories of biological processes based on Gene Ontologies from AmiGO Slim (http://old.genedb.org/amigo-cgi/slimmer). Only three genes resulted as entities involved in DNA repair: *rhp18*, *rhp54* and *rhp55* (table 5.1a/5.1b).

*rhp18*-d appeared to be synthetic sick with *fan1*-d, although no such phenotype was shown in previous experiments (see 4.3.8). The tetrad analysis on this combination of genes was

hampered by the proximity of the two ORFs. However, when the computational analysis of colony size was applied to better refine the categories of synthetic sickness and alleviating interaction, *rhp18* was classified under a low confidence SS/SL interaction (table 5.3), as the consistency across independent screens was unsatisfactory. Although it cannot be excluded that some form of genetic interaction between the two genes is at the basis of this abnormal behaviour, no further conclusion can be drawn from this data without additional experimental work.

*rhp54* represents another example of how the computational analysis led to a more accurate dataset of genetic interactions. From the visual approach, *rhp54*-d was found to be synthetic lethal with *fan1*-d (table 5.1a). With the computational analysis, the size of single mutant colonies was also taken into account. Indeed, the *rhp54* single deletion mutant was significantly smaller than the median colony size in all the screens performed. Thus, it was assumed that the reason underlying the absence of a *fan1*-d *rhp54*-d double mutant could be explained by the poor viability of the parental single mutant, rather than to true synthetic lethality. This criterion was applied to the whole screen and other few similar cases were excluded accordingly. This exclusion from the refined dataset is consistent with the analysis by tetrad dissection, which showed that *fan1*-d *rhp54*-d spores can indeed germinate (supplementary fig. 9.15).

*rhp55*-d was synthetic lethal with *fan1* in the visual screen, and in this case this finding was confirmed by the computational analysis (tables 5.1b and 5.2). The size of the single mutant was consistently close to the median value of colony size on the same plate, so the apparent synthetic lethality could not be explained by poor viability of the parental single mutant. However, when tested by tetrad analysis, *fan1*-d *rhp55*-d spores were viable (supplementary fig. 9.15). A possible explanation for this result is that the absence of Rhp55 provides an insurmountable obstacle for a correct sporulation specifically in the genetic background used for this screen. Rhp55 has shown to play important roles in mitotic recombination and meiosis,

although sporulation efficiency and spore viability are only reduced and not abolished in *rhp55*-d (Khasanov et al., 1999). Thus, it can be envisaged that the particular arrangement of the mating type locus in the query mutant may be incompatible with the deletion of genes involved in the recombination process during sporulation, such as *rhp55*. Accordingly, this might also be the case for other genes screened in this study. One way to exclude these false positives from the dataset would be to repeat the screens using a neutral NAT-resistant query mutant. With such query mutant, apparent synthetic lethality would in fact highlight obstacles in mating or sporulation processes. Without such additional controls, no further conclusion can be drawn with the only data available thus far.

### 5.4.2    Validations for the cisplatin automated screen

In the automated cisplatin screen presented in 5.3.5, *fan1*-d *rad13*-d showed a progressive and reproducible reduction in colony size upon increasing concentrations of cisplatin. The non-epistatic interaction between *fan1* and *rad13* had been already demonstrated by *in vivo* survival assays in the previous chapter. Although it would be difficult to trace a direct correspondence between the two methods, this data provided a first important validation for the computational approach applied to the cisplatin screen. Furthermore, other important validations derived from *in vivo* survival assays showing that three other genes pulled out in the screen (*rad1*, *hus1* and *rad17*) were indeed hypersensitive to cisplatin, although this was not dependent on the presence or absence of *fan1* (fig. 5.5). Further to the significance in validating the method underlying the cisplatin automated screen, this result suggests that the Fan1 pathway of ICL repair is epistatic to the 9-1-1 (Rad9-Rad1-Hus1) complex, required for DNA damage checkpoint activation. This aspect will be further discussed in 8.1.4.

### 5.4.3    SUMOylation is involved in the DNA interstrand cross-link response

Another potentially interesting candidate, the SUMO E3 ligase Pli1, was also pulled out in the screen. When tested by standard *in vivo* survival assays, the hypersensitivity to cisplatin was shown only for the combined *fan1 pli1* deletion (fig. 5.6). This result highlights a novel role for

this elusive component of DNA repair, placing SUMOylation in a pathway of ICL response alternative to the one where Fan1$^{Sp}$ is involved.

Post-translational modifications such as conjugation of ubiquitin (ubiquitylation) and ubiquitin-like substrates (i.e. SUMOylation) are important regulators of biological processes in eukaryotes. The importance of these classes of reversible modifications in DNA repair is highlighted by the fact that all the major components of DNA repair pathways are modified by ubiquitin, SUMO or both (Bergink and Jentsch, 2009). Interestingly, deubiquitylation plays a central regulatory role in the human ICL resolution pathway, where the deletion of the deubiquitylation enzyme USP1 leads to increased MMC-dependent chromosomal aberrations (Nijman et al., 2005). Likewise, in chicken cells the loss of USP1 causes hypersensitivity to DNA intercross-linkers (Oestergaard et al., 2007). Recent work has suggested that the recruitment of SNM1$^{Hs}$ (Pso2$^{Sc,Sp}$) to DNA ICLs is mediated by its UBZ (ubiquitin binding zinc finger) domain (Yang et al., 2010). Remarkably, FAN1$^{Hs}$ appears to be recruited to sites of damage in a similar fashion (Smogorzewska et al., 2010; MacKay et al., 2010; Kratz et al., 2010; Liu et al., 2010). As neither Fan1$^{Sp}$ nor Pso2$^{Sp}$ possess a UBZ domain, a different scenario can be envisaged where ubiquitylation is not required for recruitment of Fan1$^{Sp}$ to damage sites. Based on the data presented in this chapter, SUMOylation appears to play a still unidentified role in a Fan1$^{Sp}$ – independent pathway in the fission yeast. To date, no clear role has been identified for SUMOylation in the response to ICL formation. Thus, this novel role would indicate a further level of molecular control over the resolution of these DNA lesions. It would be interesting to establish whether a similar regulation exists in mammalian cells, either as an alternative or as an addition to the ubiquitylation system. Furthermore, extensive epistasis analysis in *S. pombe* could identify other components of the Pli1$^{Sp}$ pathway, including effectors such as nucleases that would be required for the repair process.

## 5.5    Conclusions

In this chapter, the use of high-throughput methodologies has led to the identification of novel genetic interactions between Fan1$^{Sp}$ and other various cellular components. Most importantly, the application of computational approaches has led to a better refinement of genetic interactions previously identified by a simple visual inspection. When these methods were applied to a screen for sensitivity to cisplatin, a novel genetic relationship could be established which pointed at a role for SUMOylation in processing of DNA interstrand cross-links.

In the next chapter, the focus is on the molecular level, where point mutations helped identify residues that are essential for Fan1 activity in *S. pombe*.

Chapter Six

PHENOTYPIC ANALYSIS OF FAN1$^{SP}$ POINT MUTANTS

## 6.1    Introduction

### 6.1.1    **Domain organisation of Fan1Sp**

In this chapter, *in vivo* survival assays are used to establish whether specific substitutions in the primary structure of Fan1Sp lead to a reduced or abolished biological function. FAN1Hs possesses three conserved domains: a UBZ-type ubiquitin-binding domain, a SAP-type DNA binding motif and a VRR_nuc domain (Virus-type Replication-Repair Nuclease). SAP (SAF-A/B, Acinus and PIAS) denotes putative DNA binding domains thought to be involved in chromosomal reorganisation (Aravind and Koonin, 2000). However, the specific function of these domains is still unclear. The VRR_nuc domain is associated with DNAses involved in repair and is characterized by a relatively conserved PD-(D/E)XK motif (Kinch et al., 2005; Iyer et al., 2006). Fan1Sp does not possess a UBZ domain, although the SAP and VRR_nuc domains are conserved (fig. 6.1 and Smogorzewska *et al.*, 2010). In particular, four residues are conserved between FAN1Hs and Fan1Sp: one residue in the SAP domain (SpL159) and three in
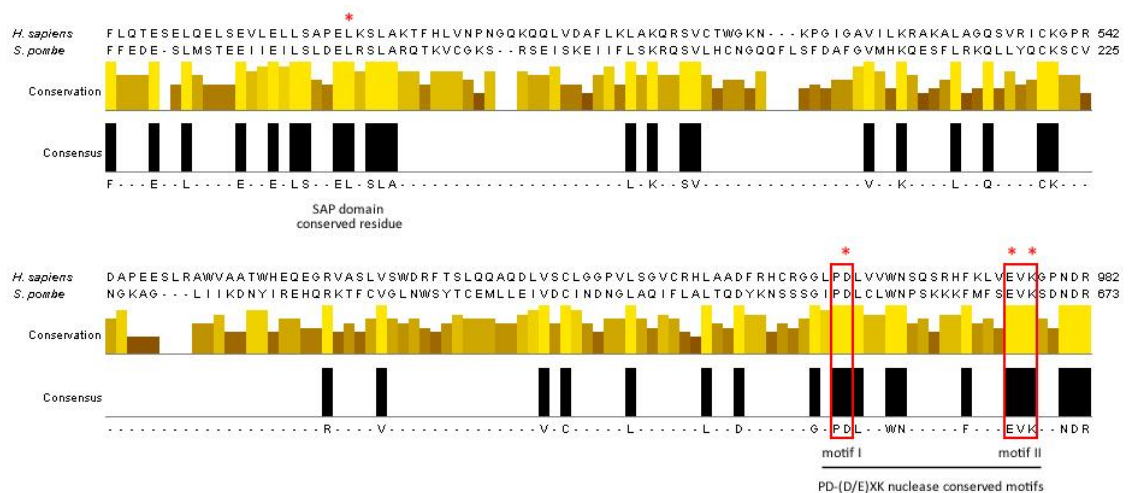


**Figure 6.1 | Alignment between FAN1Hs and Fan1Sp.** Screenshots manually annotated from ClustalW2 alignment (http://www.ebi.ac.uk/Tools/clustalw2/index.html). Boxes indicate two key conserved motifs of PD-(D/E)XK nucleases (Kinch *et al.*, 2005). Stars indicate the conserved residues mutated in this study.

the VRR_nuc domain (D651, E666, K668 in the *S. pombe* homolog) (fig. 6.1).

In order to assess the requirement for key residues for the biological function of Fan1$^{Sp}$, a series of point mutants were tested for sensitivity to cisplatin by *in vivo* survival assays.

## 6.2   Aim

The aim of this chapter is to associate specific key conserved residues to the biological activity of *S. pombe* Fan1. A series of point mutants were created, crossed into a *pso2::kanMX6* background and tested for sensitivity to increasing concentrations of cisplatin. In this context, an augmented sensitivity shown by a particular mutant can indicate the requirement for the corresponding residue in the biological function of Fan1$^{Sp}$.

## 6.3   Results

### 6.3.1   Combination of site-directed mutagenesis and recombinase-mediated cassette exchange

The possibility of introducing specific substitutions in the primary sequence of proteins of interest is a precious tool to link prospective key residues with biological activities. In the present study, site-directed mutagenesis was combined with recombinase-mediated cassette exchange as outlined in fig. 6.2. The initial step was the introduction of the point mutations by mutagenic PCR, where primers carrying the mutations of interest were used to amplify a wt *fan1* cassette on a pAW8 vector (fig. 6.2, step 1). In this way, mutated copies of the wt PAW8_fan1 vector, named PAW8_fan1_mut vector, were synthesized. The PAW8_fan1_mut vector was transformed in the previously constructed *loxP-fan1::ura4$^{+}$-loxM3* base strain (fig. 6.2, step 2 and 3). At this locus, recombinase-mediated cassette exchange replaced the mutant allele in the genome (fig. 6.2, step 4). The final product is a version of the *fan1* base strain carrying the point mutation of interest in the *fan1* ORF (*loxP-fan1_mut-loxM3*).
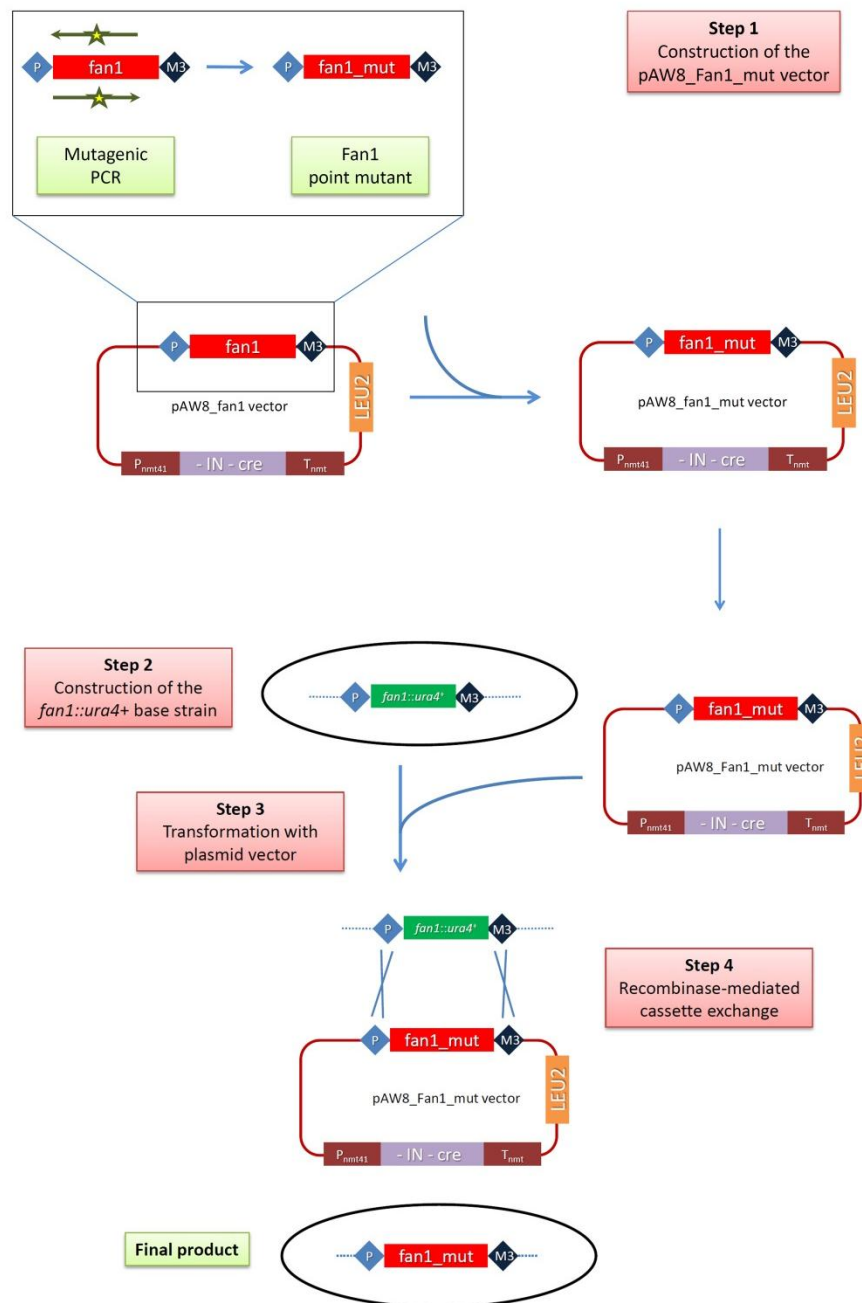
**Figure 6.2 | Combined approach of site-directed mutagenesis and recombinase-mediated cassette exchange used in this study.** The construction of pAW8_*fan1* vector and *fan1*::*ura4+* deletion base strain were obtained by standard molecular biology techniques. Fan1 point mutants on pAW8 vector were obtained by mutagenic PCR with primers described in 2.7.1. Dotted lines indicate cassettes located on a *S. pombe* chromosome. Crosses represent homologous recombination between loxP and loxM3 cassettes. Abbreviations: *ura4+*, *S. pombe* uracil marker; *LEU2*, *S. cerevisiae* leucine marker; *fan1*_mut, Fan1 point mutant; P, loxP site; M3, mutant loxM3 site; P$_{nmt41}$, *S. pombe nmt41* promoter; T$_{nmt}$, *nmt* terminator sequence; IN, *S. pombe rad50* intron 1; cre, gene coding for the recombinase Cre. Adapted from Watson et al., 2008.

## 6.3.2    **Point mutations in the nuclease domain abolish Fan1$^{Sp}$ activity**

Based on the combined analysis of sequence homology between Fan1$^{Sp}$, FAN1$^{Hs}$ and conserved

key residues in PD-(D/E)XK nucleases (fig. 6.1), three residues in the VRR_nuc domain were

mutated in this study: D651, E666, K668. The requirement for a functional SAP domain was

also tested by substituting the conserved residue L159. Substitute amino acids were chosen

with the aim of minimising possible distortions in the protein structure while removing the key

moiety of the original residue. As the deletion of *fan1* leads to only a mild sensitivity to

interstrand cross-linking agents (see 4.3.1), the point mutants were crossed into a

*pso2::kanMX6* background, since this combined deletion was expected to aggravate the

sensitivity to cisplatin of a non-functional Fan1. As a relevant control for the abolishment of

Fan1$^{Sp}$ activity, the *ura4+* deletion cassette in the *fan1::ura4+* base strain (fig. 6.2, step 2) was

replaced with a *natMX*6 cassette exploiting the same recombinase-mediated cassette

exchange employed to generate the point mutants. The *fan1*::*natMX6* base strain was then

crossed into a *pso2::kanMX6* background. It could be anticipated that the resulting double

mutant would phenocopy the hypersensitive *pso2*-d *fan1*-d (see 4.3.2).

As expected, the *pso2*-d *fan1*-d double mutant base strain displayed a marked hypersensitivity

when exposed to doses of cisplatin as low as 50 μM. All the three nuclease domain mutants

*fan1*-D651A,   *fan1*-E666Q   and   *fan1*-K668A   phenocopied   exactly   the   *pso2::kanMX6*

*fan1*::*natMX6* double mutant (fig. 6.3). The substitution of D651 with the structurally similar

residue asparagine (Fan1-D651N) showed the same hypersensitivity of the *fan1*-D651A. In

contrast, the SAP domain mutant *fan1*-L159A displayed a milder sensitivity to cisplatin, and

only at higher doses of agent (fig. 6.4). Taken together, these results indicate that the nuclease

activity is required for the biological activity of Fan1$^{Sp}$ in ICL repair. In contrast, the SAP domain

is not strictly necessary for this activity, although its absence markedly reduces Fan1$^{Sp}$

proficiency in ICL repair.
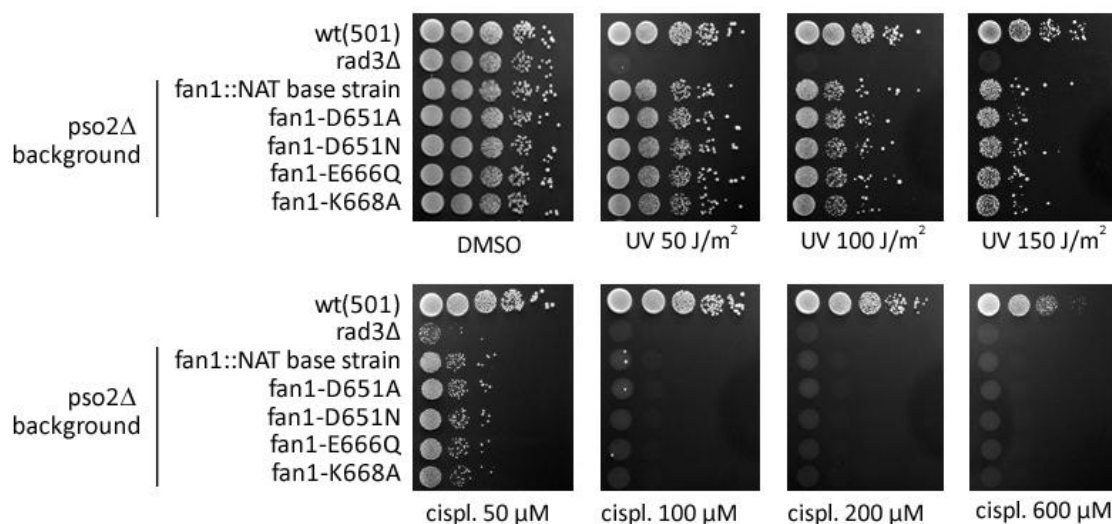
**Figure 6.3 | Sensitivity of Fan1 nuclease point mutants to UV and cisplatin.** Logarithmically grown cultures were spotted in four 1:10 serial dilutions starting from $10^7$ cells (first spot on the left) on YEA plates containing the agents in the amount indicated. *rad3*-d is used as a standard hypersensitive control for the efficacy of the agents used. Mutations in the Fan1$^{Sp}$ nuclease domain (D651A, D651N, E666Q, K668A) cause hypersensitivity to cisplatin. Abbreviations used: UV, Ultra-Violet irradiation; cispl, cisplatin.
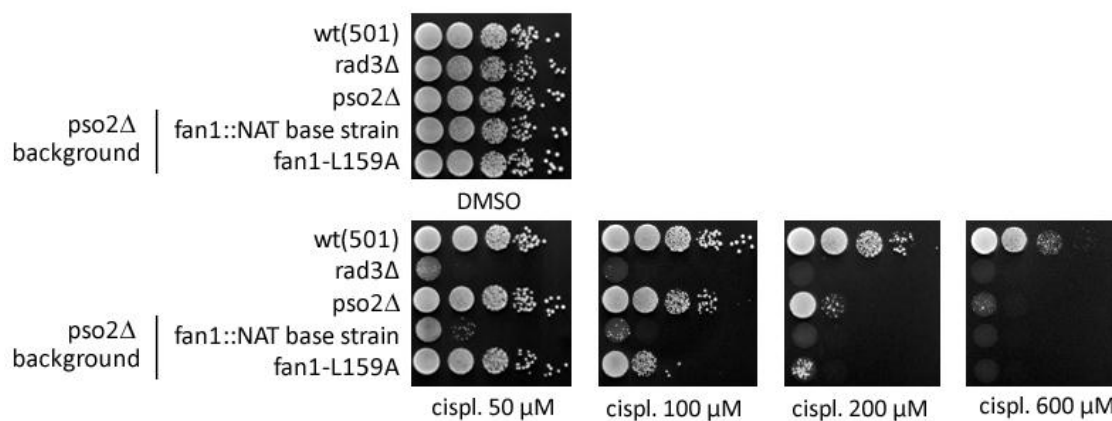


**Figure 6.4 | Sensitivity of the Fan1$^{Sp}$ SAP domain point mutant to cisplatin.** Logarithmically grown cultures were spotted in four 1:10 serial dilutions starting from $10^7$ cells (first spot on the left) on YEA plates containing the agents in the amount indicated. *rad3*-d is used as a standard hypersensitive control for the efficacy of the agents used. A mild hypersensitivity is shown for the SAP domain mutant (L159A) compared to wt Fan1$^{Sp}$ in a *pso2*-d background. Abbreviation used: cispl, cisplatin.

## 6.4    Discussion

### 6.4.1    The nuclease domain in *S. pombe* Fan1 is required for its biological activity in ICL response

In this chapter, site-directed mutagenesis has been coupled with recombinase-mediated cassette exchange in order to create a series of point mutants where Fan1 functional moieties were removed from key conserved residues. Three key residues were targeted in the VRR_nuc nuclease domain (D651, E666, K668), one in the SAP domain (L159). When mutated to residues lacking the functional amino acid moieties (D651A, D651N, E666Q, K668A), the corresponding mutants in the nuclease domain phenocopied the deletion of Fan1 in a common *pso2*-d background (fig. 6.3). This result suggests that the three conserved residues are required for Fan1 activity at interstrand cross-links. *In vivo* studies in human cells have shown that mutations in the nuclease domain of human FAN1 do not affect FAN1 localisation to laser-induced damage (Smogorzewska et al., 2010). However, the mutations in the corresponding residues in the human FAN1 (D960A, E975A, K977A) impair the protein activity in biochemical assays (Smogorzewska et al., 2010; Kratz et al., 2010; Liu et al., 2010). In this study, a link has been found *in vivo* between *S. pombe* Fan1 nuclease residues and the efficient response to interstrand cross-links. It is then possible to suggest that Fan1[Sp] acts in the ICL repair pathway as a nuclease.

### 6.4.2    The SAP domain is only partially required for efficient response to ICL-inducing agents

SAP domains have been identified in a variety of proteins involved in various aspects of chromosomal reorganisation (Aravind and Koonin, 2000). The conserved SAP domain in FAN1 in *S. pombe* and higher eukaryotes (fig. 6.1 and Smogorzewska *et al.*, 2010) suggests a function in DNA binding, as previously hypothesized for this domain (Aravind and Koonin, 2000). *In vivo* studies with human FAN1 have shown that a mutation (L477P) or the complete deletion of the SAP domain reduce the strength of GFP-FAN1 signal localised to laser-induced damage

(Smogorzewska et al., 2010). In *C. elegans*, a single mutation in the SAP domain (tm423) causes increased lethality in embryos treated with MMC and HN2 (Smogorzewska et al., 2010). In the present study, the mutation of a key conserved SAP residue (L159A) affects the response to cisplatin to a milder extent compared to the nuclease mutants, and only at higher doses of drug (fig. 6.4). It is tempting to speculate that the SAP domain in FAN1 in *S. pombe* and higher eukaryotes is involved in the localisation and possibly direct protein-DNA contacts. In this context, the mutation of only one residue (L159 in the case of Fan1[Sp]) might impair DNA binding only partially, explaining why FAN1 is still proficient in response to lower doses of cisplatin (fig. 6.4). However, such hypothesis should be properly supported by additional experimental work.

## 6.5    Conclusions

The availability of flexible tools for site-directed mutagenesis of protein residues in *S. pombe* allows for rapid investigation of the requirement for specific residues in the biological activities of proteins of interest. In this study, four residues have been mutated and tested for increased sensitivity to cisplatin. Three key conserved nuclease residues have been found to be required for Fan1[Sp] biological activity in response to cisplatin, whereas a conserved residue in a putative DNA binding domain is only partially required for this function.

Chapter Seven

FINAL DISCUSSION AND CONCLUSIONS

## 7.1 Final discussion

### 7.1.1 The rationale underlying this study

The investigation presented in this thesis stems from parallel work in mammalian cells which showed that human FAN1 (initially named KIAA1018/MTMR15) physically interacts with components of the mismatch repair pathway [Cannavo et al. (2007) and Dr J. Rouse, personal communication, 2008]. It was then assumed that the parallel characterisation of the *S. pombe* homolog (GeneDB systematic name: SPBC146.06c) would have shed further light on a potential unknown aspect of the DNA damage response in eukaryotes. The study of this protein in the fission yeast was thought to be particularly valuable for at least two reasons. Firstly, the amenable genetics and the tools available for the fission yeast would have provided a powerful model to rapidly identify the biological role of this protein. In this respect, the setup of a high-throughput screen would have served the purpose of completing and expanding the standard genetic analyses usually employed in this type of characterisation (*in vivo* viability assays such as spot tests and survival curves). Secondly, the absence of a homolog in *S. cerevisiae* (Dr J. Rouse, personal communication, 2008) suggested the presence of an additional DNA repair mechanism that could have been potentially interesting from an evolutionary perspective. Successively, in the process of completing the study presented in this thesis, five independent laboratories reported the characterisation of the mammalian KIAA1018, consequently named FAN1 (Fanconi anemia- associated nuclease 1, or FANCD2/FANCI-associated nuclease 1) (Smogorzewska et al., 2010; MacKay et al., 2010; Kratz et al., 2010; Yoshikiyo et al., 2010; Liu et al., 2010; Shereda et al., 2010). These works provided an additional value to the present study, as FAN1 was shown to be associated with the Fanconi anemia pathway of DNA interstrand cross-link repair, a pathway absent in *S. pombe* with the exception of a single component (Fml1$^{Sp}$, ortholog of FANCM in higher eukaryotes). Thus, the

study of Fan1 in *S. pombe* bears the potential of revealing the existence of possible mechanisms of ICL repair in higher eukaryotes which act in parallel with the FA pathway.

### 7.1.2 A missing crosstalk between the MMR and the ICL repair pathways in *S. pombe*?

Following initial indications that human FAN1 interacts *in vivo* with components of the mismatch repair pathway (Cannavo et al., 2007 and Dr J. Rouse, personal communication, 2008), the first step in this project was taken to assess the existence of similar protein-protein interactions for Fan1[Sp]. Western blot analyses of co-immunoprecipitation experiments did not identify the presence of either the MMR component Mlh1[Sp] or Pms1[Sp] with Fan1[Sp] (figures 3.4 - 3.7). Furthermore, the absence of Fan1 did not lead to any increase in the spontaneous mutation rate, excluding any direct role in the repair of DNA mismatches (table 3.1 and fig. 3.8). Reciprocally, the data presented in chapter five excludes a role for the MMR factors Msh2[Sp], Mlh1[Sp] and Pms1[Sp] in the response to DNA interstrand cross-links generated by cisplatin (fig. 4.8 and supplementary fig. 9.7). The exclusion of a crucial role for the MMR pathway in ICL resolution in *S. pombe* is also consistent with the data found in the *exo1* epistasis analysis (section 4.3.6). Exo1 is a nuclease involved in the late stages of MMR and in several other aspects of DNA processing (reviewed in Tran et al., 2004). The scenario in *S. pombe* appears to differ from the one in *S. cerevisiae*, where MMR factors have been associated with ICL repair, and a strong overlap has been reported between Exo1[Sc] and Pso2[Sc] in the ICL response (Barber et al., 2005; Lam et al., 2008). In the present study, the deletion of *pso2* and *exo1* led only to a mild increased sensitivity, indicating the lack of the significant redundancy between Exo1 and Pso2 observed in *S. cerevisiae* (figures 4.10 and 4.11). As the *fan1*-d *exo1*-d mutant shows an even milder combined sensitivity (fig. 4.10), it can be concluded that Exo1 does not play a central function in ICL resolution in *S. pombe*.

Taken together, these data indicate that *S. pombe* would lack a functional link between the MMR and the ICL pathway. Importantly, Fan1[Sp] would not serve as a possible ring of connection between the two pathways, as proposed for human FAN1 (Smogorzewska et al.,

2010). However, as discussed in section 4.4.3, it cannot be excluded that this crosstalk may exist also in the fission yeast, but it is confined to a specific phase of the cell cycle, as shown for the budding yeast (Barber et al., 2005). Being based on the growth of asynchronous cultures and the chronic treatment with damaging agents, the genetic analysis presented in chapter five would fail to identify this cell cycle-dependent role.

### 7.1.3 The novel Fan1[Sp]-dependent pathway of ICL resolution

The genetic analysis presented in chapter five was aimed at the identification of a possible role for Fan1[Sp] in the response to DNA damage. A first clue that Fan1 is a component of one of the DNA repair pathways in *S. pombe* was the sensitivity shown by the deletion mutant to the interstrand cross-linking agents cisplatin and mitomicin C (figures 4.2 and 4.3). The prospective role for Fan1[Sp] in the resolution of this type of adducts was further confirmed by the dramatic increase in sensitivity to the same agents when the deletion of *fan1* and *pso2* were combined (fig. 4.4). As the nuclease Pso2[Sp] was previously identified as a key component of the ICL response in *S. pombe* (Lambert et al., 2003), this result suggested that Fan1[Sp] is a key component of a novel pathway of ICL repair acting in parallel with the one where Pso2[Sp] is involved. This hypothesis was further supported by the hypersensitivity shown by the double mutant *fan1*-d *pso2*-d for a third widely used DNA cross-linking agent, the bifunctional nitrogen mustard HN2 [bis(2-chloroethyl) methylamine] (fig. 4.5). In the light of the data reported for the mammalian FAN1 (Smogorzewska et al., 2010; MacKay et al., 2010; Kratz et al., 2010; Yoshikiyo et al., 2010; Liu et al., 2010; Shereda et al., 2010), it is possible to conclude that FAN1 has a conserved role in the response to DNA interstrand cross-links across eukaryotes.

The systematic genetic analysis with other double and triple deletion mutants presented in chapter five identified only one other dramatic increased combined sensitivity to interstrand cross-linkers: the *fan1*-d *rad13*-d double mutant (fig. 4.12). Interestingly, the hypersensitivity of this combination of mutants was also shown clearly when the cisplatin high-throughput

screen was performed (table 6.5). Rad13[Sp] (homolog of Rad2[Sc] and XPG[Hs]) is a core nuclease involved in the double incision step of the nucleotide excision repair pathway, 3' to the lesion (O'Donovan et al., 1994). Interestingly, the fact that the combination of *pso2*-d and *rad13*-d did not lead to increased sensitivity to cross-linkers (fig. 4.12) places this nuclease uniquely in the Pso2-dependent pathway of ICL resolution.

Consistently with other studies in eukaryotes, in chapter five the E3 ubiquitin ligase Rhp18 has been found to be required for wild-type resistance to interstrand cross-links (fig. 4.13; Lambert et al., 2003; Wu et al., 2004; Tateishi et al., 2003; Nojima et al., 2005). However, neither the combined deletion *rhp18*-d *fan1*-d nor *rhp18*-d *pso2*-d showed increased sensitivity to cisplatin compared to the sickest single mutants (fig. 4.13 and fig. 4.14), suggesting that Rhp18 is required for both the Pso2- and the Fan1-dependent pathways. The involvement of Rhp18[Sp] in ICL repair might echo what has been proposed in *S. cerevisiae*, where Rad18 would be implicated in controlling DNA synthesis at late stages of ICL processing in conjunction with Rad6, although further work is needed to support this hypothesis.

A fourth gene found to be sensitive to cisplatin is *rhp51*, coding for the homolog of the recombination protein Rad51 (Sung, 1994; Namsaraev and Berg, 1997). Interestingly but not unexpectedly, the deletion of *rhp51* showed increased sensitivity following exposure to cisplatin when combined with either *fan1* or *pso2*, compared to the single mutants (fig. 4.14). Rhp51 has been already implicated in ICL repair in the fission yeast (Lambert et al., 2005). However, the data presented in this study suggests that indeed Rhp51 would be involved in both the Fan1- and Pso2-dependent pathways (fig. 4.15). In particular, the hypersensitivity of *rhp51*-d seems to be more dramatic in combination with *fan1*-d, suggesting that the Fan1 pathway would rely on Rad51-dependent homologous recombination to a lesser extent compared to the Pso2 pathway. It is also interesting to note that the triple deletion strain *fan1*-d *pso2*-d *rhp51*-d appears to be even more sensitive compared to any of the cognate strains (fig. 4.15 and supplementary fig. 9.12). This observation suggests that Rhp51 has

additional functions in the response to ICLs which are independent of the two Fan1 and Pso2 pathways.

Overall, the genetic analysis presented here delineates the existence of a novel pathway of ICL repair in the fission yeast *S. pombe*. This pathway is parallel to the one where the nuclease Pso2$^{Sp}$ is required and appears to require the presence of functional homologous recombination machinery (Rhp51$^{Sp}$) and the E3 ubiquitin ligase Rhp18$^{Sp}$. In contrast, the Fan1 pathway does not appear to require the activity of the nuclease Rad13$^{Sp}$. It would be interesting to assess the requirement for additional components acting in the Fan1$^{Sp}$ pathway. This could be done with an approach similar to the one presented in chapter six, where a *pso2*-deleted mutant could be used as a query strain, crossed with a series of deletion mutants from the Bioneer® library and the derived double mutants tested for sensitivity to increasing doses of cisplatin.

### 7.1.4 The DNA damage and replication checkpoint control of the Fan1 pathway

Despite the limitations of the analysis presented in chapter five (namely the chronic treatment of asynchronous populations of cells), some interesting observations emerged in respect to the control of ICL response by the DNA damage checkpoint system. A first interesting observation is that the deletion of the main DNA damage checkpoint effector Chk1 in the absence of Fan1 led to a slight hypersensitivity only in response to mitomycin C (MMC) and not to cisplatin (fig. 4.6). The spectrum of DNA lesions caused by MMC is considerably more enriched in interstrand cross-links than intrastrand cross-links or monoadducts compared to cisplatin (see 4.1.2). A possible explanation for the increased sensitivity of *fan1*-d *chk1*-d is that Fan1$^{Sp}$ is involved in the response to DNA interstrand cross-links in a pathway that is partially independent of the Chk1$^{Sp}$ control. This could be either a distinct repair pathway that does not require the effector kinase Chk1$^{Sp}$ or, more probably, the consequence of the resolution of interstrand cross-links in the S phase of the cell cycle. It has been shown that ICLs in yeast and mammalian cells are mainly repaired via recombinational repair in logarithmically growing cells

(Legerski, 2010). This hypothesis would be consistent with the finding that *cds1* (coding for the S-phase checkpoint kinase Cds1$^{Sp}$) and *fan1* seem indeed to be epistatic in response to treatment with cisplatin (fig. 4.7). However, it would be interesting to extend the epistasis analysis of *cds1* to the treatment with MMC, as this would further test this genetic relationship in the context of a cleaner preponderance of interstrand cross-links compared to other types of adducts. Thus, a scenario can be envisaged where the DNA damage checkpoint controlled by Chk1$^{Sp}$ acts in response to monoadducts, interstrand and intrastrand cross-links outside the S phase of the cell cycle, whereas Cds1$^{Sp}$ is involved more specifically in the response to interstrand cross-links, which hamper the progression of replication forks.

A second interesting observation is that the combined double deletions of *fan1* and *rad1*, *hus1* or *rad17* were identified as hypersensitive mutants in the cisplatin automated screen (table 6.5). Rad1$^{Sp}$ and Hus1$^{Sp}$ are part of the heterotrimeric complex 9-1-1 (Rad9-Rad1-Hus1 in *S. pombe*), coding for components of the DNA checkpoint complex and proposed to be an emergency sliding clamp, circling the damaged DNA and acting as a recruitment platform for downstream factors (see section 1.4; evidence reviewed in Parrilla-Castellar et al., 2004). Rad17$^{Sp}$ has been proposed to act as a loading factor for the 9-1-1 complex (Carr, 2002). When tested for sensitivity to cisplatin with standard spot tests, all the three mutants displayed a dramatic hypersensitivity, independently of the concomitant deletion of *fan1* (fig. 5.5). The extreme sensitivity of these mutants requires additional experiments with significantly lower doses of DNA damaging agents to check that indeed *fan1* and the 9-1-1 complex are epistatic. However, other repeats of the same experiment and the result shown in supplementary fig. 9.19 for *rad9*-d, where cisplatin has a slightly reduced cytotoxicity, appear to confirm that indeed this is the case. It would be interesting to determine the sensitivity of the 9-1-1 mutants (single and combined with *fan1*-d) to MMC, in order to establish whether a difference in sensitivity can be observed for a fraction of sublesions enriched in interstrand cross-links, similarly to the *chk1* disruptants.

Taken together, these results could indicate that the novel Fan1 pathway of ICL resolution is controlled by the DNA damage and replication checkpoints. It is possible that specific responses by either checkpoint are triggered dependently on the type of adducts created by the cross-linkers used and on the phase of the cell cycle where these lesions occur.

### 7.1.5    The molecular function of Fan1 in ICL resolution

Very limited conclusions can be drawn about the function of Fan1[Sp] in this novel pathway of ICL repair. Data from the analysis of Fan1[Sp] point mutants lead to the conclusion that at least three key residues in the VRR_nuc nuclease domain are required for the function of the protein in the ICL response: D651, E666 and K668 (fig. 6.3). In human cells, point mutations in the corresponding residues D960, E975, K977 compromise Fan1 exo- and endonucleolytic activities (Smogorzewska et al., 2010; Kratz et al., 2010; Liu et al., 2010). Although biochemical studies with *S. pombe* Fan1 have not been done in the present study, it is possible to suggest that Fan1[Sp] acts in the *S. pombe* ICL resolution pathway as a nuclease. Interestingly, the mutation in the conserved SAP domain (conserved domain involved in various aspects of chromosomal reorganisation; Aravind and Koonin, 2000) affects the response to ICLs only to very mild extent (fig. 6.4). However, it is still possible that the SAP motif mediates the contact with the damaged substrate DNA, similarly to what has been proposed for other proteins possessing this domain (Aravind and Koonin, 2000). In this context, a single SAP mutation in Fan1[Sp] would not be sufficient to abolish completely its contacts with the DNA molecule.

From the limited data available thus far, it is not possible to assign a specific function to Fan1 in the processing of ICL lesions. However, it is interesting to note that the nuclease Rad13[Sp] has been found to be non-epistatic with Fan1[Sp] and epistatic to Pso2[Sp] (fig. 4.12). It is tempting to speculate that another nuclease may be needed in the Fan1[Sp] pathway to cover the role performed by Rad13[Sp]. This nuclease (homolog of Rad2[Sc]/XPG[Hs]) is a crucial component of the nucleotide excision repair pathway, involved in the endonucleolytic incision 3' to the adduct (O'Donovan et al., 1994). Consistently with its role in NER, it has been proposed that in

mammalian cells XPG would be involved in the unhooking step of the ICL pathway (3' of the lesion), although the finding that XPG-depleted cells are only mildly sensitive to ICL agents suggests that in fact other nucleases (such as MUS81-EME1) have a more prominent importance in this role (De Silva et al., 2002; Wood, 2010). It is possible that in *S. pombe*, as well as in higher eukaryotes, multiple nucleases are involved in the endonucleolytic unhooking step of ICL resolution. In the light of the biochemical studies with mammalian FAN1 (Smogorzewska et al., 2010; MacKay et al., 2010; Kratz et al., 2010), it can be suggested that FAN1$^{Hs}$/Fan1$^{Sp}$ may be implicated in this reaction, either 3' or 5' to the ICL. It would be interesting to test the requirement for the various nucleases that may be involved at this stage in the fission yeast, such as Mus81$^{Sp}$/Eme1$^{Sp}$, the XPF homolog Rad16$^{Sp}$, Rad13$^{Sp}$ and Fan1$^{Sp}$ itself.

The biochemical data for human FAN1 indicates that this enzyme may be additionally involved in other stages of ICL repair. Firstly, its exonuclease activity might be required in the trimming of the unhooked ICL. Secondly and more importantly, the significant defects shown for FAN1-depleted cells at late stages of homologous repair indicate that this nuclease might be predominantly involved in the processing of recombination intermediates generated by treatments with DNA cross-linkers (MacKay et al., 2010; Kratz et al., 2010). However, the data presented in this study does not allow any further conclusion on a similar role for Fan1$^{Sp}$.

### 7.1.6 The role of SUMOylation in the DNA interstrand cross-link pathway

Another interesting outcome of the cisplatin high-throughput screen was the identification of the increased sensitivity of the combined *fan1*-d *pli1*-d mutant compared to the parental single mutants (table 5.5 and fig. 5.6). Pli1$^{Sp}$ is a ligase involved in the post-translational conjugation of small proteins called SUMO (small ubiquitin-related modifier). Although the exact significance of this conjugation (called SUMOylation) is still debated, it is clear that this class of reversible modifications plays a widespread and important role in the regulation of eukaryotic biological processes including DNA repair (reviewed in Bergink and Jentsch, 2009). In the

context of this study, the hypersensitivity of the *fan1*-d *pli1*-d mutant to cisplatin highlights a crucial involvement of SUMOylation in an ICL resolution pathway distinct from the one where Fan1[Sp] is implicated. Further epistasis analysis could establish whether this is the Pso2[Sp]-dependent, or a third unknown pathway. Whatever the outcome of these investigations, this study shows an unprecedented role for SUMOylation in the resolution of interstrand cross-links in *S. pombe* which might be conserved in higher eukaryotes. However, on the basis of the data presented in this study, it is not possible to speculate on the functional significance for this mechanism in the response to ICL formation.

### 7.1.7    A model for ICL resolution in S. pombe

Based on the data presented in this study, it is possible to delineate the participation of some of the components of the DNA repair machinery in the resolution of interstrand cross-links in the fission yeast *S. pombe*. A schematic is presented in fig. 8.1 where the known Pso2 pathway of ICL resolution is paralleled by the newly discovered Fan1 pathway. The results from the high-throughput cisplatin screen (section 5.3.5) highlighted the non-epistatic relationship of Fan1 and the SUMO ligase Pli1 (fig. 5.6). However, as the epistasis analysis has not been extended to Pso2, it is not possible to discuss whether Pli1 is involved in the Pso2 pathway, and/or in a third, independent pathway of ICL response. Fig. 7.1 (left panel) shows also the possible molecular roles for Fan1 in the ICL resolution pathway, as discussed in section 7.1.5.
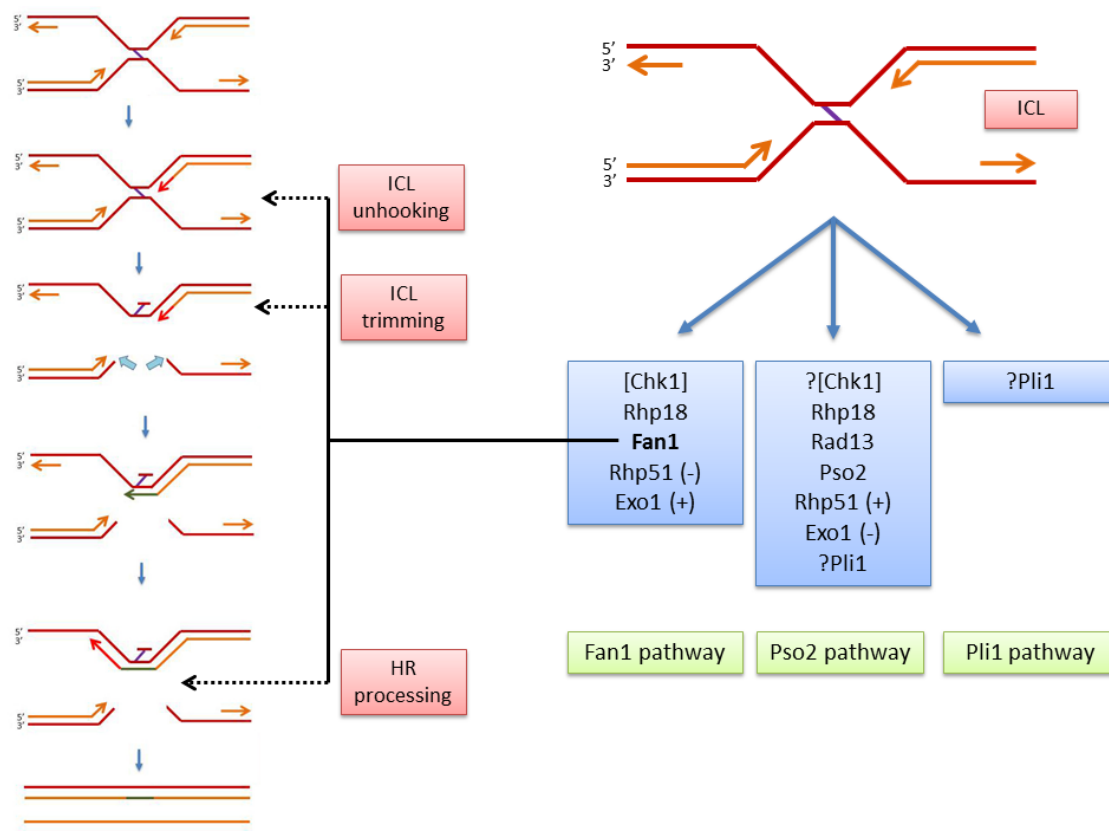
**Figure 7.1 | Proposed schematic of ICL resolution in S. pombe.** The components of the various DNA repair pathways are shown in the relevant boxes, as assigned from the genetic analysis presented in this study. (+) and (-) highlight the differential involvement of the component in the different pathways [e.g. Exo1 showed to be more implicated in the Fan1 pathway (+) than in the Pso2 pathway (-), see fig. 4.10]. As the analysis with *pli1* has not been extended further to the combination *pli1*-d *fan1*-d double disruptant (fig. 5.6), it is not possible to exclude the participation of Pli1 in the Pso2 pathway, and/or in a third unknown pathway of ICL repair. Left panel: possible roles for Fan1 in the Fan1-dependent resolution pathway. For simplicity, only the double fork model is shown (see fig. 1.5 for a detailed description of the model).

## 7.2   Conclusions

This study profited from the use of the fission yeast *S. pombe* as a model organism to investigate the role of a novel component of the DNA interstrand cross-link pathway. Standard biochemical and genetic characterisation were expanded into the exploration of the yeast genetic landscape through the setup of a high-throughput sensitivity screen. Taken together, the present investigation unravels novel unsuspected genetic relationships between the

interstrand cross-link repair pathway and other compensatory mechanisms of DNA metabolism and processing. This study reveals fresh insights into the repair of DNA interstrand cross-links, one of the most insidious threats posed to genomic stability. DNA interstrand cross-linking agents are amongst the most widely used treatments of a wide range of cancers. Studies in mammalian systems stemming from the outcome of the present work may translate in the increased efficacy of the current clinical options, for instance by simultaneous targeting parallel ICL repair pathways to selectively aggravate the cytotoxicity of the current oncological treatments.

Appendix 1

USE OF THE Ch16 DOUBLE-STRAND BREAK REPAIR SYSTEM TO INVESTIGATE THE FUNCTIONAL INTERACTION BETWEEN Rqh1$^{Sp}$ AND Crb2$^{Sp}$ IN RECOMBINATIONAL DNA REPAIR

## 8.1 Introduction

### 8.1.1 Crb2$^{Sp}$ as a regulator of Rqh1$^{Sp}$ activity

Caspari et al. (2002) suggested a role for the checkpoint mediator Crb2 in modulating the activity of the RecQ helicase Rqh1$^{Sp}$ in the fission yeast *S. pombe*. The link between Crb2 and the activity of Rqh1-Top3 was proposed to be mediated by the CDK phosphorylation of Crb2. This crosstalk emerged following the analysis of a *cdc13* mutant which contained a mutation in the cyclin box and had reduced CDK activity (Caspari et al., 2002). In *S. pombe*, the CDK-cyclin B complex consists of Cdc2 and Cdc13. *cdc13*-245 is hypersensitive to IR despite being proficient in the G2/M arrest. The significant proportion of cells undergoing catastrophic mitosis suggested a defect in DNA repair. Analysis of Rhp51 (homolog of Rad51 in *S. pombe*) foci formation led to the conclusion that *cdc13*-245 was defective in both the early and late stages of HR-dependent DNA repair. At early stages, Cdc13 was redundant with the activity of Rad50, as the double mutant *cdc13*-245 *rad50*-d was more sensitive to IR than *rad50*-d and the formation of Rhp51 foci was impaired in this strain. The defect at late stages of recombinational repair was highlighted by the restoration of IR resistance of *cdc13*-245 in an *rqh1*-d background, indicating that Cdc2-Cdc13 affects intermediates generated by Rqh1 activity.

Crb2 is phosphorylated by CDK-CyclinB kinase both in undamaged and in damaged cells and this phosphorylation is required for cell-cycle arrest in response to UV irradiation and defective replication (Saka et al., 1997; Esashi and Yanagida, 1999). Caspari et al. (2002) showed a genetic interaction between Cdc13 and Crb2 when *cdc13*-245 was combined with the non-phosphorylatable *crb2*-T215A mutation. *crb2*-T215A was initially characterised as showing a deficiency in the checkpoint function of Crb2 where the checkpoint can be initiated but not maintained (Nakamura et al., 2005). However, different lines of evidence suggest that this checkpoint defect is partial and depends on factors such as the dose of DNA damaging agent

used and the method used for cell cycle synchronisation. Nakamura et al. (2005) showed that this defect in checkpoint maintenance was displayed following exposure to doses of IR above 90 Gy after synchronisation by *cdc25-22* block and release. However, unpublished work in our laboratory showed that this defect did not occur when cell cultures were synchronised by elutriation prior to irradiation (Jo Murray, personal communication). The T215A mutation markedly affects the DNA repair function of Crb2, as *crb2*-T215A cells are more sensitive to IR than wt (Caspari et al., 2002).

*crb2*-T215A displayed sensitivity to IR more marked than *cdc13*-245, but the double mutant was as sensitive as *crb2*-T215A, suggesting that Crb2 and Cdc13 act in the same pathway in response to IR. Furthermore, the deletion of *rqh1*-d suppressed the sensitivity of *crb2*-T215A to ionizing radiation, but the resistance was only restored to the level of *rqh1*-d, suggesting that Crb2 function requires Rqh1. Consistent with a role in the late stages of homologous recombination, Rqh1 foci appeared late following IR irradiation. Interestingly, the finding that the overexpression of Top3, binding partner of Rqh1, suppressed the IR sensitivity of *crb2*-T215A and *cdc13*-245 suggested that these mutations impair Top3 activity. The molecular mechanism behind the IR sensitivity of *crb2*-T215A and *cdc13*-245 is still obscure. However, the IR-induced (Rqh1-dependent) hyperrecombination observed in *crb2*-T215A and *cdc13*-245 may provide a plausible explanation for this increased sensitivity. Intriguingly, the relationship between Crb2 and Cdc13 does not appear to be direct, as the phosphorylation status of Crb2 is not affected in a *cdc13*-245 background (Caspari et al., 2002).

Taken together, these data suggest that the regulation of Crb2 by Cdc2-Cdc13 in *S. pombe* may mirror the situation proposed in human cells, where the BRCT-domain protein BRCA1 acts as a scaffold which favours the assembly of checkpoint proteins and repair enzymes at the site of damage (Wang et al., 2000). Thus, upon IR treatment, the checkpoint-dependent hyperphosphorylation of Crb2 would be responsible for regulating the activity of Rqh1-Top3 at repair sites. In particular, it has been proposed that Crb2 could aid the convergence of two

Holliday junctions to form a hemicatenane that would then be resolved by the Rqh1-Top3 complex (Carr, 2002). Crb2 may also act in the processing of recombination intermediates generated by Rqh1-Top3, as proposed in Caspari et al. (2002).

The genetic relationship between Rqh1 and Crb2 through Cdc2-Cdc13 reported by Caspari et al. (2002) provides the basis for the work presented in this chapter.

### 8.1.2 Ch16 double-strand break repair system

In order to investigate the functional interaction between Rqh1 and Crb2 in recombinational repair in *S. pombe*, a genetic system has been used where a non-essential minichromosome (Ch16) derived from chromosome III is artificially introduced in *S. pombe* cells (Prudden et al., 2003b). This genetic element is maintained by heteroallelic complementation between the *ade6-M216* allele on Ch16 and the *ade6-M210* on the native chromosome III. The main features of the Ch16 used in the present study are a *MATa* cassette, a target site for the HO endonuclease, and a *kanMX6* cassette, adjacent to *MATa*, that confers resistance to the drug G418 (Geneticin). A further marker, *his3*$^+$, is located 25 kb centromere-distal to the *MATa* site and confers prototrophy to histidine (fig. 8.1; Cullen et al., 2007). The expression of the HO endonuclease is regulated by the *nmt1* promoter, induced in the absence of thiamine. Upon removal of thiamine from the medium, the HO endonuclease introduces a double-strand break (DSB) at the target *MATa* site, and subsequent repair events can be followed by assessing the loss of the three markers flanking the DSB. Minichromosome loss leads to an ade- G418-sensitive his- phenotype, as all the three markers are lost (fig. 8.1b). Repair by homologous recombination (HR) leads to gene conversion and consequent *kanMX6* loss (fig. 8.1a). Long-tract gene conversion (LTGC) leads to loss of both *ade6-M216* and *kanMX6* markers (fig. 8.1c). Non-homologous end joining or repair by sister-chromatid conversion lead to both the markers being retained (fig. 8.1e). The fate of the additional *his3*$^+$ marker is indicative of break-induced loss of heterozygosity (LOH), which leads to loss of *kanMX6* and *his3*$^+$ markers but

retention of *ade6* (fig. 8.1d; Cullen et al., 2007). Clearly, the *his3*+ marker is lost along with the other two markers if the minichromosome itself is lost.
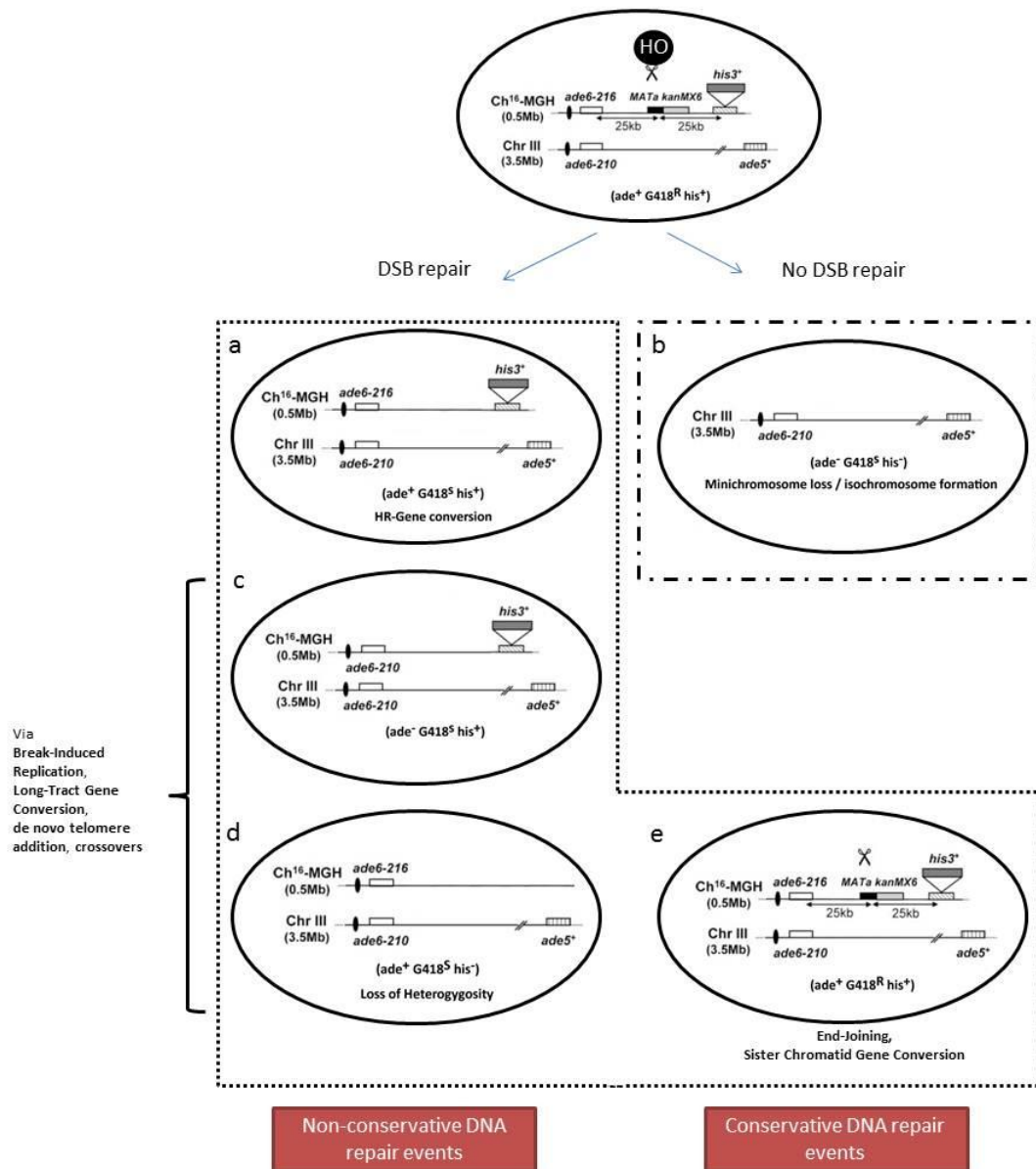


**Figure 8.1 | Ch16 double-strand break repair system.** As the expression of the HO endonuclease is regulated by the nmt promoter, removal of thiamine from the medium induces the HO nucleolytic activity targeted at the *MATa* site. DSB repair events can be assessed by scoring the loss of one or more genetic markers. The minichromosome system used in this study (MGH: *MATa*, G418, His) carries three markers flanking the *MATa* site: *ade6-216*, *kanMX6*, *his3*+. a. Repair of the HO break by homologous recombination (HR) leads to loss of the *kanMX6* marker and retention of the *ade6-216* and *his3*+ markers. b. The loss of the minichromosome leads to an ade- G418s his- phenotype. c. Long-tract gene conversion leads to the loss of the two markers *ade6-216* and *kanMX6* and retention of *his3*+. d. loss of heterogygosity leads to loss of the two markers on the right arm of the *MATa* site, *kanMX6* and *his3*+. e. Non-homologous end joining or repair by sister chromatid gene conversion are conservative events which lead to retention of all the markers.

## 8.2 Aim

The aim of this chapter is to test the use of the Ch16 double-strand break repair system to investigate the functional role of the interaction between Rqh1 and Crb2 in *S. pombe*. In order to achieve a tighter control over the activity of the endonuclease HO, inducible systems alternative to the standard *nmt1* promoter (ER-HBD-HO, invHO) were also tested.

## 8.3 Results

### 8.3.1 Gene conversion events are decreased in *rqh1*-d cells

This analysis started by investigating repair events occurring in the absence of the RecQ helicase Rqh1. To this aim, the Ch16 double-strand break repair system as described in Cullen et al., 2007 (MGH: *MATa*, G418, His) was used. 24 and 48 hours after the removal of thiamine
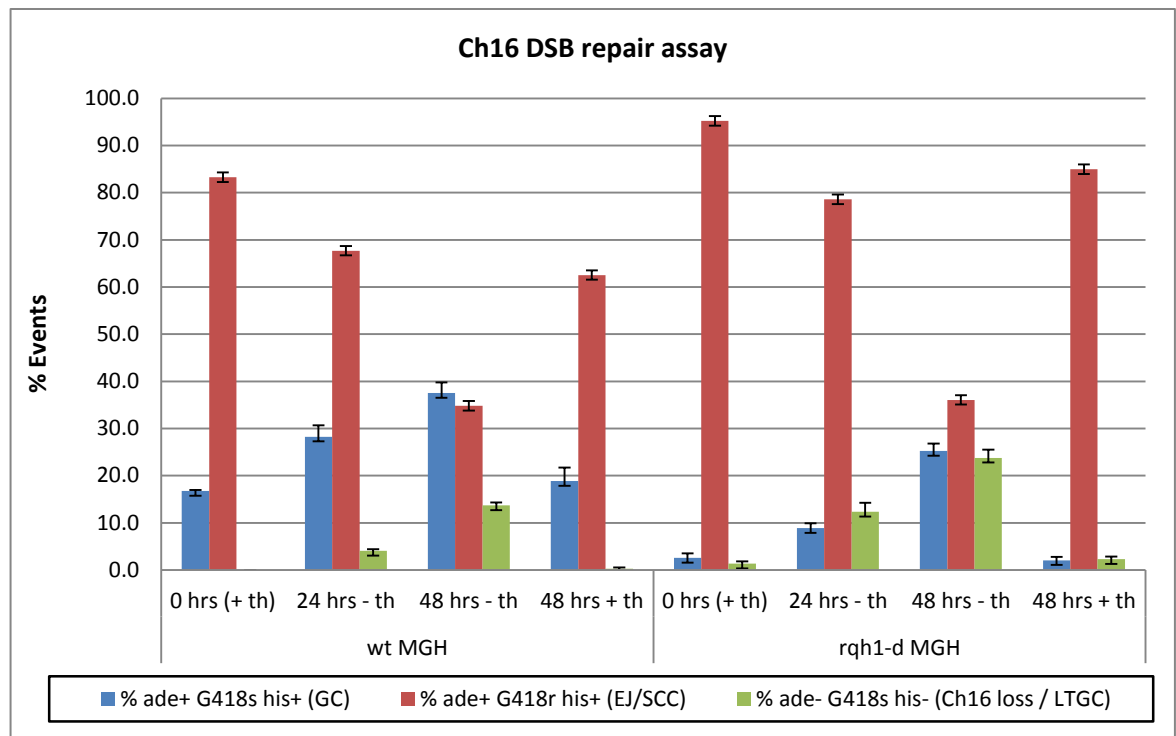


**Figure 8.2 | DNA repair events in wt and *rqh1*-deleted MGH Ch16 double-strand repair system.** The timepoints refer to growth time following the removal of thiamine from the medium: –th, thiamine absent from the medium. 48 hrs +th refers to cultures grown in parallel to the 48 hrs –th cultures: +th, thiamine present in the medium. *rqh1*-d cells display a decrease in non-conservative events and a corresponding increase in conservative events compared to wt MGH. GC, gene conversion; EJ, end-joining; SCC, sister-chromatid conversion; LTGC, long-tract gene conversion.

from the medium (24 hrs -th, 48 hrs –th) *rqh1*-d MGH cells showed a decrease in non-conservative events (i.e. events leading to marker loss such as gene conversion), and a corresponding increase in conservative events compared to wt MGH (fig. 8.2, compare blue bars with red bars; table 8.1). This result confirms data published in Hope et al. (2006). However, an increase in conservative (EJ/SCC) events may in fact be just a consequence of the reduction in the HO cutting efficiency in *rqh1*-d cells compared to the wt. A way to rule out this possibility is to assess the HO cutting efficiency in *rqh1*-d and wt MGH. This experiment has been done in Hope et al. (2006), showing that the HO cutting efficiency is comparable in the two backgrounds. Thus, the most plausible explanation for the decrease of non-conservative events in *rqh1*-d compared to wt MGH is that Rqh1 is responsible for this shift in repair events, either by favouring gene conversion or by suppressing EJ/SCC events.

It should be noticed that levels of gene conversion at 0 hrs (+ th) in wt MGH are higher than expected compared to similar experiments (fig. 8.4; Prudden et al., 2003). However, as a full repression of *nmt1* is not achievable (Maundrell, 1990; Basi et al., 1993), this effect can be attributed to unusually high leakage from this inducible promoter. Although it cannot be confirmed that higher levels of GC in wt MGH are only due to this initial leakage, it should be noticed that at 24 hours in the absence of thiamine the difference in GC events is still higher in wt MGH compared to *rqh1*-d (28.3% and 8.9% respectively). Thus, this result still confirms the shift in repair events between the two backgrounds.

Surprisingly, at a closer inspection the sum of all the repair events occurring at 48 hours (either in the absence or in the presence of thiamine) in both the backgrounds does not add up to 100% (table 8.1). Although alternative minor repair events occur normally in the Ch16 system (Cullen et al., 2007), levels up to 18.3% (wt MGH, 48 hours +th) are unusually high. This occurrence in minor repair events is similar in both the backgrounds. Insights on this unusual occurrence can be gained by analysing the percentage of the loss of the three individual markers (supplementary fig. 9.3). The shift from common to minor repair events corresponds

| Genetic background | Time / induction | % ade+ G418s his+ (GC) | % ade+ G418r his+ (EJ/SCC) | % ade- G418s his- (Ch16 loss / LTGC) | TOT | % Alternative repair events |
|---|---|---|---|---|---|---|
| wt MGH | 0 hrs (+ th) | 16.7±0.3 | 83.3±0.3 | 0±0 | 100 | 0.0 |
| | 24 hrs - th | 28.3±2.4 | 67.7±2.7 | 4.1±0.4 | 100 | 0.0 |
| | 48 hrs - th | 37.5±2.3 | 34.8±0.4 | 13.7±0.7 | 86 | 14.0 |
| | 48 hrs + th | 18.8±2.9 | 62.5±2.5 | 0.3±0.3 | 81.7 | 18.3 |
| rqh1-d MGH | 0 hrs (+ th) | 2.5±1 | 95.2±1.2 | 1.3±0.5 | 99.1 | 0.9 |
| | 24 hrs - th | 8.9±1.1 | 78.6±2.2 | 12.3±1.9 | 99.8 | 0.2 |
| | 48 hrs - th | 25.2±1.6 | 36.1±1.6 | 23.8±1.8 | 85.1 | 14.9 |
| | 48 hrs + th | 2.1±0.7 | 85±0.8 | 2.3±0.6 | 89.3 | 10.7 |

**Table 8.1 | Occurrence of repair events as plotted in fig. 8.2 and occurrence of alternative repair events.** Alternative repair events are calculated as the difference between 100 and the sum of scored standard repair events ("TOT" column). GC, gene conversion; EJ, end-joining; SCC, sister-chromatid conversion; LTGC, long-tract gene conversion.

to exceptional disparity between the loss of *ade6* and *his3+* markers, in particular a low *his3* marker loss compared to *ade6* marker loss. However, it should be noticed that this unusual event occurs in all the 48 hrs samples, irrespectively of genetic background or presence of thiamine. Thus, this unexpected result can be explained by possible alterations in the composition of the solid media on which the cultures were plated. It is possible that small quantities of histidine were present in the media used to score *his3+* marker loss for the 48 hrs timepoints, thereby leading to an erroneously low score of *his3+* marker loss. However, despite this unexpected result, when only the most common repair events are taken into consideration, the shift towards an increase of EJ/SCC events in *rqh1*-d cells can still be confirmed.

### 8.3.2 Ch16 loss/LTGC events are increased in *crb2*-T215A

To investigate the functional interaction between Rqh1 and Crb2, the analysis of marker loss in the Ch16 system was performed in genetic backgrounds either devoid of Crb2 (*crb2*-d) or lacking a phosphorylatable T215 residue (*crb2*-T215A). At 48 hrs in the absence of thiamine, while *crb2*-T215A MGH shows rates of GC events comparable to wt MGH, Ch16 loss/LTGC

events are increased by approximately 100% in this background (from 15.78% to 29.77%), at

the expense of a reduced percentage of EJ/SCC events (fig. 8.3). This increase is not dependent

on Rqh1, as the same occurrence of GC and Ch16 loss/LTGC events is shown in its absence in a

*crb2*-T215A background (*crb2*-T215A *rqh1*-d). However, interestingly the increase in Ch16

loss/LTGC events seems to be dependent on the mutated Crb2, as *crb2*-d *rqh1*-d cells show

rates of Ch16 loss/LTGC repair events comparable to wt levels (17.50% compared to 15.78%,

respectively). Furthermore, the presence of Crb2 (either wt or T215A) seems to be responsible

for the maintenance of wt levels of GC events, as these are reduced by approximately a half

when *crb2* is deleted (fig. 8.3, compare blue bars at 48hrs –th).

Taken together, this data suggests that T215 in Crb2 is a key residue responsible for a shift in

repair events, either by suppressing Ch16 loss/LTGC events or by promoting EJ/SCC events,

through an unknown mechanism independent of Rqh1.

### 8.3.3 Isochromosome formation in the *crb2*-T215A background

To further investigate the shift in repair events caused by the mutated T215 residue in Crb2,

randomly selected triple-negative colonies (*ade*⁻ G418s *his*⁻) were processed by PFGE to



| | +th | -th | +th | +th | -th | +th | +th | -th | +th | +th | -th | +th |
|---|---|---|---|---|---|---|---|---|---|---|---|---|
| | 0 hrs | 48 hrs | 48 hrs | 0 hrs | 48 hrs | 48 hrs | 0 hrs | 48 hrs | 48 hrs | 0 hrs | 48 hrs | 48 hrs |
| | Wt MGH | | | crb2-T215A MGH | | | crb2-T215A rqh1-d MGH | | | crb2-d rqh1-d MGH | | |
| % ade+ G418s his+ (GC) | 5.14 | 18.48 | 12.90 | 13.92 | 18.16 | 10.47 | 0.86 | 15.60 | 0.74 | 1.68 | 9.46 | 1.41 |
| % ade+ G418r his+ (EJ/SCC) | 94.24 | 65.75 | 85.90 | 85.26 | 52.07 | 86.20 | 98.16 | 53.98 | 96.90 | 95.87 | 73.05 | 91.37 |
| % ade- G418s his- (Ch16 loss/LTGC) | 0.61 | 15.78 | 1.20 | 0.82 | 29.77 | 3.33 | 0.98 | 30.42 | 2.36 | 2.45 | 17.50 | 7.22 |

**Figure 8.3 | DNA repair events in *crb2*-T215A and *crb2*-d backgrounds.** 48 hrs +th refers to cultures

grown in parallel to the 48 hrs –th cultures: +th, thiamine present in the medium (HO off); -th, thiamine

absent (HO on). Ch16 loss/LTGC events are doubled in a *crb2*-T215A background, at the expense of a

reduced percentage of EJ/SCC events. GC, Gene Conversion; EJ, End-Joining; SCC, Sister-Chromatid

Conversion; LTGC, Long-Tract Gene Conversion.

discriminate between loss of minichromosome or LTGC as the cause of the triple-negative phenotype. Data from a limited number of colonies (23 and 27 colonies for *crb2*-T215A and *crb2*-T215A *rqh1*-d, respectively) would suggest that, despite comparable rates of Ch16 loss/LTGC events (fig. 8.3), the actual contribution of the distinct outcomes are different between *crb2*-T215A and *crb2*-T215A *rqh1*-d, with a greater incidence of minichromosome loss in a *rqh1* null background (fig. 8.4). Although this would be consistent with a role for Rqh1 in preserving chromosomal stability (Stewart et al., 1997), further work is needed in order to confirm this finding.

In order to confirm the presence or the absence of the minichromosome, the agarose pulse-field gels used in the above experiment were blotted with probes homologous to sequences on each minichromosome arm. As expected, the chk1 probe (left arm of chromosome III)

| | Ch16 present | Ch16 absent | Tot. Colonies Analysed | % Ch16 present | % Ch16 absent |
|---|---|---|---|---|---|
| *crb2*-T215A | 11 | 12 | 23 | 47.8 | 52.2 |
| *crb2*-T215A, *rqh1*-d | 9 | 18 | 27 | 33.3 | 66.7 |
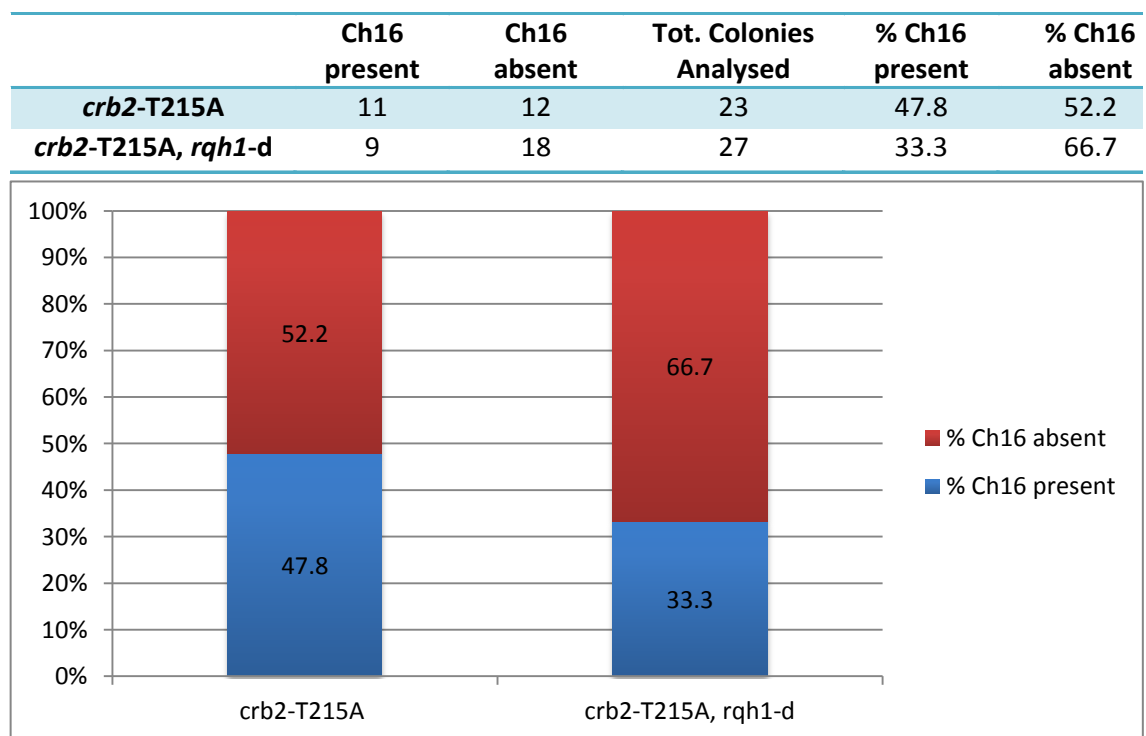


**Figure 8.4 | Percentage of minichromosome presence in *crb2*-T215A and *crb2*-T215A *rqh1*-d cells.** Presence was scored by visualisation of ethidium bromide – stained pulse-field gels, and confirmed by Southern blot analysis (see fig. 3.5).

annealed with both the minichromosome and chromosome III (fig. 8.5a, top gels). Weaker minichromosome signals in some tracts are probably due to significant progressive loss of the minichromosome in the population of cells grown in rich media prior to PFGE treatment. Interestingly, *crb2*-T215A *rqh1*-d showed two colonies where an alternative form of chromosome arises, probably due to exchange of genetic material between ChIII and the minichromosome. This form of chromosome (namely ChX) has been previously described (Prudden et al., 2003; Cullen et al., 2007).

Surprisingly, the probe spcc4b3.18 (right arm of the minichromosome, proximal to the HO site)
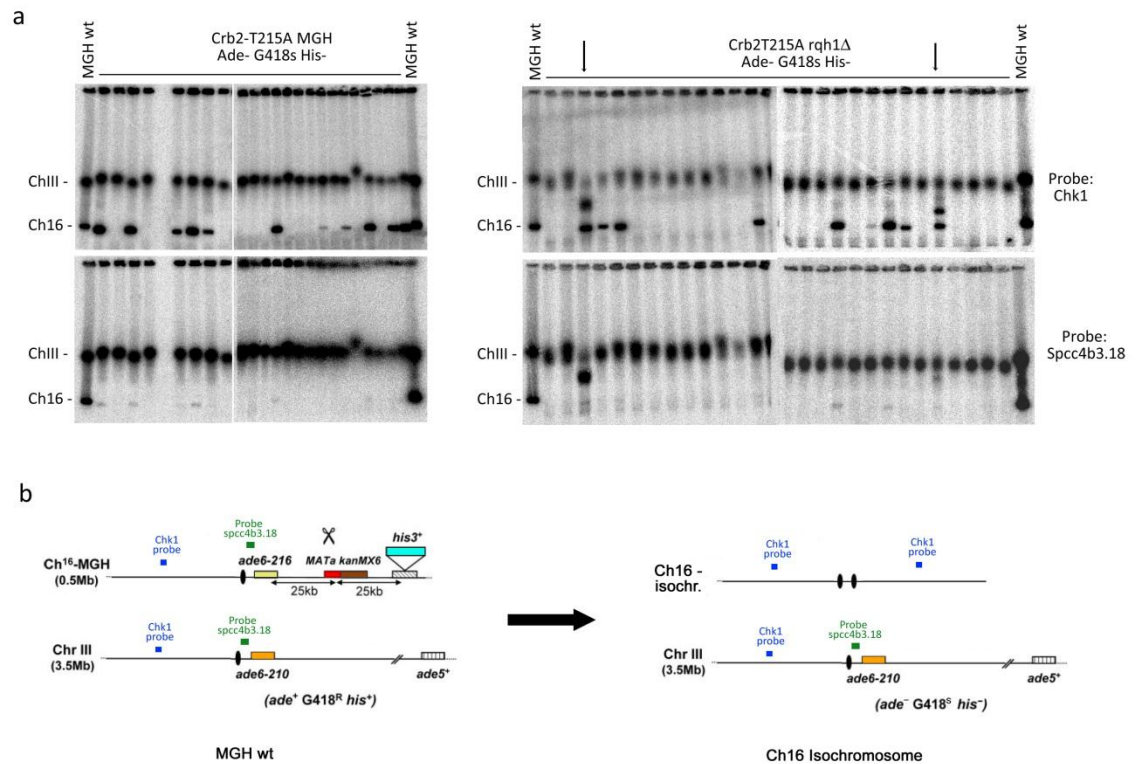


**Figure 8.5 | Pulse-field gel analysis of Ch16 from *ade*- G418s *his*- colonies in *crb2*-T215A and *crb2*-T215A *rqh1*-d mutants.** a. Pulse-field gels blotted with probes either side of ChIII and minichromosome centromeres (*chk1*, top row; *spcc4b3.18*, bottom row). Each lane represents a single *ade*- G418s *his*- colony. Two colonies in *crb2*-T215A *rqh1*-d (indicated by arrows) showed formation of intermediate forms of chromosomes, probably due to transfer of chromosomal material between ChIII and the minichromosome (ChX). b. Proposed schematic for the formation of isochromosomes from minichromosomes.

annealed only with chromosome III and not with the minichromosome in all the relevant colonies (fig. 8.6a, bottom gels). Weak minichromosome signals on membranes can be attributed to faint signals due to incomplete removal of the previous chk1 probe. This result can be explained by invoking the formation of an isochromosome, a particular type of gross chromosomal rearrangement where one of the two chromosomal arms is lost and replaced with a copy of the opposite arm (see proposed schematic in fig. 8.6b). This type of rearrangement in this system has been previously described (Tinline-Purvis et al., 2009). This is an interesting finding, which should be extended to a statistically significant number of samples, including wt MGH triple-negative colonies, in order to assess whether the formation of isochromosomes is specifically increased in a *crb2*-T215A background.

### 8.3.4  Regulation of HO by Estradiol Receptor-Hormone Binding Domain (ER-HBD-HO)

The *nmt1* (no message in thiamine) promoter is the most widely used regulatory element in *S. pombe.* However, although optimisations of the upstream TATA box of the promoter have been obtained, its repression by thiamine cannot be achieved fully (Basi et al., 1993). Furthermore, *nmt1* activation is induced at a maximum steady-state level 16 hours after the removal of thiamine from the medium (Maundrell, 1990). In an attempt to overcome these limitations, a novel approach was tested where the HO endonuclease is regulated at a post-translational level. In this system, the protein of interest is confined in the cytoplasm by molecular chaperones. Upon addition of $\beta$-Estradiol, the protein is released and translocated to the cell nucleus, and thus activated (Picard, 1993; Picard, 1994). Examples of such regulation have been described (Picard, 2000; Bøe et al., 2008). A cloning strategy was designed where the HO cassette was cloned into modular constructs either on the N- or the C-terminal side to an inducible Estradiol Receptor-Hormone Binding Domain (ER-HBD) (see supplementary fig. 9.1 and 9.2 for the detailed cloning strategy). In addition, the presence of the *nmt1* promoter in these vectors was expected to provide a further level of regulation. In these experiments, the MG system (lacking the *his3+* marker compared to MGH; Prudden et al., 2003) was used. In

the N-terminal construct, HO showed a dramatically reduced activity where the maximum level of G418 marker loss reached only 18.5% after 48 hours from the removal of thiamine (fig. 8.7). This indicates that the N-terminal tagging of the HO nuclease inactivates the protein. In contrast, in the C-terminal construct the HO endonuclease was induced by the removal of thiamine from the medium, but it was not affected by the presence or absence of β-Estradiol (fig. 8.8). This suggests that the C-terminal-tagged HO is functional but not regulatable. Taken together, these data show that the constructed vectors described here cannot be used as a tool for a rapid activation of the HO endonuclease in *S. pombe*.

### 8.3.5  **Regulation of HO by the Invertase promoter (InvHO)**

A further attempt was made to achieve a more rapid induction of the HO endonuclease by using the invertase promoter as a regulatory element (*inv1*). *Inv1* is activated within 1 hour following a shift from glucose to sucrose as a main source of carbon in the medium (Iacovoni et al., 1999). Wt MGH and *crb2*-d *rqh1*-d cells transformed with vectors carrying the invHO cassette (kind gift of Dr Tim Humphrey) showed low levels of background leakage at 2 hours of growth in the presence of extra glucose (fig. 8.8). However, the percentage of GC events was low at 2 hours of growth in the presence of sucrose in both wt MGH and double mutant (fig. 8.8, light blue bars at 2 hrs, sucrose). In other experiments performed in wt MGH and *crb2*-T215A *rqh1*-d MGH backgrounds, the invHO promoter showed variable results, with high levels of marker loss at 3 hrs following shift to sucrose but high levels of leakage at 0 hrs, before the induction (supplementary fig. 9.4). Moreover, levels of GC seem to decrease at 6 hours following induction (supplementary fig. 9.4, compare blue bars for 3 hrs and 6 hrs timepoints), probably reflecting an increased repression due to progressive hydrolysis of sucrose into glucose, a limitation of the invertase promoter that has already been reported (Iacovoni et al., 1999). Taken together, these data on the *inv1*-regulated HO endonuclease suggest that further optimisation of the system are needed to achieve a rapid induction coupled with reduced levels of leakage.

**N-terminal ER-HBD-HO**

| | +th -E 24 hrs | +th +E 24 hrs | -th -E 24 hrs | -th +E 24 hrs | -th -E 48 hrs | -th +E 48 hrs |
|---|---|---|---|---|---|---|
| ■ % ade- | 1.4 | 0.2 | 0.2 | 0.5 | 0.8 | 0.8 |
| ■ % G418- | 11.8 | 10.6 | 12.5 | 11.3 | 13.5 | 18.5 |
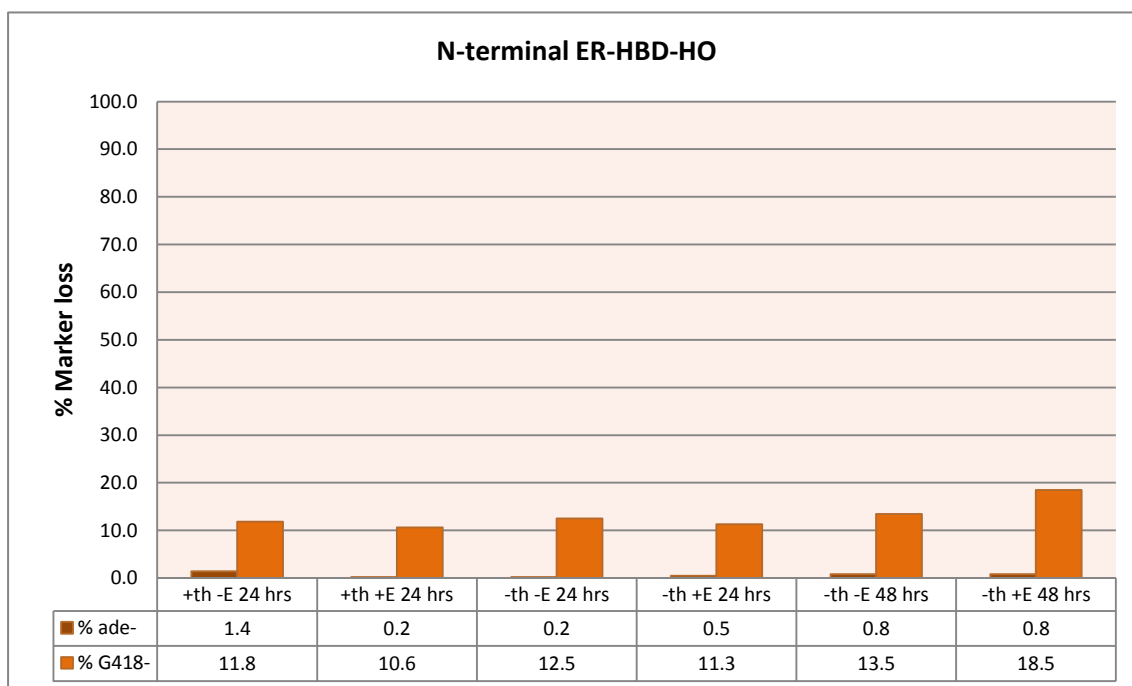
**Figure 8.6 | Marker loss in wt MG transformed with the N-terminal ER-HBD-HO construct.** +th, thiamine added to the medium; -th, thiamine absent; +E, β-Estradiol added to the medium;- E, β-Estradiol absent. Time points refer to hours from the start of the experiment (+ th cultures were grown in parallel with – th cultures). The N-terminal ER-HBD-HO constructs display a reduced activity as assessed by low level of *ade* and *G418* marker loss.



**C-terminal ER-HBD-HO**

| | +th -E 24 hrs | +th +E 24 hrs | -th -E 24 hrs | -th +E 24 hrs | -th -E 48 hrs | -th +E 48 hrs |
|---|---|---|---|---|---|---|
| ■ % ade- | 0.0 | 0.4 | 2.5 | 0.8 | 4.0 | 5.8 |
| ■ % G418- | 3.2 | 7.7 | 17.4 | 11.9 | 40.0 | 38.8 |
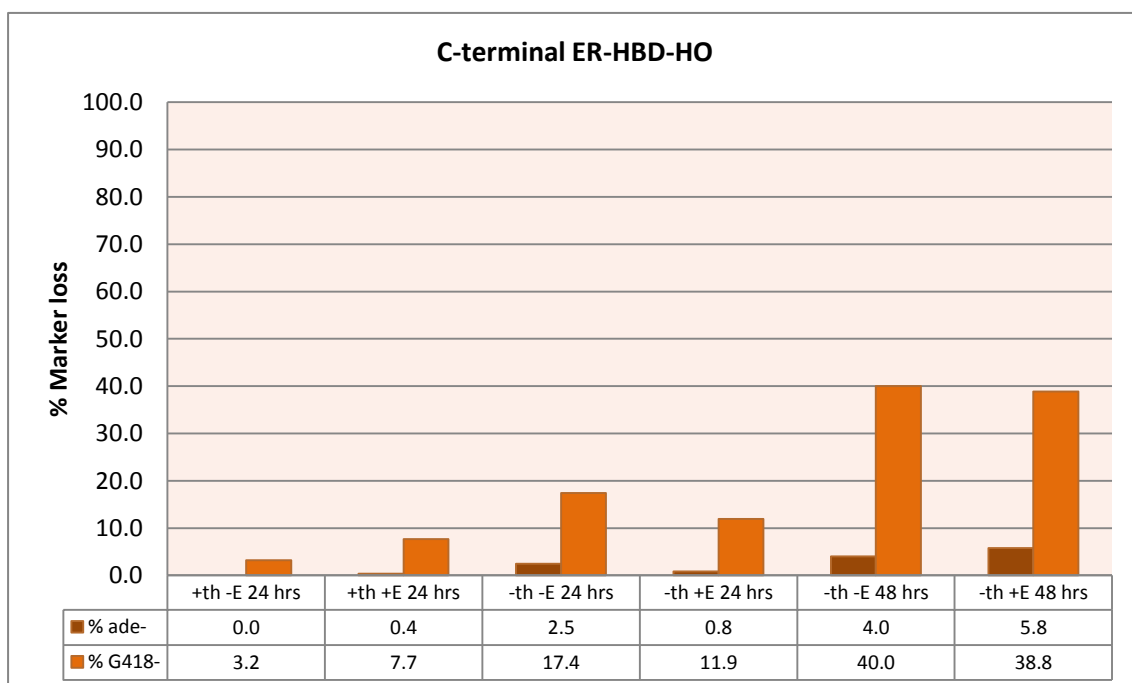
**Figure 8.7 | Marker loss in wt MG transformed with the C-terminal ER-HBD-HO construct.** +th, thiamine added to the medium; -th, thiamine absent; +E, β-Estradiol added to the medium;- E, β-Estradiol absent. Time points refer to hours from the start of the experiment (+ th cultures were grown in parallel with – th cultures). The HO endonuclease in the C-terminal construct is induced by removal of thiamine from the media, but its control is unaffected by the presence or absence of β-Estradiol.

| | 0 hrs extra glucose (HO off) MGH wt | 0 hrs extra glucose (HO off) crb2-d rqh1-d | 2 hrs extra glucose (HO off) MGH wt | 2hrs extra glucose (HO off) crb2-d rqh1-d | 2hrs sucrose (HO on) MGH wt | 2hrs sucrose (HO on) crb2-d rqh1-d |
|---|---|---|---|---|---|---|
| ■ % ade+ G418s his+ (GC) | 0.0 | 0.0 | 1.9 | 1.0 | 3.8 | 2.1 |
| ■ % ade+ G418r his+ (EJ/SCC) | 96.2 | 84.1 | 98.1 | 91.3 | 84.6 | 80.0 |
| ■ % ade- G418s his- (Ch16 loss) | 3.8 | 11.1 | 0.0 | 4.8 | 11.5 | 7.4 |
| ■ % ade+ G418s his- (LOH) | 0.0 | 4.8 | 0.0 | 2.9 | 0.0 | 10.5 |
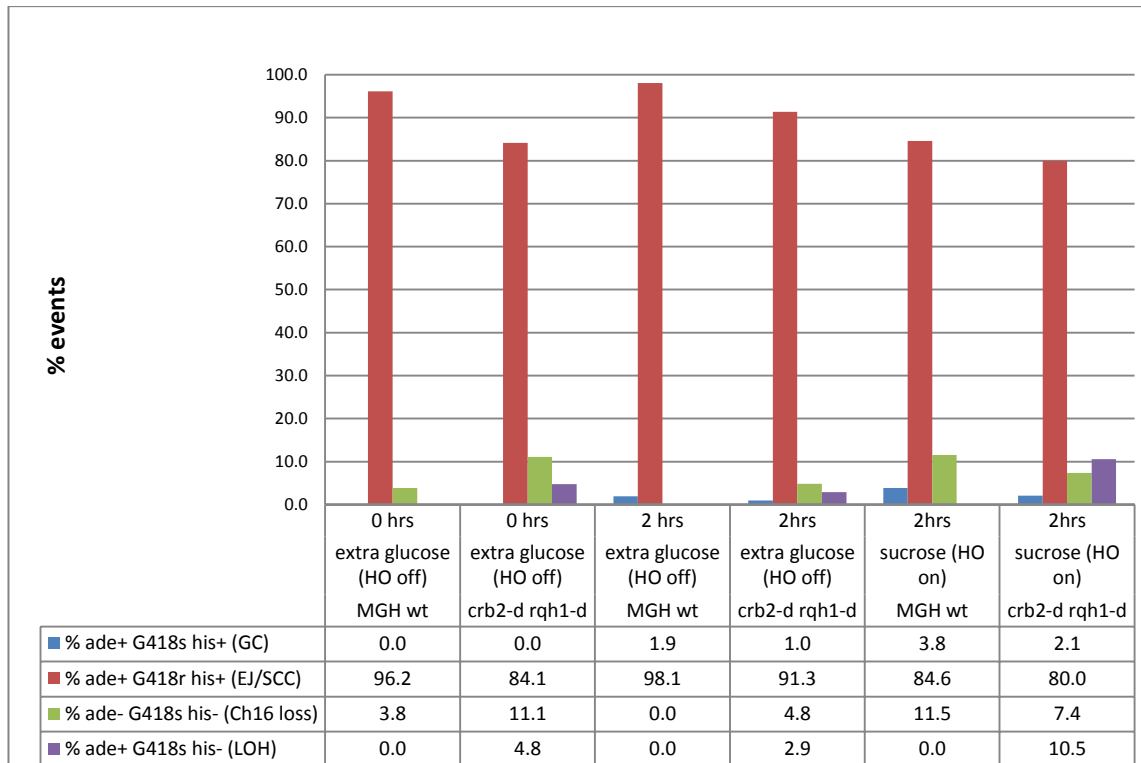
**Figure 8.8 | DNA repair events in wt MGH and *crb2*-d *rqh1*-d cells transformed with vectors carrying the HO endonuclease under regulation of the invertase promoter (InvHO).** Timepoints (0, 2 hrs) refer to time after the switch of carbon source from glucose (HO off) to sucrose (HO on). The induction of HO in sucrose does not induce a significant increase in HO activity as scored by increased marker loss. GC, Gene Conversion; EJ, End-Joining; SCC, Sister-Chromatid Conversion; LTGC, Long-Tract Gene Conversion; LOH, loss of herozigosity.

## 8.4 Discussion

### 8.4.1 DNA repair events in Rqh1 and Crb2 mutants

The aim of this work was to set up a system to study the functional relationship between the checkpoint mediator Crb2 and the helicase Rqh1 in *S. pombe*. The genetic relationship between the two proteins, suggested by preceding work by Caspari et al. (2002), provided the starting point for the project presented in this chapter. The use of the minichromosome system as presented in works by Prudden et al. (2003) and Cullen et al. (2007) was chosen as a tool to investigate the functional relationship that may link the two enzymes in the context of the recombinational repair of a site-specific DSB.

Initial results confirmed that gene conversion events are decreased in an *rqh1*-d background, as already reported by Hope et al., 2006. The following step in this project focused on Crb2. In particular, the Crb2-T215A (mutated in the CDK phosphorylation site) was shown to be responsible for a shift in repair events towards Ch16 loss/LTGC, favoured over EJ/SCC events (fig. 8.3). This data suggests a role for Crb2$^{Sp}$ in the choice of the DNA repair pathway utilised to repair an HO-induced DSB in which CDK phosphorylation of Crb2-T215 would favour conservative events such as end-joining or sister-chromatid conversion. This could occur either by promotion of this class of repair events or by suppression of non-conservative events (namely long-tract gene conversion). Interestingly, the importance of the Crb2-T215 phosphorylation as a pathway switch seems to be confirmed by the finding that the absence of Crb2 leads to levels of conservative events and triple marker loss similar to wt (fig. 8.3, -th 48hrs, red and green bars). However, the lack of data from *crb2*-d limits the conclusions that can be drawn in this respect. The presence of the checkpoint mediator may be required for higher levels of gene conversion compared to the wt and *crb2*-T215A backgrounds (fig. 8.3, -th 48hrs, blue bars), although a reduction in GC events and a corresponding increase in EJ/SCC events may be due to the deletion of *rqh1*, as shown in fig. 8.2. Thus, in order to further define the apparent importance of the Crb2-T215 phosphorylation event in this context, it would be interesting to assess whether an opposite shift in repair events is shown in a *crb2*-T215 phospho-mimetic mutant.

Further work is needed to elucidate the significance of this pathway switch, but Rqh1 does not seem to be involved, as its deletion does not affect the overall distribution of repair events in a *crb2*-T215A background (fig. 8.3).

### 8.4.2 **Isochromosome formation in *crb2*-T215A**

A random selection of *crb2*-T215A colonies showing a triple-negative phenotype was subsequently analysed by Pulse-Field Gel Electrophoresis. Interestingly, the colonies that showed retention of the minichromosome, previously classified as "Long-tract Gene

Conversion" events, represented in fact a specific type of gross chromosomal rearrangements leading to formation of isochromosomes. The generation of these chromosomal structures has been previously reported. Nakamura and co-workers showed that two types of spontaneous gross chromosomal rearrangements involving the minichromosome can occur in fission yeast. Type II minichromosome rearrangements were identified as isochromosomes, where the original right arm was replaced by a copy of the left arm. Rhp51[Sp] was shown to be crucially involved in suppressing the formation of these structures (Nakamura et al., 2008). Work by Tinline-Purvis et al. (2009) using an HO inducible DSB system showed that the occurrence of isochromosomal rearrangements is generally increased in genetic backgrounds in which gene conversion is abrogated or inefficient (*rhp51*-d, *rhp55*-d, *rhp57*-d, *nbs1*-d). As extensive LOH and minichromosome loss showed the same trend, a plausible conclusion is that all these dramatic non-conservative events are the result of failed gene conversion (Tinline-Purvis et al. 2009). In the present study, gene conversion events did not show significant changes in a *crb2*-T215A background compared to wt (fig. 8.3). However, all the colonies analysed that were presumed to have lost the minichromosome were in fact shown to possess isochromosomes (fig. 8.5). Although it could be speculated that a phosphorylatable Crb2-T215 residue might be crucially involved in the suppression of isochromosome formation, the limited number of colonies analysed and the absence of any comparison with other genetic backgrounds does not allow any further conclusion from these data.

It is interesting to note that the PFGE analysis (fig. 8.5) highlighted the formation of two forms of chromosomal rearrangements in *crb2*-T215A *rqh1*-d probably arising from transfer of chromosome material between ChIII and the minichromosome. Although the number of samples analysed here is very limited, a similar observation has been seen previously in our laboratory where an increase in translocations occurred in an *rqh1*-d background compared to wt (Dr S. Gill, personal communication). This finding would be consistent with the role shown for Rqh1 in preserving chromosomal stability (Stewart et al., 1997).

### 8.4.3    Limitations of the Ch16 double-strand break repair system

The genetic system employed in this study provides a useful tool to detect the pathway chosen by cells to repair a DSB at a specific site. However, some limitations which are intrinsic to the system have to be considered.

The first limitation is the impossibility to distinguish between an uncut target DNA and an error-free repair pathway, as in both cases the phenotypic outcome will be a wild-type combination of genetic traits. It is thereby assumed that in the presence of thiamine or at earlier time-points, when the induction of the HO endonuclease is either repressed or at its initial onset, the vast majority of wild-type colonies represent cells where the *MATa* site on the minichromosome has not been cleaved yet.

The second limitation of the system is that further analysis by PFGE is required in order to assess whether the triple marker loss is due to occurrence of long-tract gene conversion or due to loss of the minichromosome.

A third limitation is that, in order to allow comparisons between different genetic backgrounds, it is assumed that the efficiency of the HO endonuclease is consistently similar in different genetic backgrounds and at different time-points following induction. Although studies of HO cutting efficiency *in vivo* have not yet been performed, Hope et al. (2006) showed that indeed the HO cutting efficiency in wt and *rqh1*-depleted cells is comparable.

The fourth limitation of the system is due to the use of the *nmt1* promoter as a regulatory element for the HO induction: despite optimisations of the upstream TATA box of the promoter, its full repression by thiamine cannot be achieved (Basi et al., 1993). Furthermore, its activation is induced at a maximum steady-state level 16 hours after the removal of thiamine from the medium (Maundrell, 1990). To overcome this limitation, two alternative regulatory elements were tested, where the HO endonuclease can be regulated by the presence of β-Estradiol (ER-HBD-HO) or sucrose (InvHO). However, most of the data obtained

in this chapter is based on the use of the well-established thiamine-regulated promoter and its intrinsic limitation taken into account, where appropriate.

Finally, it should be also noticed that due to the prolonged status of activation of the HO endonuclease following its induction, the *MATa* site will undergo repeated rounds of re-cutting, assuming the previous DNA repair events generate re-cleavable substrates. As a consequence, it could be postulated that over time repair events will be biased towards non-conservative events, these being end-points for the occurrence of further cuttings. However, it has been shown that levels of G418 marker loss do not decrease significantly at 48 hours and 72 hours following induction (Prudden et al., 2003, fig. 2 and suppl. fig. C). Thus, it can be assumed that the system is not affected by a bias towards non-conservative events in the time frame considered in this study.

### 8.4.4 Use of the Ch16 system to investigate the functional relationship between Rqh1 and Crb2

The data presented in this chapter indicate that while the Ch16 system can be used to investigate the relationship between Crb2 and Rqh1, as discussed above a limitation of the system is the impossibility of exerting a fine control over the HO activity. The requirement for 16 hours to obtain maximum levels of HO induction translates into the difficulty in investigating functional protein-protein interactions on a molecular level. This limitation precludes cell cycle synchronisation studies as reported for other DNA damaging agents. Furthermore, the experimental procedure requiring colonies growing on selective plates excludes the possibility of detecting reduced cell viability following HO induction. Decreased cell viability in specific mutants caused by HO DSBs would be an important indicator of molecular events needed for wild-type survival and response to this subset of DNA damage. As shown in Caspari et al. (2002), the reduction in cell survival following IR in *crb2*-T215A and the restored resistance by the additional deletion of *rqh1* highlighted a genetic relationship between the two proteins. It would be interesting to assess whether the same interplay occurs

following HO induction. This validation would be important, as it cannot be excluded that the above interaction may occur following specific types of DNA damage (e.g. IR-induced damage, as shown in Caspari et al., 2002) and may not be relevant in the context of a site-specific DSB generated by the HO endonuclease.

In conclusion, the most evident finding obtained by the use of this system is that a cross-talk between Rqh1$^{Sp}$ and Crb2$^{Sp}$ does not seem to influence the choice of the pathway to repair an HO-induced DSB.

### 8.4.5 **Alternative HO regulatory elements**

Soon after the employment of this system, it became clear that the limitations of the Ch16 system were hampering further developments towards the establishment of a reliable tool to address the specific questions posed by the project. As seen above, the delay in induction dictated by the use of the *nmt1* promoter can impede analyses aimed at investigating the properties of components of functional molecular pathways on a dynamic level. For this reason, two alternative systems were tested where the HO endonuclease could be regulated in a rapid and reversible fashion. However, neither of the two systems, regulated by means of β-Estradiol (ER-HBD-HO) or sucrose (InvHO) could provide the reliability and the versatility required. Thus, further attempts to use the Ch16 system to establish the functional relationship between Crb2 and Rqh1 were abandoned.

## 8.5   Conclusions

The Ch16 system has proven to be a useful tool to investigate the choice of DNA repair pathway followed by cells bearing different genetic backgrounds (Prudden et al., 2003; Hope et al., 2006; Cullen et al., 2007; Tinline-Purvis et al., 2009). Due to the nature of the Ch16 DSB assay, the employment of this system addresses questions regarding the choice of repair pathways at steady-state levels of DNA repair, and would not be suitable to address the specific question posed by the project, namely the investigation of the functional relationship

between Rqh1 and Crb2. Indeed, the observation that the deletion of both Crb2 and Rqh1 does not affect the choice of repair pathway compared to the wt background (fig. 8.3) would suggest that the relationship between the two proteins should be investigated by using a different set of tools. Likewise, the shift in DNA repair events observed in a *crb2*-T215A background does not seem to be affected by the concomitant absence of Rqh1. It cannot be excluded that the relationship between the two proteins could be resolved at early stages of HO induction, where an alternative, flexible and rapid way of regulating its activity was to be used. However, the two alternative systems of HO regulation failed to provide these improvements. Taken together, these results indicate that the Ch16 system would not be suitable to investigate the functional relationship between Crb2 and Rqh1.

Appendix 2

SUPPLEMENTARY FIGURES
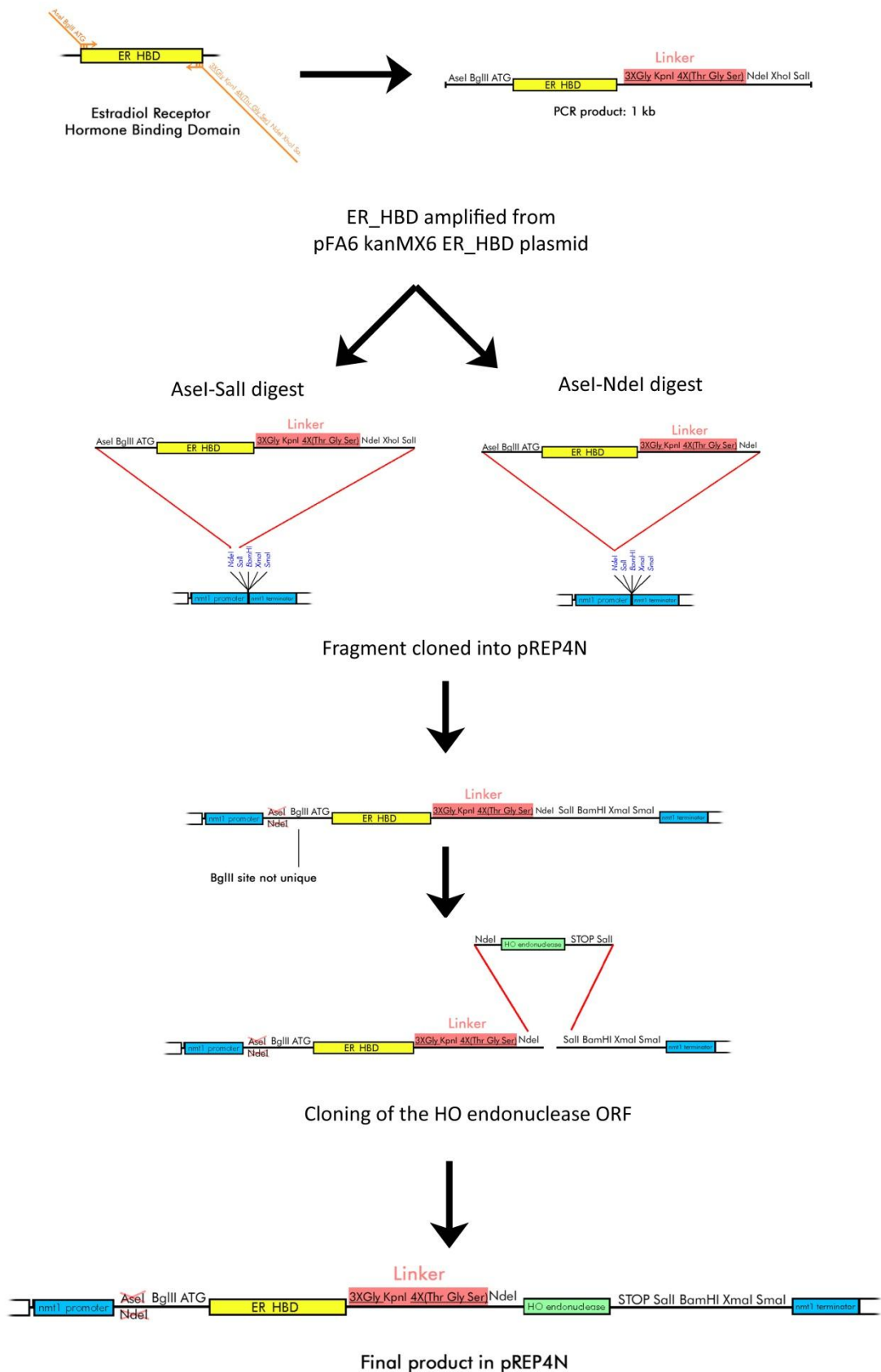
**Figure 9.1 | N-terminal ER-HBD HO: cloning strategy.** Standard molecular biology techniques were used to obtain the construct of interest. Two distinct strategies were followed. In the first strategy (left side), the PCR product amplified from pFA6-kanMX6_ER-HBD is digested with AseI-*SalI*, while in the second strategy (right side) the plasmid is digested with AseI-NdeI. As AseI and NdeI generate compatible ends, the downstream steps are common to the two approaches.
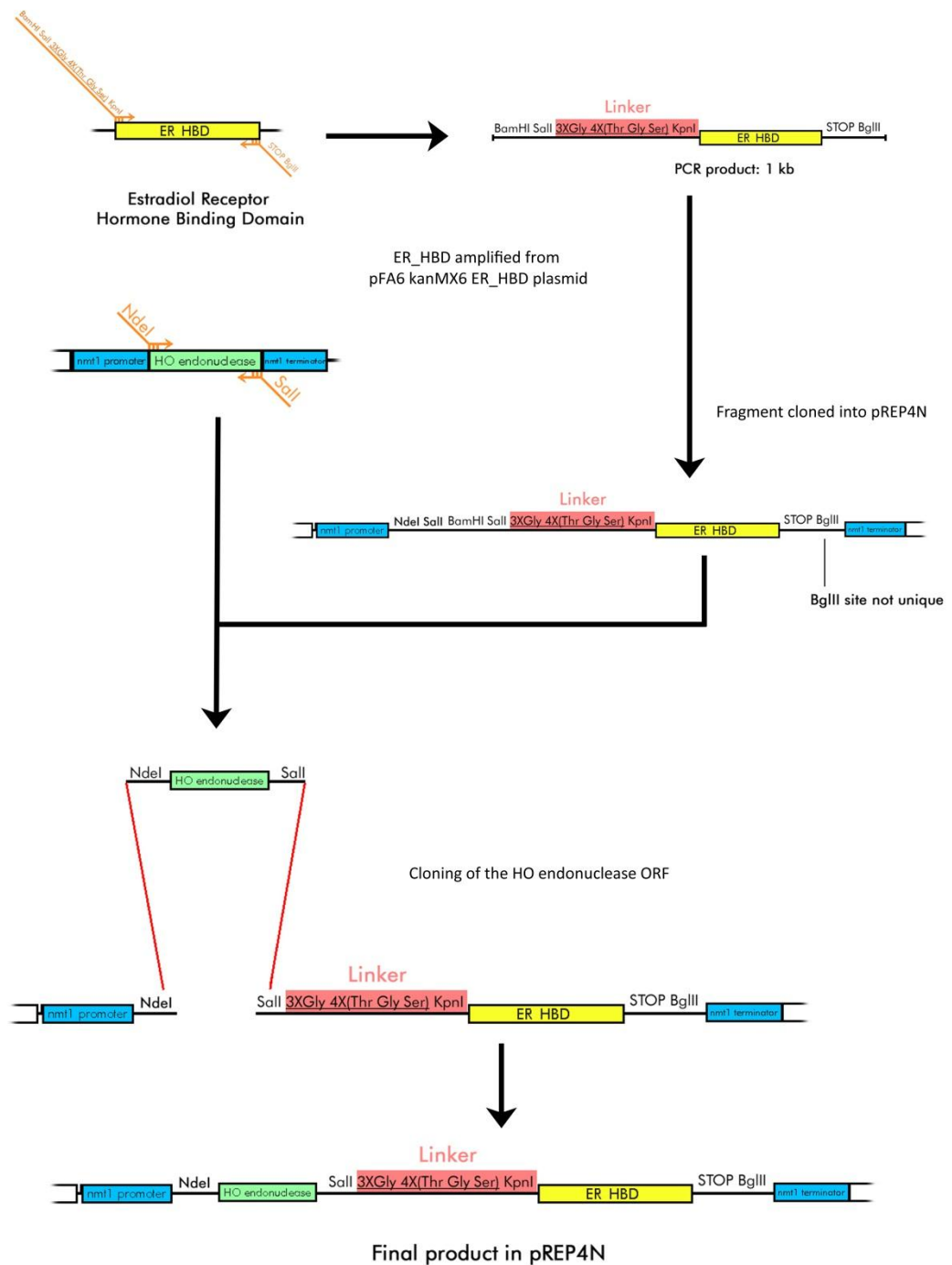
**Figure 9.2 | C-terminal ER-HBD HO: cloning strategy.** Standard molecular biology techniques were used to obtain the construct of interest.
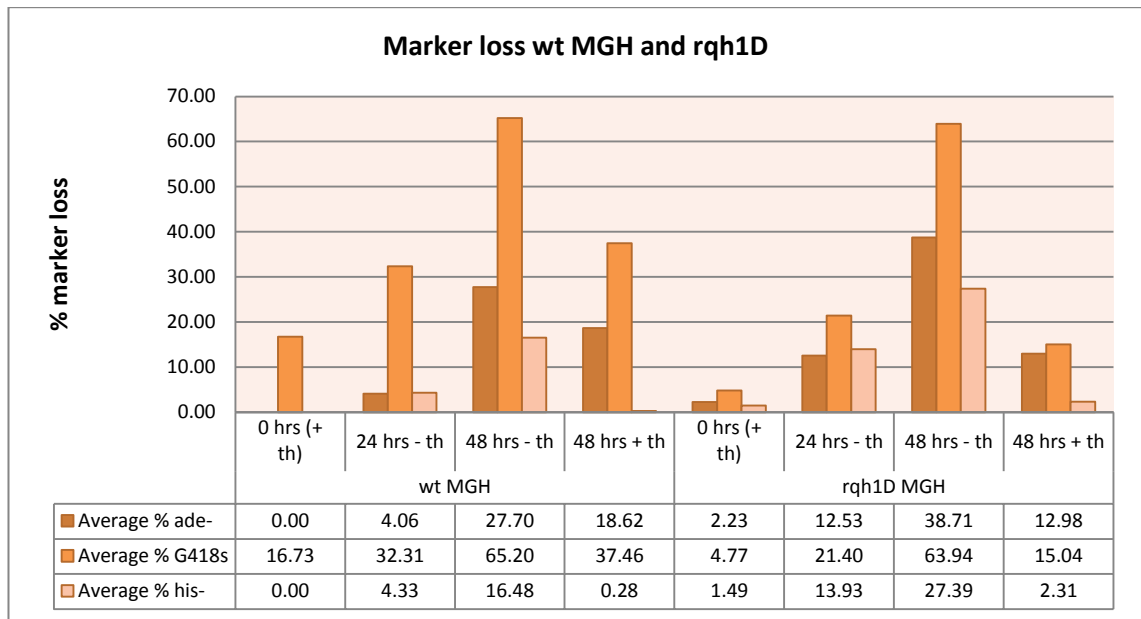
**Figure 9.3 | Loss of individual markers in wt and rqh1-d MGH.** The data in this graph represents the initial scoring of the loss of the three individual markers ade6, G418, his3 prior to the assignment to categories of DNA repair events shown in fig. 3.2. The data presented in this graph highlight an exceptionally low his3 marker loss compared to ade6 marker loss. See section 8.3.1 for a discussion about this unusual occurrence. The timepoints refer to growth time following the removal of thiamine from the medium: –th, thiamine absent from the medium. 48 hrs +th refers to cultures grown in parallel to the 48 hrs –th cultures: +th, thiamine present in the medium.

**InvHO DSB assay - Crb2-T215A rqh1-d (+ sucrose only)**

| | + HO 0 hrs MGH wt | + HO 0 hrs | + HO 0 hrs | + HO 0 hrs | no HO 0 hrs | + HO 3 hrs MGH wt | + HO 3 hrs | + HO 3 hrs | + HO 3 hrs | no HO 3 hrs | + HO 6 hrs MGH wt | + HO 6 hrs | + HO 6 hrs | + HO 6 hrs | no HO 6 hrs |
|---|---|---|---|---|---|---|---|---|---|---|---|---|---|---|---|
| | | Crb2-T215A rqh1-d MGH | | | | | Crb2-T215A rqh1-d MGH | | | | | Crb2-T215A rqh1-d MGH | | | |
| ■ % ade+ G418s his+ (GC) | 10.3 | 50.1 | 62.0 | 46.3 | 0.0 | 34.9 | 73.9 | 83.3 | 60.6 | 0.0 | 24.0 | 67.3 | 83.3 | 55.3 | 0.0 |
| ■ % ade+ G418r his+ (EJ/SCC) | 87.1 | 49.1 | 37.1 | 52.9 | 99.4 | 60.5 | 21.7 | 16.7 | 30.3 | 99.0 | 76.0 | 26.5 | 0.0 | 38.3 | 99.7 |
| ■ % ade- G418s his- (Ch16 loss) | 1.1 | 0.8 | 0.9 | 0.8 | 0.6 | 0.0 | 2.2 | 0.0 | 1.5 | 1.0 | 0.0 | 0.0 | 16.7 | 0.0 | 0.3 |
| ■ % ade+ G418s his- (LOH) | 1.4 | 0.0 | 0.0 | 0.0 | 0.0 | 2.3 | 2.2 | 0.0 | 7.6 | 0.0 | 0.0 | 4.1 | 0.0 | 6.4 | 0.0 |
| ■ ade- G418s his+ (reverse LOH) | 0.0 | 0.0 | 0.0 | 0.0 | 0.0 | 2.3 | 0.0 | 0.0 | 0.0 | 0.0 | 0.0 | 2.0 | 0.0 | 0.0 | 0.0 |
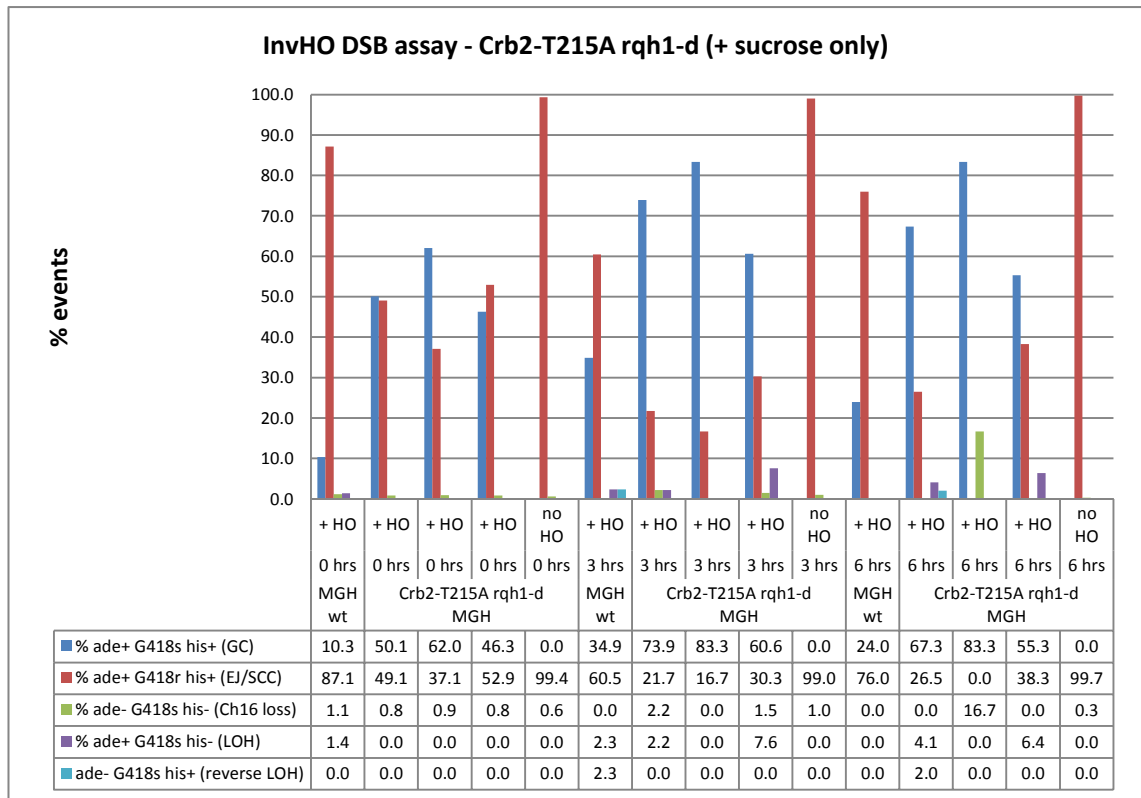
**Figure 9.4 | DNA repair events in wt MGH and crb2-T215A rqh1-d cells transformed with vectors carrying the HO endonuclease under regulation of the invertase promoter (+ HO) or Inv empty vectors (no HO).** The experiment was performed with three different isolates for each crb2-T215A rqh1-d strain (second, third and fourth column for each timepoint). All timepoints refer to hours of growth in medium containing sucrose (HO on). The strains show a significant leakage in HO activity at 0 hrs, before the induction with sucrose. GC, Gene Conversion; EJ, End-Joining; SCC, Sister-Chromatid Conversion; LTGC, Long-Tract Gene Conversion; LOH, loss of heterozigosity.
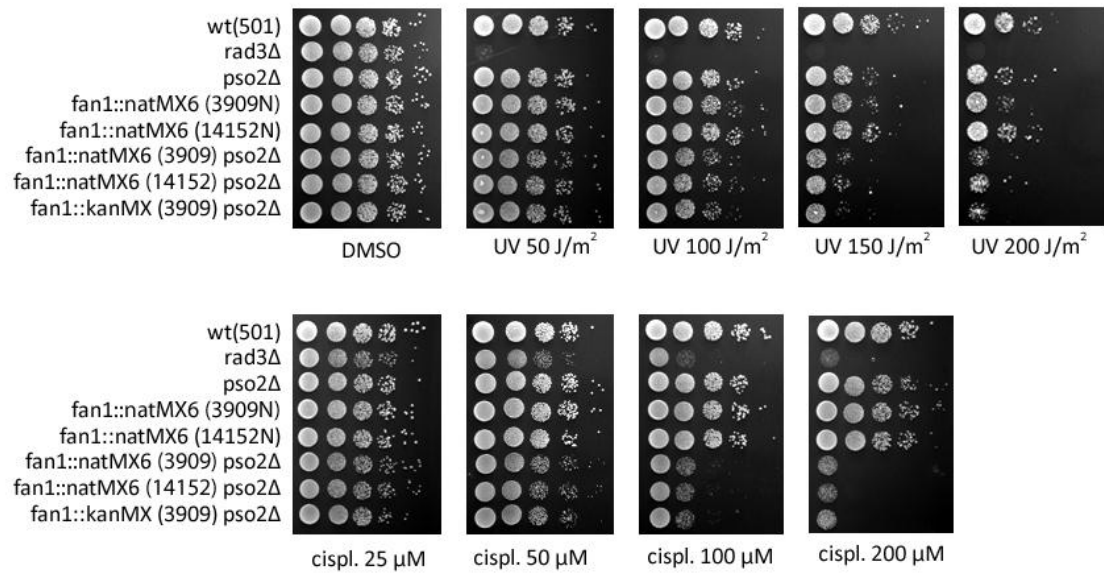
**Figure 9.5 | Sensitivity of *fan1*::*kanMX6 pso2*::*kanMX6* mutants to UV and cisplatin.** Logarithmically grown cultures were spotted in four 1:10 serial dilutions starting from $10^7$ cells (first spot on the left) on YEA plates containing the agents in the amount indicated. *rad3*-d is used as a standard hypersensitive control for the efficacy of the agents used. The insertion of the *kanMX6* instead of the *natMX6* cassette to disrupt the *fan1* ORF in a *pso2*-d background does not affect the sensitivity to the DNA damaging agents tested. UV, Ultra-Violet irradiation; cispl., cisplatin.
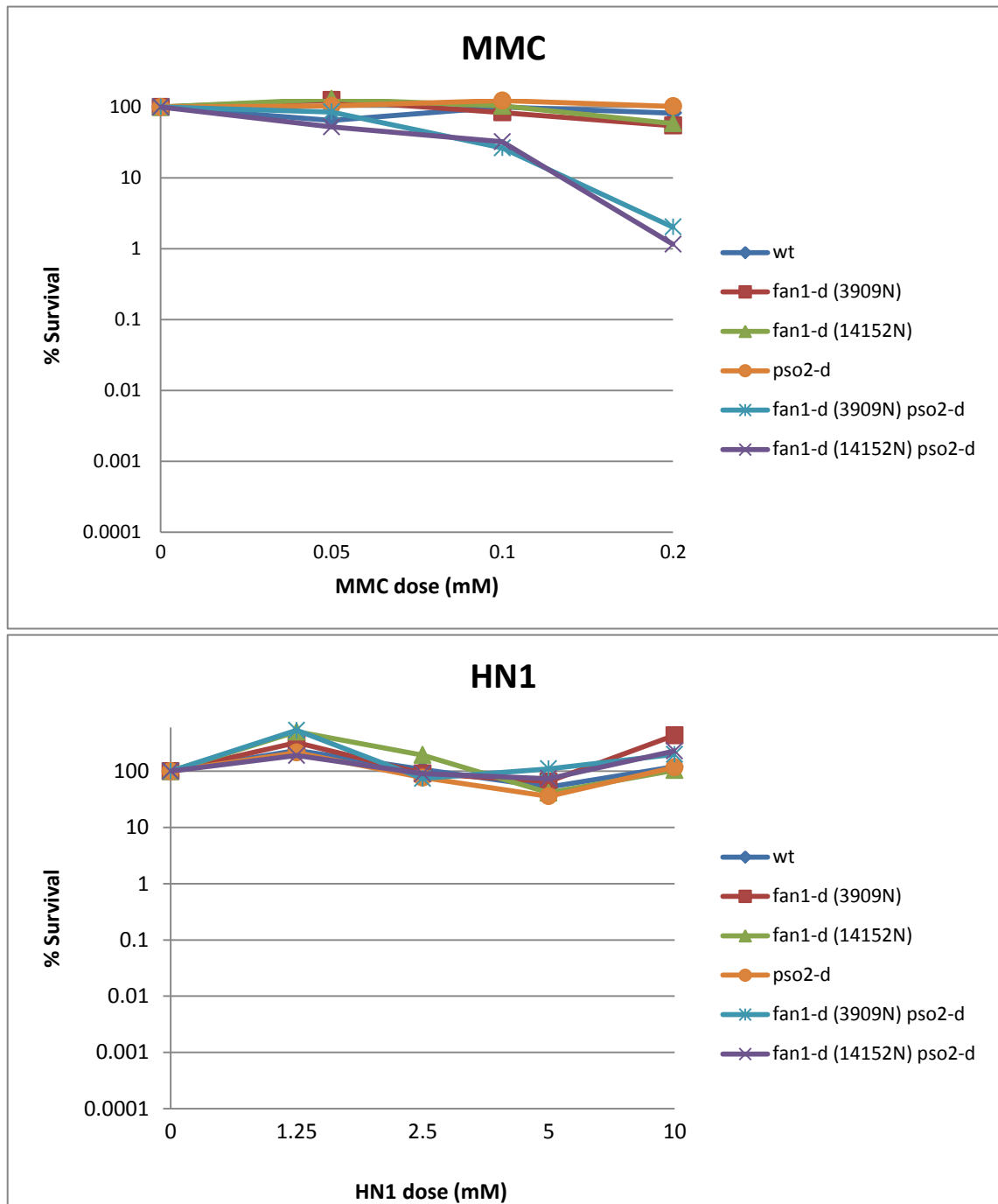
**Figure 9.6 | Sensitivity of *fan1*-d mutants, alone and in combination with *pso2*-d, to MMC and the mono-functional nitrogen mustard HN1 (2-dimethylaminoethylchloride hydrochloride).** $4 \times 10^7$ cells from logarithmically growing cultures were exposed to each indicated dose of damaging agents. Approximately 200 cells were plated on YEA and grown for 3-4 days at 30°C. The combination of the deletions of *fan1* and *pso2* causes the most marked sensitivity to MMC among the mutants tested. No significant sensitivity is shown to the mono-functional nitrogen mustard HN1. MMC, Mitomycin C; HN1, mono-functional nitrogen mustard (2-dimethylaminoethylchloride hydrochloride).
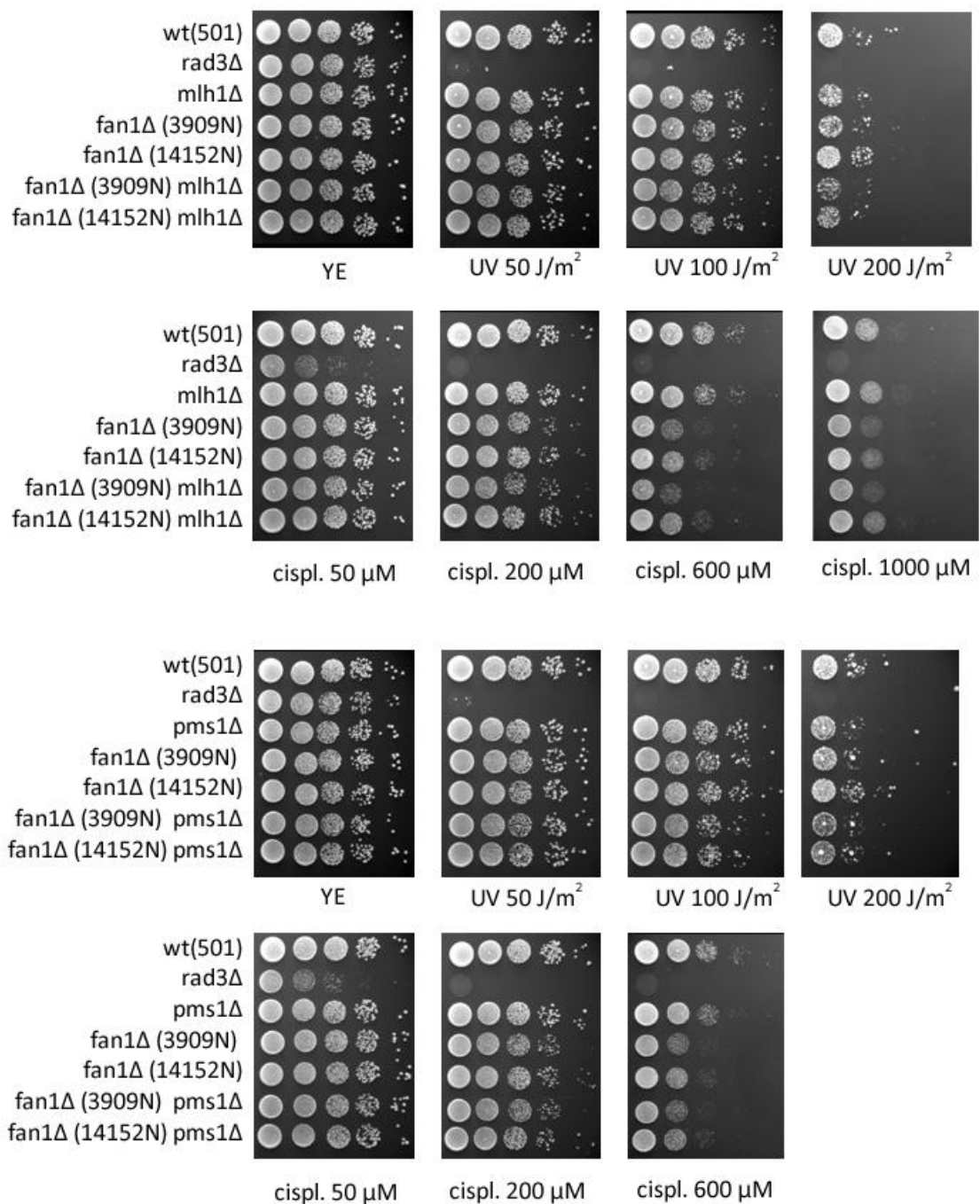
**Figure 9.7 | Sensitivity of *mlh1*-d and *pms1*-d strains, alone and in combination with *fan1*-d, to UV and cisplatin.** Logarithmically grown cultures were spotted in four 1:10 serial dilutions starting from $10^7$ cells (first spot on the left) on YEA plates containing the agents in the amount indicated. *rad3*-d is used as a standard hypersensitive control for the efficacy of the agents used. The combined deletion of *fan1* with *mlh1* and *pms1* does not affect the sensitivity to UV and cisplatin compared to the respective single mutants. Abbreviations used: UV, Ultra-Violet irradiation; cispl, cisplatin.
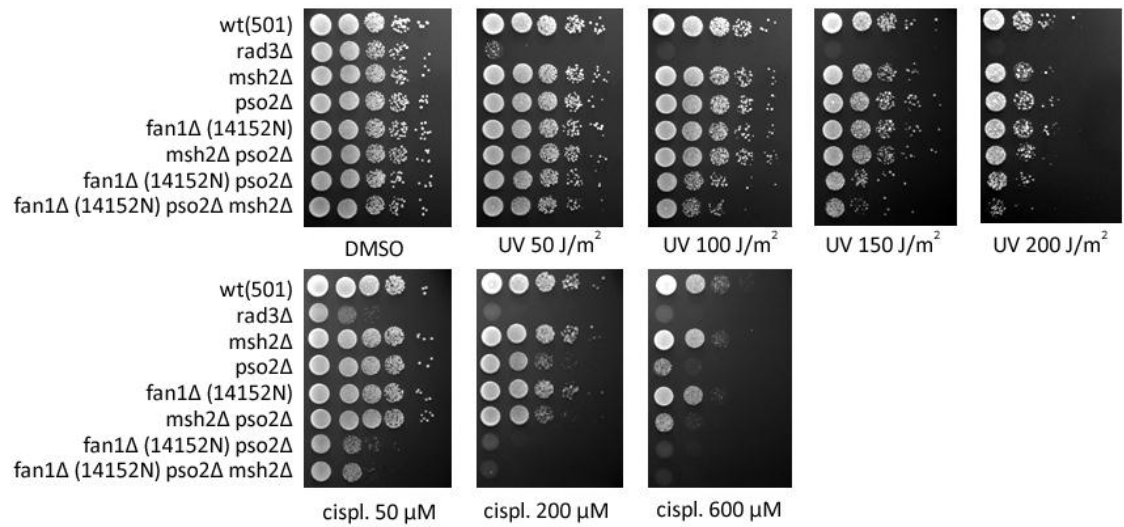
**Figure 9.8 | Sensitivity of *fan1*-d (14152N) *pso2*-d *msh2*-d triple mutant to UV and cisplatin.** Logarithmically grown cultures were spotted in four 1:10 serial dilutions starting from $10^7$ cells (first spot on the left) on YEA plates containing the agents in the amount indicated. *rad3*-d is used as a standard hypersensitive control for the efficacy of the agents used. A subtle increased sensitivity to cisplatin is noticed only for the combined triple mutant *fan1*-d *pso2*-d *msh2*-d when exposed to UV. Abbreviations used: UV, Ultra-Violet irradiation; cispl, cisplatin.
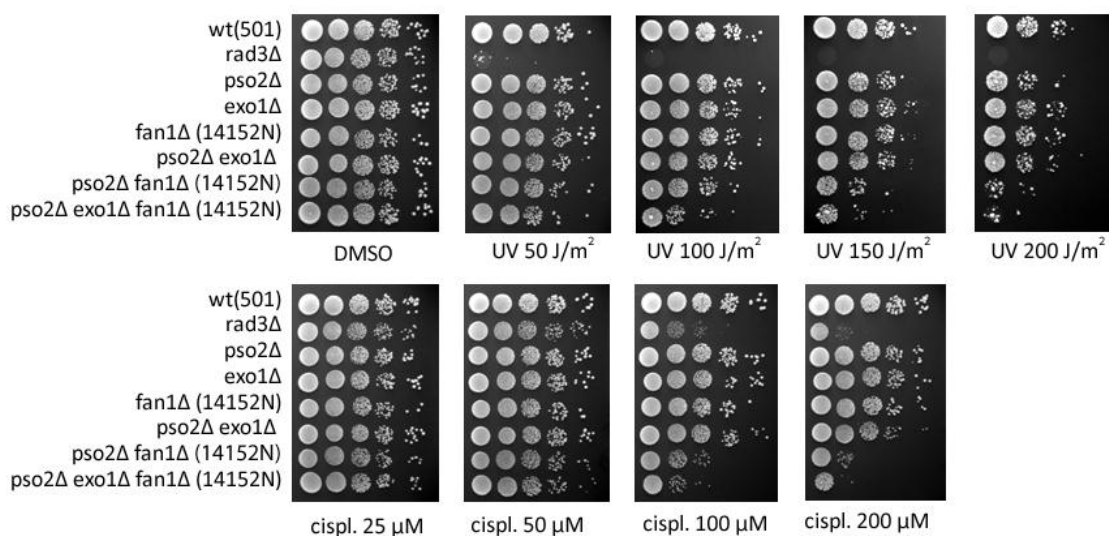
**Figure 9.9 | Sensitivity of different combinations of *fan1*-d (14152N background), *exo1*-d and *pso2*-d mutants to UV and cisplatin.** Logarithmically grown cultures were spotted in four 1:10 serial dilutions starting from $10^7$ cells (first spot on the left) on YEA plates containing the agents in the amount indicated. *rad3*-d is used as a standard hypersensitive control for the efficacy of the agents used. The triple deletion of *fan1*, *pso2* and *exo1* does not aggravate the sensitivity of the cognate double mutant *fan1 pso2*. Abbreviations used: UV, Ultra-Violet irradiation; cispl, cisplatin.
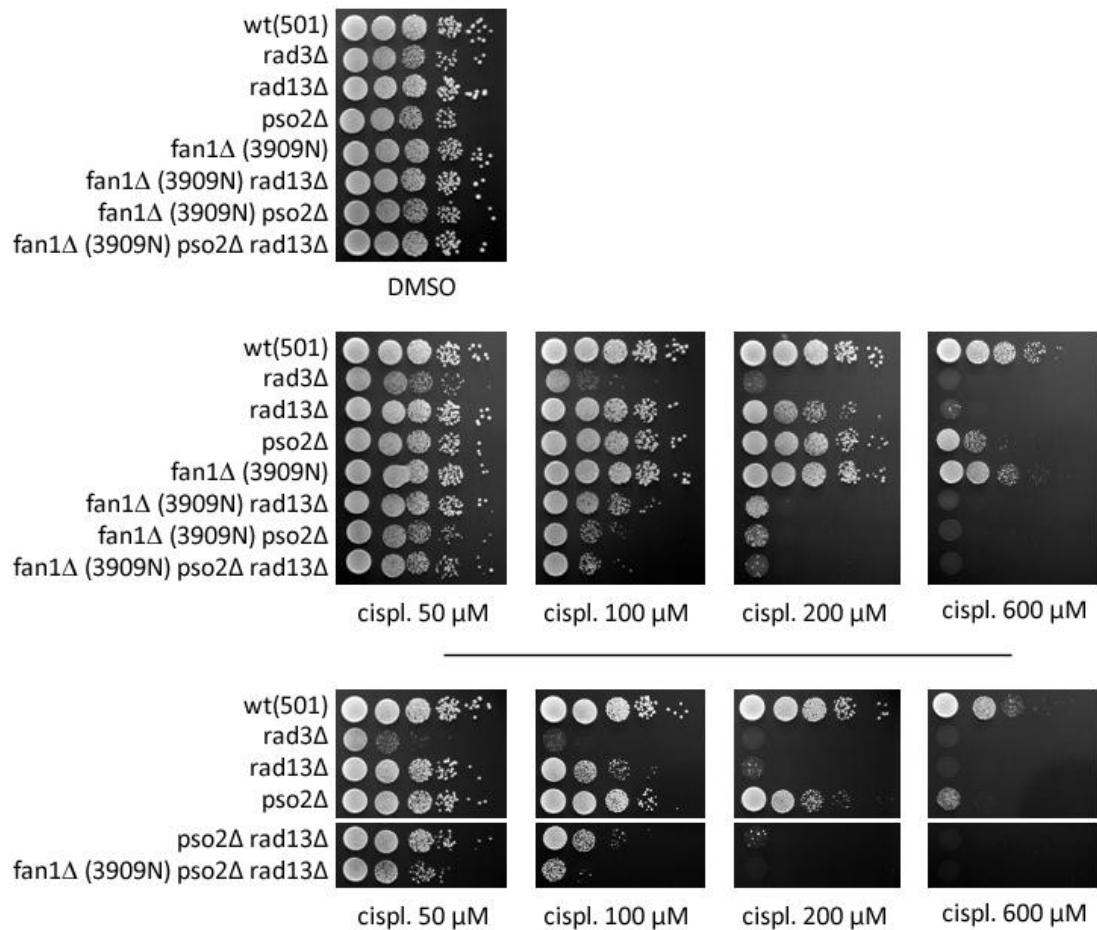
**Figure 9.10 | Sensitivity of *rad13* mutants exposed to increasing doses of cisplatin (*fan1*-d: 14152N background).** Logarithmically grown cultures were spotted in four 1:10 serial dilutions starting from $10^7$ cells (first spot on the left) on YEA plates containing the agents in the amount indicated. *rad3*-d is used as a standard hypersensitive control for the efficacy of the agents used. The deletion of both *fan1* and *rad13* causes a marked hypersensitivity to cisplatin. Bottom panel: independent experiment showing the compared sensitivity of *pso2*-d *rad13*-d and the respective single mutants. Abbreviations used: MMC, mitomycin C; cispl, cisplatin.
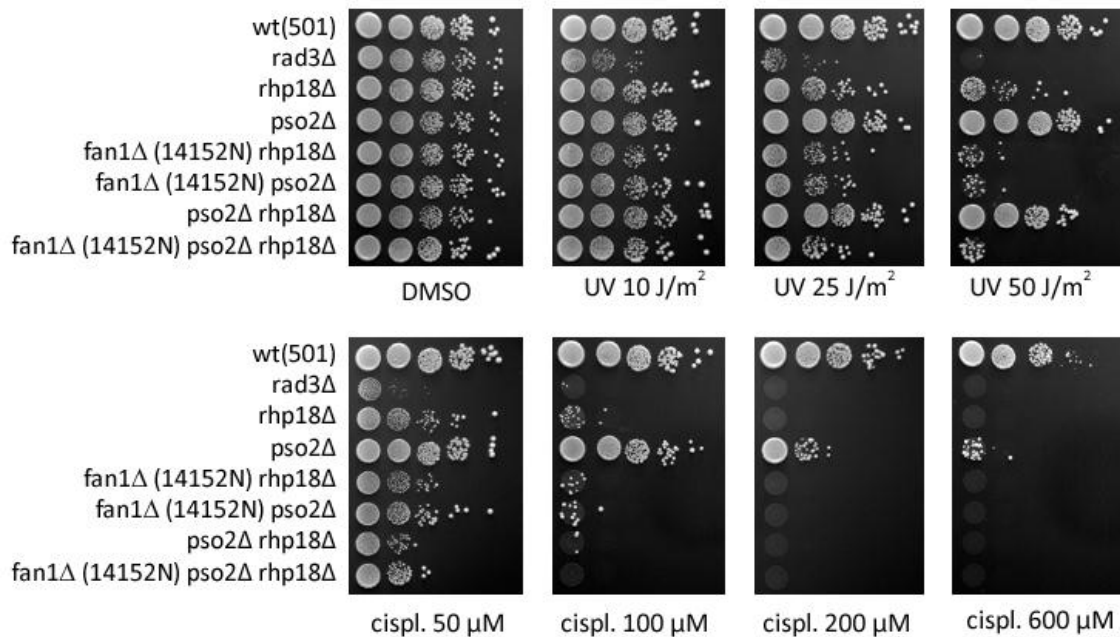
**Figure 9.11 | Sensitivity of combinations of *rhp18* mutants to UV and cisplatin (*fan1*-d: 14152N background).** Logarithmically grown cultures were spotted in four 1:10 serial dilutions starting from $10^7$ cells (first spot on the left) on YEA plates containing the agents in the amount indicated. *rad3*-d is used as a standard hypersensitive control for the efficacy of the agents used. The additional deletion of *rhp18* does not affect the sensitivity of *pso2*-d to cisplatin. Abbreviations used: UV, Ultra-Violet irradiation; cispl, cisplatin.
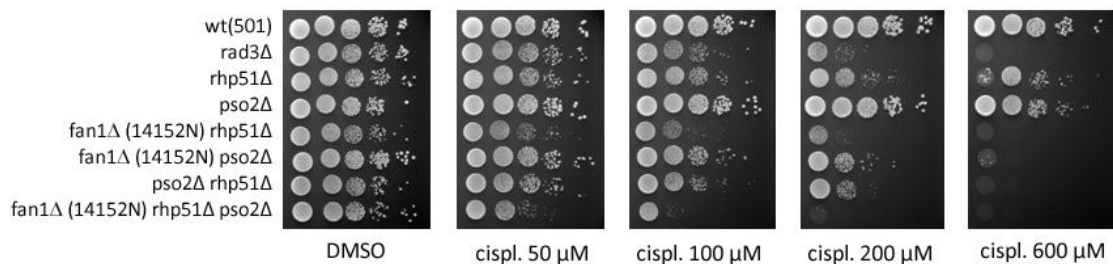


**Figure 9.12 | Sensitivity to cisplatin of various combinations of *rhp51* mutants to cisplatin (*fan1*-d: 14152N background).** Logarithmically grown cultures were spotted in four 1:10 serial dilutions starting from $10^7$ cells (first spot on the left) on YEA plates containing cisplatin in the amount indicated. *rad3*-d is used as a standard hypersensitive control for the efficacy of the agents used. The combined deletion of *pso2* and *rhp51* causes a lower sensitivity to cisplatin compared to *fan1*-d *rhp51*-d. Abbreviation used: cispl, cisplatin.

| | | | | |
|---|---|---|---|---|
| ecl2 | 1661 | 1915 | c | extender of the chronological lifespan protein Ecl2 |
| SPBP35G2.02 | 6111 | 6734 | | poteasome interacting protein (predicted) |
| sgo1 | 7146 | 8167 | c | shugoshin Sgo1 |
| SPBP35G2.04c | 8408 | 9434 | c | sequence orphan |
| cki2 | 10357 | 11848 | c | serine/threonine protein kinase Cki2 |
| nup131 | 12449 | 16032 | c | nucleoporin Nup131 |
| ilv1 | 16509 | 18518 | | acetolactate synthase catalytic subunit |
| SPBP35G2.08c | 18929 | 19974 | c | zinc knuckle TRAMP complex subunit Air1 |
| usp103 | 20640 | 21293 | | U1 snRNP-associated protein Usp103 (predicted) |
| mit1 | 21468 | 25724 | | SHREC complex subunit Mit1 |
| SPBP35G2.11c | 26044 | 27237 | c | transcription related zf-ZZ type zinc finger protein |
| SPBP35G2.12 | 28958 | 29575 | | ADP-ribose diphosphatase (predicted) |
| swc2 | 29817 | 30767 | c | Swr1 complex complex subunit Swc2 |
| SPBP35G2.14 | 32287 | 35469 | | RNA-binding protein |
| SPBP35G2.15 | 36243 | 39480 | | mediator complex subunit Med15 (predicted) |
| SPBC146.02 | 40411 | 41202 | | sequence orphan |
| cut3 | 41889 | 45863 | c | condensin complex subunit Cut3 |
| SPBC146.04 | 47418 | 47996 | | sulfhydryl oxidase (predicted) |
| cwf25 | 48199 | 49391 | c | complexed with Cdc5 protein Cwf25 |
| SPBC146.06c | 50001 | 52112 | c | VRR-NUC nuclease associated domain, human MTMR15 homolog |
| prp2 | 52955 | 54508 | | U2AF large subunit (U2AF-59) |
| SPBC146.08c | 54732 | 55167 | c | translation initiation factor eIF1A-like |
| lsd1 | 55400 | 58402 | c | histone demethylase SWIRM1 |
| mug57 | 59153 | 59722 | | meiotically upregulated gene Mug57 |
| CDS | 59696 | 60703 | c | meiotically upregulated gene Mug97 |
| coq6 | 61855 | 63255 | | monooxygenase Coq6 |
| myo1 | 63633 | 67330 | c | myosin type I |
| sec26 | 68516 | 71338 | c | coatomer beta subunit (predicted) |
| SPBC337.02c | 72257 | 73176 | c | cell surface glycoprotein (predicted), DUF1773 family protein 6 |
| SPBC337.03 | 74938 | 76264 | | RNA polymerase II transcription termination factor (predicted) |
| ppk27 | 76477 | 77785 | | serine/threonine protein kinase Ppk27 (predicted) |
| cct8 | 77947 | 79978 | c | chaperonin-containing T-complex theta subunit Cct8 |
| Cwf15 | 80517 | 81373 | c | complexed with Cdc5 protein Cwf15 |
| SPBC337.07c | 81695 | 83359 | c | carboxypeptidase (predicted) |
| ubi4 | 83818 | 84966 | c | ubiquitin |
| erg28 | 86935 | 87520 | | Erg28 protein |
| SPBC337.10c | 87964 | 88830 | c | anamorsin family protein, involved in iron-sulphur cluster assembly |
| SPBC337.11 | 89715 | 90692 | | mitochondrial peptidase (predicted) |
| SPBC337.12 | 91480 | 92871 | | human ZC3H3 homolog |
| gtr1 | 93178 | 94104 | c | Gtr1/RagA G protein Gtr1 |
| rpb4 | 95062 | 95626 | | DNA-directed RNA polymerase II complex subunit Rpb4 |
| coq7 | 96025 | 96675 | c | ubiquinone biosynthesis protein Coq7 |
| cho1 | 97747 | 98467 | | phosphatidyl-N-methylethanolamine N-methyltransferase (predicted) |
| SPBC1734.01c | 98922 | 100970 | c | pre-rRNA processing protein Esf1 (predicted) |
| cdc27 | 101370 | 102112 | c | DNA polymerase delta subunit Cdc27 |

Colour key:
- ● Present in the Bioneer V2 library
- ● Pulled out in the screening
- ■ Known gene
- ■ function inferred from similarity to known gene
- ■ Conserved protein of unknown function
- ■ Sequence orphan

**Figure 9.13 | Genome view of ORFs proximal to the MTMR15 ortholog *fan1* in *S. pombe* (± 50 kb)**. List assembled by using the Artemis web applet (http://old.genedb.org/genedb/pombe).

**Results**

**47** result(s) in slim set with 245 terms and 66 gene products from your gene product list:

Please note that ontology roots nodes (marked with '*') only show direct associations.

You may also refine your input parameters.

Jump to Biological Process

**Missed Gene Products**

The following gene products could not be mapped to non-root nodes in the ontology using this slim. This may mean that the slim is incomplete.

| |
|---|
| SPAC1F12.04c |
| SPAC25B8.18 |
| SPBC146.06c |
| ape2 |
| mug110 |
| SPBC337.07c |
| SPBP35G2.14 |
| SPCC1827.04 |
| SPCC553.12c |

**Biological Process**

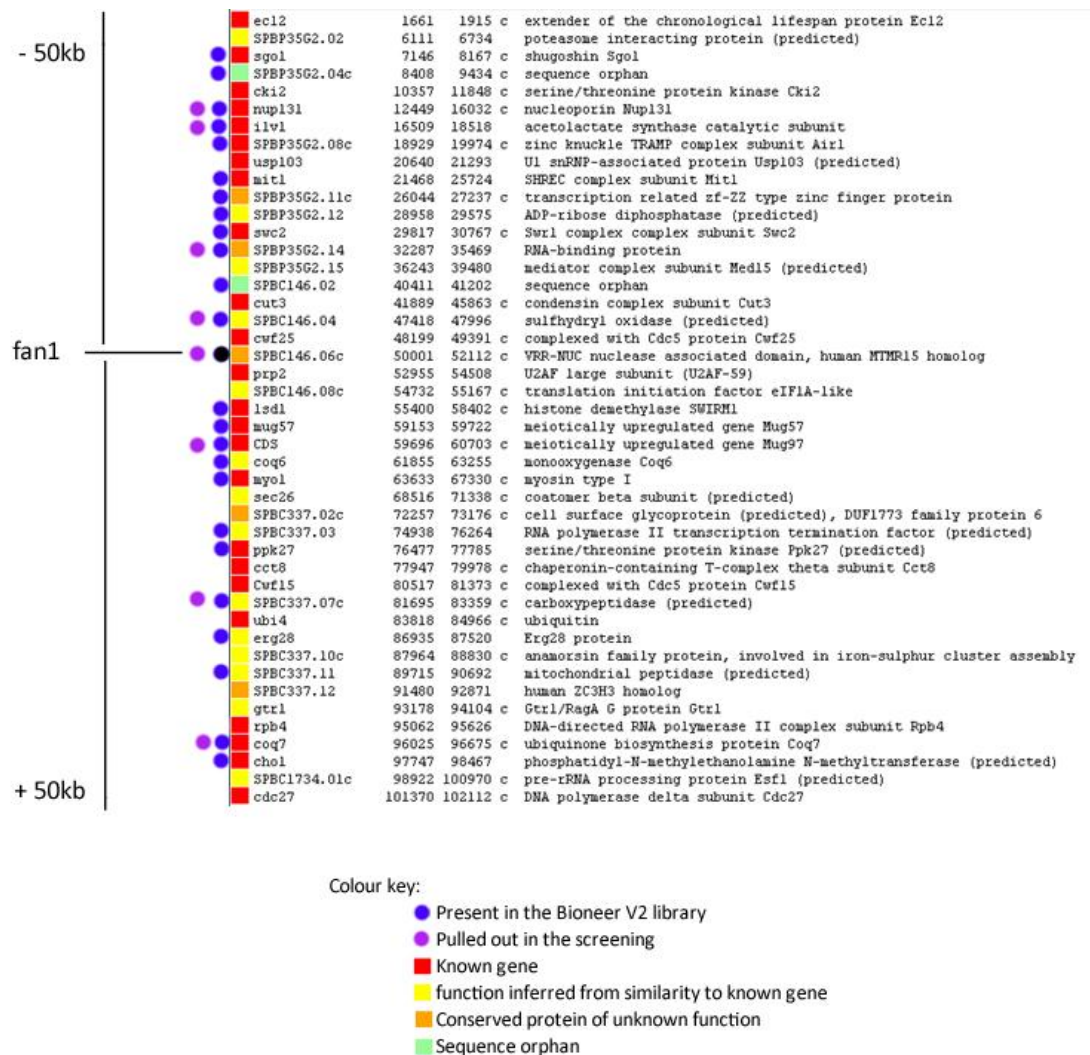| GO Slim Term | Total # GPs |
|---|---|
| GO:0006950 response to stress | 14 ( SPAC15E1.02c  sds23  nup131  rhp18  byr1  SPAC15E1.10  SPAC22E12.03c  byr2  ste20  rhp55  rad25  rhp54  SPBC8E4.05c  tif452 ) |
| GO:0023052 signaling | 12 ( gpa1  pef1  sds23  ste6  rhp18  byr1  ste7  ste20  byr2  rad25  csk1  ral2 ) |
| GO:0000747 conjugation with cellular fusion | 11 ( gpa1  sds23  ste6  byr1  ste7  ste20  byr2  tht1  mug138  mam4  ral2 ) |
| GO:0006810 transport | 9 ( dic1  nup131  atp16  apl5  SPAC11D3.18c  tom7  lys1  SPBC1734.07c  pub1 ) |
| GO:0051276 chromosome organization | 6 ( bqt2  sgo2  rhp54  mst2  swd2  hif2 ) |
| GO:0006412 translation | 6 ( ubi1  SPAC1F12.02c  tif452  csk1  rpl1002  rpl702 ) |
| GO:0006796 phosphate metabolic process | 6 ( pef1  rad25  atp16  byr1  csk1  byr2 ) |
| GO:0007126 meiosis | 6 ( dic1  rhp55  mug97  bqt2  sgo2  rhp54 ) |
| GO:0006259 DNA metabolic process | 5 ( rhp55  rad25  bqt2  rhp18  rhp54 ) |
| GO:0055086 nucleobase, nucleoside and nucleotide metabolic process | 5 ( rhp55  gpa1  atp16  rhp54  SPBC651.02 ) |
| GO:0006350 transcription | 4 ( pef1  mst2  hif2  php5 ) |
| GO:0006520 cellular amino acid metabolic process | 4 ( SPBC3B8.03  ilv1  SPAC644.08  lys1 ) |
| GO:0007346 regulation of mitotic cell cycle | 4 ( pef1  rad25  sds23  csk1 ) |
| GO:0016568 chromatin modification | 4 ( rhp54  mst2  swd2  hif2 ) |
| GO:0030437 ascospore formation | 4 ( dic1  gpa1  mug97  bqt2 ) |
| GO:0055085 transmembrane transport | 4 ( atp16  SPAC11D3.18c  tom7  pub1 ) |
| GO:0070647 protein modification by small protein conjugation or removal | 4 ( ubi1  ubr1  rhp18  pub1 ) |
| GO:0007059 chromosome segregation | 3 ( mug97  bqt2  sgo2 ) |
| GO:0006281 DNA repair | 3 ( rhp55  rhp18  rhp54 ) |
| GO:0006310 DNA recombination | 3 ( rhp55  bqt2  rhp54 ) |
| GO:0030163 protein catabolic process | 3 ( ubr1  SPAC15E1.10  pub1 ) |
| GO:0042254 ribosome biogenesis | 2 ( ubi1  rpl1002 ) |
| GO:0016192 vesicle-mediated transport | 2 ( apl5  SPBC1734.07c ) |
| GO:0007010 cytoskeleton organization | 2 ( bud6  ain1 ) |
| GO:0005975 carbohydrate metabolic process | 2 ( alg12  php5 ) |
| GO:0006091 generation of precursor metabolites and energy | 2 ( coq7  atp16 ) |
| GO:0006629 lipid metabolic process | 2 ( alg12  SPAC15E1.05c ) |
| GO:0007005 mitochondrion organization | 2 ( SPCC1672.04c  tom7 ) |
| GO:0016071 mRNA metabolic process | 2 ( SPBC13E7.03c  tif452 ) |
| GO:0032569 gene-specific transcription from RNA polymerase II promoter | 2 ( hif2  php5 ) |
| GO:0006260 DNA replication | 1 ( rad25 ) |
| GO:0000910 cytokinesis | 1 ( ain1 ) |
| GO:0006457 protein folding | 1 ( SPBC146.04 ) |
| GO:0007155 cell adhesion | 1 ( ral2 ) |
| GO:0006461 protein complex assembly | 1 ( SPCC1672.04c ) |
| GO:0006486 protein amino acid glycosylation | 1 ( alg12 ) |
| GO:0006605 protein targeting | 1 ( tom7 ) |
| GO:0006766 vitamin metabolic process | 1 ( nmt1 ) |
| GO:0006913 nucleocytoplasmic transport | 1 ( nup131 ) |
| GO:0007031 peroxisome organization | 1 ( SPBC1734.07c ) |
| GO:0007163 establishment or maintenance of cell polarity | 1 ( bud6 ) |
| GO:0019725 cellular homeostasis | 1 ( pub1 ) |
| GO:0051186 cofactor metabolic process | 1 ( coq7 ) |
| GO:0070882 cellular cell wall organization or biogenesis | 1 ( pal1 ) |
| GO:0071554 cell wall organization or biogenesis | 1 ( pal1 ) |
| GO:0007033 vacuole organization | 0 |
| GO:0006399 tRNA metabolic process | 0 |

**Figure 9.14 | Gene Ontologies from AmiGO Slim relative to the ORFs shown in tables 5.1a and 5.1b.**

Screenshots assembled from http://old.genedb.org/amigo-cgi/slimmer.
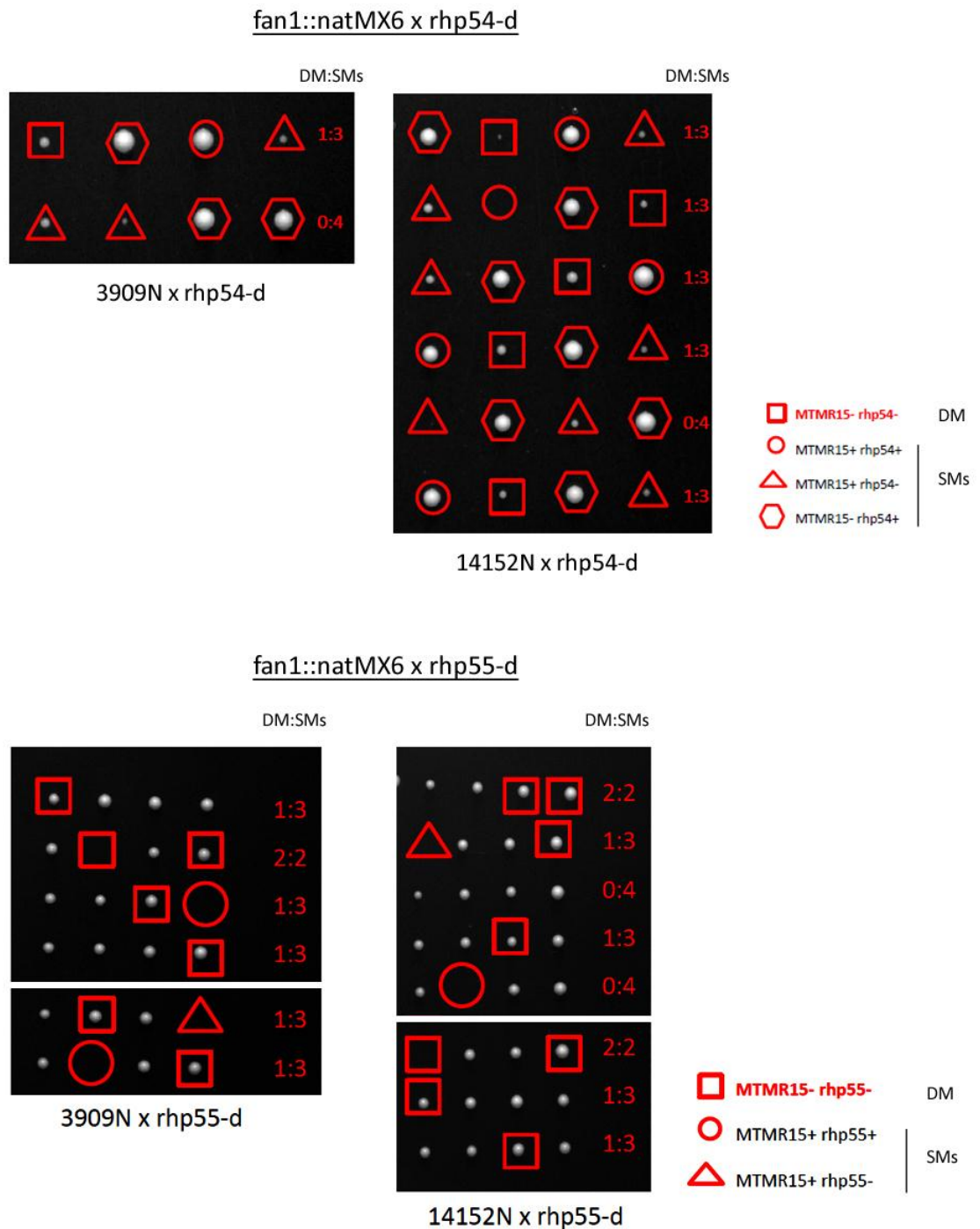
Figure 9.15 | Tetrad dissection analysis on *fan1*-d *rhp54*-d and *fan1*-d *rhp55*-d double mutant strains. Only YEA plates shown. *rhp54*-d, *rhp54*::*hphMX6* (hygromycin B – resistance cassette); *rhp55*-d, *rhp55*::ura4+. Independently derived mutants show that the combinations of *fan1*-d with *rhp54*-d and *rhp55*-d are not synthetically lethal. DM, double mutant; SMs, single mutants. DM:SMs is the ratio between the number of double mutant (DM) spores and the number of single mutant spores (SMs) in the respective tetrad on the left. DM and SMs spores were assessed by replica plating spores grown on YEA plates onto selective plates (YEA-hygromycin B and YEA-NAT plates for *fan1*-d *rhp54*-d; YNB-ura- and YEA-NATplates for *fan1*-d *rhp55*-d).

| row | column | size-1 (DM) | size-1 (SM) | Median DM | Median SM | Innermost colonies (excl. first 2 rows and columns) | Corrected median innermost colonies (DM) | Outermost colonies (first 2 rows and columns) | Median outermost colonies (DM) | Double mutants: deviation from median (pixels) | Single mutants: deviation from median (pixels) |
|---|---|---|---|---|---|---|---|---|---|---|---|
| 1 | 1 | 0 | 231 | 171 | 76 | 0 | 169 | 0 | 175 | -171 | 155 |
| 1 | 2 | 279 | 187 | -85.5 | -38 | 0 | | 279 | | 108 | 111 |
| 1 | 3 | 0 | 166 | 256.5 | 114 | 196 | | 0 | | -171 | 90 |
| 1 | 4 | 228 | 148 | | | 208 | | 228 | | 57 | 72 |
| 1 | 5 | 0 | 0 | | | 127 | | 0 | | -171 | -76 |
| 1 | 6 | 263 | 180 | | | 0 | | 263 | | 92 | 104 |
| 1 | 7 | 249 | 153 | | | 0 | | 249 | | 78 | 77 |
| 1 | 8 | 232 | 152 | | | 0 | | 232 | | 61 | 76 |
| 1 | 9 | 247 | 121 | | | 121 | | 247 | | 76 | 45 |
| 1 | 10 | 262 | 139 | | | 225 | | 262 | | 91 | 63 |
| 1 | 11 | 231 | 129 | | | 0 | | 231 | | 60 | 53 |
| 1 | 12 | 0 | 0 | | | 241 | | 0 | | -171 | -76 |
| 1 | 13 | 107 | 115 | | | 243 | | 107 | | -64 | 39 |
| 1 | 14 | 0 | 0 | | | 0 | | 0 | | -171 | -76 |
| 1 | 15 | 263 | 129 | | | 224 | | 263 | | 92 | 53 |
| 1 | 16 | 174 | 119 | | | 0 | | 174 | | 3 | 43 |
| 1 | 17 | 0 | 0 | | | 0 | | 0 | | -171 | -76 |
| 1 | 18 | 205 | 105 | | | 139 | | 205 | | 34 | 29 |
| 1 | 19 | 0 | 0 | | | 147 | | 0 | | -171 | -76 |
| 1 | 20 | 216 | 76 | | | 0 | | 216 | | 45 | 0 |
| 1 | 21 | 90 | 45 | | | 0 | | 90 | | -81 | -31 |
| 1 | 22 | 190 | 70 | | | 17 | | 190 | | 19 | -6 |
| 1 | 23 | 190 | 40 | | | 171 | | 190 | | 19 | -36 |
| 1 | 24 | 148 | 62 | | | 183 | | 148 | | -23 | -14 |
| 2 | 1 | 59 | 130 | | | 245 | | 59 | | -112 | 54 |
| 2 | 2 | 155 | 146 | | | 237 | | 155 | | -16 | 70 |
| 2 | 3 | 193 | 125 | | | 0 | | 193 | | 22 | 49 |

**Figure 9.16 | Example of spreadsheet with analysis of colony size relative to one synthetic genetic array.** Colony size values of single mutants (SMs) were included here as a control for the presence of colonies on the single mutant array. DM, double mutant; SM, single mutant. "Row" and "column" refer to the position of the strain in the 384-format plate. "Median DM" and "Median SM" columns show the median value of colony size on the double mutants and single mutants plates, respectively (cells not highlighted in the columns, in this example: 171 and 76). The cells highlighted in light blue are intervals used for the assignment of colour-coded categories (see fig. 5.3). The correction of the median for innermost and outermost colonies are displayed here, but they were not considered in the final analysis. Colour coded categories shown in the final two columns: (see fig. 5.3).

| row | column | ORF | Screening 2 (GNC) | | Screening 2 (GNC-GNC) | | Screening 4 (GNC) | | Screening 4 (GNC-GNC) | | Screening 5 (GNC) | | |
|---|---|---|---|---|---|---|---|---|---|---|---|---|---|
| | | | Double mutants: deviation from median (pixels) | Single mutants: deviation from median (pixels) | Double mutants: deviation from median (pixels) | Single mutants: deviation from median (pixels) | Double mutants: deviation from median (pixels) | Single mutants: deviation from median (pixels) | Double mutants: deviation from median (pixels) | Single mutants: deviation from median (pixels) | Double mutants: deviation from median (pixels) | Single mutants: deviation from median (pixels) | |
| 1 | 1 | SPCC4B3.07 | -113 | -158.5 | -129.5 | -158.5 | -148 | -179 | -143.5 | -179 | -134.5 | -71 | |
| 1 | 2 | SPBC1709.13c | -61 | -64.5 | -69.5 | -64.5 | -148 | 162 | -143.5 | 162 | -134.5 | 79 | SS/SL |
| 1 | 3 | SPAC30D11.05 | -113 | -158.5 | -129.5 | -158.5 | -148 | -179 | -143.5 | -179 | -134.5 | -71 | |
| 1 | 4 | SPBC19F8.06c | 28 | 15.5 | 30.5 | 15.5 | 31 | 229 | 121.5 | 229 | 77.5 | 98 | |
| 1 | 5 | SPAC1093.03 | -113 | -158.5 | -129.5 | -158.5 | -148 | -179 | -143.5 | -179 | -134.5 | -71 | |
| 1 | 6 | SPBC24C6.06 | -113 | 19.5 | -129.5 | 19.5 | -148 | 115 | -143.5 | 115 | -134.5 | 100 | SL |
| 1 | 7 | SPAC12B10.01c | 47 | -108.5 | 55.5 | -108.5 | 61 | 40 | 121.5 | 40 | 45.5 | 44 | |
| 1 | 8 | SPBC2G2.02 | 50 | 28.5 | 56.5 | 28.5 | -31 | 96 | 108.5 | 96 | 154.5 | 95 | |
| 1 | 9 | SPAC1B3.17 | 31 | 45.5 | 35.5 | 45.5 | -135 | 102 | -143.5 | 102 | -134.5 | -3 | |
| 1 | 10 | SPBC365.07c | 43 | 49.5 | 45.5 | 49.5 | 37 | 139 | 118.5 | 139 | 141.5 | 86 | |
| 1 | 11 | SPAC222.07c | 41 | 45.5 | 38.5 | 45.5 | 91 | 101 | 124.5 | 101 | 86.5 | 87 | |
| 1 | 12 | SPBC530.08 | -113 | -158.5 | -116.5 | -158.5 | -133 | -179 | -143.5 | -179 | -134.5 | -71 | |
| 1 | 13 | SPAC23G3.07c | 42 | 38.5 | 43.5 | 38.5 | 107 | 180 | 120.5 | 180 | 149.5 | 23 | |
| 1 | 14 | SPBC839.15c | -113 | -158.5 | -119.5 | -158.5 | -148 | -179 | -143.5 | -179 | -134.5 | -71 | |
| 1 | 15 | SPAC31G5.10 | 33 | -26.5 | 32.5 | -26.5 | 60 | 96 | 102.5 | 96 | 135.5 | 27 | |
| 1 | 16 | SPCC1020.10 | -14 | 136.5 | -16.5 | 136.5 | 79 | 248 | 91.5 | 248 | 132.5 | 65 | |
| 1 | 17 | SPAC4H3.02c | -113 | -158.5 | -129.5 | -158.5 | -148 | -179 | -143.5 | -179 | -134.5 | -71 | |
| 1 | 18 | SPCC1322.02 | -9 | 130.5 | -12.5 | 130.5 | 60 | 201 | 73.5 | 201 | 55.5 | 45 | |
| 1 | 19 | SPAC821.09 | -113 | -158.5 | -129.5 | -158.5 | -148 | -179 | -143.5 | -179 | -134.5 | -71 | |
| 1 | 20 | SPCC1753.02c | -9 | 93.5 | -12.5 | 93.5 | -23 | 134 | 20.5 | 134 | -76.5 | -11 | |
| 1 | 21 | SPBC106.11c | -113 | -158.5 | -129.5 | -158.5 | -148 | -179 | -143.5 | -179 | -134.5 | -71 | |
| 1 | 22 | SPCC18B5.01c | -113 | -158.5 | -129.5 | -158.5 | -148 | -179 | -143.5 | -179 | -134.5 | -71 | |
| 1 | 23 | SPBC13G1.08c | -113 | -158.5 | -129.5 | -158.5 | -148 | -179 | -143.5 | -179 | -134.5 | -71 | |

Array: YFL14c-15c-16c-17c

**Figure 9.17 | Example of spreadsheet with colour-coded categories of genetic interaction relative to a single synthetic array.** Categories of genetic interaction were finally assigned taking into account consistency across different screens and healthiness of the single mutant. Three independent screens were performed ("GNC" screens). Additionally, two further repeats were carried out by replicating GNC plates onto fresh GNC plates ("GNC-GNC" screens). See fig. 5.3 for the legend for colour-coded categories. SS, synthetic sick; SL, synthetic lethal; GNC, geneticin, nurseothricin, cycloheximide plates.

Q2xYFL2c-3c-4c-5c

*39hrs*

| row | column | size-1 DMSO | size-1 cisp50 | size-1 cisp200 | size-1 cisp600 | Median values of colony size | | | | Difference from median values of | | | | % difference of colony size | |
|---|---|---|---|---|---|---|---|---|---|---|---|---|---|---|---|
| | | | | | | DMSO | cisp50 | cisp200 | cisp600 | DMSO | cisp50 | cisp200 | cisp600 | cisp50-cisp200 | cisp200-cisp600 |
| 1 | 1 | 0 | 0 | 0 | 0 | 151 | 164 | 116 | 55 | -151 | -164 | -116 | -55 | - | - |
| 1 | 2 | 345 | 316 | 149 | 81 | | | | | 194 | 152 | 33 | 26 | -112 | -84 |
| 1 | 3 | 0 | 0 | 0 | 0 | | | | | -151 | -164 | -116 | -55 | - | - |
| 1 | 4 | 0 | 0 | 0 | 0 | | | | | -151 | -164 | -116 | -55 | - | - |
| 1 | 5 | 0 | 0 | 0 | 0 | | | | | -151 | -164 | -116 | -55 | - | - |
| 1 | 6 | 0 | 0 | 0 | 0 | | | | | -151 | -164 | -116 | -55 | - | - |
| 1 | 7 | 423 | 435 | 306 | 138 | | | | | 272 | 271 | 190 | 83 | -42 | -122 |
| 1 | 8 | 360 | 364 | 311 | 199 | | | | | 209 | 200 | 195 | 144 | -17 | -56 |
| 1 | 9 | 0 | 0 | 0 | 0 | | | | | -151 | -164 | -116 | -55 | - | - |
| 1 | 10 | 395 | 394 | 309 | 108 | | | | | 244 | 230 | 193 | 53 | -28 | -186 |
| 1 | 11 | 0 | 0 | 0 | 0 | | | | | -151 | -164 | -116 | -55 | - | - |
| 1 | 12 | 381 | 375 | 320 | 111 | | | | | 230 | 211 | 204 | 56 | -17 | -188 |
| 1 | 13 | 0 | 0 | 0 | 0 | | | | | -151 | -164 | -116 | -55 | - | - |
| 1 | 14 | 289 | 312 | 277 | 81 | | | | | 138 | 148 | 161 | 26 | -13 | -242 |
| 1 | 15 | 0 | 0 | 0 | 0 | | | | | -151 | -164 | -116 | -55 | - | - |
| 1 | 16 | 0 | 0 | 0 | 0 | | | | | -151 | -164 | -116 | -55 | - | - |
| 1 | 17 | 0 | 0 | 0 | 0 | | | | | -151 | -164 | -116 | -55 | - | - |
| 1 | 18 | 291 | 248 | 251 | 94 | | | | | 140 | 84 | 135 | 39 | 1 | -167 |
| 1 | 19 | 0 | 0 | 0 | 0 | | | | | -151 | -164 | -116 | -55 | - | - |
| 1 | 20 | 0 | 0 | 0 | 0 | | | | | -151 | -164 | -116 | -55 | - | - |
| 1 | 21 | 0 | 0 | 0 | 0 | | | | | -151 | -164 | -116 | -55 | - | - |
| 1 | 22 | 140 | 90 | 79 | 19 | | | | | -11 | -74 | -37 | -36 | -14 | -316 |
| 1 | 23 | 140 | 91 | 65 | 24 | | | | | -11 | -73 | -51 | -31 | -40 | -171 |
| 1 | 24 | 128 | 77 | 55 | 25 | | | | | -23 | -87 | -61 | -30 | -40 | -120 |
| 2 | 1 | 0 | 0 | 0 | 0 | | | | | -151 | -164 | -116 | -55 | - | - |
| 2 | 2 | 272 | 173 | 49 | 22 | | | | | 121 | 9 | -67 | -33 | -253 | -123 |

**Figure 9.18 | Example of spreadsheet with colony size analysis at increasing concentrations of cisplatin**. In this example, two possible candidates are shown (highlighted with a yellow square). However, only the second entry (row 2, column 2) was included in the final list of candidates, as consistency was shown across independent repeats of the screen. The main parameter taken into account in this analysis is the percentage reduction in colony size from cisplatin 50 µM to cisplatin 200 µM and cisplatin 200 µM to cisplatin 600 µM. Cells circled in red highlight the top 10% values in the column. Median values and deviation from median values were used only as a further control.
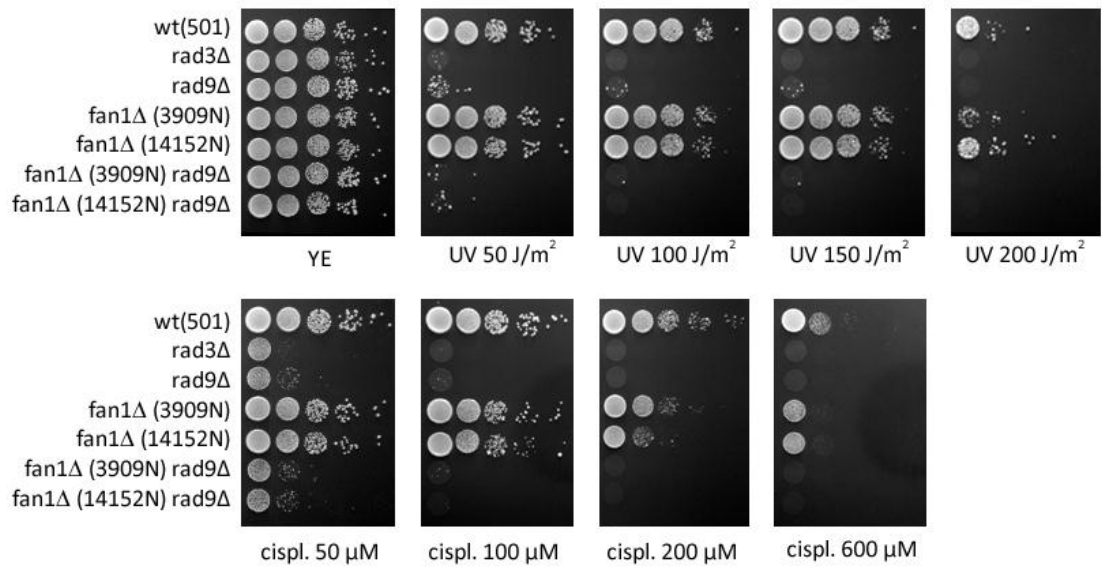
**Figure 9.19 | Sensitivity of *rad9* mutants to UV and cisplatin.** Logarithmically grown cultures were spotted in four 1:10 serial dilutions starting from $10^7$ cells (first spot on the left) on YEA plates containing the agents in the amount indicated. *rad3*-d is used as a standard hypersensitive control for the efficacy of the agents used. The double mutant tested in this experiment is derived from independently constructed single deletion mutants. *rad9*-d, alone or in combination with *fan1*-d, shows a dramatic hypersensitivity to both UV and cisplatin. Abbreviations used: UV, Ultra-Violet irradiation; cispl, cisplatin.
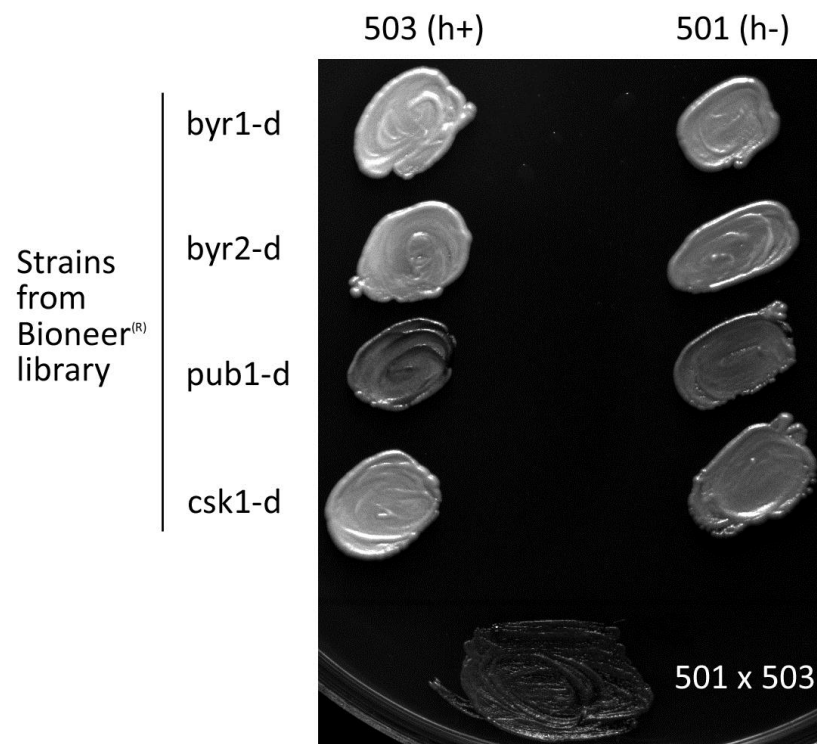
**Figure 9.20 | Test crosses with four selected strains from the prospective synthetic lethality set.** The four deletion mutants *byr1*-d, *byr2*-d, *pub1*-d and *csk1*-d were freshly streaked from the prospective synthetic lethality set and crossed with the wild-type strains 501 (h-) and 503 (h+) on an ELN plate. The crosses were incubated at 25°C for three days. Following iodine staining, none of the crosses turned dark red, indicating defective mating/sporulation processes. In contrast, the cross between 501 and 503 turned dark red as expected, indicating that the ELN media is not responsible for the inefficient crosses.
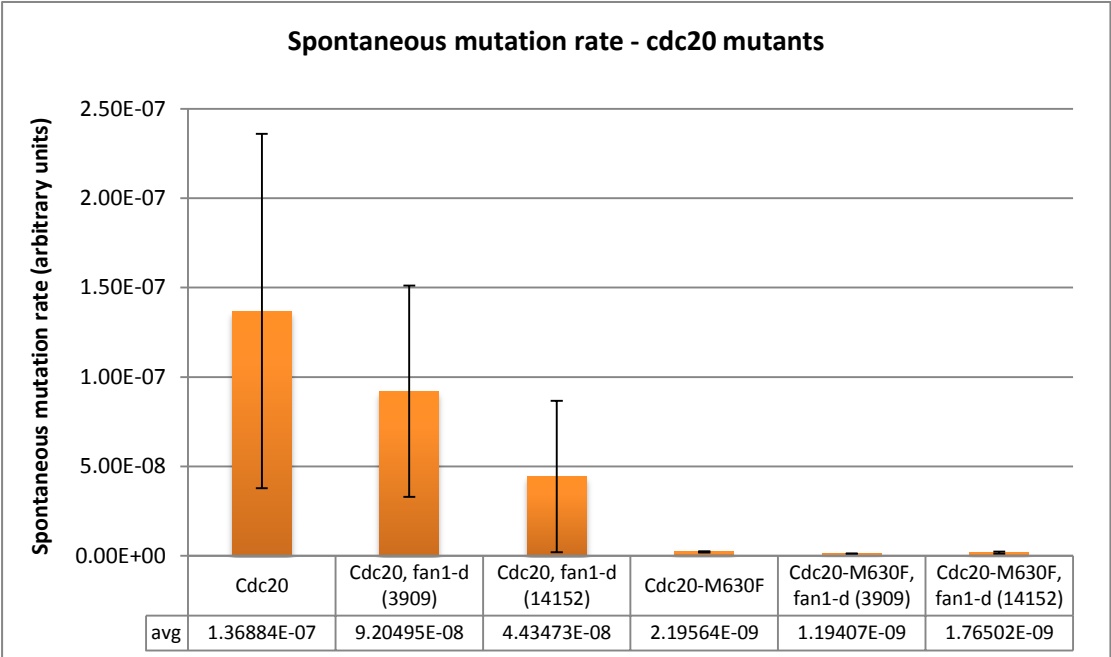
**Figure 9.21 | Spontaneous mutation rate of *fan1*-d mutants in *cdc20* wt and *cdc20*-M630F backgrounds.** The average of three independent experiments is shown. Error bars represent the standard error of the mean, calculated as standard deviation divided by $\sqrt{3}$. High standard error in all the samples is due to the low mutation rate falling outside the detection limit of the assay (errors in the order of $10^{-8}/10^{-9}$).
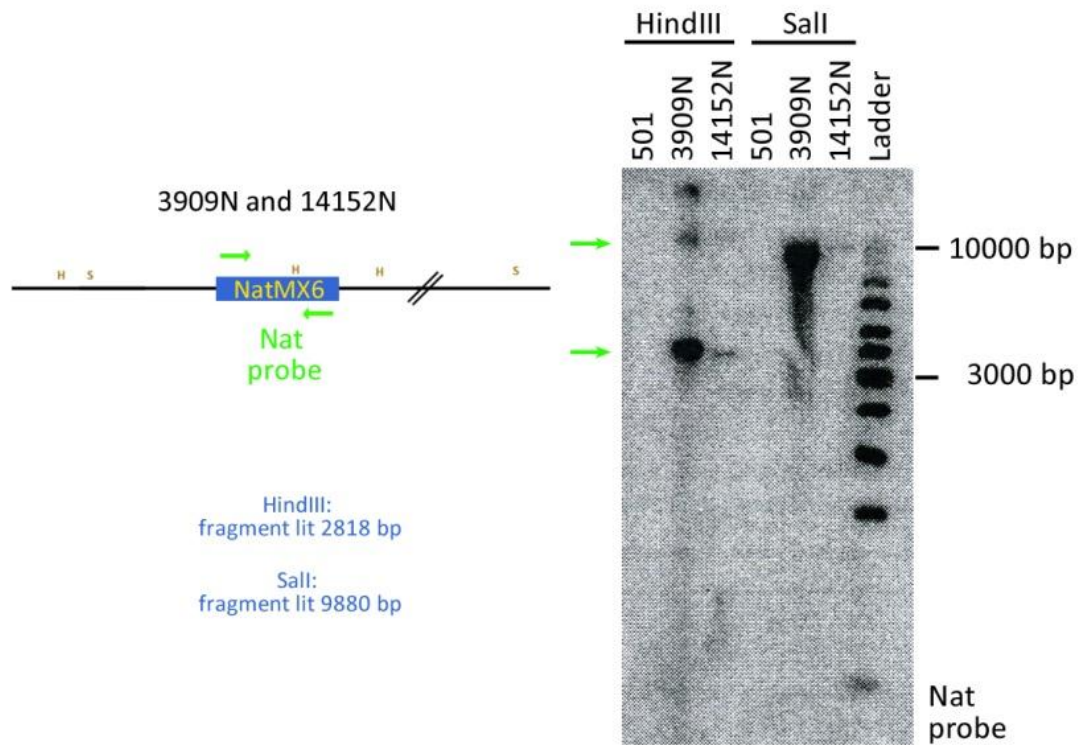
**Figure 9.22 |Southern blot analysis of the two *fan1*-deleted strains 3909N and 14152N.** 3909N and 14152N were obtained from the 3909 and 14152 strains, respectively, by replacing the *kanMX6* cassette with the *natMX6* cassette. Left: schematic showing the expected size for *HindIII* and *SalI* digests. H, *HindIII*; S, *SalI*. Right: Southern blot analysis. The genomic DNA digested with the indicated restriction enzymes and lit with the nat probe confirms the identity of the two strains.

# References

Adams, M. D., McVey, M., and Sekelsky, J. J. (2003). Drosophila BLM in double-strand break repair by synthesis-dependent strand annealing. Science *299*, 265-7.

Akkari, Y. M., Bateman, R. L., Reifsteck, C. A., Olson, S. B., and Grompe, M. (2000). DNA replication is required To elicit cellular responses to psoralen-induced DNA interstrand cross-links. Mol. Cell. Biol *20*, 8283-8289.

Alcasabas, A. A., Osborn, A. J., Bachant, J., Hu, F., Werler, P. J., Bousset, K., Furuya, K., Diffley, J. F., Carr, A. M., and Elledge, S. J. (2001). Mrc1 transduces signals of DNA replication stress to activate Rad53. Nat. Cell Biol *3*, 958-965.

Al-Khodairy, F., and Carr, A. M. (1992). DNA repair mutants defining G2 checkpoint pathways in Schizosaccharomyces pombe. EMBO J *11*, 1343-1350.

Al-Khodairy, F., Fotou, E., Sheldrick, K. S., Griffiths, D. J., Lehmann, A. R., and Carr, A. M. (1994). Identification and characterization of new elements involved in checkpoint and feedback controls in fission yeast. Mol. Biol. Cell *5*, 147-160..

Alpi, A. F., and Patel, K. J. (2009). Monoubiquitylation in the Fanconi anemia DNA damage response pathway. DNA Repair (Amst.) *8*, 430-435.

Araki, M., Masutani, C., Takemura, M., Uchida, A., Sugasawa, K., Kondoh, J., Ohkuma, Y., and Hanaoka, F. (2001). Centrosome protein centrin 2/caltractin 1 is part of the xeroderma pigmentosum group C complex that initiates global genome nucleotide excision repair. J. Biol. Chem *276*, 18665-18672..

Aravind, L., and Koonin, E. V. (2000). SAP - a putative DNA-binding motif involved in chromosomal organization. Trends Biochem. Sci *25*, 112-114.

Aten, J. A., Stap, J., Krawczyk, P. M., van Oven, C. H., Hoebe, R. A., Essers, J., and Kanaar, R. (2004). Dynamics of DNA double-strand breaks revealed by clustering of damaged chromosome domains. Science *303*, 92-95.

Au, K. G., Welsh, K., and Modrich, P. (1992). Initiation of methyl-directed mismatch repair. J. Biol. Chem *267*, 12142-12148.

Aylon, Y., Liefshitz, B., and Kupiec, M. (2004). The CDK regulates repair of double-strand breaks by homologous recombination during the cell cycle. EMBO J *23*, 4868-4875.

Bøe, C. A., Garcia, I., Pai, C.-C., Sharom, J. R., Skjølberg, H. C., Boye, E., Kearsey, S., Macneill, S. A., Tyers, M. D., and Grallert, B. (2008). Rapid regulation of protein activity in fission yeast. BMC Cell Biol *9*, 23.

Bachrati, C. Z., Borts, R. H., and Hickson, I. D. (2006). Mobile D-loops are a preferred substrate for the Bloom's syndrome helicase. Nucleic Acids Res *34*, 2269-79.

Barber, L. J., Ward, T. A., Hartley, J. A., and McHugh, P. J. (2005). DNA interstrand cross-link repair in the Saccharomyces cerevisiae cell cycle: overlapping roles for PSO2 (SNM1) with MutS factors and EXO1 during S phase. Mol. Cell. Biol *25*, 2297-2309.

Basi, G., Schmid, E., and Maundrell, K. (1993). TATA box mutations in the Schizosaccharomyces pombe nmt1 promoter affect transcription efficiency but not the transcription start point or thiamine repressibility. Gene *123*, 131-136.

Bebenek, K., Roberts, J. D., and Kunkel, T. A. (1992). The effects of dNTP pool imbalances on frameshift fidelity during DNA replication. J. Biol. Chem *267*, 3589-3596.

Beljanski, V., Marzilli, L. G., and Doetsch, P. W. (2004). DNA damage-processing pathways involved in the eukaryotic cellular response to anticancer DNA cross-linking drugs. Mol. Pharmacol *65*, 1496-1506.

Bergink, S., and Jentsch, S. (2009). Principles of ubiquitin and SUMO modifications in DNA repair. Nature *458*, 461-467.

Bernstein, K. A., Gangloff, S., and Rothstein, R. (2010). The RecQ DNA helicases in DNA repair. Annu. Rev. Genet *44*, 393-417.

Bessho, T., Mu, D., and Sancar, A. (1997). Initiation of DNA interstrand cross-link repair in humans: the nucleotide excision repair system makes dual incisions 5' to the cross-linked base and removes a 22- to 28-nucleotide-long damage-free strand. Mol. Cell. Biol *17*, 6822-6830.

Bhagwat, N., Olsen, A. L., Wang, A. T., Hanada, K., Stuckert, P., Kanaar, R., D'Andrea, A., Niedernhofer, L. J., and McHugh, P. J. (2009). XPF-ERCC1 participates in the Fanconi anemia pathway of cross-link repair. Mol. Cell. Biol *29*, 6427-6437.

Bi, X., Barkley, L. R., Slater, D. M., Tateishi, S., Yamaizumi, M., Ohmori, H., and Vaziri, C. (2006). Rad18 regulates DNA polymerase kappa and is required for recovery from S-phase checkpoint-mediated arrest. Mol. Cell. Biol *26*, 3527-3540.

Boiteux, S., O'Connor, T. R., and Laval, J. (1987). Formamidopyrimidine-DNA glycosylase of Escherichia coli: cloning and sequencing of the fpg structural gene and overproduction of the protein. EMBO J *6*, 3177-3183.

Bonilla, C. Y., Melo, J. A., and Toczyski, D. P. (2008). Colocalization of sensors is sufficient to activate the DNA damage checkpoint in the absence of damage. Mol Cell *30*, 267-76.

Boulikas, T., and Vougiouka, M. (2004). Recent clinical trials using cisplatin, carboplatin and their combination chemotherapy drugs (review). Oncol. Rep *11*, 559-595.

van Brabant, A. J., Ye, T., Sanz, M., German III, J. L., Ellis, N. A., and Holloman, W. K. (2000). Binding and melting of D-loops by the Bloom syndrome helicase. Biochemistry *39*, 14617-25.

Brabec, V. (2002). DNA modifications by antitumor platinum and ruthenium compounds: their recognition and repair. Prog. Nucleic Acid Res. Mol. Biol *71*, 1-68.

Brabec, V., and Kasparkova, J. (2002). Molecular aspects of resistance to antitumor platinum drugs. Drug Resist. Updat *5*, 147-161.

Buis, J., Wu, Y., Deng, Y., Leddon, J., Westfield, G., Eckersdorff, M., Sekiguchi, J. M., Chang, S., and Ferguson, D. O. (2008). Mre11 nuclease activity has essential roles in DNA repair and genomic stability distinct from ATM activation. Cell *135*, 85-96.

Burdett, V., Baitinger, C., Viswanathan, M., Lovett, S. T., and Modrich, P. (2001). In vivo requirement for RecJ, ExoVII, ExoI, and ExoX in methyl-directed mismatch repair. Proc. Natl. Acad. Sci. U.S.A *98*, 6765-6770.

Busso, D., Keriel, A., Sandrock, B., Poterszman, A., Gileadi, O., and Egly, J. M. (2000). Distinct regions of MAT1 regulate cdk7 kinase and TFIIH transcription activities. J. Biol. Chem *275*, 22815-22823.

Caldecott, K. W. (2008). Single-strand break repair and genetic disease. Nat. Rev. Genet *9*, 619-631.

Cannavo, E., Gerrits, B., Marra, G., Schlapbach, R., and Jiricny, J. (2007). Characterization of the interactome of the human MutL homologues MLH1, PMS1, and PMS2. J. Biol. Chem *282*, 2976-2986.

Carr, A. M. (2002). DNA structure dependent checkpoints as regulators of DNA repair. DNA Repair (Amst) *1*, 983-94.

Caspari, T., Dahlen, M., Kanter-Smoler, G., Lindsay, H. D., Hofmann, K., Papadimitriou, K., Sunnerhagen, P., and Carr, A. M. (2000). Characterization of Schizosaccharomyces pombe Hus1: a PCNA-related protein that associates with Rad1 and Rad9. Mol Cell Biol *20*, 1254-62.

Caspari, T., Murray, J. M., and Carr, A. M. (2002). Cdc2-cyclin B kinase activity links Crb2 and Rqh1-topoisomerase III. Genes Dev *16*, 1195-208.

Cassier-Chauvat, C., and Moustacchi, E. (1988). Allelism between pso1-1 and rev3-1 mutants and between pso2-1 and snm1 mutants in Saccharomyces cerevisiae. Curr. Genet *13*, 37-40.

Cattell, E., Sengerová, B., and McHugh, P. J. (2010). The SNM1/Pso2 family of ICL repair nucleases: from yeast to man. Environ. Mol. Mutagen *51*, 635-645.

Chanet, R., Cassier, C., and Moustacchi, E. (1985). Genetic control of the bypass of mono-adducts and of the repair of cross-links photoinduced by 8-methoxypsoralen in yeast. Mutat. Res *145*, 145-155.

Chang, M., Bellaoui, M., Zhang, C., Desai, R., Morozov, P., Delgado-Cruzata, L., Rothstein, R., Freyer, G. A., Boone, C., and Brown, G. W. (2005). RMI1/NCE4, a suppressor of genome instability, encodes a member of the RecQ helicase/Topo III complex. EMBO J *24*, 2024-33.

Ciccia, A., and Elledge, S. J. (2010). The DNA damage response: making it safe to play with knives. Mol. Cell *40*, 179-204.

Cimprich, K. A., and Cortez, D. (2008). ATR: an essential regulator of genome integrity. Nat. Rev. Mol. Cell Biol *9*, 616-627.

Clerici, M., Mantiero, D., Guerini, I., Lucchini, G., and Longhese, M. P. (2008). The Yku70-Yku80 complex contributes to regulate double-strand break processing and checkpoint activation during the cell cycle. EMBO Rep *9*, 810-818.

Clingen, P. H., Arlett, C. F., Hartley, J. A., and Parris, C. N. (2007). Chemosensitivity of primary human fibroblasts with defective unhooking of DNA interstrand cross-links. Exp. Cell Res *313*, 753-760.

Cohn, M. A., Kowal, P., Yang, K., Haas, W., Huang, T. T., Gygi, S. P., and D'Andrea, A. D. (2007). A UAF1-containing multisubunit protein complex regulates the Fanconi anemia pathway. Mol. Cell *28*, 786-797.

Coin, F., Oksenych, V., and Egly, J.-M. (2007). Distinct roles for the XPB/p52 and XPD/p44 subcomplexes of TFIIH in damaged DNA opening during nucleotide excision repair. Mol. Cell *26*, 245-256.

Collins, S. R., Miller, K. M., Maas, N. L., Roguev, A., Fillingham, J., Chu, C. S., Schuldiner, M., Gebbia, M., Recht, J., Shales, M., et al. (2007). Functional dissection of protein complexes involved in yeast chromosome biology using a genetic interaction map. Nature *446*, 806-810.

Collins, S. R., Schuldiner, M., Krogan, N. J., and Weissman, J. S. (2006). A strategy for extracting and analyzing large-scale quantitative epistatic interaction data. Genome Biol *7*, R63.

Couvé-Privat, S., Macé, G., Rosselli, F., and Saparbaev, M. K. (2007). Psoralen-induced DNA adducts are substrates for the base excision repair pathway in human cells. Nucleic Acids Res *35*, 5672-5682.

Cullen, J. K., Hussey, S. P., Walker, C., Prudden, J., Wee, B.-Y., Davé, A., Findlay, J. S., Savory, A. P., and Humphrey, T. C. (2007). Break-induced loss of heterozygosity in fission yeast: dual roles for homologous recombination in promoting translocations and preventing de novo telomere addition. Mol Cell Biol *27*, 7745-57.

Daley, J. M., Palmbos, P. L., Wu, D., and Wilson, T. E. (2005). Nonhomologous end joining in yeast. Annu. Rev. Genet *39*, 431-451.

De Silva, I. U., McHugh, P. J., Clingen, P. H., and Hartley, J. A. (2000). Defining the roles of nucleotide excision repair and recombination in the repair of DNA interstrand cross-links in mammalian cells. Mol. Cell. Biol *20*, 7980-7990.

De Silva, I. U., McHugh, P. J., Clingen, P. H., and Hartley, J. A. (2002). Defects in interstrand cross-link uncoupling do not account for the extreme sensitivity of ERCC1 and XPF cells to cisplatin. Nucleic Acids Res *30*, 3848-3856.

Dixon, S. J., Costanzo, M., Baryshnikova, A., Andrews, B., and Boone, C. (2009). Systematic mapping of genetic interaction networks. Annu. Rev. Genet *43*, 601-625.

Donahue, B. A., Fuchs, R. P., Reines, D., and Hanawalt, P. C. (1996). Effects of aminofluorene and acetylaminofluorene DNA adducts on transcriptional elongation by RNA polymerase II. J. Biol. Chem *271*, 10588-10594.

Dronkert, M. L., de Wit, J., Boeve, M., Vasconcelos, M. L., van Steeg, H., Tan, T. L., Hoeijmakers, J. H., and Kanaar, R. (2000). Disruption of mouse SNM1 causes increased sensitivity to the DNA interstrand cross-linking agent mitomycin C. Mol. Cell. Biol *20*, 4553-4561.

Du, L.-L., Nakamura, T. M., Moser, B. A., and Russell, P. (2003). Retention but not recruitment of Crb2 at double-strand breaks requires Rad1 and Rad3 complexes. Mol Cell Biol *23*, 6150-8.

Du, L.-L., Nakamura, T. M., and Russell, P. (2006). Histone modification-dependent and - independent pathways for recruitment of checkpoint protein Crb2 to double-strand breaks. Genes Dev *20*, 1583-96.

Edwards, R. J., Bentley, N. J., and Carr, A. M. (1999). A Rad3-Rad26 complex responds to DNA damage independently of other checkpoint proteins. Nat Cell Biol *1*, 393-8.

Enoch, T., Carr, A. M., and Nurse, P. (1992). Fission yeast genes involved in coupling mitosis to completion of DNA replication. Genes Dev *6*, 2035-2046.

Esashi, F., and Yanagida, M. (1999). Cdc2 phosphorylation of Crb2 is required for reestablishing cell cycle progression after the damage checkpoint. Mol. Cell *4*, 167-174.

Evans, E., Moggs, J. G., Hwang, J. R., Egly, J. M., and Wood, R. D. (1997). Mechanism of open complex and dual incision formation by human nucleotide excision repair factors. EMBO J *16*, 6559-6573.

Fekairi, S., Scaglione, S., Chahwan, C., Taylor, E. R., Tissier, A., Coulon, S., Dong, M.-Q., Ruse, C., Yates, J. R., Russell, P., et al. (2009). Human SLX4 is a Holliday junction resolvase subunit that binds multiple DNA repair/recombination endonucleases. Cell *138*, 78-89.

Fisher, A. E. O., Hochegger, H., Takeda, S., and Caldecott, K. W. (2007). Poly(ADP-ribose) polymerase 1 accelerates single-strand break repair in concert with poly(ADP-ribose) glycohydrolase. Mol. Cell. Biol *27*, 5597-5605.

Fisher, L. A., Bessho, M., and Bessho, T. (2008). Processing of a psoralen DNA interstrand cross-link by XPF-ERCC1 complex in vitro. J. Biol. Chem *283*, 1275-1281.

Fiumicino, S., Martinelli, S., Colussi, C., Aquilina, G., Leonetti, C., Crescenzi, M., and Bignami, M. (2000). Sensitivity to DNA cross-linking chemotherapeutic agents in mismatch repair-defective cells in vitro and in xenografts. Int. J. Cancer *85*, 590-596.

Fleck, O., Lehmann, E., Schär, P., and Kohli, J. (1999). Involvement of nucleotide-excision repair in msh2 pms1-independent mismatch repair. Nat. Genet *21*, 314-317.

Foster, P. L. (2006). Methods for determining spontaneous mutation rates. Meth. Enzymol *409*, 195-213.

Fousteri, M., Vermeulen, W., van Zeeland, A. A., and Mullenders, L. H. F. (2006). Cockayne syndrome A and B proteins differentially regulate recruitment of chromatin remodeling and repair factors to stalled RNA polymerase II in vivo. Mol. Cell *23*, 471-482.

Frampton, J., Irmisch, A., Green, C. M., Neiss, A., Trickey, M., Ulrich, H. D., Furuya, K., Watts, F. Z., Carr, A. M., and Lehmann, A. R. (2006). Postreplication repair and PCNA modification in Schizosaccharomyces pombe. Mol. Biol. Cell *17*, 2976-2985.

Frankenberg-Schwager, M., Kirchermeier, D., Greif, G., Baer, K., Becker, M., and Frankenberg, D. (2005). Cisplatin-mediated DNA double-strand breaks in replicating but not in quiescent cells of the yeast Saccharomyces cerevisiae. Toxicology *212*, 175-184.

Frosina, G., Fortini, P., Rossi, O., Carrozzino, F., Raspaglio, G., Cox, L. S., Lane, D. P., Abbondandolo, A., and Dogliotti, E. (1996). Two pathways for base excision repair in mammalian cells. J. Biol. Chem *271*, 9573-9578.

Gangloff, S., McDonald, J. P., Bendixen, C., Arthur, L., and Rothstein, R. (1994). The yeast type I topoisomerase Top3 interacts with Sgs1, a DNA helicase homolog: a potential eukaryotic reverse gyrase. Mol Cell Biol *14*, 8391-8.

van Gent, D. C., Hoeijmakers, J. H., and Kanaar, R. (2001). Chromosomal stability and the DNA double-stranded break connection. Nat Rev Genet *2*, 196-206.

Gravel, S., Chapman, J. R., Magill, C., and Jackson, S. P. (2008). DNA helicases Sgs1 and BLM promote DNA double-strand break resection. Genes Dev *22*, 2767-2772.

Greenwell, P. W., Kronmal, S. L., Porter, S. E., Gassenhuber, J., Obermaier, B., and Petes, T. D. (1995). TEL1, a gene involved in controlling telomere length in S. cerevisiae, is homologous to the human ataxia telangiectasia gene. Cell *82*, 823-829.

Greeson, N. T., Sengupta, R., Arida, A. R., Jenuwein, T., and Sanders, S. L. (2008). Di-methyl H4 lysine 20 targets the checkpoint protein CRB2 to sites of DNA damage. J Biol Chem.

Grossmann, K. F., Brown, J. C., and Moses, R. E. (1999). Cisplatin DNA cross-links do not inhibit S-phase and cause only a G2/M arrest in Saccharomyces cerevisiae. Mutat. Res *434*, 29-39.

Grossmann, K. F., Ward, A. M., Matkovic, M. E., Folias, A. E., and Moses, R. E. (2001). S. cerevisiae has three pathways for DNA interstrand crosslink repair. Mutat. Res *487*, 73-83.

Grossmann, K. F., Ward, A. M., and Moses, R. E. (2000). Saccharomyces cerevisiae lacking Snm1, Rev3 or Rad51 have a normal S-phase but arrest permanently in G2 after cisplatin treatment. Mutat. Res *461*, 1-13.

Gu, J., Lu, H., Tippin, B., Shimazaki, N., Goodman, M. F., and Lieber, M. R. (2007). XRCC4:DNA ligase IV can ligate incompatible DNA ends and can ligate across gaps. EMBO J *26*, 1010-1023.

Guo, C., Sonoda, E., Tang, T.-S., Parker, J. L., Bielen, A. B., Takeda, S., Ulrich, H. D., and Friedberg, E. C. (2006). REV1 protein interacts with PCNA: significance of the REV1 BRCT domain in vitro and in vivo. Mol. Cell *23*, 265-271.

Haber, J. E. (2000). Partners and pathwaysrepairing a double-strand break. Trends Genet *16*, 259-64.

Hanada, K., Budzowska, M., Modesti, M., Maas, A., Wyman, C., Essers, J., and Kanaar, R. (2006). The structure-specific endonuclease Mus81-Eme1 promotes conversion of interstrand DNA crosslinks into double-strands breaks. EMBO J *25*, 4921-4932.

Hanlon Newell, A. E., Hemphill, A., Akkari, Y. M. N., Hejna, J., Moses, R. E., and Olson, S. B. (2008). Loss of homologous recombination or non-homologous end-joining leads to radial formation following DNA interstrand crosslink damage. Cytogenet. Genome Res *121*, 174-180.

Hartsuiker, E., Vaessen, E., Carr, A. M., and Kohli, J. (2001). Fission yeast Rad50 stimulates sister chromatid recombination and links cohesion with repair. EMBO J *20*, 6660-6671.

Hartsuiker, E., Neale, M. J., and Carr, A. M. (2009). Distinct requirements for the Rad32(Mre11) nuclease and Ctp1(CtIP) in the removal of covalently bound topoisomerase I and II from DNA. Mol Cell *33*, 117-23.

Hazrati, A., Ramis-Castelltort, M., Sarkar, S., Barber, L. J., Schofield, C. J., Hartley, J. A., and McHugh, P. J. (2008). Human SNM1A suppresses the DNA repair defects of yeast pso2 mutants. DNA Repair (Amst.) *7*, 230-238.

Hemphill, A. W., Bruun, D., Thrun, L., Akkari, Y., Torimaru, Y., Hejna, K., Jakobs, P. M., Hejna, J., Jones, S., Olson, S. B., et al. (2008). Mammalian SNM1 is required for genome stability. Mol. Genet. Metab *94*, 38-45.

Henriques, J. A., Brozmanova, J., and Brendel, M. (1997). Role of PSO genes in the repair of photoinduced interstrand cross-links and photooxidative damage in the DNA of the yeast Saccharomyces cerevisiae. J. Photochem. Photobiol. B, Biol *39*, 185-196.

Henriques, J. A., and Moustacchi, E. (1980). Isolation and characterization of pso mutants sensitive to photo-addition of psoralen derivatives in Saccharomyces cerevisiae. Genetics *95*, 273-288.

Hentges, P., Van Driessche, B., Tafforeau, L., Vandenhaute, J., and Carr, A. M. (2005). Three novel antibiotic marker cassettes for gene disruption and marker switching in Schizosaccharomyces pombe. Yeast *22*, 1013-1019.

Herrmann, G., Lindahl, T., and Schär, P. (1998). Saccharomyces cerevisiae LIF1: a function involved in DNA double-strand break repair related to mammalian XRCC4. EMBO J *17*, 4188-4198.

Hess, M. T., Gunz, D., Luneva, N., Geacintov, N. E., and Naegeli, H. (1997). Base pair conformation-dependent excision of benzo[a]pyrene diol epoxide-guanine adducts by human nucleotide excision repair enzymes. Mol. Cell. Biol *17*, 7069-7076.

Hinz, J. M. (2010). Role of homologous recombination in DNA interstrand crosslink repair. Environ. Mol. Mutagen *51*, 582-603.

Ho, T. V., and Schärer, O. D. (2010). Translesion DNA synthesis polymerases in DNA interstrand crosslink repair. Environ. Mol. Mutagen *51*, 552-566.

Hoege, C., Pfander, B., Moldovan, G.-L., Pyrowolakis, G., and Jentsch, S. (2002). RAD6-dependent DNA repair is linked to modification of PCNA by ubiquitin and SUMO. Nature *419*, 135-141.

Hope, J. C., Mense, S. M., Jalakas, M., Mitsumoto, J., and Freyer, G. A. (2006). Rqh1 blocks recombination between sister chromatids during double strand break repair, independent of its helicase activity. Proc. Natl. Acad. Sci. U.S.A *103*, 5875-5880.

Howlett, N. G., Taniguchi, T., Olson, S., Cox, B., Waisfisz, Q., De Die-Smulders, C., Persky, N., Grompe, M., Joenje, H., Pals, G., et al. (2002). Biallelic inactivation of BRCA2 in Fanconi anemia. Science *297*, 606-609.

Huertas, P., Cortés-Ledesma, F., Sartori, A. A., Aguilera, A., and Jackson, S. P. (2008). CDK targets Sae2 to control DNA-end resection and homologous recombination. Nature *455*, 689-92.

Iacovoni, J. S., Russell, P., and Gaits, F. (1999). A new inducible protein expression system in fission yeast based on the glucose-repressed inv1 promoter. Gene *232*, 53-58.

Ip, S. C. Y., Rass, U., Blanco, M. G., Flynn, H. R., Skehel, J. M., and West, S. C. (2008). Identification of Holliday junction resolvases from humans and yeast. Nature *456*, 357-361.

Ira, G., Malkova, A., Liberi, G., Foiani, M., and Haber, J. E. (2003). Srs2 and Sgs1-Top3 suppress crossovers during double-strand break repair in yeast. Cell *115*, 401-11.

Ira, G., Pellicioli, A., Balijja, A., Wang, X., Fiorani, S., Carotenuto, W., Liberi, G., Bressan, D., Wan, L., Hollingsworth, N. M., et al. (2004). DNA end resection, homologous recombination and DNA damage checkpoint activation require CDK1. Nature *431*, 1011-1017.

Ivanov, E. L., Sugawara, N., White, C. I., Fabre, F., and Haber, J. E. (1994). Mutations in XRS2 and RAD50 delay but do not prevent mating-type switching in Saccharomyces cerevisiae. Mol. Cell. Biol *14*, 3414-3425.

Iyer, L. M., Babu, M. M., and Aravind, L. (2006). The HIRAN domain and recruitment of chromatin remodeling and repair activities to damaged DNA. Cell Cycle *5*, 775-782.

Iyer, R. R., Pohlhaus, T. J., Chen, S., Hura, G. L., Dzantiev, L., Beese, L. S., and Modrich, P. (2008). The MutSalpha-proliferating cell nuclear antigen interaction in human DNA mismatch repair. J. Biol. Chem *283*, 13310-13319.

de Jager, M., van Noort, J., van Gent, D. C., Dekker, C., Kanaar, R., and Wyman, C. (2001). Human Rad50/Mre11 is a flexible complex that can tether DNA ends. Mol. Cell *8*, 1129-1135.

Jiricny, J. (2006). The multifaceted mismatch-repair system. Nat. Rev. Mol. Cell Biol *7*, 335-346.

Johnson, F. B., Lombard, D. B., Neff, N. F., Mastrangelo, M. A., Dewolf, W., Ellis, N. A., Marciniak, R. A., Yin, Y., Jaenisch, R., and Guarente, L. (2000). Association of the Bloom syndrome protein with topoisomerase IIIalpha in somatic and meiotic cells. Cancer Res *60*, 1162-7.

Johnson, S. W., Ferry, K. V., and Hamilton, T. C. (1998). Recent insights into platinum drug resistance in cancer. Drug Resist. Updat *1*, 243-254.

Kannouche, P. L., Wing, J., and Lehmann, A. R. (2004). Interaction of human DNA polymerase eta with monoubiquitinated PCNA: a possible mechanism for the polymerase switch in response to DNA damage. Mol. Cell *14*, 491-500.

Kaye, J., Smith, C. A., and Hanawalt, P. C. (1980). DNA repair in human cells containing photoadducts of 8-methoxypsoralen or angelicin. Cancer Res *40*, 696-702.

Kee, Y., and D'Andrea, A. D. (2010). Expanded roles of the Fanconi anemia pathway in preserving genomic stability. Genes Dev *24*, 1680-1694.

Khasanov, F. K., Savchenko, G. V., Bashkirova, E. V., Korolev, V. G., Heyer, W. D., and Bashkirov, V. I. (1999). A new recombinational DNA repair gene from Schizosaccharomyces pombe with homology to Escherichia coli RecA. Genetics *152*, 1557-1572.

Kim, J. M., Kee, Y., Gurtan, A., and D'Andrea, A. D. (2008). Cell cycle-dependent chromatin loading of the Fanconi anemia core complex by FANCM/FAAP24. Blood *111*, 5215-5222.

Knipscheer, P., Räschle, M., Smogorzewska, A., Enoiu, M., Ho, T. V., Schärer, O. D., Elledge, S. J., and Walter, J. C. (2009). The Fanconi anemia pathway promotes replication-dependent DNA interstrand cross-link repair. Science *326*, 1698-1701.

Kratz, K., Schöpf, B., Kaden, S., Sendoel, A., Eberhard, R., Lademann, C., Cannavó, E., Sartori, A. A., Hengartner, M. O., and Jiricny, J. (2010). Deficiency of FANCD2-associated nuclease KIAA1018/FAN1 sensitizes cells to interstrand crosslinking agents. Cell *142*, 77-88.

Krogh, B. O., and Symington, L. S. (2004). Recombination proteins in yeast. Annu Rev Genet *38*, 233-71.

Kubota, Y., Nash, R. A., Klungland, A., Schär, P., Barnes, D. E., and Lindahl, T. (1996). Reconstitution of DNA base excision-repair with purified human proteins: interaction between DNA polymerase beta and the XRCC1 protein. EMBO J *15*, 6662-6670.

Kunkel, T. A., and Erie, D. A. (2005). DNA mismatch repair. Annu. Rev. Biochem *74*, 681-710.

Kunz, C., Saito, Y., and Schär, P. (2009). Mismatched repair: variations on a theme. Cell Mol Life Sci.

Kuraoka, I., Kobertz, W. R., Ariza, R. R., Biggerstaff, M., Essigmann, J. M., and Wood, R. D. (2000). Repair of an interstrand DNA cross-link initiated by ERCC1-XPF repair/recombination nuclease. J. Biol. Chem *275*, 26632-26636.

Lam, A. F., Krogh, B. O., and Symington, L. S. (2008). Unique and overlapping functions of the Exo1, Mre11 and Pso2 nucleases in DNA repair. DNA Repair (Amst.) *7*, 655-662.

Lamarche, B. J., Orazio, N. I., and Weitzman, M. D. (2010). The MRN complex in double-strand break repair and telomere maintenance. FEBS Lett *584*, 3682-3695.

Lambert, S., Froget, B., and Carr, A. M. (2007). Arrested replication fork processing: interplay between checkpoints and recombination. DNA Repair (Amst) *6*, 1042-61.

Lambert, S., Mason, S. J., Barber, L. J., Hartley, J. A., Pearce, J. A., Carr, A. M., and McHugh, P. J. (2003). Schizosaccharomyces pombe Checkpoint Response to DNA Interstrand Cross-Links. Mol. Cell. Biol. *23*, 4728-4737.

Lau, P. J., and Kolodner, R. D. (2003). Transfer of the MSH2.MSH6 complex from proliferating cell nuclear antigen to mispaired bases in DNA. J. Biol. Chem *278*, 14-17.

Laursen, L. V., Ampatzidou, E., Andersen, A. H., and Murray, J. M. (2003). Role for the fission yeast RecQ helicase in DNA repair in G2. Mol Cell Biol *23*, 3692-705.

Legerski, R. J. (2010). Repair of DNA interstrand cross-links during S phase of the mammalian cell cycle. Environ. Mol. Mutagen *51*, 540-551.

Lehmann, A. R. (2003). DNA repair-deficient diseases, xeroderma pigmentosum, Cockayne syndrome and trichothiodystrophy. Biochimie *85*, 1101-1111.

Lehmann, A. R., Niimi, A., Ogi, T., Brown, S., Sabbioneda, S., Wing, J. F., Kannouche, P. L., and Green, C. M. (2007). Translesion synthesis: Y-family polymerases and the polymerase switch. DNA Repair (Amst.) *6*, 891-899.

Lehoczký, P., McHugh, P. J., and Chovanec, M. (2007). DNA interstrand cross-link repair in Saccharomyces cerevisiae. FEMS Microbiol. Rev *31*, 109-133.

Li, X., Hejna, J., and Moses, R. E. (2005). The yeast Snm1 protein is a DNA 5'-exonuclease. DNA Repair (Amst.) *4*, 163-170.

Li, X., and Moses, R. E. (2003). The beta-lactamase motif in Snm1 is required for repair of DNA double-strand breaks caused by interstrand crosslinks in S. cerevisiae. DNA Repair (Amst.) *2*, 121-129.

Liberi, G., Maffioletti, G., Lucca, C., Chiolo, I., Baryshnikova, A., Cotta-Ramusino, C., Lopes, M., Pellicioli, A., Haber, J. E., and Foiani, M. (2005). Rad51-dependent DNA structures accumulate at damaged replication forks in sgs1 mutants defective in the yeast ortholog of BLM RecQ helicase. Genes Dev *19*, 339-50.

Lieber, M. R. (2010). The mechanism of double-strand DNA break repair by the nonhomologous DNA end-joining pathway. Annu. Rev. Biochem *79*, 181-211.

Limbo, O., Chahwan, C., Yamada, Y., de Bruin, R. A. M., Wittenberg, C., and Russell, P. (2007). Ctp1 is a cell-cycle-regulated protein that functions with Mre11 complex to control double-strand break repair by homologous recombination. Mol. Cell *28*, 134-146.

Lindsay, H. D., Griffiths, D. J., Edwards, R. J., Christensen, P. U., Murray, J. M., Osman, F., Walworth, N., and Carr, A. M. (1998). S-phase-specific activation of Cds1 kinase defines a subpathway of the checkpoint response in Schizosaccharomyces pombe. Genes Dev *12*, 382-95.

Lipkin, S. M., Moens, P. B., Wang, V., Lenzi, M., Shanmugarajah, D., Gilgeous, A., Thomas, J., Cheng, J., Touchman, J. W., Green, E. D., et al. (2002). Meiotic arrest and aneuploidy in MLH3-deficient mice. Nat. Genet *31*, 385-390.

Lisby, M., Barlow, J. H., Burgess, R. C., and Rothstein, R. (2004). Choreography of the DNA damage response: spatiotemporal relationships among checkpoint and repair proteins. Cell *118*, 699-713.

Liu, T., Ghosal, G., Yuan, J., Chen, J., and Huang, J. (2010). FAN1 acts with FANCI-FANCD2 to promote DNA interstrand cross-link repair. Science *329*, 693-696.

Llorente, B., and Symington, L. S. (2004). The Mre11 nuclease is not required for 5' to 3' resection at multiple HO-induced double-strand breaks. Mol. Cell. Biol *24*, 9682-9694.

Love, J. D., Nguyen, H. T., Or, A., Attri, A. K., and Minton, K. W. (1986). UV-induced interstrand cross-linking of d(GT)n.d(CA)n is facilitated by a structural transition. J. Biol. Chem *261*, 10051-10057.

Ma, Y., Pannicke, U., Schwarz, K., and Lieber, M. R. (2002). Hairpin opening and overhang processing by an Artemis/DNA-dependent protein kinase complex in nonhomologous end joining and V(D)J recombination. Cell *108*, 781-794.

MacDougall, C. A., Byun, T. S., Van, C., Yee, M.-ching, and Cimprich, K. A. (2007). The structural determinants of checkpoint activation. Genes Dev *21*, 898-903.

MacKay, C., Déclais, A.-C., Lundin, C., Agostinho, A., Deans, A. J., MacArtney, T. J., Hofmann, K., Gartner, A., West, S. C., Helleday, T., et al. (2010). Identification of KIAA1018/FAN1, a DNA repair nuclease recruited to DNA damage by monoubiquitinated FANCD2. Cell *142*, 65-76.

Macé-Aimé, G., Couvé, S., Khassenov, B., Rosselli, F., and Saparbaev, M. K. (2010). The Fanconi anemia pathway promotes DNA glycosylase-dependent excision of interstrand DNA crosslinks. Environ. Mol. Mutagen., NA-NA.

Maillard, O., Camenisch, U., Clement, F. C., Blagoev, K. B., and Naegeli, H. (2007). DNA repair triggered by sensors of helical dynamics. Trends Biochem. Sci *32*, 494-499.

Manderfeld, M. M., Schafer, H. W., Davidson, P. M., and Zottola, E. A. (1997). Isolation and identification of antimicrobial furocoumarins from parsley. J. Food Prot *60*, 72-77.

Mansour, A. A., Tornier, C., Lehmann, E., Darmon, M., and Fleck, O. (2001). Control of GT repeat stability in Schizosaccharomyces pombe by mismatch repair factors. Genetics *158*, 77-85.

Marti, T. M., Kunz, C., and Fleck, O. (2002). DNA mismatch repair and mutation avoidance pathways. J Cell Physiol *191*, 28-41.

Marti, T. M., Mansour, A. A., Lehmann, E., and Fleck, O. (2003). Different frameshift mutation spectra in non-repetitive DNA of MutSalpha- and MutLalpha-deficient fission yeast cells. DNA Repair (Amst.) *2*, 571-580.

Matsuoka, S., Ballif, B. A., Smogorzewska, A., McDonald, E. R., Hurov, K. E., Luo, J., Bakalarski, C. E., Zhao, Z., Solimini, N., Lerenthal, Y., et al. (2007). ATM and ATR substrate analysis reveals extensive protein networks responsive to DNA damage. Science *316*, 1160-1166.

Maundrell, K. (1990). nmt1 of fission yeast. A highly transcribed gene completely repressed by thiamine. J. Biol. Chem *265*, 10857-10864.

McCabe, K. M., Olson, S. B., and Moses, R. E. (2009). DNA interstrand crosslink repair in mammalian cells. J. Cell. Physiol.

McCulloch, S. D., Kokoska, R. J., Chilkova, O., Welch, C. M., Johansson, E., Burgers, P. M. J., and Kunkel, T. A. (2004). Enzymatic switching for efficient and accurate translesion DNA replication. Nucleic Acids Res *32*, 4665-4675.

McCulloch, S. D., and Kunkel, T. A. (2008). The fidelity of DNA synthesis by eukaryotic replicative and translesion synthesis polymerases. Cell Res *18*, 148-161.

McHugh, P. J., Gill, R. D., Waters, R., and Hartley, J. A. (1999). Excision repair of nitrogen mustard-DNA adducts in Saccharomyces cerevisiae. Nucleic Acids Res *27*, 3259-3266.

McHugh, P. J., Sones, W. R., and Hartley, J. A. (2000). Repair of intermediate structures produced at DNA interstrand cross-links in Saccharomyces cerevisiae. Mol. Cell. Biol *20*, 3425-3433.

McHugh, P. J., Spanswick, V. J., and Hartley, J. A. (2001). Repair of DNA interstrand crosslinks: molecular mechanisms and clinical relevance. Lancet Oncol *2*, 483-490.

McHugh, P. J., and Sarkar, S. (2006). DNA interstrand cross-link repair in the cell cycle: a critical role for polymerase zeta in G1 phase. Cell Cycle *5*, 1044-1047.

McVey, M., Larocque, J. R., Adams, M. D., and Sekelsky, J. J. (2004). Formation of deletions during double-strand break repair in Drosophila DmBlm mutants occurs after strand invasion. Proc Natl Acad Sci U S A *101*, 15694-9.

Mellon, I., and Champe, G. N. (1996). Products of DNA mismatch repair genes mutS and mutL are required for transcription-coupled nucleotide-excision repair of the lactose operon in Escherichia coli. Proc. Natl. Acad. Sci. U.S.A *93*, 1292-1297.

Mellon, I. (2005). Transcription-coupled repair: a complex affair. Mutat. Res *577*, 155-161.

Meniel, V., Magaña-Schwencke, N., and Averbeck, D. (1995). Preferential repair in Saccharomyces cerevisiae rad mutants after induction of interstrand cross-links by 8-methoxypsoralen plus UVA. Mutagenesis *10*, 543-548.

Mimitou, E. P., and Symington, L. S. (online). Sae2, Exo1 and Sgs1 collaborate in DNA double-strand break processing. Nature.

Mochida, S., Esashi, F., Aono, N., Tamai, K., O'Connell, M. J., and Yanagida, M. (2004). Regulation of checkpoint kinases through dynamic interaction with Crb2. EMBO J *23*, 418-428.

Moggs, J. G., Szymkowski, D. E., Yamada, M., Karran, P., and Wood, R. D. (1997). Differential human nucleotide excision repair of paired and mispaired cisplatin-DNA adducts. Nucleic Acids Res *25*, 480-491.

Moore, J. K., and Haber, J. E. (1996). Cell cycle and genetic requirements of two pathways of nonhomologous end-joining repair of double-strand breaks in Saccharomyces cerevisiae. Mol. Cell. Biol *16*, 2164-2173.

Moreau, S., Morgan, E. A., and Symington, L. S. (2001). Overlapping functions of the Saccharomyces cerevisiae Mre11, Exo1 and Rad27 nucleases in DNA metabolism. Genetics *159*, 1423-1433.

Moser, J., Kool, H., Giakzidis, I., Caldecott, K., Mullenders, L. H. F., and Fousteri, M. I. (2007). Sealing of chromosomal DNA nicks during nucleotide excision repair requires XRCC1 and DNA ligase III alpha in a cell-cycle-specific manner. Mol. Cell *27*, 311-323.

Mu, D., Bessho, T., Nechev, L. V., Chen, D. J., Harris, T. M., Hearst, J. E., and Sancar, A. (2000). DNA Interstrand Cross-Links Induce Futile Repair Synthesis in Mammalian Cell Extracts. Mol. Cell. Biol. *20*, 2446-2454.

Muñoz, I. M., Hain, K., Déclais, A.-C., Gardiner, M., Toh, G. W., Sanchez-Pulido, L., Heuckmann, J. M., Toth, R., Macartney, T., Eppink, B., et al. (2009). Coordination of structure-specific nucleases by human SLX4/BTBD12 is required for DNA repair. Mol. Cell *35*, 116-127.

Mueller, J. P., and Smerdon, M. J. (1995). Repair of plasmid and genomic DNA in a rad7 delta mutant of yeast. Nucleic Acids Res *23*, 3457-3464.

Mullen, J. R., Nallaseth, F. S., Lan, Y. Q., Slagle, C. E., and Brill, S. J. (2005). Yeast Rmi1/Nce4 controls genome stability as a subunit of the Sgs1-Top3 complex. Mol Cell Biol *25*, 4476-87.

Murakami, H., and Okayama, H. (1995). A kinase from fission yeast responsible for blocking mitosis in S phase. Nature *374*, 817-819.

Muris, D. F., Vreeken, K., Carr, A. M., Murray, J. M., Smit, C., Lohman, P. H., and Pastink, A. (1996). Isolation of the Schizosaccharomyces pombe RAD54 homologue, rhp54+, a gene involved in the repair of radiation damage and replication fidelity. J. Cell. Sci *109 ( Pt 1)*, 73-81.

Murray, J. M., Lindsay, H. D., Munday, C. A., and Carr, A. M. (1997). Role of Schizosaccharomyces pombe RecQ homolog, recombination, and checkpoint genes in UV damage tolerance. Mol Cell Biol *17*, 6868-75.

Nagase, T., Ishikawa, K., Suyama, M., Kikuno, R., Hirosawa, M., Miyajima, N., Tanaka, A., Kotani, H., Nomura, N., and Ohara, O. (1999). Prediction of the coding sequences of unidentified human genes. XIII. The complete sequences of 100 new cDNA clones from brain which code for large proteins in vitro. DNA Res *6*, 63-70.

Nakamura, T. M., Du, L.-L., Redon, C., and Russell, P. (2004). Histone H2A phosphorylation controls Crb2 recruitment at DNA breaks, maintains checkpoint arrest, and influences DNA repair in fission yeast. Mol Cell Biol *24*, 6215-30.

Nakamura, T. M., Moser, B. A., Du, L.-L., and Russell, P. (2005). Cooperative control of Crb2 by ATM family and Cdc2 kinases is essential for the DNA damage checkpoint in fission yeast. Mol Cell Biol *25*, 10721-30.

Namsaraev, E., and Berg, P. (1997). Characterization of strand exchange activity of yeast Rad51 protein. Mol. Cell. Biol *17*, 5359-5368.

Nelson, J. R., Lawrence, C. W., and Hinkle, D. C. (1996). Thymine-thymine dimer bypass by yeast DNA polymerase zeta. Science *272*, 1646-1649.

Nichols, A. F., and Sancar, A. (1992). Purification of PCNA as a nucleotide excision repair protein. Nucleic Acids Res *20*, 2441-2446.

Niedernhofer, L. J., Daniels, J. S., Rouzer, C. A., Greene, R. E., and Marnett, L. J. (2003). Malondialdehyde, a product of lipid peroxidation, is mutagenic in human cells. J. Biol. Chem *278*, 31426-31433.

Niedernhofer, L. J., Garinis, G. A., Raams, A., Lalai, A. S., Robinson, A. R., Appeldoorn, E., Odijk, H., Oostendorp, R., Ahmad, A., van Leeuwen, W., et al. (2006). A new progeroid syndrome reveals that genotoxic stress suppresses the somatotroph axis. Nature *444*, 1038-1043.

Niedernhofer, L. J., Odijk, H., Budzowska, M., van Drunen, E., Maas, A., Theil, A. F., de Wit, J., Jaspers, N. G. J., Beverloo, H. B., Hoeijmakers, J. H. J., et al. (2004). The structure-specific endonuclease Ercc1-Xpf is required to resolve DNA interstrand cross-link-induced double-strand breaks. Mol. Cell. Biol *24*, 5776-5787.

Nijman, S. M. B., Huang, T. T., Dirac, A. M. G., Brummelkamp, T. R., Kerkhoven, R. M., D'Andrea, A. D., and Bernards, R. (2005). The deubiquitinating enzyme USP1 regulates the Fanconi anemia pathway. Mol. Cell *17*, 331-339.

Nojima, K., Hochegger, H., Saberi, A., Fukushima, T., Kikuchi, K., Yoshimura, M., Orelli, B. J., Bishop, D. K., Hirano, S., Ohzeki, M., et al. (2005). Multiple repair pathways mediate tolerance to chemotherapeutic cross-linking agents in vertebrate cells. Cancer Res *65*, 11704-11711.

Nouspikel, T. (2009). DNA repair in mammalian cells : Nucleotide excision repair: variations on versatility. Cell. Mol. Life Sci *66*, 994-1009.

O'Connor, T. R., and Laval, J. (1989). Physical association of the 2,6-diamino-4-hydroxy-5N-formamidopyrimidine-DNA glycosylase of Escherichia coli and an activity nicking DNA at apurinic/apyrimidinic sites. Proc. Natl. Acad. Sci. U.S.A *86*, 5222-5226.

O'Donovan, A., Davies, A. A., Moggs, J. G., West, S. C., and Wood, R. D. (1994). XPG endonuclease makes the 3' incision in human DNA nucleotide excision repair. Nature *371*, 432-435.

Oestergaard, V. H., Langevin, F., Kuiken, H. J., Pace, P., Niedzwiedz, W., Simpson, L. J., Ohzeki, M., Takata, M., Sale, J. E., and Patel, K. J. (2007). Deubiquitination of FANCD2 is required for DNA crosslink repair. Mol. Cell *28*, 798-809.

Oh, S. D., Lao, J. P., Hwang, P. Y.-H., Taylor, A. F., Smith, G. R., and Hunter, N. (2007). BLM ortholog, Sgs1, prevents aberrant crossing-over by suppressing formation of multichromatid joint molecules. Cell *130*, 259-72.

Osman, F., Dixon, J., Doe, C. L., and Whitby, M. C. (2003). Generating crossovers by resolution of nicked Holliday junctions: a role for Mus81-Eme1 in meiosis. Mol. Cell *12*, 761-774.

Paques, F., and Haber, J. E. (1999). Multiple pathways of recombination induced by double-strand breaks in Saccharomyces cerevisiae. Microbiol Mol Biol Rev *63*, 349-404.

Pan, X., Ye, P., Yuan, D. S., Wang, X., Bader, J. S., and Boeke, J. D. (2006). A DNA integrity network in the yeast Saccharomyces cerevisiae. Cell *124*, 1069-1081.

Pan, X., Yuan, D. S., Xiang, D., Wang, X., Sookhai-Mahadeo, S., Bader, J. S., Hieter, P., Spencer, F., and Boeke, J. D. (2004). A robust toolkit for functional profiling of the yeast genome. Mol. Cell *16*, 487-496.

Pani, E., Stojic, L., El-Shemerly, M., Jiricny, J., and Ferrari, S. (2007). Mismatch repair status and the response of human cells to cisplatin. Cell Cycle *6*, 1796-1802.

Papouli, E., Cejka, P., and Jiricny, J. (2004). Dependence of the cytotoxicity of DNA-damaging agents on the mismatch repair status of human cells. Cancer Res *64*, 3391-3394.

Parrilla-Castellar, E. R., Arlander, S. J. H., and Karnitz, L. (2004). Dial 9-1-1 for DNA damage: the Rad9-Hus1-Rad1 (9-1-1) clamp complex. DNA Repair (Amst.) *3*, 1009-1014.

Petukhova, G., Van Komen, S., Vergano, S., Klein, H., and Sung, P. (1999). Yeast Rad54 promotes Rad51-dependent homologous DNA pairing via ATP hydrolysis-driven change in DNA double helix conformation. J. Biol. Chem *274*, 29453-29462.

Picard, D. (2000). Posttranslational regulation of proteins by fusions to steroid-binding domains. Meth. Enzymol *327*, 385-401.

Picard, D. (1994). Regulation of protein function through expression of chimaeric proteins. Curr. Opin. Biotechnol *5*, 511-515.

Picard, D. (1993). Steroid-binding domains for regulating the functions of heterologous proteins in cis. Trends Cell Biol *3*, 278-280.

Pierce, A. J., Stark, J. M., Araujo, F. D., Moynahan, M. E., Berwick, M., and Jasin, M. (2001). Double-strand breaks and tumorigenesis. Trends Cell Biol *11*, S52-9.

Popanda, O., and Thielmann, H. W. (1992). The function of DNA polymerases in DNA repair synthesis of ultraviolet-irradiated human fibroblasts. Biochim. Biophys. Acta *1129*, 155-160.

Prakash, S., and Prakash, L. (2000). Nucleotide excision repair in yeast. Mutat. Res *451*, 13-24.

Prudden, J., Evans, J. S., Hussey, S. P., Deans, B., O'Neill, P., Thacker, J., and Humphrey, T. (2003a). Pathway utilization in response to a site-specific DNA double-strand break in fission yeast. EMBO J *22*, 1419-1430.

Prudden, J., Evans, J. S., Hussey, S. P., Deans, B., O'Neill, P., Thacker, J., and Humphrey, T. (2003b). Pathway utilization in response to a site-specific DNA double-strand break in fission yeast. EMBO J *22*, 1419-30.

Pursell, Z. F., Isoz, I., Lundström, E.-B., Johansson, E., and Kunkel, T. A. (2007). Regulation of B family DNA polymerase fidelity by a conserved active site residue: characterization of M644W, M644L and M644F mutants of yeast DNA polymerase epsilon. Nucleic Acids Res *35*, 3076-3086.

Qiu, J., Guan, M. X., Bailis, A. M., and Shen, B. (1998). Saccharomyces cerevisiae exonuclease-1 plays a role in UV resistance that is distinct from nucleotide excision repair. Nucleic Acids Res *26*, 3077-3083.

Räschle, M., Marra, G., Nyström-Lahti, M., Schär, P., and Jiricny, J. (1999). Identification of hMutLbeta, a heterodimer of hMLH1 and hPMS1. J. Biol. Chem *274*, 32368-32375.

Räschle, M., Knipscheer, P., Knipsheer, P., Enoiu, M., Angelov, T., Sun, J., Griffith, J. D., Ellenberger, T. E., Schärer, O. D., and Walter, J. C. (2008). Mechanism of replication-coupled DNA interstrand crosslink repair. Cell *134*, 969-980.

Rahn, J. J., Adair, G. M., and Nairn, R. S. (2010). Multiple roles of ERCC1-XPF in mammalian interstrand crosslink repair. Environ. Mol. Mutagen *51*, 567-581.

Raji, H., and Hartsuiker, E. (2006). Double-strand break repair and homologous recombination in Schizosaccharomyces pombe. Yeast *23*, 963-976.

Raynard, S., Bussen, W., and Sung, P. (2006). A double Holliday junction dissolvasome comprising BLM, topoisomerase IIIalpha, and BLAP75. J Biol Chem *281*, 13861-4.

Richie, C. T., Peterson, C., Lu, T., Hittelman, W. N., Carpenter, P. B., and Legerski, R. J. (2002). hSnm1 colocalizes and physically associates with 53BP1 before and after DNA damage. Mol. Cell. Biol *22*, 8635-8647.

Roberts, J. D., and Kunkel, T. A. (1988). Fidelity of a human cell DNA replication complex. Proc. Natl. Acad. Sci. U.S.A *85*, 7064-7068.

Robertson, A. B., Klungland, A., Rognes, T., and Leiros, I. (2009). DNA repair in mammalian cells: Base excision repair: the long and short of it. Cell. Mol. Life Sci *66*, 981-993.

Robson, C. N., and Hickson, I. D. (1991). Isolation of cDNA clones encoding a human apurinic/apyrimidinic endonuclease that corrects DNA repair and mutagenesis defects in E. coli xth (exonuclease III) mutants. Nucleic Acids Res *19*, 5519-5523.

Roguev, A., Wiren, M., Weissman, J. S., and Krogan, N. J. (2007). High-throughput genetic interaction mapping in the fission yeast Schizosaccharomyces pombe. Nat. Methods *4*, 861-866.

Rosche, W. A., and Foster, P. L. (2000). Determining mutation rates in bacterial populations. Methods *20*, 4-17.

Roth, F. P., Lipshitz, H. D., and Andrews, B. J. (2009). Q&A: epistasis. J. Biol *8*, 35.

Rowley, R., Subramani, S., and Young, P. G. (1992). Checkpoint controls in Schizosaccharomyces pombe: rad1. EMBO J *11*, 1335-1342.

Rudolph, C., Fleck, O., and Kohli, J. (1998). Schizosaccharomyces pombe exo1 is involved in the same mismatch repair pathway as msh2 and pms1. Curr. Genet *34*, 343-350.

Rudolph, C., Kunz, C., Parisi, S., Lehmann, E., Hartsuiker, E., Fartmann, B., Kramer, W., Kohli, J., and Fleck, O. (1999). The msh2 gene of *Schizosaccharomyces pombe* is involved in mismatch repair, mating-type switching, and meiotic chromosome organization. Mol. Cell. Biol *19*, 241-250.

Ruhland, A., and Brendel, M. (1979). Mutagenesis by cytostatic alkylating agents in yeast strains of differing repair capacities. Genetics *92*, 83-97.

Ruhland, A., Kircher, M., Wilborn, F., and Brendel, M. (1981). A yeast mutant specifically sensitive to bifunctional alkylation. Mutat. Res *91*, 457-462.

Saka, Y., Esashi, F., Matsusaka, T., Mochida, S., and Yanagida, M. (1997). Damage and replication checkpoint control in fission yeast is ensured by interactions of Crb2, a protein with BRCT motif, with Cut5 and Chk1. Genes Dev *11*, 3387-3400.

Santocanale, C., and Diffley, J. F. (1998). A Mec1- and Rad53-dependent checkpoint controls late-firing origins of DNA replication. Nature *395*, 615-618.

Sarkar, S., Davies, A. A., Ulrich, H. D., and McHugh, P. J. (2006). DNA interstrand crosslink repair during G1 involves nucleotide excision repair and DNA polymerase zeta. EMBO J *25*, 1285-1294.

Sartori, A. A., Lukas, C., Coates, J., Mistrik, M., Fu, S., Bartek, J., Baer, R., Lukas, J., and Jackson, S. P. (2007). Human CtIP promotes DNA end resection. Nature *450*, 509-514.

Schär, P., Baur, M., Schneider, C., and Kohli, J. (1997). Mismatch repair in Schizosaccharomyces pombe requires the mutL homologous gene pms1: molecular cloning and functional analysis. Genetics *146*, 1275-1286.

Schär, P., and Kohli, J. (1993). Marker effects of G to C transversions on intragenic recombination and mismatch repair in Schizosaccharomyces pombe. Genetics *133*, 825-835.

Schär, P., Munz, P., and Kohli, J. (1993). Meiotic mismatch repair quantified on the basis of segregation patterns in Schizosaccharomyces pombe. Genetics *133*, 815-824.

Schuldiner, M., Collins, S. R., Weissman, J. S., and Krogan, N. J. (2006). Quantitative genetic analysis in Saccharomyces cerevisiae using epistatic miniarray profiles (E-MAPs) and its application to chromatin functions. Methods *40*, 344-352.

Schuldiner, M., Collins, S. R., Thompson, N. J., Denic, V., Bhamidipati, A., Punna, T., Ihmels, J., Andrews, B., Boone, C., Greenblatt, J. F., et al. (2005). Exploration of the function and organization of the yeast early secretory pathway through an epistatic miniarray profile. Cell *123*, 507-519.

Shen, X., Do, H., Li, Y., Chung, W.-H., Tomasz, M., de Winter, J. P., Xia, B., Elledge, S. J., Wang, W., and Li, L. (2009). Recruitment of fanconi anemia and breast cancer proteins to DNA damage sites is differentially governed by replication. Mol. Cell *35*, 716-723.

Shen, X., Jun, S., O'Neal, L. E., Sonoda, E., Bemark, M., Sale, J. E., and Li, L. (2006). REV3 and REV1 play major roles in recombination-independent repair of DNA interstrand cross-links mediated by monoubiquitinated proliferating cell nuclear antigen (PCNA). J. Biol. Chem *281*, 13869-13872.

Shereda, R. D., Machida, Y., and Machida, Y. J. (2010). Human KIAA1018/FAN1 localizes to stalled replication forks via its ubiquitin-binding domain. Cell Cycle *9*, 3977-3983.

Shivji, K. K., Kenny, M. K., and Wood, R. D. (1992). Proliferating cell nuclear antigen is required for DNA excision repair. Cell *69*, 367-374.

Shrivastav, M., De Haro, L. P., and Nickoloff, J. A. (2008). Regulation of DNA double-strand break repair pathway choice. Cell Res *18*, 134-147.

Singh, T. R., Bakker, S. T., Agarwal, S., Jansen, M., Grassman, E., Godthelp, B. C., Ali, A. M., Du, C.-hu, Rooimans, M. A., Fan, Q., et al. (2009). Impaired FANCD2 monoubiquitination and hypersensitivity to camptothecin uniquely characterize Fanconi anemia complementation group M. Blood *114*, 174-180.

Singh, T. R., Saro, D., Ali, A. M., Zheng, X.-F., Du, C.-hu, Killen, M. W., Sachpatzidis, A., Wahengbam, K., Pierce, A. J., Xiong, Y., et al. (2010). MHF1-MHF2, a histone-fold-containing protein complex, participates in the Fanconi anemia pathway via FANCM. Mol. Cell *37*, 879-886.

Smith, M. L., Gregory, P., Bafi-Yeboa, N. F. A., and Arnason, J. T. (2004). Inhibition of DNA polymerization and antifungal specificity of furanocoumarins present in traditional medicines. Photochem. Photobiol *79*, 506-509.

Smogorzewska, A., Desetty, R., Saito, T. T., Schlabach, M., Lach, F. P., Sowa, M. E., Clark, A. B., Kunkel, T. A., Harper, J. W., Colaiácovo, M. P., et al. (2010). A genetic screen identifies FAN1, a Fanconi anemia-associated nuclease necessary for DNA interstrand crosslink repair. Mol. Cell *39*, 36-47.

Sobol, R. W., Horton, J. K., Kühn, R., Gu, H., Singhal, R. K., Prasad, R., Rajewsky, K., and Wilson, S. H. (1996). Requirement of mammalian DNA polymerase-beta in base-excision repair. Nature *379*, 183-186.

Soutoglou, E., and Misteli, T. (2008). Activation of the cellular DNA damage response in the absence of DNA lesions. Science *320*, 1507-1510.

Spampinato, C. P., Gomez, R. L., Galles, C., and Lario, L. D. (2009). From bacteria to plants: a compendium of mismatch repair assays. Mutat. Res *682*, 110-128.

Stelter, P., and Ulrich, H. D. (2003). Control of spontaneous and damage-induced mutagenesis by SUMO and ubiquitin conjugation. Nature *425*, 188-191.

Stewart, E., Chapman, C. R., Al-Khodairy, F., Carr, A. M., and Enoch, T. (1997). rqh1+, a fission yeast gene related to the Bloom's and Werner's syndrome genes, is required for reversible S phase arrest. EMBO J *16*, 2682-92.

Sugasawa, K., Ng, J. M., Masutani, C., Maekawa, T., Uchida, A., van der Spek, P. J., Eker, A. P., Rademakers, S., Visser, C., Aboussekhra, A., et al. (1997). Two human homologs of Rad23 are functionally interchangeable in complex formation and stimulation of XPC repair activity. Mol. Cell. Biol *17*, 6924-6931.

Sugasawa, K., Okamoto, T., Shimizu, Y., Masutani, C., Iwai, S., and Hanaoka, F. (2001). A multistep damage recognition mechanism for global genomic nucleotide excision repair. Genes Dev *15*, 507-521.

Sugasawa, K., Okuda, Y., Saijo, M., Nishi, R., Matsuda, N., Chu, G., Mori, T., Iwai, S., Tanaka, K., Tanaka, K., et al. (2005). UV-induced ubiquitylation of XPC protein mediated by UV-DDB-ubiquitin ligase complex. Cell *121*, 387-400.

Sugawara, N., and Haber, J. E. (1992). Characterization of double-strand break-induced recombination: homology requirements and single-stranded DNA formation. Mol. Cell. Biol *12*, 563-575.

Sugiyama, T., and Kowalczykowski, S. C. (2002). Rad52 protein associates with replication protein A (RPA)-single-stranded DNA to accelerate Rad51-mediated displacement of RPA and presynaptic complex formation. J. Biol. Chem *277*, 31663-31672.

Sun, W., Nandi, S., Osman, F., Ahn, J. S., Jakovleska, J., Lorenz, A., and Whitby, M. C. (2008). The FANCM ortholog Fml1 promotes recombination at stalled replication forks and limits crossing over during DNA double-strand break repair. Mol. Cell *32*, 118-128.

Sung, P. (1994). Catalysis of ATP-dependent homologous DNA pairing and strand exchange by yeast RAD51 protein. Science *265*, 1241-1243.

Sung, P. (1997). Yeast Rad55 and Rad57 proteins form a heterodimer that functions with replication protein A to promote DNA strand exchange by Rad51 recombinase. Genes Dev *11*, 1111-1121.

Svendsen, J. M., and Harper, J. W. (2010). GEN1/Yen1 and the SLX4 complex: Solutions to the problem of Holliday junction resolution. Genes Dev *24*, 521-536.

Szostak, J. W., Orr-Weaver, T. L., Rothstein, R. J., and Stahl, F. W. (1983). The double-strand-break repair model for recombination. Cell *33*, 25-35.

Tateishi, S., Niwa, H., Miyazaki, J.-I., Fujimoto, S., Inoue, H., and Yamaizumi, M. (2003). Enhanced genomic instability and defective postreplication repair in RAD18 knockout mouse embryonic stem cells. Mol. Cell. Biol *23*, 474-481.

Tinline-Purvis, H., Savory, A. P., Cullen, J. K., Davé, A., Moss, J., Bridge, W. L., Marguerat, S., Bähler, J., Ragoussis, J., Mott, R., et al. (2009). Failed gene conversion leads to extensive end processing and chromosomal rearrangements in fission yeast. EMBO J *28*, 3400-3412.

Tomita, K., Matsuura, A., Caspari, T., Carr, A. M., Akamatsu, Y., Iwasaki, H., Mizuno, K.-ichi, Ohta, K., Uritani, M., Ushimaru, T., et al. (2003). Competition between the Rad50 complex and the Ku heterodimer reveals a role for Exo1 in processing double-strand breaks but not telomeres. Mol. Cell. Biol *23*, 5186-5197.

Tong, A. H., Evangelista, M., Parsons, A. B., Xu, H., Bader, G. D., Pagé, N., Robinson, M., Raghibizadeh, S., Hogue, C. W., Bussey, H., et al. (2001). Systematic genetic analysis with ordered arrays of yeast deletion mutants. Science *294*, 2364-2368.

Tong, A. H. Y., Lesage, G., Bader, G. D., Ding, H., Xu, H., Xin, X., Young, J., Berriz, G. F., Brost, R. L., Chang, M., et al. (2004). Global mapping of the yeast genetic interaction network. Science *303*, 808-813.

Tornaletti, S. (2009). DNA repair in mammalian cells: Transcription-coupled DNA repair: directing your effort where it's most needed. Cell. Mol. Life Sci *66*, 1010-1020.

Tornier, C., Bessone, S., Varlet, I., Rudolph, C., Darmon, M., and Fleck, O. (2001). Requirement for Msh6, but not for Swi4 (Msh3), in Msh2-dependent repair of base-base mismatches and mononucleotide loops in Schizosaccharomyces pombe. Genetics *158*, 65-75.

Tran, P. T., Erdeniz, N., Symington, L. S., and Liskay, R. M. (2004). EXO1-A multi-tasking eukaryotic nuclease. DNA Repair (Amst.) *3*, 1549-1559.

Tsai, C. J., Kim, S. A., and Chu, G. (2007). Cernunnos/XLF promotes the ligation of mismatched and noncohesive DNA ends. Proc. Natl. Acad. Sci. U.S.A *104*, 7851-7856.

Van Komen, S., Petukhova, G., Sigurdsson, S., Stratton, S., and Sung, P. (2000). Superhelicity-driven homologous DNA pairing by yeast recombination factors Rad51 and Rad54. Mol. Cell *6*, 563-572.

Venkatesan, R. N., Hsu, J. J., Lawrence, N. A., Preston, B. D., and Loeb, L. A. (2006). Mutator phenotypes caused by substitution at a conserved motif A residue in eukaryotic DNA polymerase delta. J. Biol. Chem *281*, 4486-4494.

Verhage, R., Zeeman, A. M., de Groot, N., Gleig, F., Bang, D. D., van de Putte, P., and Brouwer, J. (1994). The RAD7 and RAD16 genes, which are essential for pyrimidine dimer removal from the silent mating type loci, are also required for repair of the nontranscribed strand of an active gene in Saccharomyces cerevisiae. Mol. Cell. Biol *14*, 6135-6142.

Verweij, J., and Pinedo, H. M. (1990). Mitomycin C: mechanism of action, usefulness and limitations. Anticancer Drugs *1*, 5-13.

Walworth, N., Davey, S., and Beach, D. (1993). Fission yeast chk1 protein kinase links the rad checkpoint pathway to cdc2. Nature *363*, 368-371.

Wang, J. C. (2002). Cellular roles of DNA topoisomerases: a molecular perspective. Nat. Rev. Mol. Cell Biol *3*, 430-440.

Wang, X., Peterson, C. A., Zheng, H., Nairn, R. S., Legerski, R. J., and Li, L. (2001). Involvement of nucleotide excision repair in a recombination-independent and error-prone pathway of DNA interstrand cross-link repair. Mol. Cell. Biol *21*, 713-720.

Wang, Y., Cortez, D., Yazdi, P., Neff, N., Elledge, S. J., and Qin, J. (2000). BASC, a super complex of BRCA1-associated proteins involved in the recognition and repair of aberrant DNA structures. Genes Dev *14*, 927-939.

Ward, I., Kim, J.-E., Minn, K., Chini, C. C., Mer, G., and Chen, J. (2006). The tandem BRCT domain of 53BP1 is not required for its repair function. J. Biol. Chem *281*, 38472-38477.

Watanabe, K., Tateishi, S., Kawasuji, M., Tsurimoto, T., Inoue, H., and Yamaizumi, M. (2004). Rad18 guides poleta to replication stalling sites through physical interaction and PCNA monoubiquitination. EMBO J *23*, 3886-3896.

Waters, L. S., Minesinger, B. K., Wiltrout, M. E., D'Souza, S., Woodruff, R. V., and Walker, G. C. (2009). Eukaryotic translesion polymerases and their roles and regulation in DNA damage tolerance. Microbiol. Mol. Biol. Rev *73*, 134-154.

Watkins, J. F., Sung, P., Prakash, L., and Prakash, S. (1993). The Saccharomyces cerevisiae DNA repair gene RAD23 encodes a nuclear protein containing a ubiquitin-like domain required for biological function. Mol. Cell. Biol *13*, 7757-7765.

Watson, A. T., Garcia, V., Bone, N., Carr, A. M., and Armstrong, J. (2008). Gene tagging and gene replacement using recombinase-mediated cassette exchange in Schizosaccharomyces pombe. Gene *407*, 63-74.

Wei, K., Clark, A. B., Wong, E., Kane, M. F., Mazur, D. J., Parris, T., Kolas, N. K., Russell, R., Hou, H., Kneitz, B., et al. (2003). Inactivation of Exonuclease 1 in mice results in DNA mismatch repair defects, increased cancer susceptibility, and male and female sterility. Genes Dev *17*, 603-614.

Wei, Y. F., Robins, P., Carter, K., Caldecott, K., Pappin, D. J., Yu, G. L., Wang, R. P., Shell, B. K., Nash, R. A., and Schär, P. (1995). Molecular cloning and expression of human cDNAs encoding a novel DNA ligase IV and DNA ligase III, an enzyme active in DNA repair and recombination. Mol. Cell. Biol *15*, 3206-3216.

Weinert, T. A., and Hartwell, L. H. (1988). The RAD9 gene controls the cell cycle response to DNA damage in Saccharomyces cerevisiae. Science *241*, 317-22.

Welsh, K. M., Lu, A. L., Clark, S., and Modrich, P. (1987). Isolation and characterization of the Escherichia coli mutH gene product. J. Biol. Chem *262*, 15624-15629.

Whitby, M. C. (2010). The FANCM family of DNA helicases/translocases. DNA Repair (Amst.) *9*, 224-236.

Whitehouse, C. J., Taylor, R. M., Thistlethwaite, A., Zhang, H., Karimi-Busheri, F., Lasko, D. D., Weinfeld, M., and Caldecott, K. W. (2001). XRCC1 stimulates human polynucleotide kinase activity at damaged DNA termini and accelerates DNA single-strand break repair. Cell *104*, 107-117.

Wilborn, F., and Brendel, M. (1989). Formation and stability of interstrand cross-links induced by cis- and trans-diamminedichloroplatinum (II) in the DNA of Saccharomyces cerevisiae strains differing in repair capacity. Curr. Genet *16*, 331-338.

Williams, R. S., Moncalian, G., Williams, J. S., Yamada, Y., Limbo, O., Shin, D. S., Groocock, L. M., Cahill, D., Hitomi, C., Guenther, G., et al. (2008). Mre11 dimers coordinate DNA end bridging and nuclease processing in double-strand-break repair. Cell *135*, 97-109.

Wilson, T. E., and Lieber, M. R. (1999). Efficient processing of DNA ends during yeast nonhomologous end joining. Evidence for a DNA polymerase beta (Pol4)-dependent pathway. J. Biol. Chem *274*, 23599-23609.

Winkler, G. S., Araújo, S. J., Fiedler, U., Vermeulen, W., Coin, F., Egly, J. M., Hoeijmakers, J. H., Wood, R. D., Timmers, H. T., and Weeda, G. (2000). TFIIH with inactive XPD helicase functions in transcription initiation but is defective in DNA repair. J. Biol. Chem *275*, 4258-4266.

Wood, R. D. (2010). Mammalian nucleotide excision repair proteins and interstrand crosslink repair. Environ. Mol. Mutagen *51*, 520-526.

Wu, H. I., Brown, J. A., Dorie, M. J., Lazzeroni, L., and Brown, J. M. (2004). Genome-wide identification of genes conferring resistance to the anticancer agents cisplatin, oxaliplatin, and mitomycin C. Cancer Res *64*, 3940-3948.

Wu, L., Davies, S. L., Levitt, N. C., and Hickson, I. D. (2001). Potential role for the BLM helicase in recombinational repair via a conserved interaction with RAD51. J Biol Chem *276*, 19375-81.

Wu, L., Davies, S. L., North, P. S., Goulaouic, H., Riou, J. F., Turley, H., Gatter, K. C., and Hickson, I. D. (2000). The Bloom's syndrome gene product interacts with topoisomerase III. J Biol Chem *275*, 9636-44.

Wu, L., and Hickson, I. D. (2003). The Bloom's syndrome helicase suppresses crossing over during homologous recombination. Nature *426*, 870-4.

Wu, L., and Hickson, I. D. (2006). DNA helicases required for homologous recombination and repair of damaged replication forks. Annu Rev Genet *40*, 279-306.

Wu, Q., Christensen, L. A., Legerski, R. J., and Vasquez, K. M. (2005). Mismatch repair participates in error-free processing of DNA interstrand crosslinks in human cells. EMBO Rep *6*, 551-557.

Wyman, C., and Kanaar, R. (2006). DNA double-strand break repair: all's well that ends well. Annu. Rev. Genet *40*, 363-383.

Xue, Y., Li, Y., Guo, R., Ling, C., and Wang, W. (2008). FANCM of the Fanconi anemia core complex is required for both monoubiquitination and DNA repair. Hum. Mol. Genet *17*, 1641-1652.

Yang, K., Moldovan, G.-L., and D'Andrea, A. D. (2010). RAD18-dependent recruitment of SNM1A to DNA repair complexes by a ubiquitin-binding zinc finger. J. Biol. Chem *285*, 19085-19091.

Yoshikiyo, K., Kratz, K., Hirota, K., Nishihara, K., Takata, M., Kurumizaka, H., Horimoto, S., Takeda, S., and Jiricny, J. (2010). KIAA1018/FAN1 nuclease protects cells against genomic instability induced by interstrand cross-linking agents. Proc Natl Acad Sci U S A.

Zamble, D. B., Mu, D., Reardon, J. T., Sancar, A., and Lippard, S. J. (1996). Repair of cisplatin--DNA adducts by the mammalian excision nuclease. Biochemistry *35*, 10004-10013.

Zhang, N., Liu, X., Li, L., and Legerski, R. (2007). Double-strand breaks induce homologous recombinational repair of interstrand cross-links via cooperation of MSH2, ERCC1-XPF, REV3, and the Fanconi anemia pathway. DNA Repair (Amst.) *6*, 1670-1678.

Zhang, N., Lu, X., Zhang, X., Peterson, C. A., and Legerski, R. J. (2002). hMutSbeta is required for the recognition and uncoupling of psoralen interstrand cross-links in vitro. Mol. Cell. Biol *22*, 2388-2397.

Zhao, J., Jain, A., Iyer, R. R., Modrich, P. L., and Vasquez, K. M. (2009). Mismatch repair and nucleotide excision repair proteins cooperate in the recognition of DNA interstrand crosslinks. Nucleic Acids Res *37*, 4420-4429.

Zheng, H., Wang, X., Warren, A. J., Legerski, R. J., Nairn, R. S., Hamilton, J. W., and Li, L. (2003). Nucleotide excision repair- and polymerase eta-mediated error-prone removal of mitomycin C interstrand cross-links. Mol. Cell. Biol *23*, 754-761.

Zhou, B. B., and Elledge, S. J. (2000). The DNA damage response: putting checkpoints in perspective. Nature *408*, 433-9.

Zhu, Z., Chung, W.-H., Shim, E. Y., Lee, S. E., and Ira, G. (2008). Sgs1 helicase and two nucleases Dna2 and Exo1 resect DNA double-strand break ends. Cell *134*, 981-94.

Zierhut, C., and Diffley, J. F. X. (2008). Break dosage, cell cycle stage and DNA replication influence DNA double strand break response. EMBO J *27*, 1875-85.

Zou, L., and Elledge, S. J. (2003). Sensing DNA damage through ATRIP recognition of RPA-ssDNA complexes. Science *300*, 1542-1548.